Looking for a white cat in a snowstorm - In depth thermodynamic and aggregation fingerprinting of patient-derived IgG light chains

Inaugural-dissertation
for the attainment of the title of doctor
in the Faculty of Mathematics and Natural Sciences
at the Heinrich-Heine Universität Düsseldorf
presented by

Rebecca Sternke-Hoffmann
Landau i.d. Pfalz

Düsseldorf, 12.01.2021

aus dem Institut für Physikalische Biologie
der Heinrich-Heine-Universität Düsseldorf

Gedruckt mit der Genehmigung der
Mathematisch-Naturwissenschaften Fakultät der
Heinrich-Heine-Universität Düsseldorf

Berichterstatter:
1. Prof. Alexander K. Buell
2. Prof. Rainer Haas

Tag der mündlichen Prüfung: 23.03.2021

ERKLÄRUNG

Ich versichere an Eides Statt, dass die Dissertation von mir selbstständig und ohne unzulässige fremde Hilfe under Beachtung der Grundsätze zur Sicherung guter wissenschaftlicher Paxis an der Heinrich-Heine Universität Düsseldorf erstellt worden ist.
Ich versichere, dass die eingereichte schriftliche Fassung, der auf dem Medium gespeicherten Fassun entspricht.

I declare under oath that I have complied my dissertation independently and without any undue assistance by third parties under consideration of the "Principles for the Safeguarding of Good Scientific Practices at Heinrich-Heine Universität Düsseldorf"

_____ _____

Date Signature

ACKNOWLEDGEMENTS

I would like to thank my PhD supervisor Prof. Alexander Kai Buell for his valuable personal and scientific guidance and high accessibility, even though without being physically present. Furthermore, thanks to its remarkable collaboration network, this project was feasible at all.

Therefore I also want to thank my mentor Prof. Rainer Haas, the project would not exist without his great personal commitment, and Roland Fenk and Amelie Boquoi, who could provide me their excellent medical background knowledge; my collaboration partners, Jan Hansen, Florian Platten and Stefan Egelhaaf, who assisted me from the beginning of the project; Julia Chamot-Rooke, Mathieu Dupre, Magalie Duchateau and Martial Rey, without whose support and enthusiasm we would not have been able to determine the primary structure of the LC proteins; Sabine Metzger, for their MS-expertise, and Luitgard Nagel-Steger and Thomas Pauly, who enhanced my scientific knowledge due to their thriving discussions.

I would like to thank all the people that are and were part of the AG Buell, in particular, Lena Nora Mangels, Najoua Bolakhrif, Nicola Vettore, Marie Schützmann, Alessia Peduzzo and Rasmus K. Norrild. Moreover I would like to thank Luitgard and her group, Thomas Pauly, Verena Stehl, Tao Zhang, Florian Tucholski and Sergi Gan, for their great acceptance and pleasant dinners. My thanks are due to Najoa Bolakhrif, Betka Runova and Florian Tucholsky, for their scientific contribution to this project.

This project would not have been the same without Thomas Pauly, who encouraged me to view experimental data carefully and bridged waiting times with entertaining coffee breaks together with Najoua Bolakhrif.

Generally speaking, I am very thankful for the atmosphere, both on a scientific and personal level, of the whole Institut für Physikalische Biologie. My colleagues were always available for scientific discussions, but also for private conversations. At this point I want to thank Christine Röder, Lena Mangels, Marcellino Caliqi, Emil Dandanell Agerschou and Nicola Vettore for the great night outs, the excellent food and the laugh.

Finally, I thank my parents, Sylvia and Rolf Sternke, my sister, Katharina, my father, Peter Hoffmann, and Jannik for their love and support.

ABSTRACT

The deposition of immunoglobulin light chains (IgG LCs) in the form of amorphous aggregates or amyloid fibrils in different tissues is a serious problem for patients with light chain diseases such as Multiple Myeloma (MM). MM is an incurable malignancy of plasma cells characterized by a clonal expansion of an abnormal B-cell, which leads to an overproduction of free light chain. A lot of scientific work has been carried out to correlate the different *in vivo* solubilities of LCs and their intrinsic aggregation propensity to either form highly ordered amyloid fibrils or disordered amorphous aggregates. It is generally presumed, that the origin of their different solubility is to be found in the amino acid sequence of the respective LC. Due to somatic recombination and various mutations, each LC possesses an unique primary structure. Hence the clinical picture in a patient as well as the behaviour of the LC in a test tube is very diverse.

In order to elucidate the *in vivo* solubility of a certain LC protein, I performed a detailed biochemical and biophysical analysis of light chains extracted and purified from the urine of a group of 20 patients with light chain disease. This process is described in Chapter 3. For all samples, the unfolding temperature of the LCs, their monomer-dimer distribution, the digestibility by trypsin and the formation of amyloid fibrils under various conditions of pH and reducing agent, were quantified. Neither of these properties correlated with the kidney damage as defined by clinical parameters. Most of the LC characteristics reported to be predictors of amyloid formation cannot be used to assess the degree of kidney damage. Nevertheless, I detected that LCs, which display very poor digestibility by trypsin, were derived from patients with the greatest impairment of kidney function. To perform a more detailed biophysical *in vitro* characterization, a sub-set of ten LC samples, which contained the protein at high purity, were choosen. This allows both the sequence determination, as well as a detailed biophysical study. The amino acid sequences are solved by a novel *de novo* sequencing workflow for patient-derived LCs, based on a combination of bottom-up and top-down proteomics. This is presented in Chapter 4. An in depth Thermodynamic and Aggregation Fingerprinting (ThAgg-Fip) (Chapter 5) was established to characterize the behaviour of the LCs of all of which we determined the primary structure. Our results suggest that while every pathogenic LC has an unique ThAgg-fingerprint and sequence, they can all form amyloid fibrils under physiologically relevant, mildly acidic pH conditions. Therefore we suspect that extrinsic factors are the main determinants of *in vivo* light chain aggregation behaviour. This intrinsic amyloid propensity challenges the current paradigm of the link between sequence and amyloid fibril formation of pathogenic light chains. Since the aggregation kinetics of the LC samples are affected by external factors, I could not easily examine the influence of the anti-amyloid component EGCG on their fibril formation. For this reason I performed a detailed study of the aggregation kinetics of α-synuclein to elucidate the impact of the solution conditions. This is shown in (Chapter 6). This research provides a significant contribution to the highly-relevant scientific field of LC amyloid pathology research.

CONTENTS

List of Figures

List of Tables

LIST OF SYMBOLS, ABBREVATIONS AND ACRONYMS

Aβ	Amyloid beta
ACN	Acetonitril
AD	Alzheimer's disease
AEC	Anion exchange chromatography
AFM	Atomic force microscopy
ALP	Autophagy-lysosomal pathway
ATF6	Activating transcription factor 6
AUC	Analytical ultracentrifugation
BSE	Bovine spongiform encephalopathy
BUP	Bottom-up proteomics
CD spectroscopy	Circular dichroism spectoscopy
CDR	Complementary determining region
CKD	Chronic kidney disease
CR	Congo Red
c-region	Constant region
CRAB symptoms	Hypercelcemia, renal insufficienty, anemia and bone lesions
DSC	Differential scanning calorimetry
DTT	Dithiothreitol
ER	Endoplasmic reticulum
EGCG	Epigallocatechin-3-gallate
FA	Formic acid
FLC	Free light chains
HRMS	High resolution mass spectrometry
HSA	Human serum albumin
IAA	Iodoacetamide
IAPP	Islet amyloid polypeptide
IDP	Intrinsically disordered protein
Ig	Immunoglobulin
IMWG	International Myeloma Working Group

κ	Kappa isotype of the LC
λ	Lambda isotype of the LC
LC	Light chain
LCDD	Light chain deposition disease
LC-MS	Liquid chromatography tandem mass spectrometry
MGUS	Monoclonal gammopathy of undetermined significance
MM	Multiple Myeloma
MS	Mass spectrometry
MW	Molecular weight
NAC	Non-amyloid β-component
PD	Parkinson's disease
pI	Isoelectrical point
PrP	Prion protein
PTM	Posttranslational modification
SAP	Serum amyloid P component
SDS	Size exlusion chromatography
SE	Sedimentation equilibrium
SEC	Size exlusion chromatography
SV	Sedimentation velocity
TCEP	Tris (2-carboxyethyl)phosphine
TDP	Top-down proteomics
ThT	Thioflavin-T
TOF	Time-of-flight
UPS	Ubiquitin proteasome system
V-J combination	Variable and joining gene segments recombination
v-region	Variable region

CONTRIBUTIONS

- **Chapter 3:** Biochemical and biophysical characterisation of immunoglobulin free light chains derived from an initially unbiased population of patients with light chain disease
  - Contribution 70 % (first author)
  - Purified and prepared the samples and acquired all data. Wrote the manuscript and contributed to review manuscript
- **Chapter 4:** *De novo* sequencing of antibody light chain proteoforms from patients with multiple myeloma
  - Contribution 5 %
  - Prepared the samples. Participated in writing the introduction and contributed to review manuscript.
- **Chapter 5:** Universal amyloidogenicity of patient-derived immunoglobulin light chains
  - Contribution 70 % (first author)
  - Prepared the samples, acquired data and interpreted measurements. Wrote the manuscript and contributed to review manuscript.
- **Chapter 6:** The aggregation conditions define whether EGCG is an inhibitor or enhancer of α-synuclein amyloid fibril formation
  - Contribution 80 % (first author)
  - Prepared the samples, acquired all data and interpreted measurements. Wrote the manuscript and contributed to review manuscript.

1

General introduction

The aim of this work is the biochemical and biophysical characterization of patient-derived immunoglobulin light chains (LC) and to analyse their intrinsic aggregation propensity *in vitro* in order to correlate the biophysical propensities with their *in vivo* solubility. For this, the clinical picture, in particular the severity of kidney damage has been used as a readout. Since a clear-cut correlation could not be detected, an in depth Thermodynamic and Aggregation Fingerprinting (ThAgg-Fig) of nine multiple myeloma patient-derived LC was performed. Furthermore, the potential impact of the small compound EGCG on amyloid aggregation was investigated using α-synuclein as a model protein.

1.1. Protein folding and aggregation

The majority of proteins require a highly specific three-dimensional structure in order to attain functionality in the organism [21]. The native structure is thermodynamically stable and is determined by the primary structure of the polypeptide chain and its environment [22]. Recently, DeepMind's latest artificial intelligence system AlphaFold demonstrated its ability to forecast the most accurate structure in the biennial protein-structure prediction challenge (CASP) [23, 24] and with this made a big step towards prediction of the folding process. Nevertheless, the prediction of a native protein structure from its primary sequence remains a fundamental problem of biochemistry.

Dependent on their size, proteins can fold spontaneously into their biologically active structure within microseconds [25] to hours [26, 27]. But as first pointed out by Levinthal about half a century ago [28] the number of theoretically possible conformations is too high in order to find the native structure in the conformational space in biological real-time by random searching. To overcome the "Levinthal's paradox"[29, 30] several folding models have been proposed [31, 32, 33, 34, 35, 36, 37]. The folding funnel model first described by *Leopold et al.*[38] unites several mechanisms and describes both thermodynamic and kinetic aspects of folding [39, 40]. The downhill nature of folding is explained by the assumption that all native-like intra-molecular contacts are on average more favourable than non-native ones. The contacts are formed by hydrophobic interactions, intramolecular hydrogen bonds, Van der Waals forces and electrostatic interactions.

Unfolded proteins occupy the largest conformational state. The formation of native intra-molecular contacts makes the polypeptide more compact, reduces the conformational space and drives the molecule downhill towards the thermodynamically favoured state. An example of a rugged folding funnel landscape is illustrated in Figure 1.1 A.

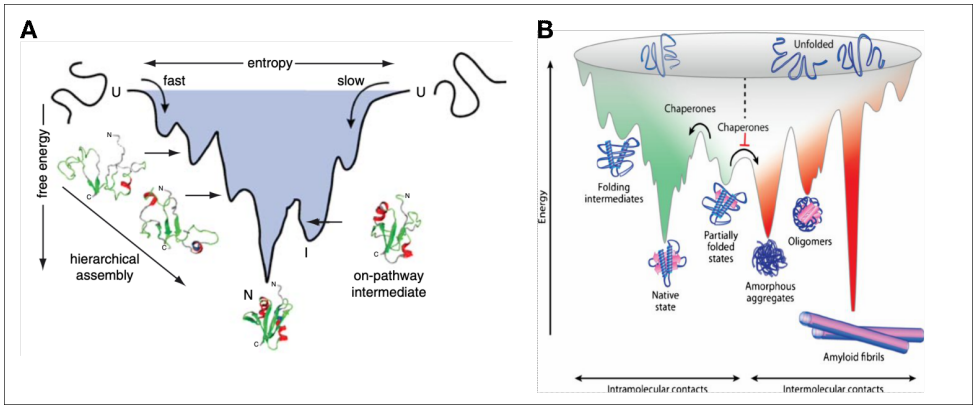

Figure 1.1: (A) A two-dimensional cross-section of a rugged folding funnel landscape illustrates the folding via a two-state model (fast) and a three-state model (slow). When the polypeptide chain descends the funnel, the entropy and free energy is decreased [1]. (B) Energy landscape of protein folding (green) combined with aggregation (red). The folding towards the native folded state and aggregation are competing reactions. Kinetically trapped intermediates are exposed to intermolecular interactions. This can lead to the formation of various aggregates such as amorphous aggregates, oligomers and amyloid fibrils. Chaperons can help to overcome kinetic barriers. [2, 3]

Folding proteins may pass through structural intermediates, which may have kinetically stable, misfolded conformations on the pathway towards the native state. Partially folded or misfolded states, in particular kinetically trapped states, are exposed to intermolecular interactions and can aggregate into a variety of aggregate structures (Figure 1.1 B). Aggregation is favoured due to exposed hydrophobic amino acid residues, which are mostly buried in the native state [41] and by an increased protein concentration, which increases the possible intermolecular interactions. The presence of molecular chaperones *in vivo* can prevent intermolecular interactions between misfolded molecules, and promote intramolecular interactions. The formed aggregates can either be amorphous like oligomers or highly ordered, such as amyloid fibrils. Amyloid fibrils have been postulated to be the most thermodynamic stable state present in the energy landscape and can consists of thousands of individual protein molecules. Amyloid fibrils are found as deposits of insoluble aggregates in patients with a wide range of diseases. However, fibril formation may be an evolutionary conserved, widely accessible, stable structure of self-assembled proteins and peptides [42, 43], hence amyloid can be formed from a range of very different polypeptide sequences. Besides disease-related peptides, also non-disease related proteins can form amyloid fibrils under certain conditions [44] and they can play important roles as "functional amyloid" in different organisms such as promotion of structure and protection [45, 46, 47].

1.2. Amyloid

Today several dozens of diseases can be linked to fibrillar proteinaceous depositions, most of which are neurodegenerative e.g. Alzheimer's disease, Parkinson's disease, Huntington's disease and transmissible spongiform encephalopathy [48]. Amyloidosis had been observed in organs since the 17^th century [49], but the first histochemical reaction for amyloidosis had been conducted by the German physician scientist Rudolpf Virchow [50, 51]. He used the iodine-sulphuric acid reaction to stain a corpora amylacea in the nervous system. He introduced the term amyloid under the assumption they would be cellulose derivatives. Nevertheless, in 1859 Schmidt [52], Friedreich and Kekulé [53] could demonstrate the absence of starch or cellulose and a high proportion of nitrogen in the amyloids.

The ability of the dye Congo Red (CR) to stain amyloid was discovered in 1922 [54], but the specificity was limited. In 1945 Ladewig [55] demonstrated that amyloid deposits exhibited green birefringence under polarized light. Since then, this Congophilia with apple green birefringence [56] is known as one of the main characteristics of amyloid and commonly used as a criterion to define amyloid species.

Under the light microscope amyloid appeared amorphous, and only with electron microscopy a first fibrillar ultrastructure could be revealed in 1959 [57] while X-ray diffraction experiments resolved another main characteristic of amyloid fibrils, namely the cross-β structure [58, 59]. This indicates a regular repeat of 4.68 Å along the fibril axis, a perpendicular spacing of 6 - 11 Å to the fibril axis and the β-sheets are organized parallel to the fibril axis [4, 60] (Figure 1.2 A-C). Nowadays high-resolution structures can be solved by a combination of cryo-electron microscopy, solid-state nuclear magnetic resonance (NMR) spectroscopy and atomic force microscopy [5, 61, 62, 63, 64, 65, 66, 67]. An example of a cryo-EM structure of amyloid fibrils of an immunoglobulin light chain is presented in Figure 1.2 D-F. The aggregation of light chains is the hallmark of amyloid light chain (AL) -amyloidosis.

Amyloid fibrils possess highly similar structures, despite the precursor proteins can differing greatly in their sequence and structure. Proteins with a natively unfolded (intrinsically disordered) structure as well as highly structured proteins can self-assemble into fibrils. The secondary structure of a folded protein appears negligible as well. Proteins with a primary helical structure such as lysozyme, insulin and myoglobin [68] and with a prominent β-sheet secondary structure such as light chains and transthyretin [69], both are able to build fibrils. Variation in local packing can lead to morphological differences [70]. Even the same precursor protein can aggregate into different morphologies due to varying the solution conditions [71, 72]. Interestingly, low-stress environments produce heterogeneous polymorphs, while environmental stress such as hydrodynamic flow results in a more homogenous fibril landscape [73]. In general, strain-specific morphologies can cause different effects [74, 75, 76].

It remains unclear whether the amyloid formation requires disordered polypeptide segments [68] or specifically structured β-sheet intermediates, which results in the questions whether native β-sheet proteins are predisposed to form amyloid fibrils or not. Transmission mode FTIR spectra recorded on native β-sheet structured monomers and amyloid fibrils revealed differences in the properties of their β-sheet structure [69], pointing out that native β-sheets are not likely predisposed to form amyloid fibrils and requires a substantial structural reorganization.

The amyloid formation of various proteins can be studied *in vitro*. Thioflavin-T (ThT) assays are a powerful and easy approach to analyse the kinetic and structural properties of amyloid fibrils [77]. The fluorescence emission at 482 nm is greatly enhanced upon selectively binding of ThT to the cross-β-structure of fibrils. Furthermore, ThT does not interfere with the aggregation into amyloid fibrils [78]. This enables the monitoring of amyloid aggregation in real time. Identifying the processes that lead to the self-assembly of proteins into amyloid fibrils is key to understanding the disease and designing a treatment. The amyloid formation is typically a complex nucleation-dependent polymerization process [79, 80].

In cases where the monomeric precursor protein is folded, an aggregation-prone species can be generated by destabilising the monomeric precursor protein. The formation of a minimal fibril from monomer is called nucleation and this process has a higher dependence on protein concentration and a higher energy barrier than the addition of a monomer to the end of a pre-formed fibril. The latter is called elongation, or growth. Once a fibril has formed and is growing,

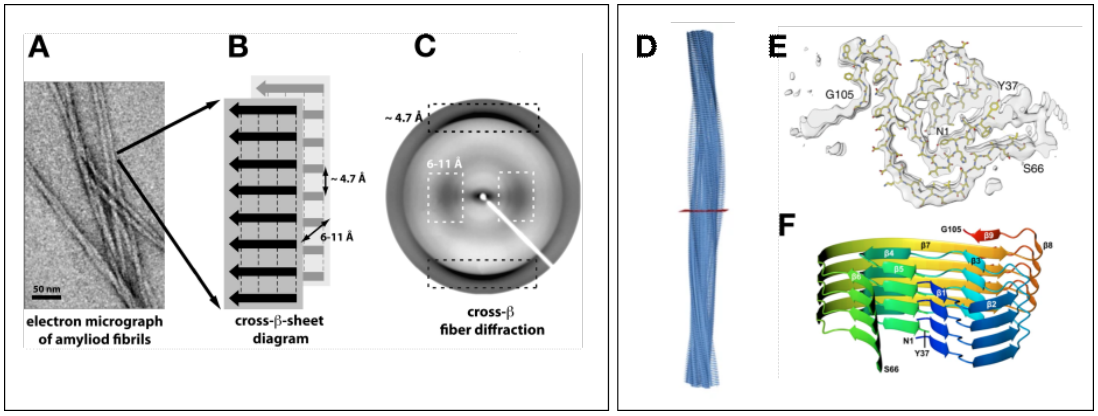

Figure 1.2: (A) Negatively stained amyloid fibrils under the electron microscope. (B) Schematic diagram of the cross-β sheets in a fibril and (C) the typical fiber diffraction pattern with a meridional reflection at 4.7 Å (black dashed line) and an equatorial reflection at 6 - 11 Å (white dashed line) [4]. (D) The post-processed 3D reconstruction of the light chain AL55 amyloid fibril structure (overall resolution of 4 Å) and (E) atomic model of the cross-section of the density map. (F) Ribbon representation of the fibril structured core [5].

it can multiply through a range of secondary processes, such as fibril breakage (fragmentation) or secondary nucleation, whereby a new fibril forms on the surface of an existing fibril [81, 82] (Figure 1.3 A).

Recently, Dear and colleagues proposed the catalytic nature of the amyloid reaction described by Michaelis-Menten-like equations [83]. Primary nucleation does not meet all criteria for Michaelis-Menten kinetics, but secondary nucleation can be well described. Surface catalysis is admittedly only efficient between peptides with the identical morphology, indicating the propagation of a fibril strain [84], however the solution conditions appear considerable more important on the morphologies [85]. During elongation, which constitutes unspecific association and dissociation of a monomer with the fibril end and subsequent conformational change to fit in the fibrillar structure, was previously described as a dock-lock mechanism [86, 87] and diffusive barrier-crossing reaction [88], the fibril ends may function as a catalytic pseudo species, because the number of free ends remains unchanged. At high concentrations, where the elongation is saturated, elongation can be modelled using Hamiltonian formulation [89].

The models are very efficient for fitting *in vitro* experimental data, but the transfer to the *in vivo* aggregation behaviour is questionable. Because of the failure of several drug trials for Alzheimer's disease (AD), Thompson and colleagues proposed a new mathematical model [90]. Besides the established mechanisms, primary and secondary nucleation, elongation and depolymerization, they included additional mechanisms such as monomer production, monomer clearance and dimer clearance. The model was applied on the aggregation of the AD peptide Aβ. In contrast to α-synuclein, Aβ is a normal metabolic waste product due to the proteolytically cleavage of amyloid-β precursor protein [91].

1.2.1 Oligomers

Besides amyloid fibrils, proteins can form different types of pre-fibrillar oligomers. Oligomers have been reported for several amyloidogenic proteins, , such as Amyloid-β [92], α-synuclein [93], tau [94], β2-microglobulin [95], transthyretin [96] and lysozyme [97]. Resolving the structure with a high resolution is a challenging task, but they share structural similarities, since

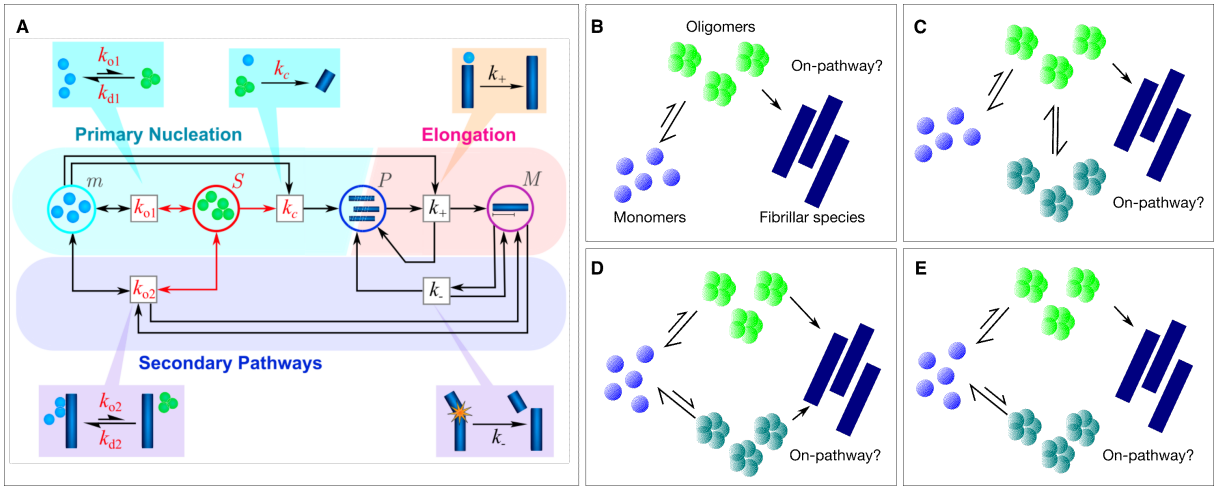

Figure 1.3: (A) Overview of the coarse-grained reaction network describing fibril formation. Reactions are represented by box and species of interest as circles. The oligomer-involving reactions are highlighted in red [6]. (B)-(E) Representative Illustration of the ambiguity of identification off- and on-pathway oligomers: (B) Oligomers dissociate into monomers instead of converting to fibrils; (C) one oligomer species forms another oligomer species through a side reaction; (D) different types of oligomers are formed from monomers, which can both convert into fibrils with different rates; (E) monomer form different oligomers, but only one converts into fibrils (adapted from)[7]).

they can be identified with an oligomer-specific antibody A11 [98, 99]. In the example of Amyloid-β, oligomers not only form in a test tube, they occur in humans and animal models as well [100, 101, 102, 103, 104, 105] before formation of plaques [106, 107] and are claimed to be the most neurotoxic species [108]. Oligomers may transfer from cell to cell and spread to specific brain regions, suggesting a prion-like manner [109]. They can be extracellular and existing in cerebrospinal fluid [110, 111, 112]. *In vitro*, oligomers form within minutes in a lag-free oligomerization reaction [113]. They are metastable and heterogeneous in size ranging from 50 to 1500 kDa and rich in β-sheet structure. They can be globular [114] or curvilinear [115] oligomers.

In vitro, the aggregation kinetics displays a biphasic behaviour. The aggregation starts immediately with the lag-free formation of oligomers, followed by a sigmoidal phase representing the growth of fibrils, which slowly replace the metastable oligomers. Oligomers increase the lag period for subsequent fibril nucleation and growth due to lateral binding to the amyloid surface [113]. The rate of oligomerization is vigorously accelerated at low pH comparatively to endosomal/lysosomal pH milieus, whereby a synaptic dysfunction and Tau pathology can be explained [116].

Compared to fibrils oligomers generally have been defined as species with a smaller size, lower growth rate, less ordered structure, distinct surface properties or higher toxicity. Cytotoxic oligomers, which can convert to amyloid fibrils are prime targets for drug design, which either prevent the formation or accelerates the conversion into amyloid fibrils to reduce the toxicity [117]. The term oligomers is widely used in literature, but it remains unclear, whether these oligomers are on-pathway or off-pathway. The majority of oligomers appear to be off-pathway and dissociate into their monomeric precursors without forming new fibrils [6, 118]. Oligomers are referred to as protofibrils, which can be misleading, if they are defined as off-pathway oligomers not terminating in a fibril [108, 109, 114, 119, 120].

Recently, different studies are debating about the terminology, establishing a non-binary definition of oligomers. Dear and colleagues used Monte Carlo simulations to identify if oligomers are contributing to fibril formation [7]. They analysed the aggregation mechanism of Aβ42, α-synuclein and tau. For Aβ in buffer under conditions where secondary nucleation dominates they saw, that all experimentally detected oligomers were fully on-pathway, although they rapidly dissociates to monomer and are constantly reformed, thereby facilitating amyloid formation. Under conditions where secondary nucleation is suppressed, α-synuclein aggregates into two kinds of oligomers, which are both on pathway. One oligomer species nucleates through monomers and is converted into the other, which builds the fibrils. One oligomer species of tau was displayed to contribute to fibril formation, whereas the other one was less productive.

1.3. Parkinson's disease (PD)

Amyloid diseases are generally categorized in localized amyloid deposits in the brain, which result in neurodegeneration such as AD, PD and prion diseases; and in systemic amyloidosis, where amyloid deposits can occur in all organs apart from the central nervous system.

Prion diseases have to be emphasised, because prions are proteinaceous infectious particle that lacks nucleic acid [121]. That proteins can be infectious was first discovered in scrapie, Creuzfeldt-Jacob disease and Bovine spongiform encephalopathy (BSE) [122]. They consist of assemblies of a cellular protein, that is misfolded from its native conformation PrP^{c} into the misfolded, self-replicating PrP^{sc} conformation. These diseases belong to the category of prion diseases and can occur in humans and mammals. Furthermore, they can conquer species barriers. BSE was caused by scrapie of the sheep [123] and can be transmitted to sheep and goats as well [124]. Prion propagation describes the templated conversion of natively folded proteins into amyloid structures and the spread from cell to cell. The templated conversion into amyloid structure is called seeding and is inherent to the self-assembly of different amyloid proteins. Prion propagation is increasingly recognized to have an important role in neurodegenerative diseases like Alzheimer's disease and Parkinson's disease (PD) [125]. Both diseases can be triggered in transgenic mice by injecting preformed seeds of α-synuclein, islet amyloid polypeptide (IAPP) or amyloid-β [74, 126, 127].

A-synuclein is the main component of Lewy Bodies, the main neuropathology of Parkinson's disease [128, 129, 130, 131]. Parkinson disease was first described two centuries ago by James Parkinson on observation of the shaking palsy [132]. PD is the second most common neurodegenerative disorder that affects 2-3 % of the population over 65 years of age [133, 134]. While the most common form of PD occurs sporadically with a usually late-onset, the amyloidogenic protein can carry certain mutations (A30P, E46K, A53T, H50Q and G51D), which can be autosomal-dominant inherited and are associated with an early onset [135, 136, 137]. It is associated with bradykinesia/akinesia, tremor, rigidity and postural instability as well as other motoric and non-motoric symptoms [138]. The main pathological feature is the loss of dopamineric neurons disrupting the micro-architecture of the substantia nigra [139, 140, 141] which is caused by proteinaceous deposits. The underlying pathology at mesoscopic scales is the aggregation and deposition of α-synuclein [129, 142, 143, 144].

One of the earliest neurological signs of PD are olfactory deficits [145]. The dysfunction occurs in more than 90 % of cases and both in familial and sporadic PD [146]. Recent studies demonstrate, that challenging TgM83 transgenic mice overexpressing mutant human α-synuclein orally or intravenously with recombinant α-synuclein fibrils leads to the development of α-

synuclein pathology [147]. This indicates that α-synuclein aggregates are transmissible by oral and intravenous routes comparable to prions. However, picogram quantities of purified PrP^{sc} could trigger pathologies, whereas the most α-synuclein transmission studies used microgram quantities [148]. Additional to the olfactory bulb, first lesions are developed at the dorsal motor nucleus of the vagal nerve, suggesting that PD may start in the digestive tract and spread from the gut to the brain by the vagal nerve [149]. A-synuclein could be detected in gastrointestinal tract tissues of PD patients [150, 151]. A potential propagation from the gut to the brain could be demonstrated in mouse/rat models as well [152, 153, 154]. A diet with uridine and fish oil prevents motor and gastrointestinal dysfunction in model organisms paving the way for new therapeutical approaches. Gastrointestinal inflammation and infection are postulated as potential factors in PD pathogenesis. It is expressed during acute and chronic gastrointestinal infection [155] and can directly activate immune cells [156].

A-synuclein is a synaptic protein attributed having an important role in neuronal communication. It is probably involved in maintaining homeostasis of neurotransmitter release by interacting with proteins involved in synaptic vesicle fusion and transportation. It can bind actin and regulate its dynamics, which are required for the regulation of synaptic vesicle mobilization [157]. Furthermore, a more general role of α-synuclein in basic cellular functions is assumed, because of its propensity to associate with membranes [158]. The protein is also important for the development of dopaminergic neurons [159]. Nevertheless, the precise biological function remains unclear.

The factors which causes α-synuclein to adopt a pathological conformation are largely unknown. The prevention of aggregation and cellular transport of α-synuclein are therapeutic goals, but until now PD is incurable and the treatment is mainly based on the alleviation of the symptoms [160].

At the present moment a prion-like propagation is only observed for amyloid proteins affecting the central nervous system, but there are indications that systemic amyloidosis could be transmissible as well [161, 162].

In the past, besides histological examinations, Congo Red was applied to detect amyloid in patients with systemic amyloidosis without awareness of it's carcinogenicity [163]. A highly diluted solution of Congo Red was injected into patients, who were clinically suspected of having amyloidosis. The CR would bind to amyloid deposits in the patient and results in a high decrease of detectable CR in the blood after 60 minutes. But also in healthy subjects up to 60 % CR disappeared [54, 164, 165]. In particular, systemic amyloidosis such as primary amyloidosis, which affects the whole body and interferes with organ function, were diagnosed with the CR test.

The term primary amyloidosis, which draws attention since 1929, was used formerly for AL-Amyloidosis and denoted an amyloidosis without any predisposing disease [166, 167]. AL-Amyloidosis is the most prevalent type of systemic amyloidosis with an incidence rate of 1.2 per 100,000 person/years [168]. It results from the extra-cellular, fibrillar deposition of monoclonal immunoglobulin (IgG) light chains in various organs. Light chains are the major component of fibrillar deposits in AL, but Ig heavy chains or heavy chain fragments.

1.4. AL-Amyloidosis

AL-amyloidosis is a fatal disease in which IgG light chains deposit as insoluble fibrillar aggregates [169, 170]. AL-amyloidosis can affect all organs, except for central nervous system, but most frequently involved are the kidney and the heart [171, 172, 173, 174]. Cardiac AL is insidious, because of a median survival of less than 6 months and a 5-year survival of less than 10 % [175]. Depending on the affected organs the clinical manifestations are very diverse and challenging in diagnosis. Soft tissues and bones can be involved as well, and can be mistakenly diagnosed as rheumatic conditions [176]. Possible symptoms range from asthenia, dyspnoea, nephrotic syndrome over diastolic heart failure, sensorimotor peripheral polyneuropathy, carpal tunnel syndrome to macroglossia and skin lesions [169, 170].

Cardiac involvement can be observed by echocardiography [174, 177], but the diagnosis generally relies on pathological examination of an involved site or with abdominal fat aspiration, when the AL is not localized [178]. The deposits are stained with Congo Red, showing typical apple-green birefringence and stained positive with anti-LC antibodies through immunohistochemistry.

1.4.1 Etiology

The aggregation of light chains is contingent due to an overproduction of monoclonal protein by a clonal expansion of an abnormal B-cell, which is called monoclonal gammopathy. The B-cells accumulate in the bone marrow and secrete large amounts of monoclonal light chains additionally to the complete immunoglobulin [179]. Upon mutation, a plasma cell that expresses a soluble monoclonal immunoglobulin can lose the capacity to express the heavy chain. 15 % of the multiple myeloma (MM)-patients produce exclusively light chains [180]. Due to an increased plasma-cell growth, the produced monoclonal light chain becomes abundant. Light chain proteins are usually either excreted or degraded by the kidney, but high monoclonal quantities and low renal clearance can induce the deposition in the kidney's extracellular matrix [181]. A monoclonal gammopathy is diagnosed by immunofixation-electrophoresis of a patient's serum or urine and by detection of serum free light chains (FLC). In healthy humans IgG light chains are produced in $10-40$ % excess of heavy chains[182]. They are filtered by the kidney, actively resorbed into lysosomes and degraded, whereby the FLC levels are minimized. Elevated FLC level overwhelm renal filtration and/or catabolism and can be detected in serum and urine by immunofixation-electrophoresis [183]. The abundant urinary proteins are often referred as Bence Jones proteins [184]. Different stages of the underlying clonal population may results in different diseases. The early stage is called monoclonal gammopathy of undetermined significance (MGUS). MGUS is characterized by LC concentration of less than 30 g/l in the serum, less than 10 % clonal plasma cells in the bone marrow and no organ damage which is characterized by CRAB [185].

CRAB summarizes typical clinical manifestations of multiple myeloma such as hypercalcemia, renal insufficiency, anemia and bone lesions (CRAB) [186]. The increase of the clonal population to over 10 % bone marrow plasma cells are the hallmark of the first multiple myeloma stage. The plasma cells can either remain in an asymptomatic (smoldering) or progress to the symptomatic stage with hypercalcemia, renal failure, anemia and lytic bone lesions (CRAB) [187, 188, 189]. In all myelomagenesis stages the patient can develop a further light chain aggregation disease, such as AL amyloidosis (proteins form amyloid fibrils [190]) and light chain deposition disease (LCDD) (proteins form amorphous aggregates [191, 192]). Several cases have been reported in which both types of deposits co-exists in the same or different organs [193, 194, 195, 196]. *In*

vitro aggregation kinetics showed that an amyloidogenic LC (e.g. SMA) forms fibrillar aggregates at physiological conditions and amorphous, granular aggregates in the presence of copper ions [197]. AL-amyloidosis can coincide with all myeloma stages with descending probability; 54 % were suffering from MGUS, 38 % from smoldering MM and 8 % from full blown MM [188]. Besides of the most common IgG LC, different types of monoclonal immunoglobulin protein can be produced and secreted [198], for instance heavy chains, that can deposit by themselves [199, 200, 201, 202, 203] or co-aggregate with LCs [204, 205, 206]. The evolution from MGUS to MM is not proceeding linearly. At each step of progression they acquire new mutations and evolve subclones, which may express altered light chain population [189]. LC which cause AL or LCDD interact mainly with components of the glomerulus especially with mesangial cells and cause glomerular dysfunction, but LCs can also be pathogenic to the proximal tubules causing Fanconi's syndrome and myeloma (cast) nephropathy [206, 207, 208].

Currently, there is no possibility to predict the *in vivo* deposition behaviour of a particular light chain found in the blood or urine of a patient with a light chain disease in particular, because only a small proportion of LCs are able to form amyloid *in vivo* [209].

1.4.2 Light chains

Immunoglobulin light chains are small (approximately 22-25 kDa) glycoproteins that are paired with heavy chains to obtain an antibody. Immunoglobulin G are the most abundant type of antibody and play an important role in the adaptive immune system [210, 211]. An antibody comprises two identical heavy and two identical light chains, which are linked to each other by disulfide bonds. An example of an antibody is shown in Figure 1.4 A. Abundant monoclonal light chains subsist as monomers and/or as dimers. The structure is stabilized by two inter- and one intramolecular disulfide bridges and formed a sandwich by two antiparallel β-pleated sheets [212, 213]. The disulfide bridge is buried in the hydrophobic interior of each domain [214]. Representatively shown are two homodimers of λ and κ light chains in Figure 1.4 B and C.

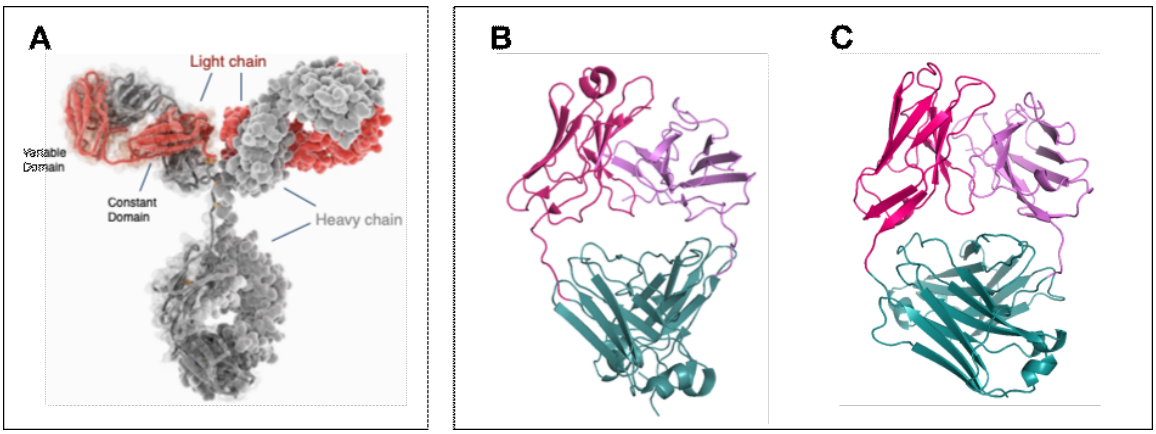

Figure 1.4: (A) Three-dimensional model of an immunoglobulin, which consists of two identical heavy (gray) and light (red) chains. Disulfide bonds are shown in yellow [8]. Three-dimensional ribbon representations of (B) λ LC homodimer 3MCG [9] and (C) κ LC homodimer 1B6D [10]. The constant region are presented in teal and the variable region in pink (visualized with PyMOL 2.4. (Schrödinger) from the RSCB protein data bank [11]).

The solubility and behaviour *in vivo* of a light chain most likely lies within the variability in the amino acid sequence and consequently certain variable subgroups and amino acid substitutions [215, 216]. However the overall topology is highly conserved in mammals containing regions

with a higher sequence variability (complementary determining region (CDR)) [217]. The sequence of a mature immunoglobulin light chain is unknown and unique for each patient-derived protein. LCs are genetically encoded in fragments, which are joined by somatic recombination and then affected by hypermutations [210, 218]. LCs consists of an N-terminal variable region (v-region) and a C-terminal constant region (c-region), which specifies the effector function of the molecule [219]. The diversity of the N-terminal variable region, which is capable to recognize the antigen [219], is created by somatic recombination of variable (V) and joining (J) gene segments (V-J combination) during the early stages of B-cell maturation [220]. Light chains occur either as a λ or a κ isotype, which are encoded by the immunoglobulin λ (IGL) (on chromosome 22 at band 22q11.2) [221] or the κ (IGK) (on chromosome 2 at band 2p11.2) [222] locus. It has been found that the majority of light chain amyloidosis cases are associated with λ light chains [223, 224] particularly with the variable λ VIa and IIIr subgroup [215, 216, 225]. There are 40 - 76 IGKV and 73 - 74 IGLV gene segments belonging to seven and eleven subgroups respectively, which are randomly joined with the corresponding joining gene segments (IGKJ and IGLJ) [226]. There are a multitude of different IGLV and IGKV gene segments, which are randomly joined with the corresponding joining gene segments IGLJ and IGKJ [226] and then affected by somatic hypermutations during the antigen dependent stages of differentiation. This sequence diversity translates into a diverse clinical picture [226], impeding the understanding of the disease mechanisms. Besides the effect of the fibril deposition, amyloidogenic LCs were denoted to be cardiotoxic.

Proteomic analyses have revealed that in most AL fibrils not the full-length LC proteins are incorporated due to a lack of different parts of their according constant region [5, 66, 202, 227, 228, 229, 230, 231, 232, 233]. However, constant regions [234, 235] and the full-length LC proteins [236, 237, 238, 239, 240] could be found in the amyloid depositions as well. So far the timing of proteolysis is unclear. Lavatelli recently presented the first high-specificity map of proteolytic cleavages in cardiac AL amyloid using mass spectrometry, suggesting that LC deposition presumably precedes the proteolytic events [241]. Nevertheless, the induced aggregation through proteolytic digestion particularly by lysosomal enzymes was demonstrated in different studies [242, 243, 244, 245, 246, 247] even of non-amyloidogenic LCs [248, 249]. The full-length LCs and fragments could also be found in deposits of LCDD patients; local tissue factors may be responsible for different processing of the light chain deposits in LCDD [193, 239].

The sequence of a LC can be determined by sequencing the RNA of the producing B-cell clone [250, 251]. However, a bone marrow aspiration is generally not conducted, because of ethical reasons it is solely allowed to improve diagnosis and treatment. Moreover sequencing of the RNA gives no insight into possible post-translational modifications (PTMs), which can play an important role in their *in vivo* behaviour [252, 253, 254].

In contrast, MS-based sequencing on protein level covers all post-translational modifications in particular inter- and intramolecular disulfide bonds and the ratio between monomeric and dimeric proteoforms. Modern MS-based sequencing identifies the peptides based on an established protein sequence database, which is solely suitable for known antibody sequences [255, 256]. Therefore a complex *de novo* sequencing based on a combination of top-down and bottom-up proteomics is required for patient-derived LCs.

Combining sequence information with biophysical information could enable the prediction of an *in vivo* light chain behaviour, which would pave the way for new diagnostics and therapeutics of light chain aggregation diseases. A large number of studies has been performed in recent years

to understand the solubility of a given LC in a patient through a detailed *in vitro* investigation of biophysical and biochemical properties in particular which properties picture amyloidogenic (*in vivo* amyloid forming) LCs. Various studies demonstrated a correlation between the thermodynamic stability and the aggregation propensity [233, 257, 258, 259, 260, 261, 262, 263, 264], though it could not be always observed [265, 266, 267]. However it was demonstrated, that LCs from MM-patients could be irreversibly heat-denatured [267] and had lower free energy of folding [265]. In addition non-amyloidogenic LCs could also be fibrillated under reducing conditions in a test tube, but in contrast to amyloidogenic LCs the aggregation kinetic showed no monomer-concentration dependence [267].

The structures of amyloidogenic and non-amyloidogenic LC monomers are very similar [209], but Qin could demonstrate that the monomeric state rather than the dimeric state, was critical for fibrillation. Intermediates with less native-like contacts showed a fast aggregation kinetic while more native-like intermediated tend to aggregate amorphously [268]. Somatic mutations that disrupts the dimer interface lead to higher amyloid propensity [269, 270], while stable dimers interfere with amyloid assembly [244, 271]. But Gatt's use of serum free light chain suggested a correlation of high degree of dimerization with AL [272] and a discriminator between malignant from premalignant monoclonal gammopathies [273, 274]. AL is usually caused by λ LCs, while κ LCs are more often involved in LCDD [171, 275]. However, AL with dominant soft tissue and bone involvement was significantly associated with κ chains [176].

λ LCs display a stronger tendency to dimerize and oligomerize [276, 277, 278], but they often show a misfolded dimer conformation [279, 280]. AL patients presented a high proportion and heterogeneity of disulfide-linked monoclonal FLCs [273, 281], λ LCs had a strong tendency to migrate abnormal on a similar height as HSA, which may increase the risk of misinterpretation of protein electrophoresis [282]. MS analysis revealed several cases of amyloidogenic κ light chains, which formed covalently bound dimers, suggesting that the dimeric nature of κ-type proteins was overlooked in previous studies [240].

Because of the increased size as a dimer, dimeric LCs are more slowly removed by glomerular filtration resulting a high protein concentration, which may promote the aggregation. Furthermore, dimerization has to be considered for the dialysis of patients. Membranes with distinct cut-offs must be used to filter monomers or dimers efficiently [283].

Lately, conformational flexibility and dynamics have been proposed to correlate with the ability to form amyloid *in vivo* [232, 284, 285].

The removal of abundant, misfolded and aggregated protein is a key factor to maintain normal physiological functions. There are two main systems which process these proteins: the autophagy-lysosomal pathway (ALP) and the ubiquitin proteasome system (UPS). UPS presents the major pathway for intracellular protein degradation. Cellular proteins are targeted for degradation with polyubiquitin chains and subsequently get degraded by the 26S proteasome [286]. Proteasomes are primarily localized in cytosol, but are also associated with plasma membrane and ER. Autophagy is activated during stress conditions such as amino acid starvation, unfolded protein response or viral infection and delivers cytoplasmic material to lysosomes for degradation [287]. Defects in either of these systems have been concatenate to neurodegenerative diseases [288].

The endoplasmic reticulum (ER) is responsible for the synthesis, folding, modification and quality control of virtually all transmembrane and secreted proteins including antibodies. This implies post-translational modifications and disulfide bond formation [289, 290]. Native folded proteins which pass the quality control are delivered to the Golgi apparatus before they are

secreted to the extracellular space [291, 292]. Excess light chains are usually secreted without assembly to the corresponding heavy chains. Only properly folded proteins can migrate to the Golgi, whereas misfolded proteins activate the unfolded protein response, which is signalled through three ER transmembrane protein sensors; inositol-requiring kinase 1, pancreatic ER eIF2a kinase and activating transcription factor 6 (ATF6) [293].

Even though amyloidogenic LCs appear to possess an more unstable and flexible conformation, they are not detected by the ER quality control, allowing their secretion to the extracellular space. However, it was demonstrated recently that inducing unfolding protein response due to activation of ATF6 and ER protein disulfide isomerase, reduces the secretion of amyloidogenic LC dramatically [294, 295, 296]. This can pave the way for the development of therapeutics. Nevertheless, the expression in different cell lines of amyloidogenic LC presenting an unstable conformation was failing and the LCs remain in the ER and were removed [297, 298].

1.4.3 Different treatment strategies

Multiple myeloma and AL amyloidosis remain incurable pathologies. The primary problem in treating AL-amyloidosis effectively is the correct and early diagnosis. First symptoms are often vague, which leads to a diagnosis at an advanced stage, where treatment is usually more difficult [299]. To adjust the convenient therapy, patients are classified using cardiac biomarkers, such as a NTproBNP cut-off [300], and glomerular filtration rate and proteinuria [301]. Currently, treatment relies mainly on suppressing the underlying B-cell dyscrasia with chemotherapy or other anti-B-cell/plasma cell agents. Depletion of the circulating free light chains is crucial, since amyloidogenic LCs with cardiac involvement, cause oxidant stress independent of fibril deposition [175].

High-dose melphalan and autologous stem cell transplantation (ASCT) is the most cytotoxic therapy against plasma cells, which can be applied to patients associated with a good overall rating, resulting in a hematologic response and improved 5-year survival high organ response rate [302, 303, 304, 305]. In particular patients with cardiac-involvement and renal impairment had a higher mortality rates [306, 307], therefore highly compatible therapeutics are required.

Many cell cycle regulatory molecules are degraded by the proteasome, but proteasome inhibitors results in an accumulation of these proteins causing apoptosis [308, 309, 310]. Malignant cells are more sensitive to proteosome inhibitors than normal cells [311], therefore they are used in the care of MM and AL amyloidosis. Bortezomib is a reversible proteasome inhibitor, that targets the myeloma cell and inhibits the binding of the myeloma cells to bone marrow stromal cells [312]. It is a standard treatment for patients with MM who are not eligible for a high-dose melphalan therapy [313, 314] and is well tolerated even in patients with advanced renal failure [315]. Treatment with Bortezomib combined with dexamethasome revealed a rapid reduction of amyloidogenic free light chains and improvement of organ function [307, 316].

The demand for novel therapeutic strategies is high, because many patients eventually experience a hematologic relapse after chemotherapy or a hardly measurable remaining LC production [304, 317, 318].

Bendamustine is an alkylating agent which enhanced the efficacy of bortezomib and dexamethasone in patients with MM especially in patients with renal impairment [319, 320, 321].

Daratumumab is a human IgGκ monoclonal antibody targeting CD38, which is located on the surface of plasma cells [322, 323]. Treatment in combination with bortezomib and dexamethasone

induced high response rates [324, 325] and was well tolerated even among patients with advanced cardiac AL involvement [326]. Daratumumab leads to a rapid decrease of circulating free LCs and improvement of organ function [327].

Antibiotic Doxycycline, which emerges as an inhibitor of amyloid formation of different proteinopathies, such as Alzheimer's disease, prion disease, dialysis-related amyloidosis and transthyretin amyloidosis [328, 329, 330, 331, 332], also displayed an impact on AL fibrils *in vitro* studies [333], in mouse models [334] and in first clinical studies [335, 336, 337, 338].

Beside suppressing the malignant B-cell clone, different antibodies were developed in order to deplete the amyloid fibril deposits. It is very important to consider the potential cardiotoxic effect of free light chains, when the fibrils are dissolved [339, 340, 341]. NEOD001 is a humanized form of the murine monoclonal antibody 2A4, which binds to a light chain epitope exposed during misfolding and aggregation [342]. *In vitro* studies suggested promising effects [343, 344], but after one of three randomized studies failed, it is no longer developed by Prothena Biosciences [336]. CAEL-101 (a chimeric form of the murine monoclonal antibody 11-1F4) is another monoclonal IgG antibody, which can bind to AL fibrils. It demonstrated an overall organ response of 63 % in a phase 1/1b study with patients with relapsed refractory AL amyloidosis [345]. Furthermore, it can be used in positron emission tomography (PET) imaging to diagnose the systemic amyloid depositions [346, 347]. Dezamizumab, an anti-SAP antibody, combined with a small molecule, CPHPC, which depletes circulating SAP (serum amyloid protein component), showed effective removal of amyloid deposits from the liver and other tissues in a phase I clinical trail [336, 348].

In some cases, the transplantation of the affected organ, in particular the heart is the only solution. But this can solely be applied to selected patients with single organ involvement, which are not too old and display a general good performance [349, 350, 351].

In 2007 Hunstein, who was suffering from AL amyloidosis himself, noticed a clear improvement of his clinical picture after drinking green tea on a daily basis [352]. In 2008 Mereles confirmed this observation with the first report of an *in vivo* effect of green tea on a patient with systemic AL and suggesting a potential new therapeutic [353]. A lot of different medical properties are attributed to green tea, it functions for example as an antioxidant, preventing oxidative damage in healthy cells and stimulating apoptosis in cancerous cells [354]. The leafs of the tea plant *Camellia sinensis* contains different polyphenols and phenolic acids. The main polyphenol found in green tea is the well-studied epigallocatechin-3-gallate (EGCG).

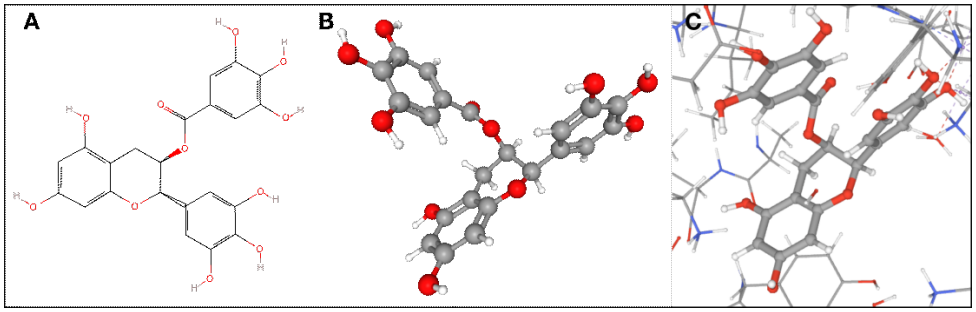

Figure 1.5: Chemical structured of epigallocatechin-3-gallate (EGCG): (A) 2D and (B) 3D conformer from the PubChem database [12] and (C) 3D crystall structure bound to influenza strain pH1N1 from the PDBe database [13] (4awm [14]). In the complex both substituents point in the same direction of the catechin ring system.

Biochemical *in vitro* studies indicated the ability to inhibit the amyloid aggregation of a number of amyloidogenic peptides and proteins effectively, including α-synuclein [355, 356, 357, 358, 359], amyloid-β (related to AD) [355, 360], islet amyloid polypeptide (related to type II diabetes) [361, 362], huntingtin exon 1 (related to Huntington's disease) [363], tau (related to AD and tauopathies) [364], superoxide dismutase (related to amyotrophic lateral sclerosis) [365], prion proteins (related to prion diseases) [366, 367] and others.

The removal of amyloid deposits is crucial to treat AL, therefore the inhibiting effect of amyloid formation of LCs upon binding was recently investigated in a test tube [267, 368, 369]. EGCG displayed a generic, sequence-independent effect on light chain aggregation through preventing the second aggregation phase and induction of formation of SDS-stable oligomers [267]. In addition to the *in vitro* studies, the clinical efficacy and toxicity of EGCG is investigated in a Phase 2 trial. Even though the therapy was well tolerated, and urinary albumin level was decreased, a clear-cut efficacy could not be observed [370].

Most of the studies are performed at physiological pH, where EGCG is unstable and oxidizes rapidly into various products [371], while a decrease in pH results in a considerable increase in stability. I tried to examine the effect of EGCG on the aggregation behaviour of the patient-derived LCs depicted in the following, but there was no impact detectable. In order to examine the mode of action of EGCG on fibril formation I therefore conducted experiments with the well-established protein α-synuclein.

1.5. Aim and approach of this work

The aggregation of immunoglobulin LCs and the triggered disorders are known for almost a century. Even though many detailed biophysical studies were conducted on patient-derived light chains, the *in vivo* behaviour of a given light chain can not fully be predicted. Thereby also the diagnosis is impeded. The main goal of this work was to resolve the biophysical and biochemical basis of patient-derived light chain aggregation, aiming to develop a quick test to improve the diagnosis.

The background of the applied methods are explained in Chapter 2. The detailed experimental conditions can be found in the material and methods sections of the following chapters.

For this *in vitro* assessment, I isolated protein from the urine of 20 patients, when the protein appeared in high concentration. All patients were suffering from a light chain disease, mainly multiple myeloma of various subtypes and one patient with AL amyloidosis. The patients were selected without bias. I investigated various characteristics, which were reported to correlate with the amyloid propensity. The outcomes are presented in Chapter 3.

Since the severity of kidney damage showed no significant correlation with any of the characteristics, the amino acid sequences of a suitable subset of samples were solved and an in depth Thermodynamic and Aggregation Fingerprinting (ThAgg-Fip) was performed. The results suggest that every pathogenic is not only unique on the level of primary structure, but also possesses an unique ThAgg fingerprinting. The results are presented in Chapter 4 and 5

I attempted to investigate the impact of the amyloid-inhibitor EGCG on the light chain aggregation. The aggregation mechanism of LCs is not a typical nucleation-dependent polymerization process, but requires additional alterations, therefore it was unfeasible to study the effect on light chain aggregation. To understand the potential course of action, I investigated the effect of the

polyphenol on the well-studied amyloid protein α-synuclein. The results presented in Chapter 4 indicate a diverse effect of EGCG which is dependent on the aggregation conditions.

2

Material and Methods

Investigated samples

2.1. Patient-derived IgG light chains

The study has been reviewed and approved by the ethics committee of the University Hospital of Düsseldorf and all patients of whom samples were used in the study have signed an informed consent (study number 5926R and registration ID 20170664320). The *in vitro* studies were performed using protein isolated from urine samples of 22 patients with multiple myeloma of various subtypes and one patient with Amyloidosis. Two samples were completely excluded from this study, because one sample did not contain a measurable amount of light chain protein and the other sample was attained using dialysate, which could not be purified in a simple manner. An overview of the patient characteristics is shown in Table 2.1. The samples were attained from patients (6 females and 14 males) with an age range between 45 and 76 years with a median age of 61.5 years.

For the majority of patients the kidney histology was unknown. Because a histopathological examination of the kidney was not available since the corresponding invasive diagnostic procedure was not necessary for the therapy decision as they were diagnosed according to International myeloma Working Group (IMWG) criteria. Two patients (P008 and P009) were diagnosed with myeloma cast nephropathy and one patient (P011) with AL-Amyloidosis. Thus, there was no initial bias in the selection of patients, as the common denominator for inclusion into the study was solely the presence of a monoclonal light chain in the peripheral blood and in the urine, while the type of light chain disease (MM vs. Amyloidosis) did not play a role.

There was a large variation with regard to the light chain concentration in the serum, with concentrations between 2.2 mg/l and 11,000 mg/l. Two of our patients presented with renal insufficiency and required dialysis, while four of them had no signs of functional renal impairment. We divided the patients into three different groups (I,II,III) according to their chronic kidney disease (CKD)-stage (1-5) at the time of diagnosis. Groups I corresponds to stages 1 and 2, group II to stage 3 and group III to stages 4 and 5. At the time when the urine samples were collected, 17 patients were diagnosed *de novo*, whereas three patients with multiple myeloma had received induction therapy with bortezomib, cyclophosphamide and dexamethasone. The duration of their disease at the time of the examination was therefore relatively short with a median of 6 weeks varying from 4 to 12 weeks. The isotype of the examined light chain protein in the study was λ in 6 samples and κ in 14 samples.

Table 2.1: Patient Characteristics at the time of examination. The patient groups are given according to CKD: Group I good Stage 1+2, n = 9 (P004, P007, P010, P011, P012, P014, P017, P018, P020), Group II intermediate Stage 3 n = 6 (P001, P005, P013, P015, P016, P019) and Group III bad Stage 4+5, n = 5 (P002, P003, P006, P008, P009)

Patient	Age	Gender	Disease type	Subtype	Subtype	Time of sample	FLC Serum [mg/l]	FLC Urine [mg/l]	TPU [g/24h]	Kidney function creatinin [mg/dl]	GFR-CKD-EPI [ml/min]	CKD Stadium	Kidney histology	Kidney function recovered? Improvement = 30%	Kidney function recovered Creatinine [mg/dl]	chronic / acute kidney injury
P001	47	male	MM	IgG	λ	at diagnosis	3.750	1.060	13	1.3	50	3	n/a	Yes	0.9	c
P002	76	male	MM	-	λ	after 1 course of therapy	4.250	n/a	0.3	dialysis dependent	<10	5	n/a	No	dialysis dependent	a
P003	52	male	MM	IgG	λ	after 1 course of therapy	2.420	n/a	0.3	dialysis dependent	15	4	n/a	No	dialysis dependent	a
P004	72	male	MM	IgG	κ	at diagnosis	5.280	7.650	4	1.1	90	1	n/a	Yes	0.9	c
P005	65	female	MM	IgG	κ	at diagnosis	1.250	6.140	3	1.2	48	3	n/a	n/a	acute kidney injury	c
P006	66	female	MM	IgG	κ	at diagnosis	2.460	6.880	3	1.9	27	4	n/a	Yes	1.3	c
P007	54	male	MM	IgG	κ	at diagnosis	0.898	n/a	1	1	83	2	n/a	No	1.3	a
P008	47	female	MM	-	κ	at diagnosis	1.370	3.990	1.5	2.1	28	4	cast nephropathy	Yes	1.5	c
P009	48	male	MM	-	λ	at diagnosis	2.590	n/a	1.4	4.2	16	4	cast nephropathy	Yes	1.3	a
P010	53	male	MM	IgA	κ	at diagnosis	2.530	n/a	6	1.1	92	1	n/a	Yes	1.1	c
P011	45	female	AL	-	λ	at diagnosis	0.120	n/a	6.2	0.7	108	1	n/a	No	0.8	c
P012	66	male	MM	IgG	κ	at diagnosis	0.101	n/a	0.2	1.2	66	2	n/a	n/a	0.9	c
P013	65	male	MM	-	κ	at diagnosis	11.000	n/a	3	1.5	50	3	n/a	No	1.7	c
P014	54	male	MM	IgG	λ	after 1 course of therapy	2.000	n/a	0.1	1.1	76	2	n/a	No	1.1	c
P015	68	male	MM	IgG	κ	at diagnosis	4.380	n/a	>6	1.5	46	3	n/a	Yes	0.9	c
P016	59	male	MM	-	κ	at diagnosis	1.150	17.50	3	1.6	45	3	n/a	No	1.2	c
P017	72	female	MM	IgG	κ	at diagnosis	1.380	n/a	4	0.7	90	1	n/a	No	0.8	c
P018	69	male	MM	IgG	κ	at diagnosis	0.369	n/a	<0.05	1.1	66	2	n/a	n/a	n/a	c
P019	56	male	MM	IgG	κ	at diagnosis	0.484	n/a	<0.05	1.8	41	3	n/a	Yes	1.4	c
P020	64	female	MM	-	κ	at diagnosis	4.120	n/a	2.4	0.8	74	2	n/a	n/a	0.9	c

The protein content of a 24 h urine collection was precipitated by ammonium sulfate (70 % saturation), generally on the same day when the urine was obtained from the patient. After incubation (for 1-2 h) at 4 °C under continuous agitation, the samples were centrifuged at 6000 xg for 25 min at 4 °C. The precipitates were dissolved in 10 mM phosphate buffer, pH 7.5, and dialyzed against the same buffer at 4 °C for 72 h (the buffer was exchanged every 24 h). The protein solution centrifuged to remove macroscopic aggregates, before loading it on a size-exclusion chromatography (SEC) column Superdex 75 10/300 GL column using an ÄKTA pure chromatography system (GE Healthcare). 10 mM phosphate buffer (for the general characterization and circular dichroism (CD) spectroscopy) or 30 mM Tris-HCl pH 7.4 (for the in depth characterization) was used as an elution buffer.

LC concentration was determined by measuring UV-absorption at 280 nm. For the experiments of the general characterization the used extinction coefficient ε (38.000 M^{-1} cm^{-1}) was estimated from a range of published light chain sequences and corresponds to an average composition of 3.5 Tryptophan and 9 Tyrosin residues. For the in depth characterization, an extinction coefficient of the determined amino acid sequence was calculated. An overview of the calculated ε is displayed in Table 2.2 together with the molecular weight (MW), theoretical isoelectric point (pI), the partial specific volume $\bar{\nu}$ and the intrinsic solubility score determined by CamSol [372].

Table 2.2: Overview of the intrinsic LC properties according their primary structure

	P001	P004a	P004b	P005	P006	P007	P013	P016	P017	P020
MS [kDa]	22.9	23.4	23.6	23.4	23.5	23.3	23.5	23.2	23.5	23.6
Theor. pI	6.34	6.12	5.73	6.91	5.2	6.35	5.73	5.7	5.19	7.75
$\bar{\nu}$ [$cm^{-2}g^{-1}$]	0.7261	0.7262	n/a	0.7255	0.7262	0.7251	0.7270	0.7262	0.7242	0.7267
ε [M^{-1} cm^{-1}]	33265	27640	33140	26150	26150	26150	33140	26150	26150	31650
Tryptophan	3	2	3	2	2	2	3	2	2	3
Tyrosin	11	11	11	10	10	10	11	10	10	10
neg. charged (Asp + Glu)	18	21	21	19	23	20	20	19	23	20
pos. charged (Asp + Glu)	17	20	19	19	19	19	18	17	18	21
Intr. solubility (Camsol)	0.155	0.428	-0.028	0.269	0.404	0.274	0.132	0.069	0.301	0.386

2.2. α-synuclein

A-synuclein is a 140-residue neuronal protein, which is the major component of Lewy Bodies, the main neuropathology of Parkinson's disease [128, 129, 130]. The underlying pathology of PD at mesoscopic scales is the aggregation and deposition of α-synuclein [129, 142, 143, 144]. The prevention of aggregation and cellular transport of α-synuclein are therapeutic targets, but until now PD is incurable and the treatment is mainly based on the alleviation of the symptoms [160].

A-synuclein is an intrinsically disordered protein (IDP) without a well defined secondary or tertiary structure at neutral pH [373, 374]. The primary structure can be subdivided into an

amphipathic N-terminal region that interacts with negatively charged surfaces, a central region referred to as the non-amyloid β-component (NAC) that has a high aggregation propensity and an acidic C-terminal region that is typically disordered. IDPs are often involved in cellular signalling and regulation, but the precise biological function of α-synuclein remains unclear. A-synuclein is enriched at the pre-synaptic terminal in almost all types of neurons in the central nervous system. Bellani proposed a potential binding and regulation of actin-dynamics, which is required for the regulation of synaptic vesicle mobilization [157].

Overproduction and/or familial mutations [135, 136, 137] cause the aggregation of α-synuclein into highly ordered, cross-β-sheet structured amyloid fibrils [375]. As described earlier the aggregation mechanism is a typical nucleation-dependent polymerization process [376]. The familial single mutation can alter the morphologies of the amyloid fibrils [377]

Amyloid formation can be observed in a wide range of physiological pH conditions such as neutral and slightly acidic pH values. At neutral pH the protein carries a net negative charge, but at low pH the normally highly acidic and extended C-terminal tail becomes fully protonated and collapses - leading to an increased hydrophobic conformation [378]. This results in a strongly enhanced aggregation kinetic, through a secondary nucleation process catalysed by the binding to the surface of pre-existing fibrils [81, 379].

A-synculein can experience such solution conditions during its life cycle in endosomes and lysosomes, which maintain an acidic pH value between pH 4 and pH 5 [380, 381, 382]. Therefore α-synuclein is an appropriate model protein to investigate the impact of EGCG on the aggregation at various environmental conditions.

Human codon-optimized wild type α-synuclein in the PT7-7 vector was expressed in *E. coli* BL21 (DE3) [85]. The expression was conducted for 24 h at 37 °C in auto-induction 2YT-medium (16 g/L trypton, 10 g/L yeast extract, 5 g/L NaCl) with 50 mM sodium phosphate pH 7.2, 2 mM $MgCl_2$, 1.8 % glycerol (v/v), 0.05 % glucose (w/v), 0.2 % lactose (w/v). The cell pellet was washed in a saline solution (0.8 % NaCl) and lysed at 95 °C for 15 minutes in 25 mM Tris-HCl pH 8.1, 1 mM EDTA and by ultrasonication using a VS70/T tip at 60 % power (15 minutes, 15 seconds pulses spaced out by 1 minute) on ice. Before centrifugation at 20,000 g for 30 minutes at 4 °C the lysed cells, the DNA was precipitated using streptomycin sulphate (final concentration 10 mg/ml per litre of initial culture) for 15 minutes at 4 °C. Ammonium sulphate was added to the supernatant (final concentration of 1.75 M) and stirred at 4 °C for 15 minutes. The precipitated protein was collected by centrifuging at 20000 g for 30 minutes. The pellet was re-suspended in 25 mM Tris-HCl pH 8.1, 1 mM EDTA and dialysed at room temperature for 2 h. The protein was filtered with a 0.42 µm pore size and subsequently loaded onto a HiTrapQHP anion exchange chromatography (AEC) column (GE Healthcare). The gradient was run stepwise: 0-35 % (in 100 ml), 35-45 % (in 50 ml) and 45-90 % (in 50 ml) of 25 mM Tris-HCL pH 8, 800 mM NaCl. A-synuclein containing fractions were combined, precipitated with ammonium sulphate and the pellet was stored at -20 °C. The expression and described purification-steps were conducted by Alessia Peduzzo.

As a last purification step, α-synuclein was purified by size-exclusion chromatography on an ÄKTA pure chromatography system (GE Healthcare) using a Superdex 200 Increase 10/300 GL (GE Healthcare) and 20 mM citric acid, pH 7 as an elution buffer.

A-synuclein concentration was determined by measuring the UV-absorbance at 275 nm (extinction coefficient of 5600 $M^{-1}cm^{-1}$.

Methods

The background of the applied methods is explained in the following sections. The exact experimental conditions can be found in the material and methods-sections in the following chapters in detail.

2.3. Spectroscopic techniques

Part of routine biophysical methods comprise spectroscopic techniques, which are based on the interaction with light [383]. Light is electromagnetic radiation composed of an electric and a perpendicular magnetic field vector. The electric field vector is essential for ultraviolet (UV)/visible (Vis) measurements, circular dichroism and fluorescence spectroscopy. The wavelength λ is the spatial distance between two consecutive peaks in the sinusoidal waveform. Energy derived from electromagnetic radiation is absorbed by electrons in molecules, leading to a transfer from the lowest energy level to an excited state. The reversion to the electronic ground state leads to emission of heat for non-fluorescent molecules. The plot of absorption probability against wavelength is called absorption spectrum.

In proteins, peptide bonds and certain amino acid side chains are important chromophores, which can interact with electromagnetic radiation. The electronic transition of peptide bonds occurs at 190 nm and 210-220 nm [384]. The aromatic side chains tryptophan (maximum at 280 nm) and tyrosine (maximum at 274 nm) dominate the typical protein spectrum [385].

The extinction coefficient describes the chance for a photon to be absorbed and is characteristic for certain macromolecules. The molar concentration (c)of a protein can be determined applying the Beer-Lambert law [386] (equation 2.1) using the corresponding extinction coefficient, which can be calculated with the amino acid sequence. Where d is the path length and A the absorbance of the sample.

$$A = \varepsilon \times c \times d \tag{2.1}$$

Beer-Lambert law can be applied at absorbances between 0.1 and 1.2, where the absorbance is linearly proportional to the concentration of chromophores. The measurement of turbid samples, in particular large aggregates in samples, can be problematic, because beside the absorbance, the light can be scattered by Rayleigh scattering, which would be recorded as absorbance.

The transition from a higher to a lower state accompanied by radiation is called fluorescence [383]. To emit fluorescence, molecules have to be brought into a state of higher energy prior to the emission. The fluorescent group in a molecule is called fluorophore. Due to the Stokes shift the wavelength of the emitted light is always longer than of the exciting light.

Proteins can possess three fluorophores (tryptophan, tyrosine and phenylalanine). The fluorescence of phenylalanine comparable to its absorbance has a very low quantum yield, whereas the fluorescence of tryptophan is highest. This phenomena is called intrinsic protein fluorescence [387]. The fluorescence is greatly influenced by the environment of the fluorophores. The emission maximum of tryptophan in solution as well as exposed on the protein surface is between 350 nm to 355 nm. If tryptophans are buried inside a protein in an environment with less polarity, the emission spectrum exhibits a hypsochromatic shift and λ_{max} is between 330 nm and 332 nm.

This principal of intrinsic fluorescence was applied to follow the thermal and chemical unfolding of the LC samples with a Prometheus Panta instrument. The fluorescence was excited at 280 nm and emission was recorded at 330 nm and 350 nm. The unfolding was pursued with the ratio of the intrinsic fluorescence emission intensity at 350 nm over the intensity at 330 nm. The experiments conducted with the Panta experiments were performed by Alexander Buell and analysed by Rasmus Norrild.

Scattering of light can reveal different properties of macromolecules, such as the molecular mass, size, diffusion coefficients and interactions [388]. Light hitting a macromolecule is scattered in all directions. In elastic light scattering also known as Rayleigh scattering, the scattered light has the same wavelength as the incident light. For small particles (particle size less than $\lambda/10$) the scattered light is equal in all directions. Due to Brownian motion macromolecules move in and out of a laser beam. This leads to a broader wavelength distribution of the scattered light and can be used to analyse the distribution of diffusion coefficients of macromolecules. Furthermore, large aggregates can be measured through turbidity, because Mie scattering occurs when the diameter of particles is larger than the wavelength [389].

Static light scattering records the average intensity of scattered light for i.e. different sample concentrations; dynamic light scattering (DLS) determines the fluctuations of scattered light over time. DLS measures Brownian motion and determines the hydrodynamic radius (r_h) from the translational diffusion coefficient (D) using the Stokes-Einstein equation (equation 2.2) [390].

$$r_h = \frac{kT}{3\phi\eta D} \tag{2.2}$$

The hydrodynamic radius represents the radius of a hypothetical hard sphere.

Light scattering is very sensitive to the formation of larger particles, because the scattering intensity is directly proportional to the sixth power of the size [391, 392]. Large particles will screen the light scattered from smaller ones. Therefore the formation of aggregates can be detected to an early time point in the aggregation kinetics, even if the amount is fairly low.

2.4. Determination of the dimer content

Different studies indicated the impact of dimerization on the *in vivo* behaviour [272, 273, 274], therefore the ratio of dimers to monomers of the various LCs were investigated. Three different approaches were applied using a denaturing, non reducing SDS-PAGE gel, analytical ultracentrifugation and MS.

Dimer-content determination using SDS-PAGE gel

The samples were run before purification via SEC on a denaturing, non-reducing SDS-PAGE gel. Tricine and Glycine sodium dodecyl sulfate polyacrylamide gel electrophoresis (SDS-PAGE) are the commonly used SDS electrophoretic techniques for separating proteins [393]. For the most experiments in the following thesis Glycine-SDS PAGE with a 5 % stacking gel and a 15 % separating gel were used to separate proteins in the mass range 10-200 kDa.

The gels were stained with Coomassie Blue (0.05 % (G/V) Coomassie Brilliant Blue R250) and parsed photometrically using the program ImageJ [394]. For this analysis only the identified monomer and dimer bands were used, no larger or smaller bands. In order to validate the

native protein, Western blots were performed. The electrophoretically separated proteins were transferred to a membrane and detected either by an antibody against anti-human κ light chain (BioLegend), against anti-human λ light chain (BioLegend) or anti-human serum albumin (Santa Cruz Biotechnology). The antibodies were used at a concentration of 0.5 µg/ml and detected by a secondary anti-mouse antibody.

Dimer-content determination using analytical ultracentrifugation

Analytical ultracentrifugation (AUC) is a precise spectroscopic method that yields information about the size, mass, shape and interaction of macromolecules in solution. Three forces act on solute particles in a gravitational field: the sedimenting force (F_s), buoyant force (F_b) and frictional force (F_f) (Figure 2.1 A) [15]. The macromolecules are detected by absorbance detection. Light of a specific wavelength is sent through the AUC sample cell inside the rotor and the transmitted light is detected with radial resolution by a detector. The wavelength can be determined specific to the sample to achieve an absorbance of 1 in order to endure an optimal resolution. The centrifugation generates a concentration distribution of the sedimenting particles over the radial position as a function of time.

The AUC can be used to either determine the distribution of macromolecules in a centrifuge cell which is rotating at low speed (sedimentation equilibrium (SE) method) or to measure the velocity of movement of macromolecules under the influence of a centrifugal field (sedimentation velocity (SV) method) (Figure 2.1 C, D) [395].

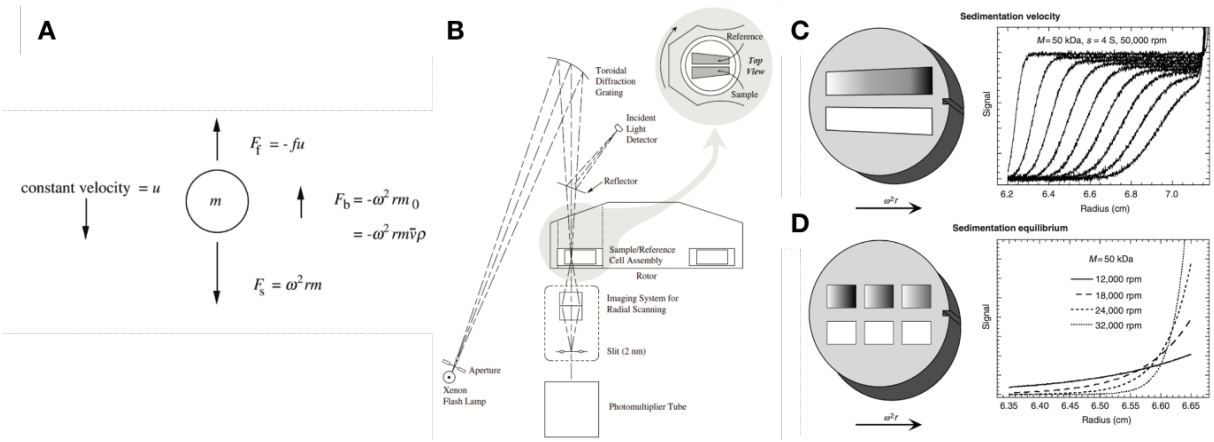

Figure 2.1: (A) The forces acting on a solute particle in a gravitational field. The buoyant force (F_b) and frictional force (F_f) are counteracting the sedimenting force (F_s) [15]. (B) Schematic diagram of the optical system of the Optima XL-A ultracentrifuge [15]. Example of a simulated (C) SV and (D) SE experiment [16]. SV experiments are usually performed in a two-sector cell and SE experiments in a six-sector cell (the performed experiments were conducted in a two-sector cell). The SV experiment was simulated with a rotor speed of 50,000 rpm and scans are recorded at 20 min intervals. The concentration of the boundary plateau decreased due to radial dilution. The SE experiment was simulated at four different rotor speeds.

In a SE measurement, the ultracentrifuge is operated at low speeds, therefore the macromolecules are concentrated at the bottom without forming a pellet and the concentration at the meniscus is decreased without building a region devoid of solute. After a considerable period of time, an equilibrium state between sedimentation and back diffusion is reached and no further changes in concentration occur. The concentration distribution of particles in solution is a function of its molecular weight. The SE method is rarely used to study proteins, because it required a long

period before the equilibrium is reached and sedimentation velocity measurements provides similar information. The SE method was only applied to the two samples displaying in SV measurements a distribution, which could not be clearly attributed as a monomer or dimer species. The equilibrium at 30.000 rpm was reached after three days, but it could not be evaluated.

In a SV measurement, the rotor is operated at high speeds so that the solute molecules are rapidly sedimented and the back diffusion is minimised. This allows the determination of the sedimentation coefficient (s).

$$s = \frac{\upsilon}{\omega^2 r} = \frac{m(1-\bar{\nu}\rho)}{f} \tag{2.3}$$

s is defined by the sedimentation velocity (υ) over the centrifugal acceleration ($\omega^2 r$) (Equation 2.3). The centrifugal acceleration ($\omega^2 r$) is defined by angular velocity (ω) and the distance from the rotor (r). s is proportional to the buoyant molar mass (m(1-$\bar{\nu}\rho$)) and inversely proportional to the frictional coefficient (f). The effective (buoyant) mass of the particle is the mass of the particle m times partial specific volume of the particle ($\bar{\nu}$) times the density of the solvent (ρ). The unit of the sedimentation coefficient is Svedberg (S) and is defined as 10^{-13} seconds.

During sedimentation in sector shaped AUC cells, the solute molecules settle towards the bottom of the cell, leaving a region containing only solvent molecules. The transition zone between the supernatant and the solution of uniform concentration (plateau region) is called boundary. The moving of the sedimentation boundaries are the principle of the SV analysis. Ideally, the boundaries are expected to be in the shape of a vertical line, but diffusion causes the sedimenting boundary to spread with time, which can be analysed to determine the diffusion coefficient. The analysis of sedimentation boundaries is based on the Lamm equation (Equation 2.4) [396]. The differential equation includes a term of diffusion ($Dr(\delta c/\delta r)$) and for sedimentation $s\omega^2 r^2 c$. The fitting of the experimental data enables the determination of the sedimentation coefficient as well as the diffusion coefficient, hence achieving the molecular weight and shape factor for the macromolecules in solution [397].

$$\frac{\delta c}{\delta t} = -\frac{1}{r}\{\frac{\delta}{\delta r}[s\omega^2 r^2 c - Dr(\frac{\delta c}{\delta r})]\} \tag{2.4}$$

Sedimentation velocity analysis was performed to determine the ratios of dimers and monomers of the LC samples. The experiments were performed in a XL-A Proteomelab ultracentrifuge equipped with absorbance optics (Figure 2.1 B). Experiments were conducted in AN-60-Ti-Rotor (Beckman) at 20 °C using a rotor speed of 60,000 rpm. Solutions of 35 µM of protein samples were investigated in standard double sector cells (optical path length 1.2 cm) and the scans were acquired at a wavelength which endures an optimal resolution to achieve an absorbance of 1 (approximately 260 nm), and 0.002 cm radial increments. At the beginning of each experiment a wavelength scan at 3000 rpm was recorded. This scan allows the determination of a potential loss of material during acceleration to final speed.

SV-data analysis was performed by applying a continuous distribution Lamm equation model (c(s)) as implemented in Sedfit.

The majority of measurements were performed by the help of Florian Tucholski and the data analysis by Thomas Pauly.

Dimer-content determination using mass spectrometry

Liquid chromatography tandem mass spectrometry (LC-MS) is an accurate method to characterize the mass of peptides. Mass spectrometry determine the exact molecular mass of a sample component by measuring the mass-to-charge ratio (m/z) after ionising the particles. Small proteins and peptides can be measured at intact level (top-down approach) [398, 399], whereas larger proteins are often indirectly measured after proteolytic digestion (bottom-up approach) [400]. The analysis of intact large proteins cannot be conducted on a frequently used triple quadrupole instrument, because of its limited resolution and mass range. But recent studies with high resolution mass spectrometry (HRMS) approaches, such as time-of-flight (TOF) and orbitrap instruments, displayed potential to analyse even intact antibodies with a molecular weight of approximately 150 kDa [401, 402, 403, 404, 405].

Intact MS analysis can disclose different proteoforms within a sample [406]. Different proteoforms of LCs in patient samples can occur because of further mutations of the plasma cell clone and post-translational modifications (PTM).

The lyophilised LC samples were diluted at 0.5 µg/L in 98 % acetonitrile and 0.1 % formic acid. In order to determine the monomer and dimer ratio, the samples were measured using low and high-resolution settings. High-resolution MS displays the accurate mass of the LCs and provides information of post-translational modifications. Low-resolution MS reveals a potential dimeric structure. Furthermore, the samples were analysed under reduced (30 minutes incubation with 5 mM TCEP at room temperature) and alkylated (30 minutes incubation at room temperature with 10 mM iodoacetamide in the dark).

The intact protein mass spectra were deconvolutes using Protein Deconvolution v3.0 software (Thermo-Scientific) either with the XtractTM algorithm for isotopically resolved charge envelopes or with the ReSpectTM algorithm for isotopically unresolved charge envelops.

The determination of the dimer ratios and the *de novo* sequencing of the amino acid sequence using mass spectrometry were performed by Mathieu Dupre and Magalie Duchateau.

2.4.1 Size determination using microfluidic diffusional sizing (MDS)

The size and structure is fundamental for the physico-chemical characterization of proteins. The determination of the size of native protein free in solution is challenging and can be conducted using e.g. AUC or DLS. AUC is a very accurate approach to determine the size of macromolecules, but is rather time-consuming. DLS measures the evolution of the scattering signal, but is susceptible for large particles. Therefore the measurement of a heterogeneous solution is complicated.

To conquer the problem of a heterogeneous solution, the components are physically separated, for instance via gel filtration, before they are measured and sized. However, the separation may modify the distribution of sizes due to dilution [407].

Fluidity One (Fluidic Analytics) is a microfluidic diffusional sizing [408] platform, which measures two-dimensional diffusion profiles in a single step. The profiles can be modelled by diffusive and advection mass transport equation without the need for any *a priori* knowledge of the analyte composition. The device measures the rate of diffusion of protein species under steady state laminar flow and determines the average particle size from the overall diffusion coefficient (Figure 2.2). Thereby requiring only a low amount of sample (6 µL) and time for the analysis.

The protein concentration is determined by fluorescence intensity, as the protein is mixed with ortho-phthalaldehyde (OPA), a compound which reacts with primary amines, producing a fluorescent compound [409], after the diffusion. Therefore an additional labelling of the proteins is not necessary.

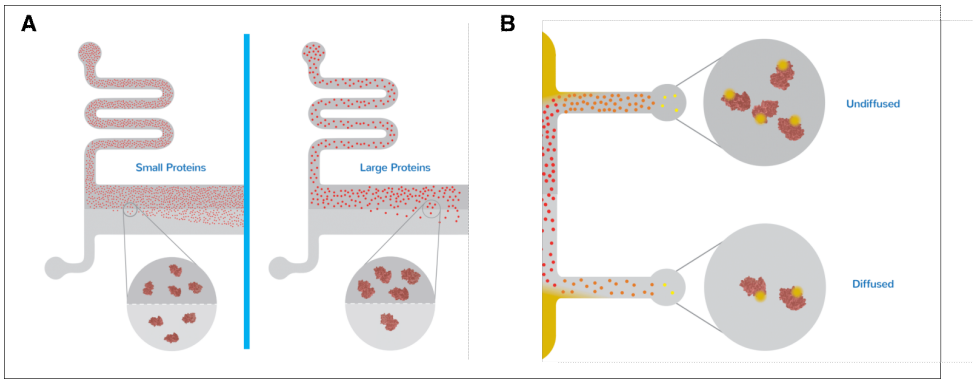

Figure 2.2: (A) Schematic diagram of the channels with laminar flow. Small molecules can diffuse faster than bigger particles. (B) The proteins mixed with OPA after the diffusion in the undiffused and diffused detection chamber (taken from Fluidic Analytics).

The Fluidity One was used to follow the change in average size of the light chain samples incubated at acidic pH values. The LC solutions were incubated in an Eppendorf tube at 37 °C under quiescent conditions and measured after different time points.

Furthermore, it was used to determine the concentration of soluble α-synuclein after the aggregation experiment. EGCG absorbs strongly at 280 nm, therefore the protein concentration could not be measured using the tyrosine-absorbance.

2.5. Aggregation

2.5.1 Fluorescent dye Thioflavin-T

Fluorophores are a useful tool for probing amyloid fibril formation. Most commonly used dyes for selectively staining and identifying amyloid fibrils both *in vivo* and *in vitro* are Congo Red and Thioflavin-T (ThT) [77]. The staining with CR is labour-intensive, sometimes difficult to interpret and requires a polarized light microscopy, whereas the benzathiole dye ThT verifies the presence of amyloid via an increased fluorescence emission. This fluorescent brightness was demonstrated for the first time in 1959. Upon binding, the peak position of absorbance (412 nm to 450 nm) and both the excitation (from 385 nm to 450 nm) and emission spectra (from 445 nm to 482 nm) are dramatically shifted. ThT acts as a fluorescent molecular rotor: it comprises a bentathiol and benzylamine ring, which can freely rotate around the shared carbon-carbon bond. Intramolecular rotation modifies the potential-energy curves of both the ground state and the excited state, resulting in a dramatically quenched excited state and in a low fluorescence emission for the unbound dye [410]. The free rotation of the rings is inhibited upon binding and leads to a stabilisation of excited states and by several orders of magnitude increased emission intensities. This enables the real-time *in situ* tracking of fibrillation.

The cationic ThT-molecule binds on the fibril surface to channels, which are caused by residues on each side of the β-sheet. It binds with its long axis parallel fibril to that of the fibrils [411]. ThT-monomer incorporation requires a minimal binding side of four to five consecutive β-strands

across a flat β-sheet surface [77, 412]. There are several studies suggesting that ThT binds to amyloid fibrils in an aggregated form in particular as excimers or micelles [413]. But the monomer model of ThT binding was validated by Sulatskaya and colleagues [414, 415, 416].

The dye does not bind to natively β-sheet rich proteins, respectively the binding is less favourable than binding to amyloid fibrils. There are some counterexamples such as the binding to acetylcholinesterase [417, 418], α-helical poly-L-glutamic acid (without fluorescence emission increase) [419] as well as (human and bovine) serum albumin [420, 421]. ThT can bind in the hydrophobic pocket of subdomain IB of the albumin monomer (as described later in Chapter 3 and 5, P020 entails a small portion of HSA, which can cause the high fluorescence signal of ThT at pH 7.4 in the beginning of the experiment). Native proteins contain fewer β strands and are more likely to be twisted, therefore the potential binding channel are more likely to be distorted and irregular. Moreover, at least five strands would be required to obtain a groove longer than the length of ThT (length 15.2±0.1 Å) [411]. Apart from protein structures, ThT can also bind to nucleic acids, in particular to G-quadruplex [422, 423], which are higher-order nucleic acid structures formed by sequences rich in guanine [424].

In moderate concentrations ThT has virtually no effect on fibrillation kinetics. But the effect on secondary nucleation, which is happening on the fibril surface, cannot be excluded. Xue *et al.* examined different ThT concentrations on the example of Aβ40, Aβ42 and the yeast protein Ure2 [425]. The highest fluorescence signal was reached with concentrations of 20-50 µM ThT and 20 µM or lower revealed a sparse effect. Hence, a concentration of 20 µM ThT was used for the following experiments, also because at this concentration the inner filter effect [426] is negligible.

Fluorescence emission is dependent on the temperature, solvent viscosity [410, 427], crowding agents [428] and pH [429]. Furthermore, amyloid fibrils of various proteins and different strains of certain protein can bind ThT differently [430, 431]. This enables the examination of conformational differences of fibrils, but raises awareness to the importance to confirm the fibrils by additional approaches [432]. But ThT is not an appropriate probe to quantify the fibril mass [433].

Apart from this, ThT-fluorescence can be altered in the presence of an exogenous anti-amyloidogenic compounds such as polyphenols. They either can interfere with the ThT fluorescence associated with fibrillar amyloid in the case of curcumin or quercetin, or can interact with ThT and/or compete with ThT for the binding on the fibril structure [434]. Therefore, the ThT-signal has to be analysed with caution when the anti-amyloidogenic properties of a compound, such as epigallocatechin-3-gallate EGCG are investigated. Nevertheless, ThT is still a valuable tool for studying kinetic aspects of fibrillation and inhibition mechanisms [435].

2.5.2 Aggregation conditions

An increase of ThT fluorescence intensity upon binding to amyloid fibrils was detected with a multi-well plate reader (BMG labtech; FLUOstar Omega or CLARIOstar) under various conditions. The experiments were conducted in an 96-well plate. The wells of the polysterol plates were coated to achieve a non-binding surface (Corning # 3881) or a high-binding surface plate (Corning # 3601), filled with 100 µL of the protein solutions. The fluorescence intensity (excitation: 450 nm; emission: 490 nm) was read through the bottom (readings were taken every 150-300 seconds). The aggregation kinetics were monitored in the presence and absence of small glass beads (SiLibeads Type M, 3.0 mm). The plates were sealed using SealPlate film

(Sigma-Aldrich #Z369667, St. Louis, MO, USA). The kinetics of amyloid fibril formation were monitored under continuous shaking (300 rpm), mild shaking conditions (every 5 min for 15 s) or quiescent conditions. Agitation of protein solutions can accelerate or induce aggregation by exposing hydrophobic amino acid residues to the air-water interface [436, 437], increasing collision frequency and inducing fragmentation of oligomers and already formed fibrils by shear forces [438, 439, 440]. Mechanical agitation can accelerate the aggregation kinetics by increasing fibril mass through fragmentation, elongation and secondary nucleation [440].

De novo aggregation

The detailed conditions are specified in the material and methods section in the following chapters. In general, different LC protein concentrations in a range from 5 µM to 100 µM were tested. The aggregation behaviour was investigated at various pH conditions: neutral pH (10 mM PB pH 7.4 or 30 mM Tris-HCl pH 7.4) and acidic pH (pH 2, pH 3 and pH 4). The final samples at acidic pH values were prepared by diluting protein solutions at neutral pH 1:1 into 300 mM citric acid buffer at the desired pH value. All aggregation kinetics were conducted at 37 °C, but the aggregation at neutral pH values was additionally examined at 47 °C and 55 °C.

The *de novo* aggregation of α-synuclein was investigated using 25 µM monomer solution, which was prepared with EGCG or $EGCG_{ox}$ solutions in a 1:1 and 1:5 (protein:compound) ratio, 20 µM ThT and 150 mM citric acid at the desired pH value (pH 3, pH 4, pH 5, pH 6 or pH 7).

Aggregation induced by trypsin

The aggregation behaviour of the LC samples was furthermore examined in the presence of trypsin at neutral pH. For this, 33 µM light chains were incubated in 10 mM phosphate buffer with 1 M urea and trypsin (molar ratio 1:100) at 37 °C in presence of ThT in a non-binding surface plate.

Aggregation under reducing conditions

The fibril formation was additionally examined under reducing conditions by adding Tris (2-carboxyethyl) phosphine (TCEP) to the protein solutions. Different TCEP conditions were tested and the majority of experiments were conducted using a final concentration of 1 or 7 mM TCEP. A stock-solution of 10 or 100 mM was prepared and the pH was adjusted to pH 7.4 using NaOH to neutralize the acidic TCEP.

Disulfide bonds are related to various protein properties, including folding kinetics and stability and more than 50 % of proteins involved in amyloidosis comprise disulfide bonds [441]. Disruption of disulfide bonds usually destabilize the protein structure [442] and enables the protein to adopt a β-sheet structure. Moreover disulfide bonds inside the hydrophobic core of a folded protein assist to protect hydrophobic residues from the access of solvent [443, 444]. Studies on the LC domains revealed, that chemical reduction of the disulfide bond and genetic removal leads to a loss of folding stability; even though it is not necessary for proper folding [246], it accelerates the folding process [214, 445].

The impact on aggregation still remains unclear [446]; reduction of disulfide bonds demonstrated to promote fibril formation [441, 447, 448, 449] and amorphous aggregation [450], as well as inhibiting aggregation processes [451, 452, 453].

Aggregates which are formed by lysozyme and BSA in the presence of dithiothreitol (DTT) and TCEP had an amorphous nature, but displayed a rapid but low increase in ThT-fluorescence (about 20 % of the signal of mature fibrils under identical experimental conditions) [450]. Andrich *et al.* could demonstrate the formation of large aggregates of patient-derived light chains in the presence of DTT at neutral pH following a biphasic aggregation behaviour [267]. These aggregates were a mixture of amorphous and fibril-like structures and displayed ThT and Congo Red fluorescence and birefringence. Moreover, LCs derived from MM-patients showed a very weak concentration dependence, indicating that a conformational conversion step limits the formation of amyloid fibrils, whereas the aggregation of LCs derived from AL-patients is dominated by protein assembly at higher concentrations [267].

Because of the potential to differentiate between amyloidogenic and non-amyloidogenic LCs, I applied the assay to the presented LC samples.

Time resolved size distribution

SV analysis of the LC samples after different incubation times with 7 mM TCEP was performed by absorbance detection under the same conditions as the measurements described before.

The samples were incubated at 37 °C in a high-binding surface plate (100 µL per well) under continuous shaking conditions before being loaded into (12 mm path length) aluminium cells. The samples were incubated for 75 min, 5 h and 15 h. Additional to the incubation times, the samples were inside the centrifuge for about 1 h before the measurement due to temperature equilibration and establishment of the vacuum.

In order to determine the loss of material during acceleration from 3000 rpm to 60.000 rpm the wavelength scan of the sample after 75 min was set as a reference for each set. The sample with no TCEP could not be used as a reference, because of a shift in the detection wavelength due to the AUC detection system.

Time resolved circular dichroism (CD) spectroscopy

The influence of reducing conditions on the light chain structure was measured by circular dichroism (CD) spectroscopy. CD spectroscopy is widely used to examine secondary structures of proteins [454]. The unequal absorbance of circularly polarized light is explained by the geometries of the polypeptide backbones. Secondary structures display distinct CD spectra. Helical structures have two minima at 222 nm and 210 nm, β-sheets a minimum at 217 nm and random coil structures have a minimum at around 200 nm [455].

A solution of 35 µM, 10 mM phosphate buffer, pH 7.4 and 7 mM TCEP was incubated in Eppendorf tubes at 37 °C under quiescent conditions and an aliquot was taken after 75 min, 5 h, 24 h, 48 h and 720 h. The sample was diluted to a concentration of 9.23 µM with 10 mM phosphate buffer. Far-UV CD spectra from 260 nm to 190 nm were recorded in a JASCO J-810 instrument (Tokyo, Japan) equipped with a Peltier thermally controlled cuvette holder.

The analysis of β-structure-rich macromolecules is often troublesome, because of spectral diversities particularly in protein aggregates and amyloid fibrils. The β-structure selection (BeStSel) is an algorithm, especially developed for β-structure-rich proteins which takes the twist of β-structures into account [456]. The recorded spectra of the different incubation times were analysed using BeStSel, because of the high β-sheet content in the native protein and in the expected amyloid fibril.

Light scattering

In order to follow the formation of ThT-negative aggregates, these samples (P001, P013, P020) as well as P006 and P017 were investigate using static and dynamic light scattering.

The experiments were performed using a 3D cross-correlation set-up (LS Instruments AG), which suppresses contributions from multiple scattering to the correlation function [457]. The measurements were done at a scattering angle of 90 °C with a He-Ne laser (wavelength 632.8 nm).

Time traces of the scattered intensities of samples containing 35 µM native LC and 7 mM TCEP were monitored for up to 20 h in consecutive 120 s intervals which, in most cases, resulted in well-defined intensity cross-correlation functions. Photon count rates were averaged over this time interval to yield total scattered intensities I (with contributions from singly and multiply scattered photons). As the correlation functions are dominated by a single exponential decay, the cumulant method up to second order [458] was applied to infer the average and variance of the decay rate. Typically, the variance ranged between 0.4 and 1.0, which indicates a broad peak of the intensity-weighted size distribution and hence a large polydispersity. The (hydrodynamic) aggregate size, i.e., the mean hydrodynamic radius, is estimated based on the average decay rate via the Stokes-Einstein equation, assuming the aggregates to be spherical and the viscosity of the surrounding medium to be equal to water [392].

Once the aggregates become very large, multiple scattering becomes important and the large aggregates are expected to sediment out of the scattering volume, such that the aggregate size can no longer be inferred from the correlation functions. Long-time data showing signs of these effects are excluded.

2.5.3 Seeded aggregation

The addition of preformed fibrils as seeds to an aggregation assay allows the investigation of different mechanisms. Seeds can strongly accelerate the overall aggregation time course and the addition of high amounts of seeds allows the study of fibril elongation in isolation [20, 379]. The use of low seed concentrations enables the investigation of secondary processes, such as fibril fragmentation or surface-catalysed secondary nucleation [379].

In the case of α-synuclein, seeded experiments were performed under quiescent conditions in a non-binding surface plate, in order to minimize *de novo* aggregation.

The seeded aggregation at acidic pH of IgLCs was monitored in high-binding plates under quiescent conditions. To investigate the seeding efficiency at physiological pH of fibrils formed from fragments, seeds were produced at pH 3 and pH 4 and added to 50 µM native light chain solutions at pH 7.4. To destabilize the native structure and enables the elongation and secondary nucleation on the fibril surface, the aggregation was monitored at 47 °C and 55 °C. To accelerate potential secondary processes, the aggregation was monitored under agitation conditions in the presence of glass beads. A non-binding surface plate was used to minimize a possible *de novo* aggregation.

2.5.4 Atomic Force Microscopy (AFM)

In order to investigate the formed aggregates and to verify the presence of fibrillar structures, the aggregated samples were imaged using a NanoScope V (Bruker) atomic force microscope (AFM). AFM is a high-resolution scanning probe microscope, which allows the imaging on the surface topography. It is equipped with one cantilever with a sharp tip (probe) by which

the surface is scanned. The image resolution is limited to the tip size; the tip radius of the used silicon cantilever ScanAsyst-Air was 2-12 nm. Besides different tip artefacts [459], the sample heights can be accurately measured. The AFM was used in the tapping mode to avoid damaging the surface of the sample [460]. In this mode, the cantilever is oscillating in the vicinity of the surface and hits the surface on each oscillation. Compared to the contact mode, the stickiness of the surface and the lateral shear force on the sample is reduced.

All samples were investigated in air, even though AFM generally provides the imaging of macromolecules under physiological conditions. Mica surfaces are negatively charged and hydrophilic [461], and were reported to induce aggregation [462, 463, 464]. The comparison between IAPP and Aβ(1-42) amyloid fibrils under liquid environment and dried in air revealed similar conformations [465]. Therefore the samples were deposited onto freshly cleaved mica. After drying, the samples were washed 5 times with 100 µL of dH_20 and died under gentle flow of nitrogen.

The images were flattened and analysed with the software Gwyddion 2.56 [466] to measure height profiles and investigate a possible twist of the fibrillar aggregates.

Nevertheless, AFM images should always be viewed carefully. The mica surface may not absorb the aggregates of different samples to the same extent, in particular at distinct pH values and salt concentrations [467]. Fibrils can clump together [468] and this complicates the localisation of fibrils as well as the characterization of their morphology.

2.6. Prediction algorithms

In general, the amyloid propensity of a protein is presumably encoded in the primary structure primarily in short sequence segments populating the aggregated β-conformation [469, 470]. The fibrillar structure is formed through adhesive segments that built a steric zipper (cross-β spine architecture) consisting of two interdigitating β-sheets mating in a dry, complementary interface with their side chains intermeshing [471]. Each sheet is hold together by hydrogen bonds and two sheets are bound into the zipper spine by van der Waals interactions. These steric zippers are also found in Ig light chain fibrils [472, 473].

Aggregation prone regions are usually buried within the hydrophobic core of the native fold. They are enriched with residues favouring β-strang formation, increased hydrophobicity and low charge [474].

Several computational tools have been developed over the last years to predict the intrinsic aggregation potential of a polypeptide sequence [469, 475, 476, 477, 478, 479, 480, 481, 482, 483]. The algorithms are either based on empirical aggregation assays or on the three dimensional protein structure. They try to find factors which cause the observed aggregation based mainly on the amino acid properties (for instance their hydrophobicity, β-propensity, solubility and steric zippers). The tools are used to identify aggregation-prone sequences and estimate the influence of particular mutations on the amyloidogenicity. This can help to investigate and validate different therapeutics. The data is mainly obtained *in vitro* in buffered solutions, therefore it is not known, whether these algorithms can predict the aggregation *in vivo*, where it is affected by the presence of different biological factors [484].

The given LC sequences were analysed with selected computational online tools: ZipperDB [485], waltz [482, 486], PASTA [470, 478] and TANGO [469].

ZipperDB evaluates aggregation-prone sequences by identifying segments with high fibrillation propensity that can form a steric zipper. Waltz contains 1416 hexapeptide entries, of which 512 peptides have experimentally determined amyloid-forming properties and 904 peptides amorphous-aggregation properties [474]. Waltz uses a position-specific scoring matrix to determine amyloid-forming hexapeptides within sequences [482]. TANGO identifies β-aggregating regions based on the physico-chemical principles of β-sheet formation with the assumption that an amino acid is fully buried in the aggregated state [487]. TANGO presented a high aggregation propensity for highly structures globular proteins [488]. PASTA uses a pairwise energy function that computes the propensity of two residues to be found within a β-sheet facing one another on neighbouring strands [489].

Best overall performance and pH 7 was used as threshold for waltz. The energy threshold for PASTA was -5, TPR 40.5 %, FPR 4.7 % and the top pairing energies 20. The parameter applied for TANGO were a temperature of 310.15 K, 0.02 M ionic strength and a concentration of 0.00035 M. Neither the n-terminal nor the c-terminal were protected. The pH values used in TANGO were pH 7, pH 4 and pH 3.

The use of different tools may reveal a distinct pattern of amyloid-prone segments within the sequences. Since the dataset comprises only one LC, which forms amyloid *in vivo*, a range of λ and κ sequences derived from different germlines selected from AL-Base [490] were used as a representative collection. The sequences were categorized depending on whether the patient was suffering from AL-Amyloidosis or MM. To compare the tendency for β-sheet aggregation the Agg parameter was determined for the sequences at pH 7 and pH 3.

3

BIOCHEMICAL AND BIOPHYSICAL CHARACTERISATION OF IMMUNOGLOBULIN FREE LIGHT CHAINS DERIVED FROM AN INITIALLY UNBIASED POPULATION OF PATIENTS WITH LIGHT CHAIN DISEASE

Article information

Authors: Rebecca Sternke-Hoffmann [1], Amelie Boquoi [2], David Lopez [2], Florian Platten [3], Roland Fenk [2], Rainer Haas [2] and Alexander K. Buell [1,4]*

[1] Institute of Physical Biology, Heinrich-Heine-University, Düsseldorf, Germany
[2] Department of Hematology, Oncology and Clinical Oncology, Heinrich-Heine-University, Düsseldorf, Germany
[3] Condensed Matter Physics Laboratory, Heinrich-Heine-University, Düsseldorf, Germany
[4] Department of Biotechnology and Biomedicine, Technical University of Denmark, Lyngby, Denmark

Correspondence: alebu@dtu.dk (A.K.B.)

Journal: PeerJ **DOI:** 10.7717/peerj.8771

3.1. Abstract

In light chain (LC) diseases, monoclonal immunoglobulin LCs are abundantly produced with the consequence in some cases to form deposits of a fibrillar or amorphous nature affecting various organs, such as heart and kidney. The factors that determine the solubility of any given LC *in vivo* are still not well understood. We hypothesize that some of the biochemical properties of the LCs that have been shown to correlate with amyloid fibril formation in patients also can be used as predictors for the degree of kidney damage in a patient group that is only biased by protein availability. We performed detailed biochemical and biophysical investigations of light chains extracted and purified from the urine of a group of 20 patients with light chain disease. For all samples that contained a sufficiently high concentration of LC, we quantified the unfolding temperature of the LCs, the monomer-dimer distribution, the digestibility by trypsin and the formation of amyloid fibrils under various conditions of pH and reducing agent. We correlated the results of our biophysical and biochemical experiments with the degree of kidney damage in the patient group and found that most of these parameters do not correlate with kidney damage as defined by clinical parameters. However, the patients with the greatest impairment of kidney function have light chains which display very poor digestibility by trypsin. Most of the LC properties reported before to be predictors of amyloid formation cannot be used to assess the degree of kidney damage. Our finding that poor trypsin digestibility correlates with kidney damage warrants further investigation in order to probe a putative mechanistic link between these factors.

3.2. Introduction

The formation of insoluble aggregates by proteins can be associated with a broad range of human disorders, many of which are neurodegenerative in nature [43, 491, 492]. Protein deposition in other organs than the central nervous system can also lead to a wide variety of diseases. In the case of the deposition of ordered fibrillar aggregates (amyloid fibrils) affecting various organs the related disorders are known as systemic amyloidoses[493]. A particular class of such protein deposition disorders is represented by the light chain diseases, which are characterized by the occurrence of monoclonal free light chains in blood and urine[179]. In general, the monoclonal free light chains of either κ or λ isotype are the secreted product of monoclonal plasma cells residing in the bone marrow. Dependent on the type of the underlying B-cell disorder, they may reflect a monoclonal gammopathy of uncertain significance (MGUS), a smoldering or full blown multiple myeloma (MM) with exclusive (Bence Jones MM) or substantial light chain secretion in addition to the complete immunoglobulin. Each light chain protein has a unique amino acid sequence which is determined by somatic recombination and various mutations[218]. The amino acid sequence, together with potential post-translational modifications and in interplay with the local conditions in the organism, such as local pH or presence of proteases, determines the *in vivo* behavior of the light chain. The sequence diversity translates into a diverse clinical picture, as far as organ involvement and severity of organ damage are concerned [229]. Aggregation of light chains and fragments of low solubility can lead to different diseases, such as light chain deposition disease (LCDD), where the LC forms amorphous aggregates [191, 192], and the AL-amyloidosis, where the LC forms amyloid fibrils[190]. At present, it is not possible to decide upon first diagnosis of a patient with light chain disease, whether the particular monoclonal light chain found in their blood at increased concentration is prone to form amyloid fibrils or amorphous deposits, or remain soluble and get excreted quantitatively through the urine. Even if the sequence of the particular light chain is known, its solubility inside the organism cannot

currently be predicted. Therefore, there is a need both for increased mechanistic understanding of LC deposition and for easy, rapid and reliable diagnostic procedures that are able to assess the potential of a given light chain to cause damage through deposition. Much work has been carried out in recent years on the study of the biophysical properties of LCs and to correlate the results with, in particular, their amyloid fibril formation *in vivo*[267, 472, 494, 495, 496]. Most of these studies have relied on the a priori knowledge that a given light chain forms, or not, amyloid fibrils *in vivo*. In this study, we set out to test the hypothesis that (some of) the biochemical and biophysical properties of light chains previously reported specifically in the context of amyloidosis also correlate with the severity of general light chain disease symptoms, in particular impairment of kidney function. In our study, we examined 20 patients presenting with light chains in their urine. Most of them had multiple myeloma with a large variety of symptoms. For our *in vitro* assessment, we isolated protein from the urine of these patients, where the proteins appear in high concentration, when the production is significantly increased and the ability to reabsorb the filtered proteins is exceeded, and characterized the samples in detail with biochemical and biophysical methods. We did not apply any particular selection criteria to include patients into the study, but excluded those samples that did not contain a sufficient concentration of light chains.

3.3. Material and Methods

3.3.1 Patients

The study described in this manuscript has been reviewed and approved by the ethics committee of the university hospital Düsseldorf and all patients of whom samples were used in the study have signed an informed consent (study number 5926R and registration ID 20170664320). The *in vitro* studies were performed using protein isolated from urine samples of 20 patients (6 females, 14 males, median age 61.5 years with a range between 45 and 76 years) with multiple myeloma of various subtypes and one patient with Amyloidosis as detailed in Table 1 (Table 2.1). For the majority of patients – P008 and 009 had a cast nephropathy - a histopathological examination of the kidney was not available since the corresponding invasive diagnostic procedure was not necessary for the therapy decision-making process as they were diagnosed according to IMWG criteria. Thus, there was no initial bias in the selection of patient, as the common denominator for inclusion into the study was solely the presence of a monoclonal light chain in the peripheral blood and in the urine, while the type of light chain disease (MM vs. Amyloidosis) did not play a role. As far as the type of light chain is concerned, 14 patients with κ and 6 patients with λ type chain were part of the study. There was a large variation with regard to the light chain concentration in the serum, with concentrations between 2.2 mg/l and 11,000 mg/l. Two of our patients presented with renal insufficiency and required dialysis, while four of them had no signs of functional renal impairment. We divided the patients into three different groups (I,II,III) according to their chronic kidney disease (CKD)-stage (1-5) at the time of diagnosis. Groups I corresponds to stages 1 and 2, group II to stage 3 and group III to stages 4 and 5. At the time when the urine samples were collected, 17 patients were diagnosed *de novo*, whereas three patients with multiple myeloma had received induction therapy with bortezomib, cyclophosphamide and dexamethasone. The duration of their disease at the time of the examination was therefore relatively short with a median of 6 weeks varying from 4 to 12 weeks.

Experimental Methods

3.3.2 Sample preparation

As first step, the protein content of a 24 h urine collection was precipitated by ammonium sulfate (70 % saturation), generally on the same day when the urine was obtained from the patient. After incubation at 4 °C under continuous agitation, the samples were centrifuged at 6000 xg for 25 min at 4 °C. The precipitates were dissolved in 10 mM phosphate buffer, pH 7.5, and dialyzed against the same buffer at 4 °C for 72 h (the buffer was exchanged every 24 h). The light chains were purified by size-exclusion chromatography on an ÄKTA pure chromatography system (GE Healthcare) using a Superdex 75 10/300 GL column equilibrated in the same buffer. The final protein concentration was estimated by the absorbance at 280 nm. The used extinction coefficient (38.000 M^{-1} cm^{-1}) was estimated from a range of published light chain sequences and corresponds to an average composition of 3.5 Tryptophan and 9 Tyrosin residues.

3.3.3 Analysis of the LC and HSA-ratio

In order to characterize the purity of the samples with respect to contamination with human serum albumin, Western blots were performed. Before (in most cases) or after the purification (P002, P014) by a size-exclusion chromatography step, the samples were diluted by a denaturing, non-reducing loading buffer and run on an SDS-PAGE gel. The separated proteins were transferred to a membrane and detected either by an antibody against anti-human κ light chain (BioLegend), against anti-human λ light chain (BioLegend) or anti-human serum albumin (Santa Cruz Biotechnology). The antibodies were used at a concentration of 0.5 µg/ml and detected by a secondary anti-mouse antibody. By correlating the bands of the SDS-PAGE gel with these blots, the relative amount of LC's compared to the HSA-content could be estimated using the program ImageJ, by integrating the degree of Coomassie staining. For this analysis the monomer and dimer band of both proteins were considered but no bigger aggregates.

3.3.4 Differential scanning calorimetry (DSC)

Thermal unfolding of the various light chains was studied using a MicroCal VP-DSC instrument (Malvern, UK) by performing temperature ramps on the LC solutions at an estimated concentration of 25 µM (based on the UV extinction coefficient mentioned above) from10 °C. to 90 °C. with a heating rate of 0.8 °C /min. For each sample, the unfolding temperature, Tm, was estimated from the peak of the thermogram. The reversibility of the unfolding was examined by a second heating of the samples after cooling down to 10 °C. The degree of refolding was estimated by the ratio of the areas under the unfolding peaks of the second to the first temperature scan.

3.3.5 Determination of the dimer content

To determine the ratio of dimers to monomers of the various LC's, the proteins were analyzed by running the samples before purification via SEC on a denaturing, non-reducing SDS-PAGE gel and staining the gels with Coomassie blue. The gels were parsed photometrically using the program ImageJ. For this analysis only the identified monomer and dimer bands were used, no larger and smaller bands.

3.3.6 Proteolysis

LCs were incubated at 37 °C. in 10 mM phosphate buffer, pH 7.5 with 1 M urea at an estimated concentration of 33 µM with bovine trypsin (molar ratio 1:100). The preparation was done on ice and the aliquot for the first time point was collected after trypsin addition and immediately inhibited by adding trypsin inhibitor (at an excess of 2:1). Further aliquots were taken 1, 2, 18, 24 and 48 h after the addition of the trypsin and quenched by the addition of trypsin inhibitor. The samples were analyzed by SDS-PAGE. Before running the samples on an SDS-PAGE gel the samples were diluted into a denaturing sample buffer without a reducing agent and heated at 95 °C for 10 min. The aggregation behavior in the presence of trypsin was examined by adding the fluorescent dye Thioflavin-T (ThT) and measurement of the fluorescence intensity (Excitation: 450 nm; Emission: 490 nm) in a multi-well plate reader (FLUOstar Omega or CLARIOstar, BMG labtech).

3.3.7 Aggregation behavior

Different solution conditions were tested for their potential to induce aggregation of the patient-derived, purified LCs. In order to examine the aggregation behavior of the LC's at pH 4, different protein concentrations in a range from 5 µM to 50 µM were tested. The final samples were prepared by diluting protein solutions of different concentrations from 10 mM PB pH 7.4 1:1 into 300 mM citric acid buffer at pH 4. The experiment was performed in a multi-well plate reader (BMG labtech; FLUOstar Omega, CLARIOstar) at 37 °C. under mild shaking conditions (every 5 min for 15 s) in a multi-well, low binding plate. The amyloid formation was monitored using 20 µM of the fluorescent dye Thioflavin-T which binds to β-sheet rich structures and displays the binding with an increase of fluorescence intensity (Excitation: 450 nm; Emission: 490 nm). Subsequently the samples were analyzed using atomic-force microscopy (AFM, instruments by JPK and Bruker were used; cantilever: QMCL-AC16OTS) to confirm the presence of amyloid fibrils.

3.4. Results and Discussion

3.4.1 Clinical data

The results presented are based on the urine samples of 20 patients with a monoclonal light chain (14 κ and 6 λ) related to different types of multiple myeloma and one patient with confirmed amyloidosis. Common denominator for inclusion into this *in vitro* study was the availability of a sufficient amount of protein extractable from the urine with a certain degree of purity. Further experiments were then performed with those samples that contained a dominant proportion of LCs. As a consequence, two samples (P008 and P009) were excluded from further analysis, as they mainly contained HSA. The data for the evaluation of LC content in the samples can be found in the Supplementary Materials (Figure 3.6). We have chosen this clinically unbiased approach (i.e. no exclusion of patients based on clinical phenotype) in terms of day-to-day practicability rather than applying restrictive inclusion criteria. By doing so, we expected a better evaluation of the utility and relevance of the biochemical and biophysical methods within the diagnostic work flow. At the time of inclusion into the study, the majority of patients were newly diagnosed without previous therapy. Two of the patients required dialysis. By investigating a potential relationship between the LC concentration in the blood and the degree of renal impairment at the time of the assessment we found no statistically relevant relationship (correlation coefficient of 0.16 with p-value of 0.54). We were also interested in the further

progress of the disease and examined the kidney looking for an improvement of the creatinine concentration in serum during the course of the treatment. Without adequate information on P005 and P013 it was interesting to note, that of the 18 patients available for assessment even patients of the category 3 showed an improved kidney function after treatment. On the other hand, the renal insufficiencies of P002 and P003 are probably irreversible. The kidney function of most of the patients of category 1 did not change significantly, as their kidney function at the time of examination was not or only moderately impaired. Previous studies have shown that patients with LCDD and active MM displayed a greater improvement of kidney function in comparison to pure LCDD [497].

3.4.2 Thermal stability

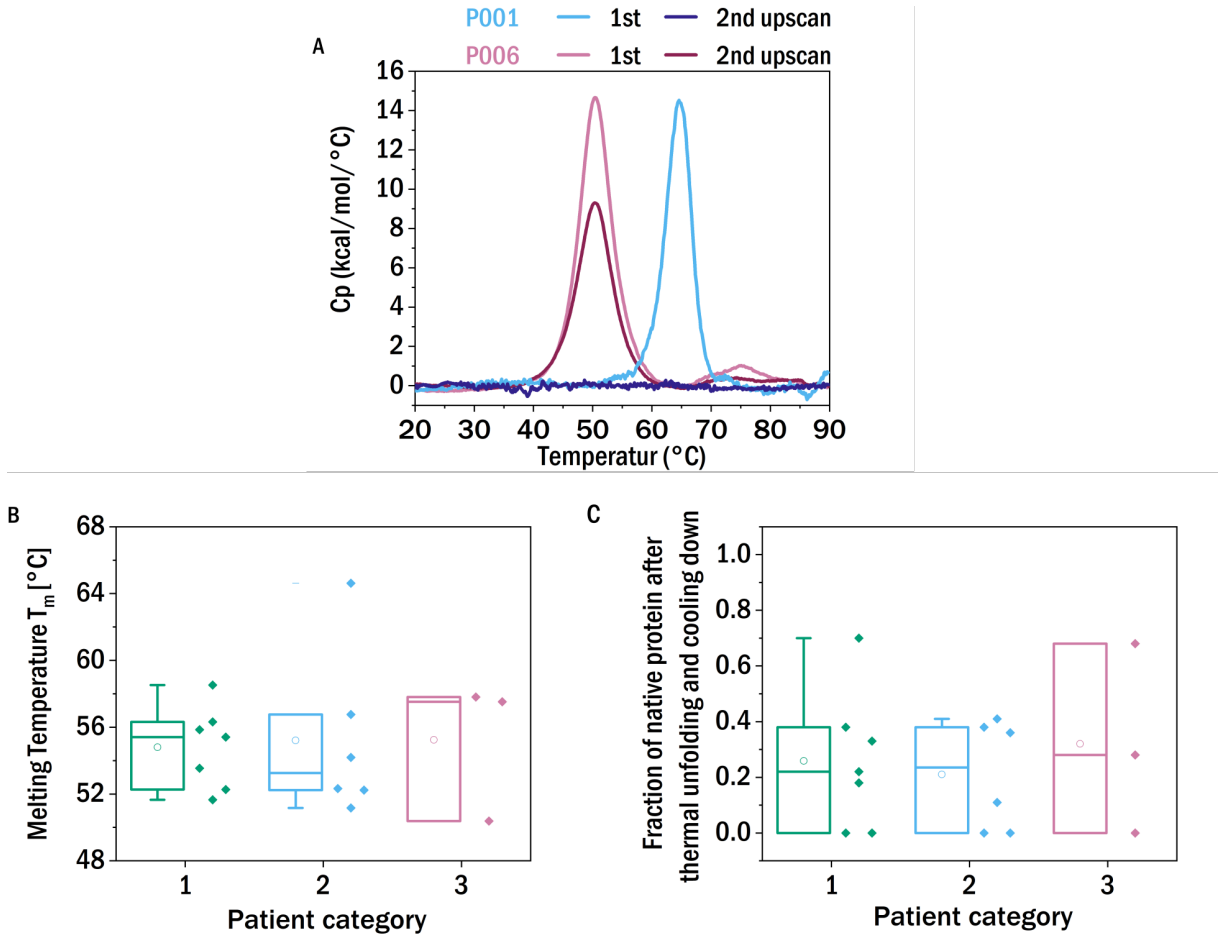

Figure 3.1: (A) Thermograms of the first and second DSC scans of P001 and P006. (B) Unfolding temperatures determined from differential scanning calorimetry (DSC) experiments of the different samples allocated in the three patient categories according to renal impairment (CDK stage): I (green), II (blue), III (red) (left). (C) The fraction of native protein that unfolds during the second scan. The boxes range between 25 and 75 percent, the median is visualized by the horizontal line and the mean by the small square. P008, P009 (low LC content), P014 and P018 (low sample availability) are excluded from this analysis.

It has been proposed that the thermodynamic stability of a light chain correlates with its tendency to form amyloid fibrils[233, 257, 262, 266, 495], but this correlation has not been observed in all studies[498]. Here we tested whether the stability against thermal unfolding correlated with the severity of the disease symptoms, independently of the fact if amyloid fibrils or other types

of aggregates cause those symptoms. The thermal stability of the proteins was investigated using differential scanning calorimetry (DSC). The transition temperatures (T_m) of the different samples range from 50 °C to nearly 70 °C (Figure 3.1B). In contrast to the other samples, which displayed one distinct peak for the unfolding of the LC, the thermogram of P004 showed two peaks; hence the presented T_m 57.7 °C is a mean of the T_m values of both peaks (53.2 °C and 62.1 °C). The mean unfolding temperature of the κ LCs of this study is 53.7 °C and the average unfolding temperature of the λ LCs is 58.6 °C. λ LC have on average a greater stability against thermal unfolding, which is in agreement with published reports[498]. No correlation was observed between the thermal stability and the severity of the patient's kidney function. It has been reported that LCs derived from MM-patients, in contrast to those from AL-patients, were not able to refold after heat denaturation [267]. Therefore it has been speculated that this experimental parameter could be predictive for the *in vivo* behavior. In order to investigate the degree of reversibility of the thermal unfolding, the samples were heated for a second time, following a first ramping from 10 °C to 90 °C and subsequent cooling down within the DSC liquid cell. If the protein can quantitatively refold into the native conformation after thermal unfolding, the thermograms of the two successive scans should not differ significantly. If only a fraction of the protein can refold into the initial structure, and the remaining fraction misfolds or aggregates, the integral of the DSC thermogram, i.e. the enthalpy of unfolding, correspondingly decreases or even vanishes. This decrease in the apparent enthalpy of unfolding is caused by the fact that only a correctly folded protein has a well-defined unfolding transition, whereas misfolded or aggregated protein comprises a multitude of states, often highly stable, that do not undergo a thermally induced transition at a well-defined temperature. The observed degree of refolding upon reheating up to 90 °C was highly variable. Some LCs did not display a peak in the thermogram at the second temperature ramp, whereas other examined LCs show a high reversibility (up to 70 %) of folding (Figure 3.1 C). Again, we found no apparent correlation between the ability of refolding after heating to 90 °C and the patients' renal function. Although of more fundamental interest, we also tested for a correlation between thermal stability and refolding ability of the LCs (Figure 3.10) and found a weak inverse correlation, i.e. the more thermostable a given LC, the smaller its ability to refold. We discuss possible origins of this connection in the SI.

3.4.3 Dimerization

The conformation of pathogenic LC proteins is typically dimeric [498, 499], and it has been proposed that the tendency to dimerize can be used as a diagnostic parameter for the tendency to form amyloid fibrils, whereby light chains in serum samples derived from AL patients show abnormally high levels of monoclonal free light chain (FLC) dimers on a western blot [272]. On the other hand, the formation of dimers seems to prevent the LC to aggregate *in vitro*. The formation of amyloid fibrils was observed when the dimer was destabilized and dissociated into monomers [271, 500]. In order to test whether the degree of dimerization can be used as a predictor for general disease severity in the form of kidney impairment in LC disease, we performed similar experiments in our study. The relative fraction of dimers of the LCs after precipitating the proteins from the urine, redissolving them in buffer and purification by dialysis was determined with a non-reducing SDS-PAGE gel and quantified photometrically (Figure 3.2). The fraction of dimers is high in some of the LC, and none of the examined LCs occurs exclusively in its monomeric form. A clear correlation between the fraction of dimerized LC and the renal function of the patients was not observed. In the case of P011, the

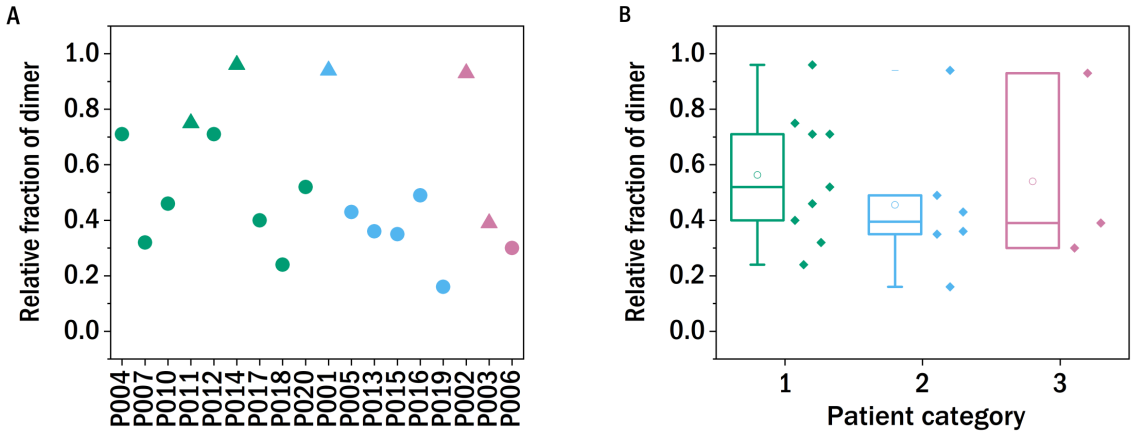

Figure 3.2: The relative fraction of dimer of the different samples measured in relation to the overall amount of native light chains (monomer and dimer), as determined by SDS-PAGE. The colors refer to the corresponding patient category defined above: I (green), II (blue), III (red), the shape indicates the isotype of the light chain: triangle: lambda, circles: kappa.

only confirmed amyloidosis case, the dimer fraction of 0.75 is in accordance with the findings of the FLC-MDPA test that amyloid prone LCs occur mainly in their dimeric forms [272].

3.4.4 Trypsin digestion

The structural flexibility and dynamics of the LC have been proposed to be correlated with the ability to form amyloid fibrils *in vivo*. LC derived from AL-patients displayed rapid proteolysis with trypsin under mildly destabilizing conditions which suggests increased dynamics of the native fold of the amyloid-forming LC [284]. These structural dynamics may be required to form amyloid fibrils under physiological conditions. In the present study, we performed such experiments in order to test whether structural flexibility of the light chains correlates with the severity of LC disease symptoms. The structural flexibility and dynamics of the LC were probed by digesting the proteins using trypsin in the presence of 1 M urea. Fast proteolysis under these conditions may suggest increased dynamics in the native fold of the LC, which allows the protease to access the cleavage sites more easily. Of course it is important to remember that the sequence variability between different light chains will lead to different numbers and accessibilities of trypsin cleavage sites. The availability of sequence information of the investigated light chains would therefore be beneficial for the detailed analysis of their proteolytic susceptibility, and will be included in a future study. The digestion time course was analyzed using SDS-PAGE gels by determining how much native protein (monomer and dimer combined) was still present after 48 h incubation with trypsin (1:100 molar ratio) at 37 °C (Figure 3.3 A, B). In addition to correlating trypsin digestion with kidney impairment, we also correlated it with the thermal stability of the LCs (Figure 3.10). A weak inverse correlation is observed, i.e. the more thermostable a LC, the less it is susceptible to be degraded by trypsin. While this connection is also of interest in a more fundamental protein science context, it does lend some support to the hypothesis underlying the digestion assay, see discussion in the SI. Additionally, these proteolysis experiments were also conducted inside a multi-well plate reader in the presence of the fluorescent, amyloid specific dye ThT. Only seven of the tested samples showed an increase in fluorescence intensity indicating amyloid fibril formation (Figure 3.3 D and Figure 3.7). Six of these seven amyloid positive LCs were almost completely digested after 48 h, suggesting that proteolytic cleavage of the LC

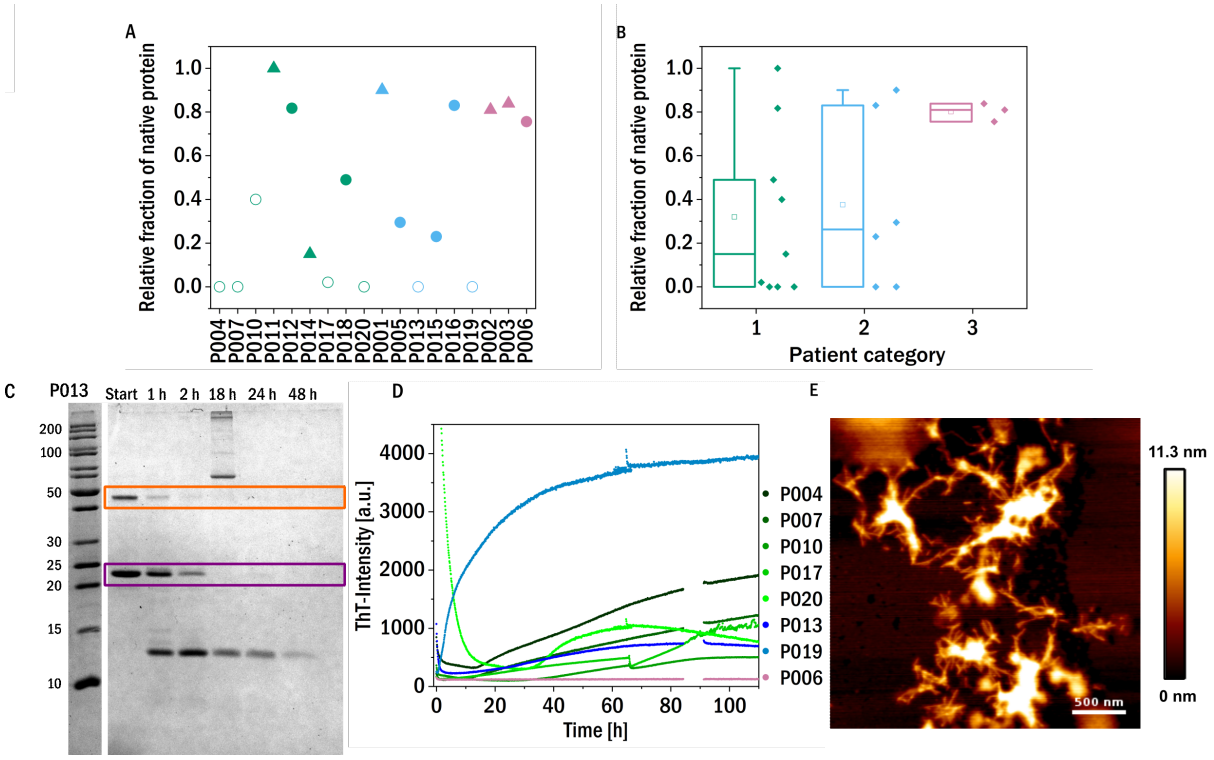

Figure 3.3: (A) and (B) The fraction of native protein (monomer and dimer combined) after 48 h incubation with trypsin is displayed. The colors refer to the corresponding patient category defined above: I (green), II (blue), III (red). The shape of the symbols represents the isotype of the LC: triangles: λ isotype, circles: κ isotype. Empty circles: amyloid fibril formation induced by proteolysis and inferred from an increased signal of ThT-fluorescence, filled circles: no evidence for amyloid formation observed. (C) SDS-PAGE gel of the trypsin digestion of P013 as a representative example. The dimer (orange) and the monomer (purple) are marked with a square. (D) ThT fluorescence aggregation assay of the amyloid forming LCs. Data for P006 is added as an example of a LC that does not from amyloid fibrils. (E) AFM-image of the aggregated sample P007 after digestion with trypsin during the kinetic experiment in a multiwell plate.

facilitates the formation of amyloid fibrils. Proteolysis-induced amyloid fibril formation of light chains is a well-established phenomenon, and even the aggregation of non-amyloidogenic light chains after acidic proteolysis was observed [248, 249]. The presence of amyloid fibrils was confirmed by atomic force microscopy (AFM, Figure 3.3 E). Interestingly, the samples of patients of category three, i.e. the patients most severely affected by impairment of kidney function, were among the least digestible proteins tested. This observed behavior should be compared to the findings on the behavior of amyloid prone LCs previously reported [284], whereby it was found that amyloidgenic LCs are most easily digested. Interestingly, the only established amyloidosis-related LC of our dataset (P011) was not digested during the investigated time period and was also not observed to form amyloid fibrils under the conditions of this experiment. However, the presence, in our data set, of only a single LC known to form amyloid fibrils *in vivo* did not allow us to test the previously reported correlation between proteolytic degradability and amyloid fibril formation. On the other hand, while easy degradability might increase the risk for amyloid formation, our data set does suggest that LCs which are difficult to proteolytically degrade tend to be associated with impairment of the renal function. A putative mechanism by which this association can be explained is the more rapid accumulation, probably in the form of amorphous aggregates, of non-cleavable LC in the kidneys. At the same time, it has to be

kept in mind that the proteases responsible for the degradation of LCs *in vivo* have cleavage patterns distinct from that of trypsin and therefore the digestibility by trypsin will only have limited predictive power for the digestibility of a given LC *in vivo*.

3.4.5 pH-dependent amyloid formation

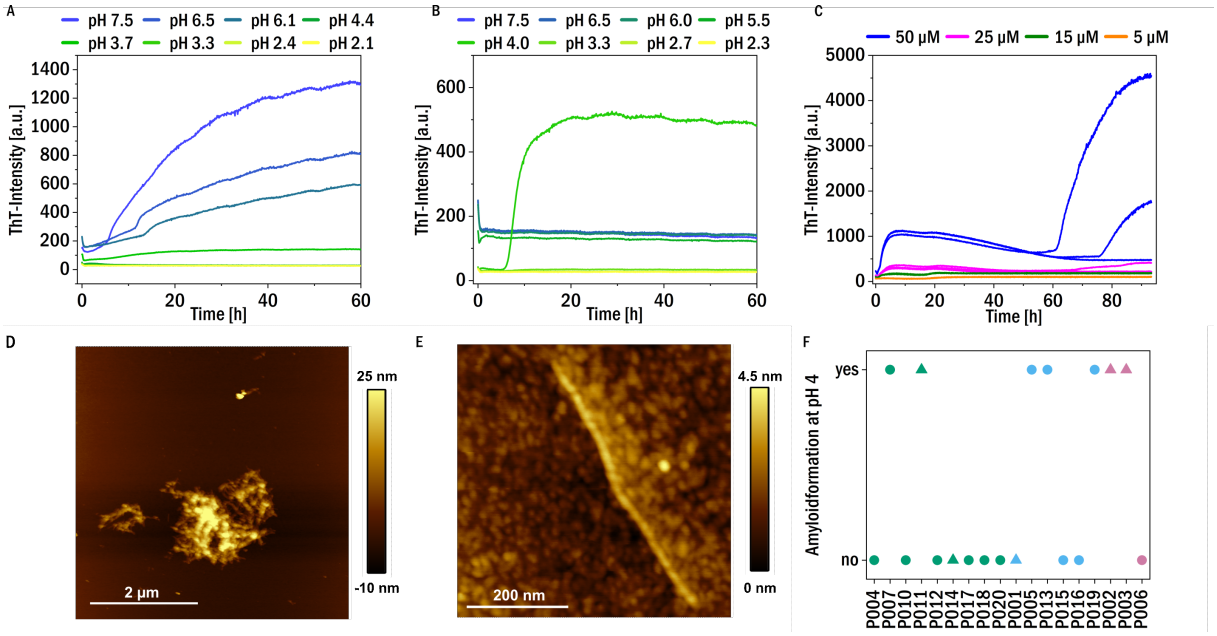

Figure 3.4: (A) Aggregation assay at different pH values in the presence of 1 mM TCEP and (B) in the absence of TCEP. (C) Aggregation assay at pH 4 at different monomer concentrations measured through ThT-fluorescence. (D) and (E) AFM images of the sample P005 at 50 µM, at the end of the experiment shown in (C). (F) The amyloid fibril formation behavior at pH 4 of the LCs monitored by an increase in the fluorescence intensity of the dye ThT: yes: if the amyloid formation was observed; no: no evidence of amyloid fibril formation was observed. The colors refer to the corresponding patient category defined above: I (green), II (blue), III (red). The shape typify the isotype of the LC: triangles: λ isotype, circles: κ isotype.

Given our findings that digestion by trypsin facilitated amyloid fibril formation of our patient-derived LCs, we further tested whether variations in solution conditions (pH, reducing agent) are also able to induce amyloid fibril formation in a subset of our samples. We found that at neutral pH and in the presence of the reducing agent TCEP at 37 °C almost all the samples (except P002, P013, P014, P016, P020) show an increase in ThT fluorescence over time, suggestive of amyloid fibril formation, (see Figure 3.4 A) for representative data and Figure 3.9 for an overview). It is known that a reduction of mostly intermolecular disulfide bridges of light chains can induce amyloid formation [498]. If the pH was lowered towards more acidic values (pH 4), fragmentation of the chains was observed, and in most cases amyloid fibril formation was absent at acidic pH in the presence of TCEP. Presumably, the degree of fragmentation of the LC through the combined effects of TCEP and low pH was too strong, such that the resulting short fragments were unable to form amyloid fibrils. On the other hand, no amyloid fibril formation was observed at neutral pH in the absence of a reducing agent (see Figure 3.4 B). If, however, in the absence of reducing agent the pH was decreased, some of the LCs showed formation of amyloid fibrils at pH 4, in particular also P011, derived from the patient with confirmed amyloidosis (Figure 3.8). Low pH destabilizes the proteins and mildly destabilizing conditions are known to accelerate aggregation [501]. For example, investigations of the amyloidogenic variable domain SMA

showed relatively native-like intermediates, but with significant changes of the tertiary structure, at pH 4 [413]. A summary of the aggregation behavior at pH 4, together with the corresponding patient categories of the samples, is given in Figure 3.4 F). Seven LCs formed amyloid fibrils at pH 4. Figure 3.4 C) displays a representative example of the observed aggregation kinetics of sample P005 at pH 4. The resulting amyloid fibrils were also in all cases examined using AFM imaging (see Figure 3.4 D and E) for a representative example, and Figure 3.8). The fibrils seem to form clusters/higher order assemblies at this pH, but also individual fibrils were detected. Some of the LCs displayed amyloid fibril formation only at pH 4 and did not form amyloid fibrils if the pH was decreased to pH 3 and below. Very low pH may lead to too substantial fragmentation of the LC [502], similar to the combined effect of reducing agent and less acidic pH discussed above. There is no obvious correlation observable between the impairment of kidney function at the time of diagnosis, i.e. the patient category, and the aggregation behavior under the investigated solution conditions.

3.5. Conclusions

This study provides a comprehensive evaluation of the *in vitro* biophysical and biochemical behavior of patient-derived monoclonal light chains. The majority of patients had been diagnosed *de novo* with multiple myeloma, while a histopathological examination was performed in three patients leading to the diagnosis of cast nephropathy in two patients and AL-Amyloidosis in one. We used an unbiased group of patients as they came to our hospital during our recruitment phase. Therefore, different from recent studies reporting on patients with light chain disease we cannot make an *a priori* separation into two distinct groups on the basis of the amyloid formation behavior of the respective LC proteins. However, an *a posteriori* bias was introduced into our patient group by excluding two samples from further analysis, because they did not contain a sufficient concentration of light chains, but were dominated by albumin.

Starting with the thermal stability of the LCs and their ability to refold after thermal unfolding we could not find a clear correlation with the degree of kidney damage (see Figure 3.5 for correlation coefficients). Also, the relative amount of dimer and the aggregation behavior at pH 4 were not correlated to the different patient categories. The digestibility by trypsin of the LCs yielded no clear correlation with kidney damage for our samples. According to published results [284], LCs derived from AL-amyloidosis patients could be relatively easily digested whereas LCs from patients with Multiple Myeloma seemed to be more resistant against digestion by trypsin. Trypsin digestion is here used as a proxy for structural dynamics, with the caveat that different LCs are likely to differ in the number and availability of trypsin cleavage sites. The most noteworthy result of our study is that in our dataset, the LCs of the three patients with the greatest degree of renal impairment were only digested by trypsin to a very small extent. Therefore, while easily digestible LC may have a tendency to form toxic amyloid fibrils *in vivo*, our results suggest that indigestible LCs may nevertheless be able to induce severe kidney damage, due to their overall higher structural stability their resulting ability to accumulate in the kidneys. This conclusion will, however, need to remain somewhat speculative until sequence information of the LCs of this study becomes available (ongoing work), which will allow to investigate how physiologically more relevant proteases can digest these LCs. The particular feature of LC diseases, namely that every patient displays a LC of a unique amino acid sequence, makes it necessary to substantially enlarge the currently available data set that links biophysical, biochemical and sequence information with clinical disease symptoms and the present study aims to contribute to this task. In order to obtain a better mechanistic understanding of the

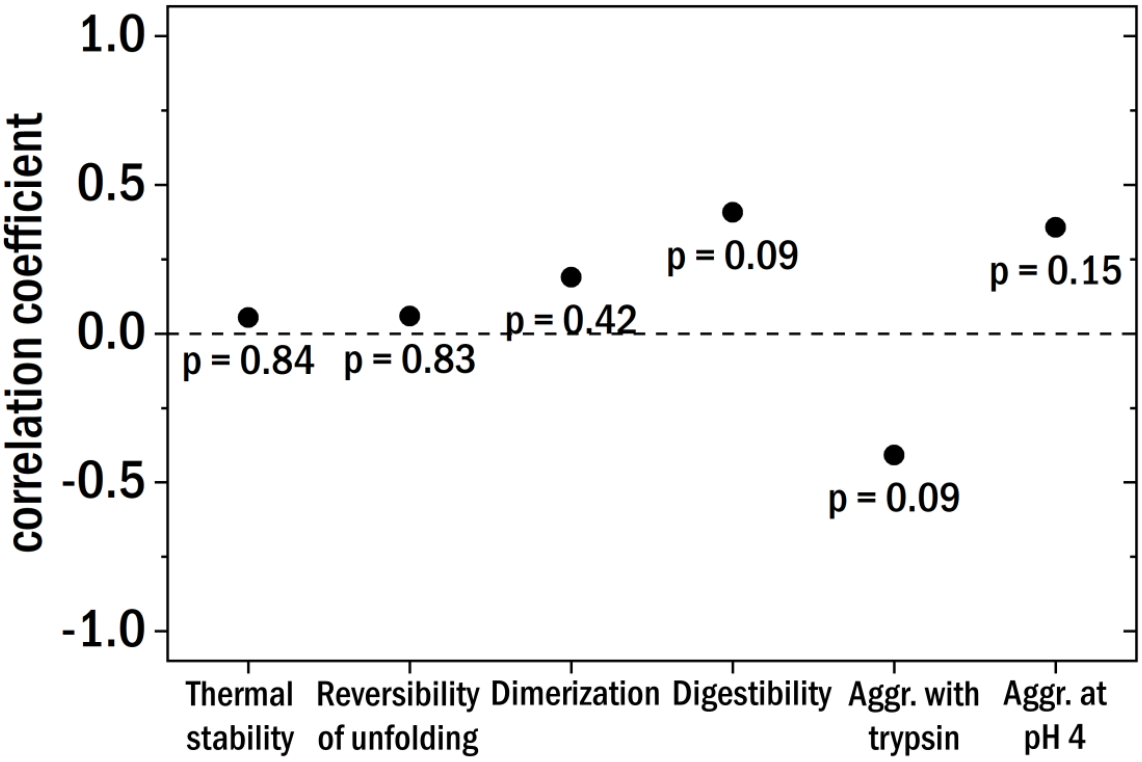

Figure 3.5: The Pearson correlation coefficient between the clinical patient categories and the different investigated biochemical and biophysical characteristics. The points are labeled with the corresponding p-value.

in vivo behavior of the LCs, a more detailed biophysical investigation, as well as sequence determinations (see above) of the extracted light chains, are required. These are the subject of ongoing studies of our groups.

3.6. Supplementary information

Sample purity: In order to characterize the purity of the samples and the relative amounts of LCs to human serum albumin (HSA) and other proteins, Western blots with anti-κ, anti-λ and anti-HSA antibodies were performed in addition to SDS-PAGE gels. The Western blots were used for identification, but not for quantification, because the binding of the antibody can be influenced by conformational changes, fragmentation or posttranslational modifications [503]. Albuminuria is often associated with kidney damage by MM and the percentage of urinary albumin excretion obtained from 24-hour urine collection among patients with AL can range between 5 and 85 % (average 70 %) [504, 505]. Some of the examined samples contain a high amount of HSA and only a small amount of LCs (see Figure 3.6). The samples from P008 and P009 contained large amounts of HSA, while also containing relevant quantities of light chains. These quantities do not show any obvious correlation with the clinical category of the individual patients. However, it is worth noting that none of the samples derived from a patient in category 1, the least severe, contains much HSA, reflecting the intact filtration unit of the glomerulus. The remaining samples were all largely dominated ($60-90$ %) by light chains. Nevertheless, the findings of the samples P008 and P009 will not be included in the subsequent experimental results, because the HSA content had an influence on the measurements and can not be immaculately distinguished.

We also tested for correlations between some of the biophysical and biochemical parameters (Figure 3.10). We find weak inverse correlation between thermal stability (as quantified by melting temperature) and on the one hand the ability to refold and on the other hand degradability by trypsin. In other words, there seems to a weak relationship in the sense that the more thermostable a LC, the smaller its ability to refold. And also, the more thermostable, the more resistant against proteolytic digestion by trypsin. A putative explanation for the first relationship is that a very hydrophobic core that stabilizes the native state against thermal unfolding can also lead to irreversible aggregation, once the LC is actually unfolded. The second relationship may be explained by the fact that more thermostable LCs are also less dynamic at room temperature and hence more difficult to degrade by trypsin. These relationships between biophysical and biochemical parameters do not have any direct relevance for the main purpose of the study, which is the elucidation between LC properties and impairment of kidney function. We report them nevertheless for their general interest and relevance to protein science.

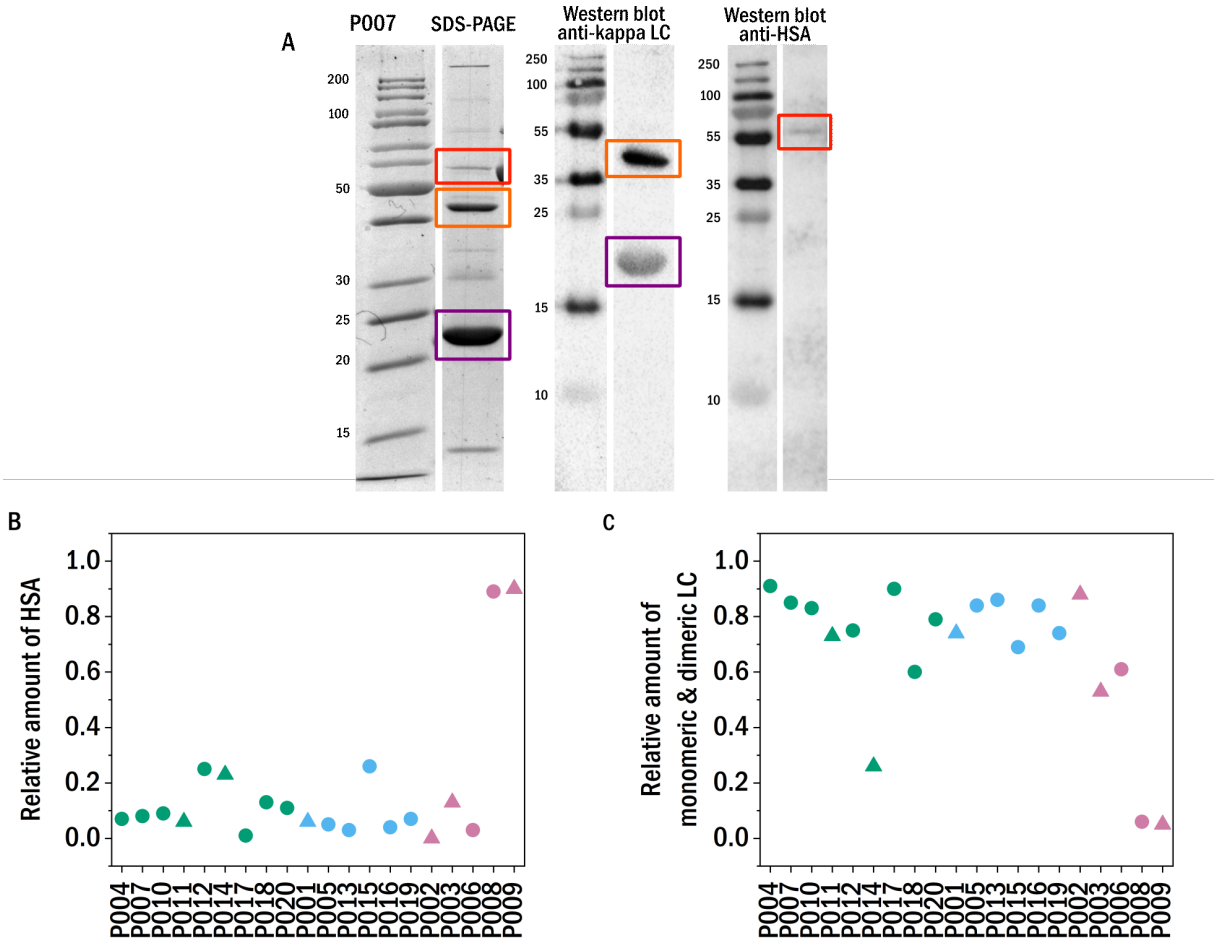

Figure 3.6: Sample purity estimates from SDS-PAGE gels and Western Blots. a) P007 as an example. The HAS-band is marked with a red square, the light chain-bands in orange (dimer) and purple (monomer). b) The relative amount of HSA in the different samples (left) b) The relative amount of light chain (monomer and dimer combined) in the different samples (right). The sorting and colors indicate the categories into which the patients were classified based on the severity of their renal impairment (CDK stage: 1+2 (green), 3 (blue), 4+5 (red). The shape symbolizes the isotype of the LC (triangle: lambda, circle: kappa).

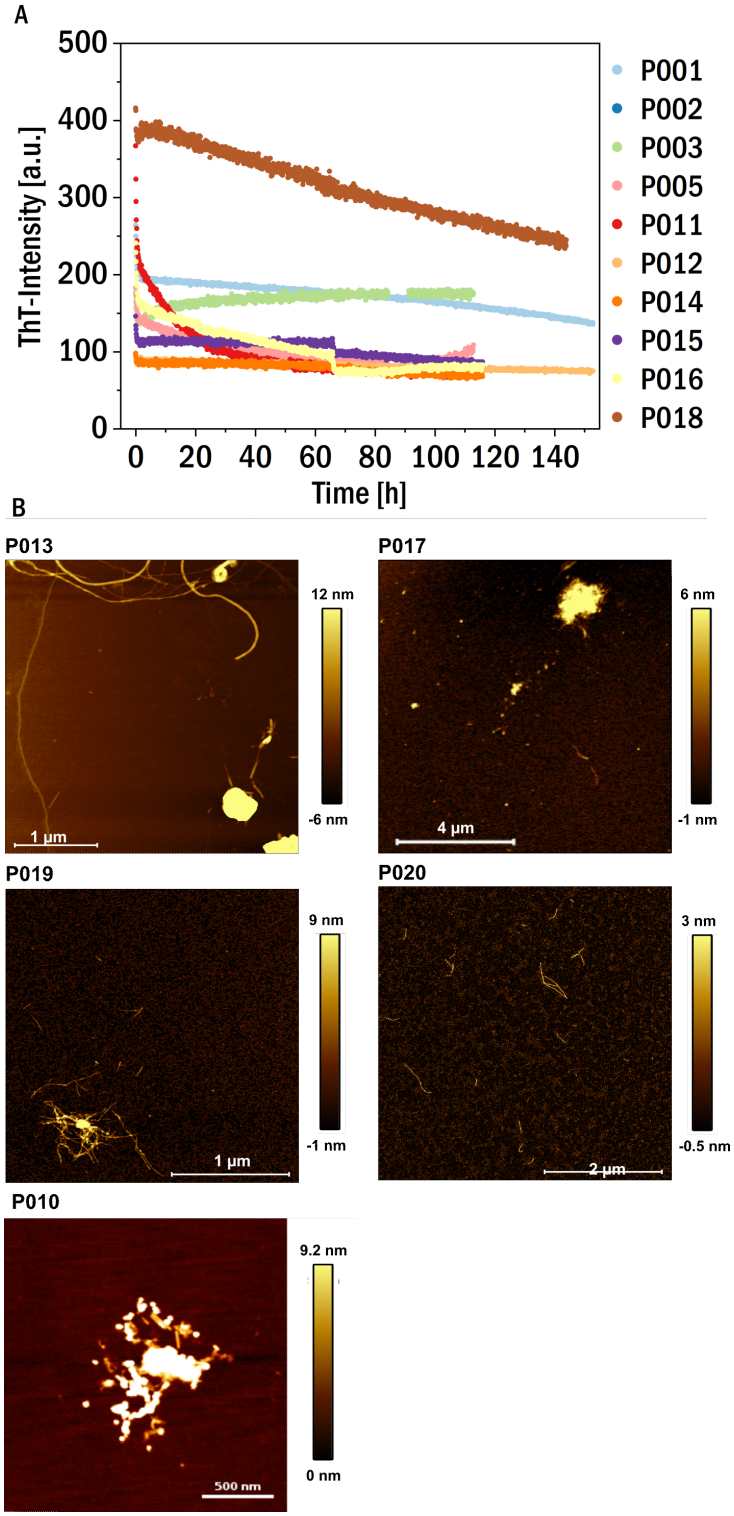

Figure 3.7: Aggregation of the LCs in the presence of trypsin. A) ThT-fluorescence aggregation assay of the non-amyloid forming LC in the presence of trypsin (P006 is already displayed in Figure 3 of the main manuscript). B) AFM-height images of the aggregated (ThT-positive) samples of P013, P017, P019, P020, P010.

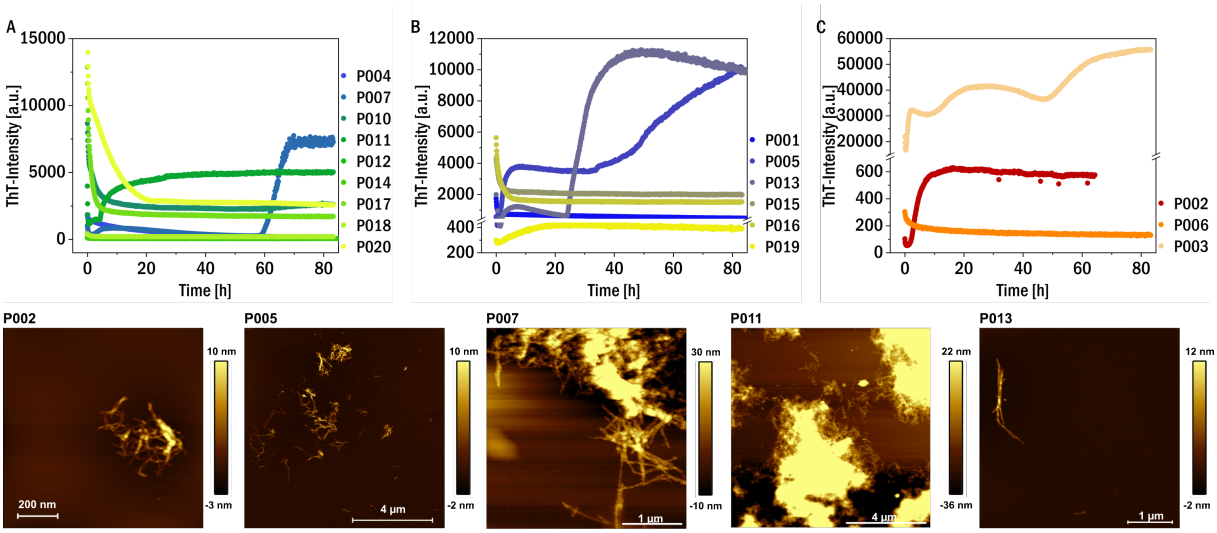

Figure 3.8: Aggregation assay at pH 4 in the absence of reducing agent. Top: ThT-fluorescence aggregation assays at pH 4 of the LCs of category I (A), II (B), III (C) corresponding to figure 4F. Bottom: AFM-height images of the aggregated samples of P002, P005, P007, P011 and P013.

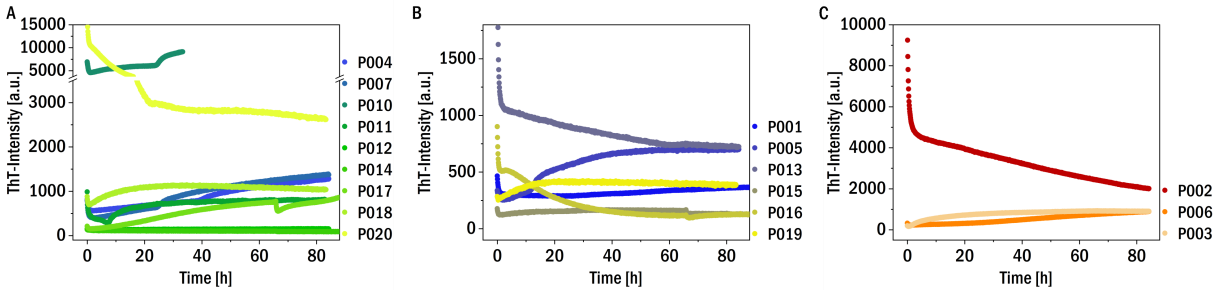

Figure 3.9: Aggregation at pH 7.5 in the presence of 1 mM TCEP. ThT-fluorescence aggregation assays at pH 7.4 in the presence of 1 mM TCEP of the LCs of category I (A), II (B), III (C).

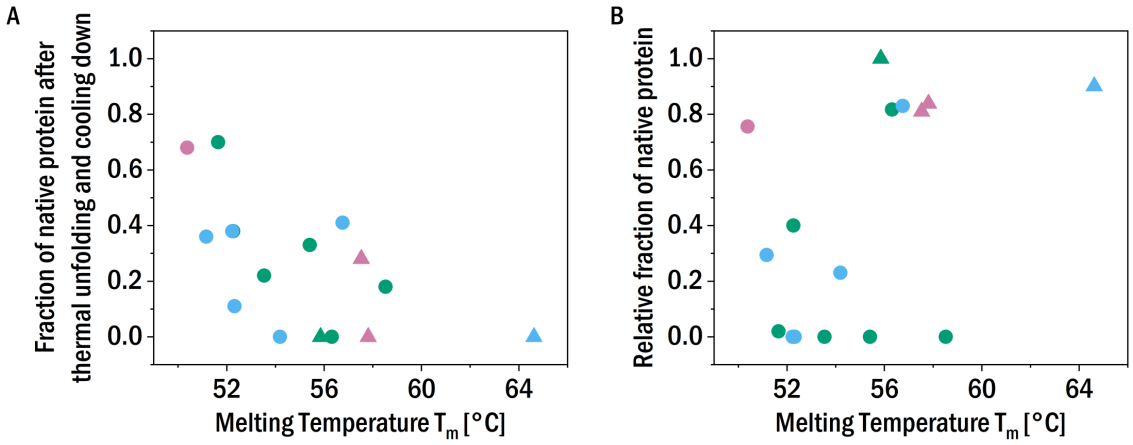

Figure 3.10: The fraction of native protein that unfolds during the second scan against the melting temperature Tm determined from the differential scanning calorimetry (DSC) experiments of the different samples allocated in the three patient categories according to renal impairment (CDK stage): I (green), II (blue), III (red). The correlation coefficient is -0.597 with a p-value of 0.015. B) The relative fraction of native protein (monomer and dimer combined) after 48 h incubation with trypsin against the melting temperature Tm determined from the differential scanning calorimetry (DSC) experiments of the different samples. The colors refer to the corresponding patient category defined above: I (green), II (blue), III (red). The correlation coefficient is 0.468 with a p-value of 0.067.

4

De novo SEQUENCING OF ANTIBODY LIGHT CHAIN PROTEOFORMS FROM PATIENTS WITH MULTIPLE MYELOMA

Article information

Authors: Mathieu Dupré[1], Magalie Duchateau[1],, Rebecca Sternke-Hoffmann[2], Amelie Boquoi[3], Christian Malosse Florian[1], Roland Fenk [3], Rainer Haas [3]* and Alexander K. Buell [4]*, Martial Rey[1], Julia Chamot-Rooke[1]*

[1] Institute Pasteur, Paris, France
[2] Institute of Physical Biology, Heinrich-Heine Universität Düsseldorf, Düsseldorf, Germany
[3] Department of Hematology, Oncology and Clinical Oncology, Heinrich-Heine Universität Düsseldorf, Düsseldorf, Germany
[4] Department of Biotechnology and Biomedicine, Technical University of Denmark, Lyngby, Denmark

Journal: -
DOI: -
not published

4.1. Abstract

In multiple myeloma diseases, monoclonal immunoglobulin light chains (LC) are abundantly produced, with the consequence in some cases to form deposits affecting various organs, such as kidney, while in other cases to remain soluble up to concentrations of several g/L in plasma. The exact factors crucial for the solubility of light chains are poorly understood, but it can be hypothesized that their amino acid sequence plays an important role. Determining the precise sequences of patient-derived light chains is therefore highly desirable. We establish here a novel de novo sequencing workflow for patient-derived LCs, based on the combination of bottom-up and top-down proteomics without database search. This pipeline is then used for the complete de novo sequencing of LCs extracted from the urine of 10 patients with multiple myeloma. We show that for the bottom-up part, digestions with trypsin and Nepenthes fluid extract are sufficient to produce overlapping peptides able to generate the best sequence candidates. For the sequencing of intact LC proteoforms, combining activation methods is key to achieve a single amino acid resolution.

4.2. Introduction

Multiple Myeloma (MM) is an incurable malignancy of plasma cells characterized by a clonal expansion of an abnormal B-cell [250, 506] The B-cells accumulate in the bone marrow and secrete large amounts of monoclonal light chains (LCs) additionally to the complete immunoglobulin. Fifteen percent of the MM-patients produce exclusively light chains [180] The 25 kDa light chain proteins are usually either excreted or degraded by the kidney, but high monoclonal quantities and low renal clearance can induce deposition in the kidney's extracellular matrix [181]. The deposits contain diverse LC aggregates, which can lead to various diseases, such as the Light Chain Deposition Disease (LCDD), where the formed aggregates have an amorphous nature,[191, 192] and the AL-amyloidosis, where aggregates consist of amyloid fibrils [190].

Currently, the in vivo aggregation behavior of a particular monoclonal LC found in the blood of a patient with light chain disease cannot be predicted. To understand better the factors affecting the solubility of LCs and their aggregation propensity, their biophysical properties have been recently explored [17, 264, 267, 472, 494, 496]. Unfortunately no clear-cut conclusion could be drawn. To achieve this goal, a database including the biophysical properties of LCs and their sequence is essential. The sequencing of monoclonal LCs is challenging, because they all have a unique amino acid sequence determined by somatic recombination and various mutations [210, 218] This sequence diversity translates into a diverse clinical picture,16 and hence the mechanisms behind a particular disease are hard to understand. LCs consist of a N-terminal variable region (v-region), which is capable of recognizing the antigen and a C-terminal constant region (c-region), which specifies the effector function of the molecule [219] Important for the antigen binding site are three hypervariable loops, so-called CDRs (Complementarity-determining regions), present in the variable region. The diversity is created by somatic recombination of variable (V) and joining (J) gene segments (V-J combination) during the early stages of B-cell maturation [220].

Light chains exist in two isotypes: kappa κ, encoded by the immunoglobulin kappa (IGK) locus on the chromosome 2[222] at band 2p11.2 and lambda λ, encoded by the immunoglobulin lambda (IGL) locus on the chromosome 22 at band 22q11.2 [221]. There are 40-76 IGKV and 73-74 IGLV gene segments belonging to seven and eleven subgroups, which are randomly joined with the corresponding joining gene segments (IGKJ and IGLJ)[226]. The rearranged

V-J genes are then affected by somatic hypermutations during the antigen dependent stages of differentiation.

The sequence of a LC can be partially determined by sequencing the RNA of the producing B-cell clone.2 [251, 507]. Admittedly, a bone marrow aspiration is allowed solely to improve diagnosis and treatment of the patients because of ethical reasons. This cannot be attained for the majority of studies. Furthermore, this approach gives no insight into potential post-translational modifications (PTMs), which can be important for solubility.

In recent years, mass spectrometry (MS) has been extensively used for antibody analysis [255, 256]. The most usual approach is bottom-up proteomics (BUP), which relies on the protein digestion and LC-MS/MS analysis of peptides. BUP can provide high sequence coverage confirming the sequence of recombinant antibodies, and the presence of expected PTMs in particular when using a combination of enzymes[508]. However, the situation is much more difficult for unknown antibodies for which de novo sequencing is required [509]. Several papers have shown that a combination of BUP and intact mass profiling can be of great help [510, 511]. For LCs, which are in the 25 kDa range, the use of top-down proteomics (TDP) based on the fragmentation of intact proteins is also possible. However, achieving a complete sequence at a single amino acid resolution is a difficult task [512, 513, 514]. A combination of BUP and TDP has also been employed recently to develop an innovative algorithm (TBnovo) allowing the de novo sequencing of small proteins, including a light chain as an example [515]. Although TBNovo can lead to high sequence coverage, many sequence gaps remain because of the lack of some fragment ions both in BUP and TDP.

We therefore developed here a complete de novo sequencing workflow for the characterization of patient-derived light chain proteoforms based on a combination of BUP and TDP with specific data analysis. This characterization covers the amino acid sequence with in most of the cases Ile/leu distinction, all post-translational modifications (including disulfide bonds), and the ratio between the monomeric and dimeric proteoforms in the clinical sample. To our knowledge such as deep characterization of LCs extracted from clinical samples has never been achieved so far.

4.3. Materials and Methods

4.3.1 Chemical and Reagents

PBS (1X, Dulbecco's Phosphate-Buffered Saline, GibcoTM), formic acid (FA), were purchased from Thermo Fischer. Ammonium bicarbonate (AB), urea, Tris 1 M HCl pH 8.5 solution, Iodoacetamide (IAA), Tris(2-carboxyethyl) phosphine 0,5 M solution (TCEP), Formic Acid (FA), glass beads (acid-washed) were purchased from Sigma-Aldrich. Ethanol (70 %), Methanol (MeOH) and Acetonitrile (ACN) were purchased from Carlo-Erba. Trypsin, Lys-C and Chymotrypsin were purchased from Promega. Sep-Pak C18 SPE cartridges were purchased from Waters. Pepsin column (ref AP-PC-001s) was purchased from affipro.cz. Nepenthes fluid was extracted from nepenthes plants of the botanical garden of Lyon and prepared as described by Rey et al. [516].

4.3.2 Ethical Considerations

All patients of whom samples were used in the study have signed an informed consent with the university hospital Düsseldorf /study number 5926R and registration ID 20170664320).

4.3.3 Light chain sample preparation

The light chains were extracted from urine samples as described in Sternke-Hoffmann *et al.* [17] (Chapter 3). Briefly, the protein content of a 24 h urine collection was precipitated by ammonium sulfate (70 % saturation) and the light chains were purified after dialysis by size-exclusion chromatography on an Äkta pure chromatography system (GE Healthcare) using a Superdex 75 10/300 GL column. 10 mM phosphate buffer pH 7.4 was used as an elution buffer. The fractions with the highest purity were chosen and dialysed against 200 mM ammonium bicarbonate and freeze-dried using a SpeedVac vacuum concentrator (ThermoFisher Scientific).

4.3.4 Light chain multiple digestions

Twenty micrograms of each LC sample were solubilized in 8 M urea, 100 mM Tris HCl pH 8.5 to obtain a final urea concentration up to 7 M. Half of the sample was kept for a direct trypsin digestion. The other half was reduced with 5 mM TCEP for 30 min and alkylated with 10 mM IAA for 30 min at room temperature in the dark. For trypsin, Lys-C and chymotrypsin digestion, the samples were diluted below 2 M urea with 100 mM Tris HCl pH 8.5. The digestion was then carried out for 3 h at 37 °C with a 1:20 ratio for each enzyme. The digestion was stopped by adding 5 % FA. For pepsin and Nepenthes fluid extract [516], urea concentration was lowered below 2 M by adding 95 % H2O, 5 % FA. The digestion was performed in solution for 10 min at 37 °C for the Nepenthes fluid and a pepsin column was used for the digestion with this enzyme. Resulting peptides were desalted and concentrated on Sep-Pak C18 SPE cartridge according to manufacturer instructions. Peptide were eluted using 50 % ACN, 0.1 % FA. Purified peptides were lyophilized and kept at −80 °C until further used.

4.3.5 Analysis of peptide digest by direct infusion

Peptide digests were analyzed in MS on an Orbitrap Fusion Lumos mass spectrometer (Thermo-Scientific) fitted an Advion TriVersa Nanomate using a chip in positive ion mode. Mass spectra were acquired at 60 K resolving power (at m/z 400), during 1 min with a scan range set to 300 – 1,700 m/z, 1 µscan per MS scan, an AGC target value of 3x106. Ions corresponding to peptides with I/L residues were then manually selected for MS2 fragmentation in EThcD (from 60 to 100 ms with additional 40 −SI60%) or MSn fragmentation using HCD (40 −SI50%). MS/MS spectra were acquired during 1 min at 60 K resolving power (at m/z 400), with a scan range set to 110 – 2,000 m/z, 10 µscans per MS scan, an AGC target value of 5x105 and maximum injection time of 50 ms.

4.3.6 LC-MS analysis of peptide digests

Peptide digests were analyzed on a Q Exactive Plus mass spectrometer (Thermo Fisher Scientific, Bremen) coupled with an EASY-nLC 1200 chromatography system (Thermo Fisher Scientific). Peptide digests (1 µg) were loaded and separated at 250 nL.min^{-1} on a in house packed 50 µcm nano-HPLC column (75 µm inner diameter) with C18 resin (1.9 µm particles, 100 Å pore size, Reprosil-Pur Basic C18-HD resin, Dr. Maisch GmbH, Ammerbuch-Entringen, Germany) equilibrated in SI98% solvent A (H2O, SI0.1% FA) and SI2% solvent B (ACN, SI0.1% FA). Peptides were eluted with a linear gradient from 2 to SI23%buffer B in 70 min, followed by a stepwise increase of buffer B to SI45% B in 30 min and finally to SI95% in 5 min. Mass spectra were acquired with a Top10 data-dependent acquisition mode, with a scan range set to 300 – 1,700 m/z, 1 µscan per MS scan, an AGC target value of 3x106. The fragmentation of precursor ions was performed by HCD (28 %) at 35K resolving power (at m/z 200) with an AGC target

value of 1×106 and a maximum injection time of 110 ms. Four µscans were accumulated per MS/MS scan. Precursors with unknown charge state or a charge state of 1 and >7 were excluded. Dynamic exclusion was set to 45 s.

4.3.7 *De novo* peptide sequencing and concatenation

PEAKS Studio X was used for peptide *de novo* sequencing. Each LC-MS experiment was processed independently. The data were refined using precursor mass correction only and the chimera scan option activated. *De novo* searches were performed with 2 ppm error for precursor mass, 0.01 Da for the fragment ions with fixed carbamidomethylation and variable oxidation as PTMs. Enzyme rules were specified for each sample, with no rules for the Nepenthes fluid and pepsin digestions. De novo sequencing results were exported and sequences, local confidence and area were used in ALPS29 to concatenate the overlapping peptides. Kmer from 6 to 10 were tested to generate putative LCs sequences. The theoretical masses of these sequences were compared to those obtained from the intact mass measurement of LCs to ensure correct concatenation and select the appropriate sequences. PEAKS DB was used to generate protein sequence coverage maps.

4.3.8 Bottom-up proteomics data analysis

All raw files were searched with MaxQuant [517] (v. 1.5.3.8) against the Uniprot Homo sapiens reference proteome (74,830 entries) concatenated with all identified LC sequences, the usual contaminants and the reversed sequences of all entries, using trypsin as specific enzyme with a maximum of 4 miscleavages. For reduced and alkylated samples, possible modifications included carbamidomethylation (Cys, fixed), oxidation (Met, variable) and Nter acetylation (variable). For non-reduced and non-alkylated samples, the following modifications were set up as variable: cysteinylation (Cys), coenzyme M (Cys), HexNAc(1)dHex(1) (Asn), oxidation (Met), Nter acetylation. The mass tolerance in MS was set to 20 ppm for the first search then 6 ppm for the main search and 10 ppm for the MS/MS. Maximum peptide charge was set to seven. Five amino acids were required as minimum peptide length. The maximum peptide mass was increased to 8,000 Da. One unique peptide to the protein group was required for the protein identification. A false discovery rate cut-off of 1 % was applied at the peptide and protein levels. Draw Map from MSTools – Web applications was used for visualization of protein sequence coverage [518]. For disulfide bridge localization, data were searched against the corresponding LC sequences with MassSpec Studio50 using the CRIMP workflow. A loss of 2 hydrogens (-2.0156 uma) was used as a virtual cross-linker mass modification. The search parameters are provided in SI. The most intense cross-linked peptides identified were used to assign disulfide bridges.

4.3.9 LC-MS analysis of intact light chains (TDP)

Intact LCs were diluted at 0.5 µg/µL in 98 % H2O, 2 % ACN and 0.1 % FA, with and without reduction (5 mM TCEP, 30 minutes at room temperature) and alkylation (10 mM iodoacetamide, 30 minutes at room temperature in the dark) steps. For reverse phase nano-liquid chromatography, a Dionex Ultimate 3000 system, equipped with a trap column (150 µm x 2.5 cm) coupled to an analytical column (75 µm x 60 cm), was used with flow rates set at 10 μL.min-1 and 0.5 μL.min-1 respectively. Both columns were packed in-house with C4 material (5 μm porous spherical particles of 300 Å pore size, Reprosil). Solvent A consisted of 98 % H2O, 2 % ACN and 0.1 % FA, and solvent B consisted of 20% H2O, 80% ACN and 0.1% FA. The following gradient was

used: 2.5 % B from 0 to10 min.; 25 % B at 11 min.; 60 % B at 20 min.; 99 % B from 21 to 30 min.; and 0.5 % B from 30.1 to 50 min. Intact light chains were analyzed both in MS and in targeted MS/MS mode on an Orbitrap Fusion Lumos mass spectrometer (Thermo-Scientific) fitted with a nano-electrospray ionization source. All experiments were performed using the intact protein mode at 2 mTorr as ion routing multipole pressure. All spectra were acquired in profile mode. The MS method includes full MS scans acquired either at 15 K or 120K resolving power (at m/z 400) with a scan range set to 750 – 2,550 m/z, 10 µscans per MS scan, an AGC target value of 5x105 and maximum injection time of 50 ms. Targeted MS/MS scans were acquired at 120 K resolving power (at m/z 400), with a scan range set to 110 – 2,000 m/z, 20 µscans per MS scan, an AGC target value of 5x105 and maximum injection time of 50 ms. In targeted experiments, selected intact protein ions were isolated with 1.2 m/z width, and fragmented with either HCD (10 %, 12 % and 15 %), CID (20 %, 25 %and 30 %), EThcD (1.5 ms/5 %, 5 ms/5 %, and 10 ms/10 %), or UVPD (25 ms, 30 ms and 35 ms).

4.3.10 TDP data analysis

Intact protein mass spectra were deconvoluted using Protein Deconvolution v3.0 software (Thermo-Scientific) either with the XtractTM algorithm for isotopically resolved charge envelopes or with the ReSpectTM algorithm for isotopically unresolved charge envelopes. MS/MS protein spectra were deconvoluted in FreeStyle 1.6 with the XtractTM algorithm. For Xtract, the following parameters were used: signal to noise ratio (S/N) of 3, fit factor of 44 %and remainder threshold of 25 %. For the Respect algorithm, a noise rejection threshold of 95 %and 20 ppm mass tolerance were used. Fragment ions were identified using Prosight Lite v1.4 with a mass tolerance of $\pm$5 ppm.

4.4. Results

4.4.1 Development of the *de novo* sequencing strategy

We used the P013 sample for optimizing the four major steps of our workflow (Figure 4.1): intact MS profiling, *de novo* peptide sequencing using multiple enzymes, proteoform characterization using TDP and proteoform validation using BUP.

4.4.2 Intact MS profiling

The intact MS profiling is an important piece of information since it allows the number of proteoforms and their isotopic molecular mass to be obtained. It also provides, using reduction/alkylation the information on the number of disulfide bridges. Since a slight band at 50 kDa was also observed in the SDS-PAGE analysis of P013 [17], we used both low and high-resolution settings to allow for the mass measurement of all species present in the sample. As shown in Figure 4.2, two protein distributions are observed in the low-resolution MS spectrum (Figure 4.2 A) corresponding respectively to 23,590.4 Da (major one) and 46,941.5 Da (average masses). As expected, only the lowest mass is observed (Figure 4.2 B) in the high-resolution spectrum (at 23,576.58 Da, monoisotopic mass). Finally, the reduced/alkylated sample (Figure 4.2 C) leads to distribution shifted toward lower m/z, due to an extensive unfolding upon S-S bond reduction and a measured mass of 23,746.74 Da (monoisotopic mass). Comparing the two monoisotopic measured masses highlights a ΔMass of 170.16 Da. This cannot only be explained by one or several carbamidomethylations (+ 57.02) following the S-S bond reduction (+ 2.02 Da) and indicates other cystein modifications.

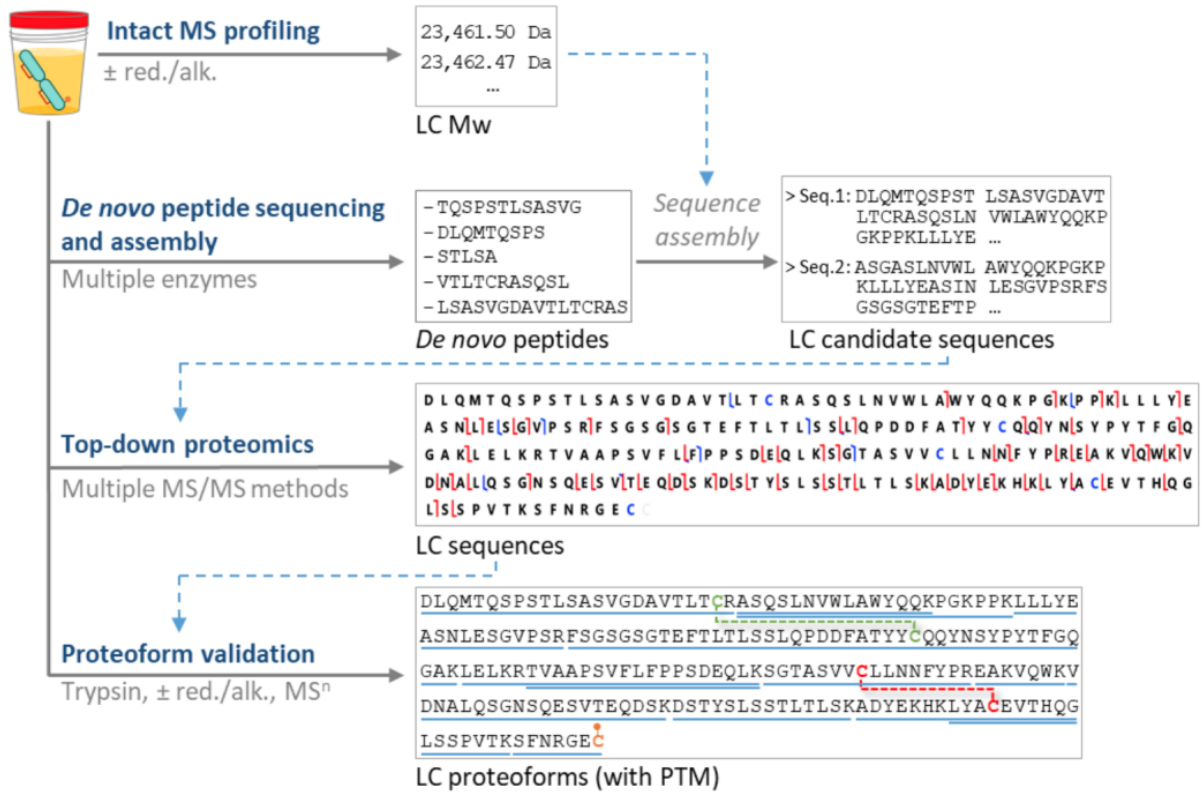

Figure 4.1: Combination of intact mass profiling, *de novo* peptide sequencing using multiple enzymes, TDP with multiple MS/MS method and BUP with and without reduction/alkylation for confident identification of light chain (LC) proteoforms.

4.4.3 *De novo* peptide sequencing and assembly

We first performed a digestion using four different enzymes (Trypsin, LysC, Pepsin and Nepenthes fluid) to maximize the probability to recover overlapping peptides. The LC-MS/MS method was optimized to obtain high quality MS/MS spectra that are required for de novo sequencing. For instance, the number of microscans was increased compared to a regular proteomics analysis. The data generated were analyzed with PEAKS to obtain *de novo* sequenced peptides. These peptides were further assembled using ALPS, with the intact mass previously measured as a constraint with 1 Da tolerance. The ALPS k-mer parameter, which represents the number of overlapping amino acids, was found to be optimal at 8. This process led to two different candidate sequences, differing only from 1 Da and a single amino acid (N/D). One of these sequences has a theoretical molecular mass of 23,746.60 Da (monoisotopic mass for the reduced/alkylated LC) matching the experimentally measured one (23,746.74 Da) within 5.8 ppm. It also contains 5 cysteines, which fits with what is expected for a LC, and was thus selected as the best candidate This allows to calculate the ΔMass due to the reduction/alkylation which is thus 289 Da. Compared to the 170.16 Da previously calculated, this leads to 119 Da, which corresponds to a cysteinylation. This LC modification was originally described by the group of Costello[254] and confirmed a few years later by Gadgil et al [519]. It has been suggested to play an important role in the stabilization of the protein.

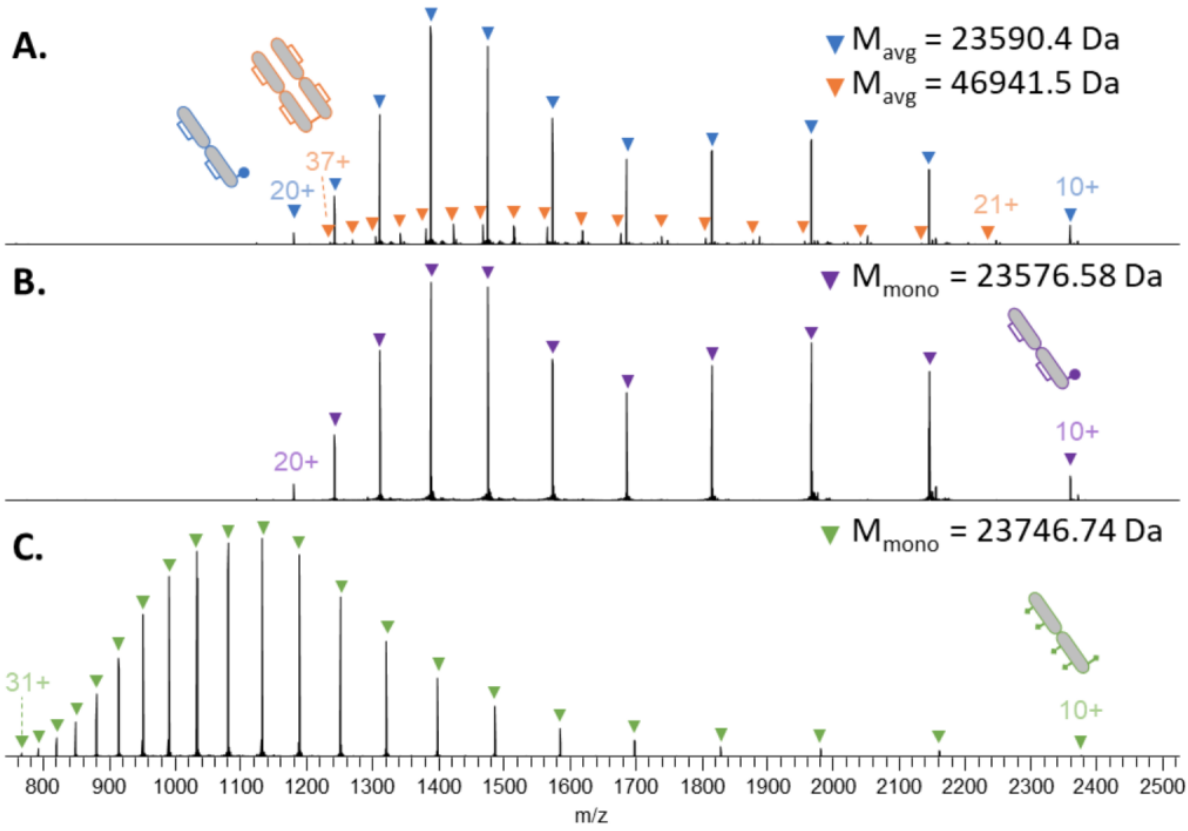

Figure 4.2: Intact mass spectra of (A) non-reduced P013 sample using low resolution MS (15k). (B) non-reduced P013 sample using high resolution MS (120k). C. reduced/alkylated P013 sample using high resolution MS (120k).

4.4.4 Top-down proteomics

The P013 sample was analyzed in its reduced and alkylated form in targeted LC-MS/MS using multiple activation techniques. The objective here was to obtain as many complementary fragment ions as possible. This is required to increase the confidence in the assembly of *de novo* peptides and identify potential errors. The Figure 4.3 shows the fragmentation map reconstructed using the 470 assigned non-redundant fragment ions. This corresponds to 89 %residue cleavage.

4.4.5 Proteoform validation

As shown in Figure 4.3, a few amino acid stretches are not covered by the TDP data and thus we decided to use the BUP information to confirm these parts of the sequence. The sequence introduced in the database for P013 is the one that is identified by Maxquant with the highest score and a 100 % sequence coverage. The MS/MS spectrum obtained for instance for the [1-24] peptide is shown in Figure 4.7. Once the P013 sequence was fully identified, we evaluated the sequence coverage obtained by each of the four enzymes. We concluded that a combination of trypsin and Nepenthes fluid is sufficient to achieve a 100 % sequence coverage and we therefore only used these enzymes for all other samples.

For the assignment of the disulfide bridges and the cysteinylation, we analyzed a non-reduced/alkylated tryptic digest of P013. Using MassSpec Studio50 the disulfide bonds were mainly identified between C23 – C88 and C134 – C194. Other combination could also be identi-

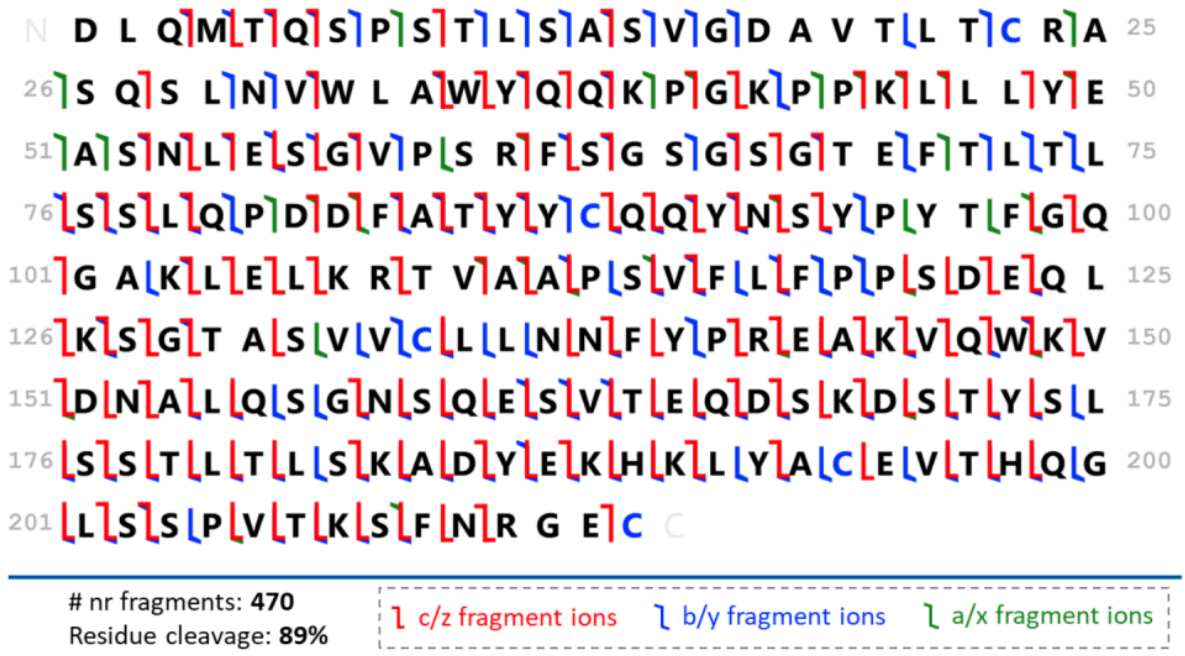

Figure 4.3: Fragmentation map obtained for P013 reduced/alkylated LC sequence using a combination of 12 top-down MS/MS analyses performed with different fragmentation methods (HCD 10 %, 12 % and 15 %, CID 20 %, 25 % and 30 %, EThcD 1.5 ms/5 %, 5 ms/5 %, and 10 ms/10 %, and UVPD 25 ms, 30 ms and 35 ms).

fied, but to a much lesser extent. The cysteinylation was primarily identified on the C-terminal cysteine (Figure 4.8), which fits with the major disulfide bond assignement. Regarding the I/L attribution, we analyzed all tryptic digests in infusion using either EThcD or HCD (MS3 and MSn) on selected I/L containing peptides. This strategy allowed about 60 % of all assignments to be performed. For the rest, I/L were assigned by homology to the described light chain sequences.

4.4.6 Application to the other clinical samples

4.4.7 P005, P006, P016 and P020

The same strategy as the one described for P013 was applied to all other samples. Four of them (P005, P006, P016 and P020) exhibited the same behaviour as P013 and could be *de novo* sequenced exactly in the same way (Table 4.1). These samples contain a single κ light chain, which exists both in a monomeric and dimeric form (with various relative abundance). These LCs contain 5 cysteines, two disulfide bonds and a cysteinylation at the C-terminus. For all samples, the dimer results from the combination of 2 monomers that are linked through a single disulfide bond. All intact MS spectra and TDP fragmentation maps are provided in Figure 4.5 and 4.6. For these LCs, sequence coverages larger than 80 % were obtained with TDP and increased to 100 % with BUP data. The sequences identified share 81 % homology (without I/L distinction) and 79.4 % when including P013.

4.4.8 P007 and P017

For these two samples, the situation is very different since the intact mass measurement indicates the presence of two proteoforms per sample. After reduction of both samples, P017 still exhibits two proteoforms although a single one is obtained for P007. All sequences were found to be part of the κ isotype, as previous ones, and contain 5 cysteines involved in two disulfide bridges. For the two samples, the two respective proteoforms were found to share the same amino acid sequence.

For P007, the first proteoform ($P007_A$) carries a cysteinylation on the C-terminal cysteine as the ones previously described (P013, P005, P006, P016, and P020). The second proteoform (P007B), which is the most abundant one, differs from $P007_A$ only by another modification present on a cysteine, since it is also removed after the reduction/alkylation process. The delta mass measured is 139.96 Da, which does not correspond to any described PTM. This mass only fits with an elemental formula of C2H6O3S2. Considering all possible thiol-based structures, we determined that P007B was probably modified by the coenzyme M, a small molecule often used as adjuvant in chemotherapy. The patient medical details confirmed this assumption. In conclusion, we characterized $P007_B$ a being modified with this small molecule on the same cysteine as the one which carries the cysteinylation. To our knowledge, such modification has never been described so far on a protein, and in particular on LCs. The fact that both modifications are on a cysteine explains why after the reduction we move from two proteoforms to a single one. This also explains that a single type of dimer is present in this sample, since it is created by the binding of the C-terminal cysteines from the two monomeric proteoforms.

For P017, the two proteoforms are cysteinylated on the C-terminus. For the second proteoform ($P017_B$), an additional oligosaccharide HexNAc(1)dHex(1) (349.14 Da) was identified probably at N153. This location fits both with our TDP results and with another LC present in the Uniprot database. The presence of this modification is unique to P017 among all clinical samples studied here. For this sample, one homodimer and the only possible heterodimer are detected as indicated by the intact mass measurements. However, this result would be explained by the low abundance of one of the glycosylated proteoform. For both P007 and P017 samples, the sequence coverage for all proteoforms were found to be 100 % when including BUP ones. The sequence homology between P007 and P017 sequences is 88.4 %.

4.4.9 P004

This sample is again different from the others, since it contains two different κ proteoforms that have different amino acid sequence. The proteoforms share a common pattern of 5 cysteines, 2 disulfide bonds and a cysteinylation at the C-terminus, but differ by eight residues present in the variable part of the LC. This mixture of two sequences, quite close from each other drastically complicates the *de novo* sequencing in particular the assembly of peptides. Note that for this sample, all dimers are formed (homo- and hetero-) and constitute the majority (95 %) of the sample.

4.4.10 P001 and P011

Finally, these two last samples are peculiar since they contain only a single LC proteoform of the λ isotype. The P001 proteoform contains 6 cysteines, with only 4 involved in a disulfide bridge. The presence of two free cysteines probably explains the easy and exclusive formation of a dimer, since the monomeric form is absent in this sample. This number of cysteines is very

unusual since LCs generally contain only five cysteines. This number of cysteines, combined to the fact that two of them are vicinal largely complicates the exact determination of disulfide bridges. It was therefore possible to formally identify only the C139–C197 disulfide bond. For P011, the sequence contains 5 cysteines, including 2 disulfide bonds, the remaining cysteine being cysteinylated as observed for the κ LCs present in the other samples. Note that the S-S bond assignment was made difficult by the very low abundance of this species in the mixture. The sequence homology between P001 and P011 is 80.1 %.

Table 4.1: Summary results obtained for all LC samples

	# Proteoforms	LC monomer proteoform	LC dimer proteoform (rel. abund., %)	LC type	LC length	LC post-translational modifications (monomer)
P013	1	P013 (100)	P013-P013 (11)	κ	214	2 disulfide bonds (C23-C88, C134-C194); 1 cysteinylation[a] (C214)
P005	1	P005 (100)	P005-P005 (48)	κ	214	2 disulfide bonds (C23-C85, C134-C194); 1 cysteinylation[a] (C214)
P006	1	P006 (100)	P006-P006 (7)	κ	213	2 disulfide bonds (C23-C87, C133-C193); 1 cysteinylation[a] (C213)
P016	1	P016 (100)	P016-P016 (12)	κ	214	2 disulfide bonds (C23-C88, C134-C194); 1 cysteinylation[a] (C214)
P020	1	P020 (100)	P020-P020 (56)	κ	214	2 disulfide bonds (C23-C88, C134-C194); 1 cysteinylation[a] (C214)
P007	2	$P007_A$ (39) $P007_B$ (100)	P007-P007 (0.5)	κ ($P007_A$) κ ($P007_B$)	214 ($P007_A$) 214 ($P007_B$)	$P007_A$: 2 disulfide bonds (C23-C88, C134-C194); 1 cysteinylation[a] (C214) $P007_B$: 2 disulfide bonds (C23-C88, C134-C194); 1 coeinzyme M[b] (C214)
P017	2	$P017_A$ (100) $P017_B$ (15)	$P017_A$-$P017_A$(42) $P017_A$-$P017_B$(26)	κ ($P017_A$) κ ($P017_B$)	215 ($P017_A$) 215 ($P017_B$)	$P017_A$: 2 disulfide bonds (C23-C88, C135-C195); 1 cysteinylation[a] (C215) $P017_B$: 2 disulfide bonds (C23-C88, C135-C195); 1 cysteinylationa (C215); 1HexNAc(a)dHex(1)[c]
P004	2	$P004_B$ (19)	$P004_A$-$P004_A$(100) $P004_A$-$P004_B$(55) $P004_B$-$P004_B$(46)	κ ($P004_A$) κ ($P004_B$)	215 ($P004_A$) nd ($P004_B$)	$P004_a$:2 disulfide bonds (C23-C89, C135-C195); 1 cysteinylation[a] (C215) $P004_b$: 2 disulfide bonds; 1 cysteinylation[a]
P001	1		P001-P001 (100)	λ	217	2 disulfide bonds
P011	1	P011 (52)	P011-P011 (100)	λ	216	2 disulfide bonds; cysteinylation[a] (C216)

nd: not determined [a] Cysteinylation: 119.00 Da [b]Coenzyme M: 138.95 Da [c]HexNACys(a)dHex(a): 349.14 Da

Figure 4.4: Multiple sequence alignment of (A.) the nine κ LC sequences and (B) the two λ LC sequences (done with Uniprot, "*" (asterix) indicates fully conserved residue, "." (colon) indicates residues with strong similar properties and "." (period) indicates residues with weak similar properties).
.

4.5. Discussion

As shown from our results, the variability observed for the LCs extracted from all clinical samples is very important, and much more than expected. First, both λ and κ isotypes are

obtained, even if the majority is constituted of this latter. Second, some samples contain a single proteoform although others contain several, which arise either from different amino acid sequences or presence of various PTMs. The sequence homology between all sequences found is $75-80\,\%$ for the κ isotypes and XX for the λ one. The presence of different LC sequences for the same patient questions the existence of several B-cell clones or point toward an unpredictable maturation process. Another difference is also the ratio between the monomeric and dimeric forms of the LCs that range from 0 to $100\,\%$. For the PTMs, we find the cysteinylation of the last cysteine of the sequence to be shared by almost all samples. We also identify a N-glycosylation and a modification with coenzyme M that are either very unusual or never described so far. Our results clearly show the added value of TDP to achieve a bird's eye view of the various proteoforms present in each sample as well as for the *de novo* sequencing. The also demonstrate that the combination of various activation techniques is required to improve the sequence coverage.

4.6. Conclusion

We developed here a novel workflow allowing the complete characterization of light chains extracted from the urine of patients with multiple myeloma. This workflow is based on the combination of bottom-up and top-down proteomics approaches, as well as the use of appropriate software tools, that are all commercially available. Using this pipeline, we could characterize for the first time a high variability in the LCs in term of sequence, PTMs and presence of monomeric or dimeric forms. These results have now to be integrated to the biophysical data already obtained for all samples. This may allow achieving the overall goal of this study, which is to identify the major factors influencing the propensity of these LCs to aggregate and lead to a disease. This is absolutely required to understand the aggregation process and be able to prevent it in the future.

4.6.1 Supplementary information

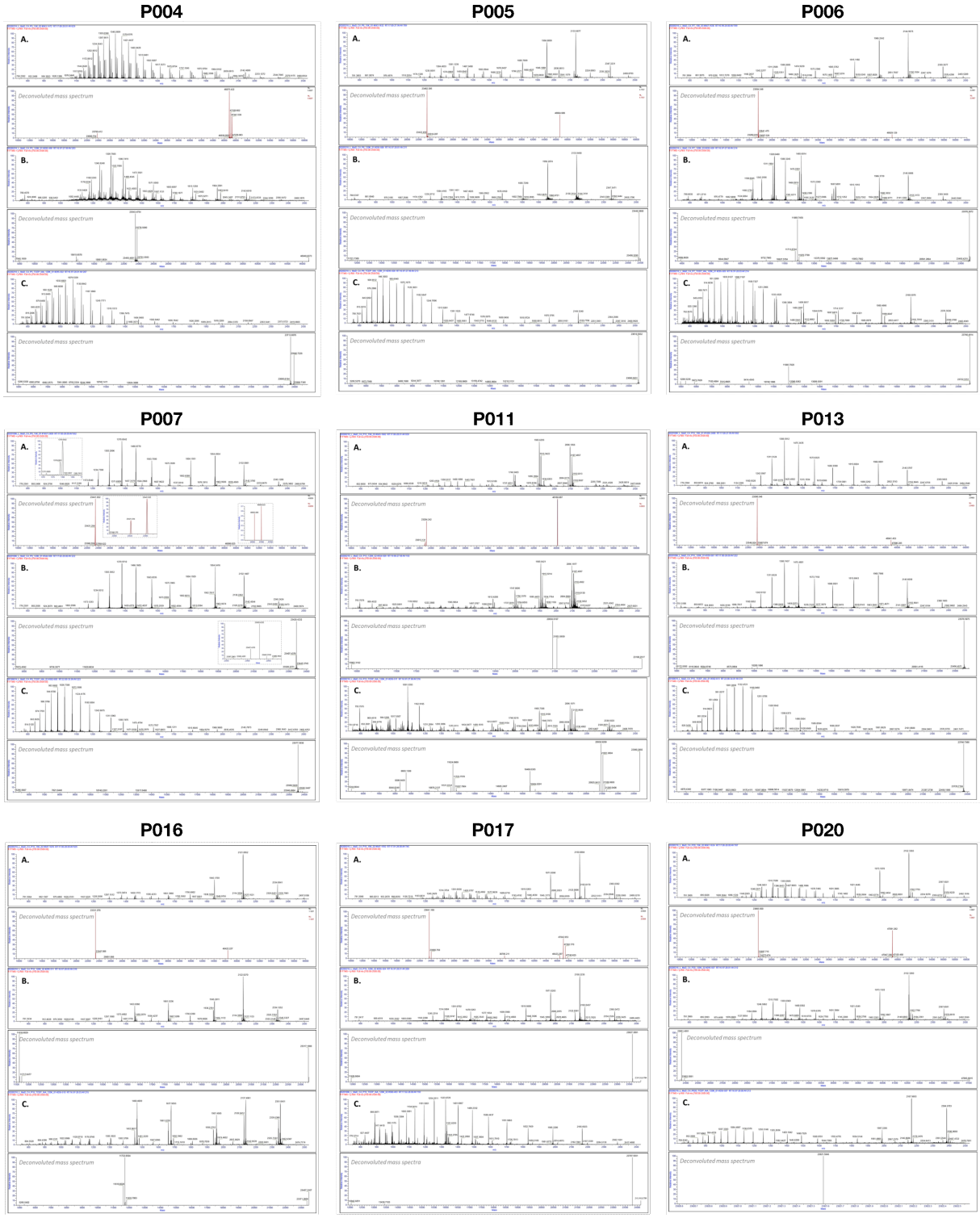

Figure 4.5: Intact mass spectra of (A) non-reduced LC samples using low resolution MS (15k). (B) non reduced LC samples using high resolution MS (120k). (C) reduced/alkylated LC samples using high resolution MS (120k).

Figure 4.6: Fragmentation maps obtained for reduced/alkylated LC sequences using a combination of 12 top-down MS/MS analyses performed with different fragmentation methods (HCD 10 %, 12 % and 15 %, CID 20 %, 25 % and 30 %, EThcD 1.5 ms/5 %, 5 ms/5 % and 10 ms/10 %, and UVPD 25 ms, 30 ms and 35 ms).

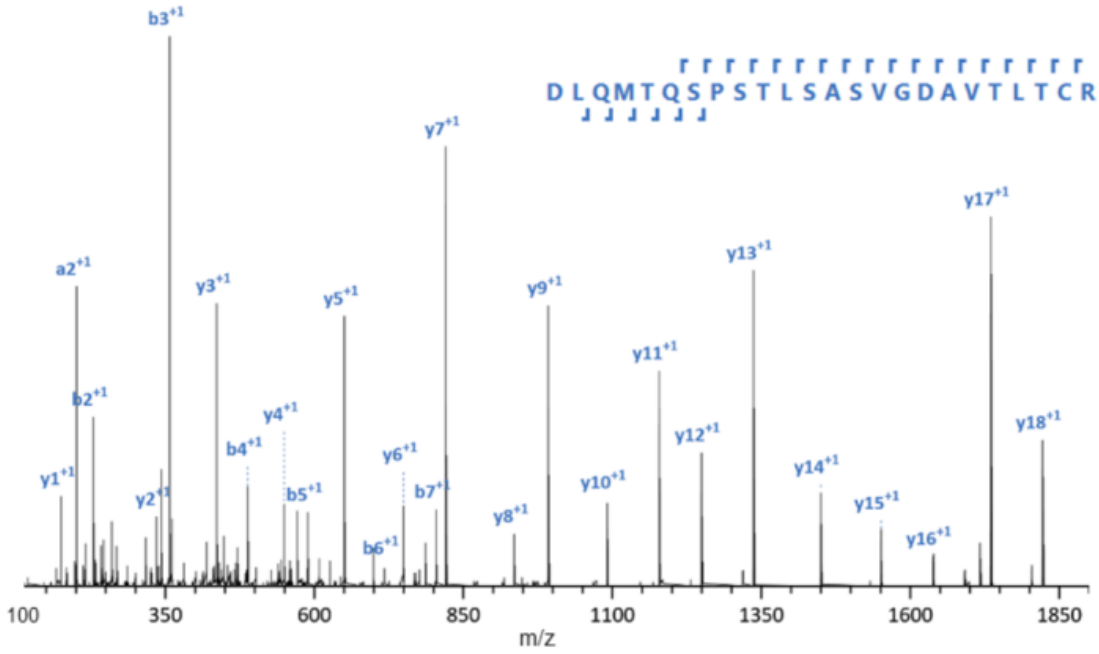

Figure 4.7: HCD fragmentation spectra of the N-terminal peptide [1-24] from sample P013.

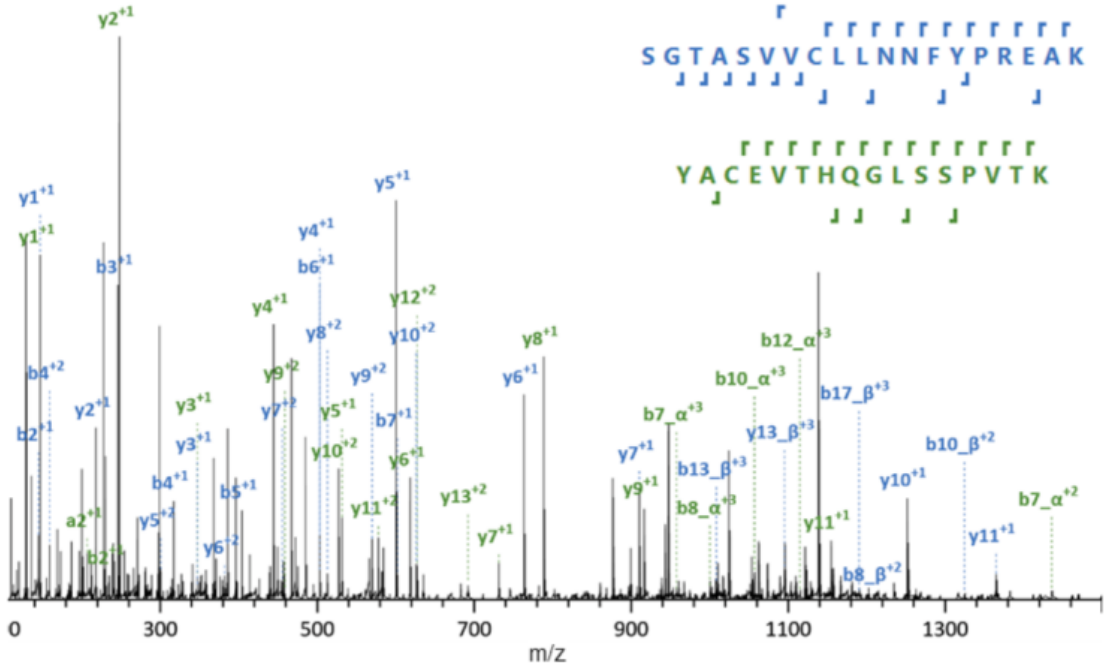

Figure 4.8: HCD fragmentation spectra of the C134-C194 disulfide-linked peptide from sample P013.

5

UNIVERSAL AMYLOIDOGENICITY OF PATIENT-DERIVED IMMUNOGLOBULIN LIGHT CHAINS

Article information

Authors: Rebecca Sternke-Hoffmann [1], Thomas Pauly [1],Jan Hansen [3],Mathieu Dupré[2], Florian Tucholski[1], Rasmus K.Norrild[5], Magalie Duchateau[2], Martial Rey[2], Sabine Metzger[6], Amelie Boquoi [4], Florian Platten [3], Stefan Egelhaaf[3], Julia Chamot-Rooke[2], Roland Fenk [4], Luitgard-Nagel-Steger[1], Rainer Haas [4]* and Alexander K. Buell [1,5]*

[1] Institute of Physical Biology, Heinrich-Heine Universität Düsseldorf, Düsseldorf, Germany
[2] Institute Pasteur, Paris, France
[3] Condensed Matter Physics Laboratory, Heinrich-Heine Universität Düsseldorf, Düsseldorf, Germany
[4] Department of Hematology, Oncology and Clinical Oncology, Heinrich-Heine Universität Düsseldorf, Düsseldorf, Germany
[5] Department of Biotechnology and Biomedicine, Technical University of Denmark, Lyngby, Denmark
[6] Cologne Biocenter, Cluster of Excellence on Plant Sciences, Mass Spectrometry Platform, University of Cologne, Cologne, Germany

Correspondence: alebu@dtu.dk (A.K.B.), Haas@med.uni-duesseldorf.de (R.H.)

Journal: -
DOI: -
not published

5.1. Abstract

The deposition of immunoglobulin light chains (IgLCs) in the form of amorphous aggregates or amyloid fibrils in different tissues of patients can lead to severe organ damage, requiring transplantation in some cases. There has been great interest in recent years to elucidate the origin of the very different *in vivo* solubilities of IgLCs, as well as the molecular determinants that drive either the formation of ordered amyloid fibrils or disordered amorphous aggregates. It is commonly thought that the origin of this differential solubility is to be found in the amino acid sequences of the respective IgLCs, i.e. that some sequences display higher intrinsic tendencies to form amyloid fibrils. Here we perform in depth Thermodynamic and Aggregation Fingerprinting (ThAgg-Fip) of 9 multiple myeloma patient-derived IgLCs, the amino acid sequences of all of which we have solved by *de novo* protein sequencing with mass spectrometry. We find that all samples also contain proteases that fragment the proteins under physiologically relevant mildly acidic pH conditions, leading to amyloid fibril formation in all cases. Our results suggest that while every pathogenic IgLC has an unique ThAgg fingerprint, all sequences have comparable amyloidogenic potential. Therefore extrinsic factors, in particular presence of, and susceptibility to, proteolytic cleavage is likely to be the main determinant of *in vivo* aggregation behaviour. This important conclusion, which is corroborated by systematic analysis of our sequences, as well as a many sequences of IgLCs from amyloidosis patients reported in the literature, challenges the current paradigm of the link between sequence and amyloid fibril formation of pathogenic light chains.

5.2. Introduction

Protein aggregates are the hallmark, and in many cases causative agents, of severe disorders, ranging from Alzheimer's diseases to systemic amyloidoses [492, 493, 520, 521]. The loss of protein solubility in these situations that leads to their deposition in various types of aggregates can have multiple origins, such as point mutations, post-translational modifications and over-production of proteins. The latter phenomenon occurs for example in Multiple Myeloma (MM), an incurable malignancy of plasma cells characterised by a clonal expansion of an abnormal B-cell [250, 506]. The B-cells accumulate in the bone marrow and secrete large amounts of monoclonal light chains (LCs) additionally to the complete immunoglobulin [179]. 15% of the MM-patients produce exclusively light chains [180]. The 25 kDa sized light chain proteins are usually either excreted or degraded by the kidney, but high monoclonal quantities and low renal clearance can induce the deposition in the kidney's extracellular matrix[181]. The deposits contain diversified kinds of LC aggregates, which can lead to different diseases, such as Light Chain Deposition Disease (LCDD), where the formed aggregates have an amorphous nature [191, 192], and AL-amyloidosis, where aggregates consist of amyloid fibrils [190].

Currently, there is no possibility to predict the *in vivo* solubility and deposition behaviour of a particular monoclonal light chain found in the blood or urine of a patient with a light chain disease. A large number of studies has been performed in recent years in order to understand the *in vivo* solubility and aggregation behaviour of a light chain through a detailed investigation of the biophysical and biochemical properties of patient-derived light chains *in vitro* [17, 258, 264, 267, 472, 494, 496]. In particular the question as to which properties distinguish the amyloid fibril forming light chains from those that are not observed to form amyloid fibrils *in vivo* has been extensively studied. Various molecular properties of the light chains, such as thermal stability [257, 258, 260, 262, 264], tendency to dimerize [268, 272, 498],

or protein dynamics [232, 284, 285] have been proposed to correlate with their deposition in the form of amyloid fibrils. Each patient-derived light chain protein has a unique amino acid sequence determined by somatic recombination and various mutations [210, 218]. The diversity of the N-terminal variable region (v-region), which is capable of recognition of the antigen [219], is created by somatic recombination of variable (V) and joining (J) gene segments (V-J combination) during the early stages of B-cell maturation [220]. Light chains occur either as a λ or a κ isotype, which are encoded by the immunoglobulin λ (IGL) [221] or the κ (IGK)[222] locus. It has been found that the majority of light chain amyloidosis cases are associated with λ light chains [223]. There are a multitude of different IGLV and IGKV gene segments, which are randomly joined with the corresponding joining gene segments (IGLJ and IGKJ) [226] and then affected by somatic hypermutations during the antigen dependent stages of differentiation. This sequence diversity translates into a diverse clinical picture [226], impedig the understanding of the disease mechanisms. An improved understanding of the causes and mechanisms of light chain deposition requires to determine the amino acid sequences of patient-derived light chains and to correlate the sequence information with the biochemical and biophysical properties. The unique nature of light chains renders their sequence determination challenging. The sequence can either be obtained through DNA sequencing of tissue from bone marrow biopsies [250, 251], or less invasively through *de novo* protein sequencing by mass spectrometry. The latter, however, is difficult because of the absence of the sequence under study in the data bases usually employed in mass spectrometry (MS)-based proteomics [511]. In order to be able to address the challenging link between light chain sequence and aggregation behaviour, we have developed a complete *de novo* protein sequencing workflow based on a combination of top-down and bottom-up proteomics with specific data analysis for patient-derived light chains. The details of this workflow are published separately (REF). We were able to determine the sequences of a range of different light chains. The light chains investigated in this study were derived from 10 patients presenting light chains in their urine (2 isotype lambda and 8 isotype kappa) and represent a sub-set of a larger collection from a patient cohort at the University Hospital Düsseldorf, which has already been subjected to an initial biochemical and biophysical characterisation [17]3. The inclusion criterion of a given sample into the present study was the availability of a sufficient amount of light chain at high purity to allow both the sequence determination, as well as the detailed Thermodynamic and Aggregation Fingerprinting (ThAgg-Fip) to be carried out. ThAgg-Fip consists of a characterisation of IgLC dimerisation, thermodynamic stability (thermal and chemical), thermally and chemically induced aggregation (amorphous and amyloid) and enzymatic digestability and represents the most comprehensive charcaterisation of disease-related IgLCs to date. We dub our approach ThAgg-Fip, because the multi-parametric characterisation we perform reveals a unique set of biophysical and biochemical properties of every individual patient-derived light chain. In addition to the 9 samples fulfilling our inclusion criteria, all stemming from multiple myeloma patients without evidence of amyloid fibril formation, we also included a sample from a confirmed amyloidosis case. Consequently our study was mostly carried out on light chain proteins, which would generally be considered to be non-amyloidogenic. However, we find that all proteins of our study are observed to form amyloid fibrils *in vitro* under physiologically relevant conditions of mildly acidic pH, where the present proteases led to the rapid digestion of the light chains into shorter fragments. We analyse our determined sequences as well as a representative collection of light chain sequences from the literature using several commonly used aggregation prediction algorithms and find no noticeable difference between amyloid forming and non-amyloid forming sequences. Our findings challenge the current paradigm that the origin of the amyloidogenicity is to be found in the amino acid sequence of the light chains alone. We conclude that all light chains have

comparable intrinsic amyloidogenicity and that the interplay of protein sequence, environmental conditions and presence and action of proteases defines whether a given light chain deposits in the form of amyloid fibrils in a given patient or not. Furthermore, our uniquely comprehensive and widely applicable ThAgg-Fip approach highlights the multiparametric nature of the problem of *in vivo* protein aggregation and opens up the possibility for the application of machine learning approaches once larger data sets will become available in the future.

5.3. Materials and Methods

5.3.1 Patient-derived samples

The study described in this manuscript is an extension of previous work [17] and has been reviewed and approved by the ethics committee of the University Hospital Düsseldorf. All patients of whom samples were used in the study have signed an informed consent (study number 5926R and registration ID 20170664320). Protein isolated from 24 h urine samples of 10 patients (5 females, 5 males, median age 64.5 years with a range between 45 and 72, 2 patients with a lambda isotype light chain and 8 patients with a kappa isotype chain) with multiple myeloma and one patient with amyloidosis as detailed in table 2.1. A histopathological examination of the patient's kidney was not available since the corresponding invasive diagnostic procedure was not necessary for the therapy decision-making process as they were diagnosed according to IMWG criteria. These samples represent a sub-set of samples of a previous study [17] (cf. Chapter 3), and they were selected, because they contained the light chain protein at sufficiently high quantity and purity to perform the detailed biochemical and biophysical experiments and to determine the protein sequence.

We divided the patients into three different groups (I, II, III) according to their chronic kidney disease (CKD)-stage at the time of diagnosis. Group I corresponds to stages 1 and 2, group II to stage 3 and group III to stages 4 and 5.

5.3.2 Protein sample preparation

The LCs were purified as described previously [17]. Briefly summarized, the protein content of a 24 h urine collection was precipitated by ammonium sulfate (70 % saturation) and the light chains were purified after dialysis by size-exclusion chromatography on an ÄKTA pure chromatography system (GE Healthcare) using a Superdex 75 10/300 GL column and 30 mM Tris-HCl, pH 7.4, as an elution buffer. LC concentration was determined by measuring UV-absorption at 280 nm (extinction coefficient of 33265 (P001), 27640 (P004), 26150 (P005, P006, P007, P016, P017), 33140 (P013) and 31650 (P020). A stock solution of tris(2-carboxyethyl)phosphine (TCEP) was prepared by dissolving 100 mM TCEP in 30 mM Tris-HCl buffer pH 7.4. Subsequently, the pH value was titrated with NaOH to 7.4. Pepstatin A and E-64 were dissolved in DSMO to prepare a stock solution of 1 mM.

5.3.3 Determination of the amino acid sequence

Mass spectrometry (MS) experiments were performed to confirm the purity of the sample, determine the monomer and dimer content of the LCs and to determine the amino acid sequence. To this end, a complete *de novo* sequencing workflow based on a combination of top-down and bottom-up proteomics with specific data analysis for patient-derived light chains was performed. For bottom-up proteomics, peptides were generated either with trypsin or *Nepenthes* fluid extract

[516, 522] and analyzed in LC-MS/MS on an Orbitrap Q-Exactive plus. PEAKS and ALPS [511] were then used for peptide *de novo* sequencing and concatenation of overlapping peptides to generate putative LC sequences. Intact light chains were analyzed in LC-MS/MS (before and after disulfide bond reduction) on an Orbitrap Fusion Lumos with different activation methods. Prosight PD was used for proteoform identification. A detailed description of the *de novo* sequencing workflow can be found in (Chapter 4).

5.3.4 Analysis of the properties of the IgLC amino acid sequences

The sequences of the IgLC samples of this study were parsed with IMGT, the international ImMuniGeneTics information system and were aligned in order to investigate the amino acid changes between the germline sequences and the sequences under study. The sequences were also analysed using different online bioinformatic tools (ZipperDB, Tango, Pasta, CamSol), which predict the aggregation propensity/solubility of the samples.

5.3.5 Determination of the dimer content

The ratio of dimers and monomers of the various LCs were determined by both top-down proteomics and analytical ultracentrifugation (AUC). Sedimentation velocity experiments were performed in a XL-A Proteomelab ultracentrifuge equipped with absorbance optics. Experiments were conducted in An-60-Ti at 20 °C using a rotor speed of 60,000 rpm. Solutions of 35 µM of LC samples were investigated and the scans were acquired at a wavelength which ensures an optimal resolution to achieve an absorbance of 1, and 0.002 cm radial increments. The sedimentation boundary was analyzed with SEDFIT (version). The fraction of dimer measured in relation to the overall amount of native light chains (monomer and dimer) investigated by the AUC measurements were compared to the results of mass spectrometry (MS) and previously reported results from non-reducing SDS-PAGE [17].

5.3.6 Combined differential scanning fluorimetry (DSF) and dynamic light scattering (DLS) experiments

The thermal unfolding experiments of the IgLC samples as a function of protein and denaturant concentration were performed with a Prometheus Panta instrument (Nanotemper, Munich, Germany). This is a microcapillary-based (10 µL sample per capillary) instrument that allows to measure up to 48 samples in parallel. Intrinsic fluorescence can be excited at 280 nm and emission is monitored at 330 nm and 350 nm. The DLS experiments are performed on the same sample with a laser at 405 nm. Thermal ramping experiments were performed by scanning from 20 °C (urea dependence) or 25 °C (concentration dependence) to 70 °C at a scan rate of 1°C/min. For the melting scans, we prepared stock solutions of the IgLCs (97 µM (P001), 150 µM (P004), 91 µM (P005), 139 µM (P006), 103 µM (P007), 97 µM (P013), 99 µM(P016), 158 µM (P017) and 81 µM (P020)). These stock solutions were filtered through a 220 nm pore size syringe filter before the DSF-DLS experiments. For the concentration-dependent measurements, the stock solutions were diluted 3 times by a factor of two, to yield 4 different concentrations per protein. For the urea-dependent experiments, the stock solutions were diluted 5 times into solutions of appropriate urea concentration. The final urea concentrations were 0, 0.67,1.34, 2.01, 2.68, 3.35, 4.02, 4.69, 5.36 M and the buffer concentration was in all cases 30 mM Tris buffer. The data was visualised as the ratio of the intrinsic fluorescence emission intensity at 350 nm over the intensity at 330 nm. For the melting temperatures at the different protein concentrations the melting temperature (T_m) and the temperature of aggregation onset (T_{agg}) were automatically

determined by the instrument software. In table 5.2 we report the values for T_m and T_{agg} for the highest and lowest concentrations of our concentration series, respectively. We also show the evolution of the size distribution of the sample as a function of temperature with a heatmap on a logarithmic scale. The aggregate size we report in table 5.2 corresponds to the maximal size reached at the upper temperature limit of the experiment (70 °C). The full sets of raw data of these experiments can be found in supplementary figures 5.16 and 5.17. For the combined chemical and thermal unfolding experiments, the data set of each protein was globally fitted to the thermodynamic model recently presented. The global fits are shown in Figure 5.18. In order to reduce the influence of aggregation on the fits, only samples containing urea were included in the fit, as the simultaneous DLS measurements had shown aggregation mostly in the absence of urea. For P004, all samples below 2 M urea were excluded on this rationale. From the global fit over all temperatures, we then determine the stability of the IgLC, ΔG, at 37 °C. We find a significant correlation between ΔG and the m-value, i.e. $m = \frac{d\Delta G}{d[\text{urea}]}$. We therefore fix the m-value to a common value for all different light chains and focus on the resulting differences between ΔG. Error estimates of the obtained values were obtained by 100-fold bootstrapping by resampling the different capillaries with replacement.

5.3.7 Measurements of aggregation kinetics

Different solution conditions (acidic pH values and reducing conditions) were tested for their potential to induce aggregation of patient-derived, purified LCs. In order to prepare the samples at different acidic pH values (pH 2, pH 3, pH 4), protein solutions of different concentrations were diluted from 30 mM Tris-HCl pH 7.4 1:1 into 300 mM citric acid buffer at the desired pH value). Reducing conditions were prepared by adding 7 mM pH-adjusted TCEP to the protein solutions of the desired concentration (5 µM, 35 µM or 100 µM). 20 µM ThT was added to allow the detection of amyloid fibril formation. Two or three replicates of each solution were then pipetted into a high-binding surface plate (Corning #3601, Corning, NY, USA). The aggregation kinetics were monitored in the presence and absence of small glass beads (SiLibeads Typ M, 3.0 mm). The plates were sealed using SealPlate film (Sigma-Aldrich #Z369667). The kinetics of amyloid fibril formation were monitored at 37 °C. either under continuous shaking (600 rpm) or under quiescent conditions by measuring ThT fluorescence intensity through the bottom of the plate using a FLUOstar (BMG LABTECH, Germany) microplate reader (readings were taken every 150 or 300 seconds). In order to compare the factor of the increase of the ThT fluorescence emission intensity between the samples, the ThT fluorescence emission intensity at the end of the experiment was compared with the lowest emission value. The halftimes of the aggregation reaction are defined as the point where the ThT intensity is halfway between the initial baseline and the final plateau. The halftimes were obtained by individually fitting the curves using the following generic sigmoidal equation [523]:

$$Y = y_i + m_i t + \frac{y_f + m_f t}{1 + e^{-(\frac{t - t_{50}}{k})}} \tag{5.1}$$

Where Y is the ThT fluorescence emission intensity, t is the time and t_{50} is the time when 50 % of maximum ThT fluorescence intensity is reached. The initial baseline is described by $y_i + m_i t$ and the final baseline is described by $y_f + m_f t$. While this equation does not describe the underlying molecular processes of aggregation, it does allow an accurate determination of the macroscopic parameters of each experiment. At the end of the experiments, the amount of aggregated protein was determined by combining the replicates and centrifuging the aggregation product for 1 h at

13200 rpm and measuring the soluble content by UV-absorbance at 280 nm, and correcting for the absorbance of the ThT. In order to investigate whether the aggregation can be seeded at acidic pH, fibrils were produced by incubating 35 µM protein solution at pH 3 and pH 4 in a high-binding plate and in a 2 ml Eppendorf tube in presence of glass beads under shaking conditions at 37 °C. The presence of fibrillar aggregates was confirmed by AFM. These aggregates were used as seeds by monitoring the aggregation kinetics in the presence of preformed fibrils obtained from the plate and from the Eppendorf tube. Before performing the experiment, the seed-solutions were homogenized using an ultra-sonication bath Sonorex RK 100 H (Bandelin, Germany) for 300 s.The seeded aggregation experiments were performed in high-binding surface plates under quiescent conditions with 35 µM P016 monomer and the preformed fibrils were added as seeds to a final concentration of 5 % of the monomer solution at the desired pH value. The seeds were added either at the beginning or after 6 h pre-incubation of the monomer solution at 37 °C. We furthermore investigated the seeding potential at neutral pH, where the protein remains largely intact. We used pre-formed fibrils, which were produced at pH 3 and pH 4 in an Eppendorf tube as described above with 100 µM. The seeds were additionally washed to remove the soluble fragments by centrifuging the sample at 40.000 rpm at 20 °C for 45 min and resuspending the pellet in 150 mM citric acid. This washing procedure was carried out three times. The seeded aggregation experiments were performed in high-binding surface plates under agitation conditions with 50 µM monomer solution and fibrils added to a final concentration of 5 %.

5.3.8 Light scattering experiments

The influence of a reducing agent on different light chain samples (P001, P006, P013, P017 and P020), in particular their aggregation behaviour, was characterized at a temperature of 37 °C under quiescent conditions by static and dynamic light scattering. The experiments were performed using a 3D cross-correlation set-up (LS Instruments AG), which suppresses contributions from multiple scattering to the correlation function [457]. These measurements were done at a scattering angle of 90° with a He-Ne laser (wavelength 632.8 nm, power 32 mW, JDSU), a pair of avalanche photodiodes (Perkin-Elmer) and a multitau digital correlator. Time traces of the scattered intensities of samples containing 35 µM LC monomer and 7 mM TCEP were monitored for up to 20 h in consecutive 120 s intervals which, in most cases, resulted in well-defined intensity cross-correlation functions. Photon count rates were averaged over this time interval to yield total scattered intensities (with contributions from singly and multiply scattered photons). As the correlation functions are dominated by a single exponential decay, the cumulant method up to second order [458] was applied to infer the average and variance of the decay rate. Typically, the variance ranged between 0.4 and 1.0, which indicates a broad peak of the intensity-weighted size distribution and hence a large polydispersity. The (hydrodynamic) aggregate size, i.e., the mean hydrodynamic radius, is estimated based on the average decay rate via the Stokes-Einstein equation, assuming the aggregates to be spherical and the viscosity of the surrounding medium to be that of water [524]. Once the aggregates become very large, multiple scattering becomes important and the large aggregates are expected to sediment out of the scattering volume, such that the aggregate size can no longer be inferred from the correlation functions. Long-time data showing signs of these effects are excluded.

5.3.9 Circular dichroism (CD) spectroscopy

The influence of reducing conditions on the light chain structure was measured by circular dichroism (CD) spectroscopy. A solution of 35 µM protein, 10 mM phosphate buffer pH 7.4

and 7 mM TCEP was incubated in Eppendorf tubes at 37 °C under quiescent conditions and an aliquot was taken after 1.25 h, 5 h, 24 h and 48 h. The sample was diluted to an concentration of 9.23 µM with 10 mM phosphate buffer and Far-UV CD spectra were recorded on a JASCO J-810 instrument (Tokyo, Japan) equipped with a Peltier thermally controlled cuvette holder. The spectra were recorded from 260 nm to 190 nm.

5.3.10 Prevention of aggregation kinetics at acidic pH values

In order to investigate whether the cleavage of the IgLCs at acidic pH values was responsible for the amyloid fibril formation, we tested whether inhibiting some of the identified proteases will prevent the formation of ThT-positive aggregates. Therefore the LCs (35 µM monomer concentration) were incubated as described above in a high binding surface plate under quiescent conditions in the presence of 10 µM pepstatin A and E-64, respectively. E-64 is an irreversible and highly selective cysteine protease inhibitor, pepstatin A is a reversible inhibitor of acidic proteases (aspartic proteases) and can be used in a mixture with other enzyme inhibitors. Further experiments were conducted with P005 and P016 in the presence of 1 µM pepstatin A or E-64 or 1 µM or 10 µM pepstatin A and E-64 under agitation conditions. The morphology of aggregates were investigated by AFM.

5.3.11 Atomic Force Microscopy (AFM)

Atomic force microscopy height-images were acquired after the aggregation kinetic measurements. 10 µL of each sample (after diluting 1:4 with dH_2O) was deposited onto freshly cleaved mica. After drying, the samples were washed 5 times with 100 µL of dH_2O and dried under gentle flow of nitrogen. AFM images were obtained using a NanoScope V (Bruker) atomic force microscope equipped with a silicon cantilever ScanAsyst-Air with a tip radius of 2-12 nm. The images were analyzed with the software Gwyddion 2.56 to measure height profiles and investigate a possible twist of the fibrillar aggregates.

5.3.12 Microfluidic diffusional sizing and concentration measurements

Fluidity One is a microfluidic diffusional sizing (MDS [408]) device, which measures the rate of diffusion of protein species under steady state laminar flow and determines the average particle size from the overall diffusion coefficient. The protein concentration is determined by fluorescence intensity, as the protein is mixed with ortho-phthalaldehyde (OPA) after the diffusion, a compound which reacts with primary amines, producing a fluorescent compound [409]. To measure the influence of pH on the average size of the molecules in the solution, the protein was pre-incubated at acidic pH values with 150 mM citric acid (pH 3 or pH 4). The LC solution was incubated in an Eppendorf tube at 37 °C under quiescent conditions. After different incubation times, 6 µL of the solutions was pipetted onto a disposable microfluidic chip and measured with the Fluidity One (F1, Fluidic Analytics, Cambridge, UK).

5.4. Results

This study is based on the detailed study of 9 different immunoglobulin light chains (1 isotype λ and 8 isotype κ) which were purified from urine samples of patients with a monoclonal light chain disease related to different types of multiple myeloma. These light chains were selected from a previous study [17] and the criterion for inclusion into the present extended *in vitro* study was the accessibility and a degree of purity of light chain proteins which enables a detailed

analysis with biophysical techniques, as well as *de novo* sequencing. We set out to perform a comprehensive characterisation of the thermodynamic and aggregation properties of these light chains with the aim to combine this information with the sequences that we obtained from a parallel sequencing effort. To this end, we have combined a wide array of state of the art biophysical and biochemical methods into the ThAgg-Fip approach, which, in the form presented here, is specifically suited for the characterisation of IgLCs, but can be easily adapted to capture the key properties of any type of aggregating protein. The resulting ThAgg fingerprints are listed in table 5.2.

5.4.1 Dimerisation of the light chains

We first set out to robustly characterise the monomer-dimer distribution of the IgLCs. The tendency of disease-related overproduced immunoglobulin light chains to dimerise has previously been proposed to correlate with the protein's tendency to form amyloid fibrils [272, 498]. In a previous study, we determined the degree of dimerization with non-reducing SDS-PAGE gels [17]. Here we aimed to improve our previous results by both sedimentation velocity analytical ultracentrifugation (AUC), as well as mass spectrometry. AUC allows the analysis under native conditions in solution and mass spectrometry allows unique identification of protein monomers and multimers. Taken together, these techniques provide a very accurate picture of the monomer-dimer distribution of the light chain proteins in solution. None of the examined LCs occurs exclusively in its monomeric form, but P001 is exclusively dimeric. The results of the three different methods are displayed in Figure 5.1 C. The three techniques exhibit similar outcomes. Especially P001, P004 and P006 behaved in the AUC- and the MS-measurement very similar, despite the different sample treatments before the measurements. The light chains were purified by size-exclusion chromatography (SEC), aliquoted, frozen and thawed before the AUC-measurement. Prior to the MS-measurements the samples were dialyzed against ammonium bicarbonate after the SEC and freeze-dried. The chromatograms of the different samples with the fractions used for the experiments marked can be found in the supplementary information (Figure 5.13). All experiments of the current study were conducted with specific fractions in order to standardise the preparation since the peaks are not always symmetrical. Therefore a bias of the measured dimer fraction due to differences in sampling can not be fully excluded.

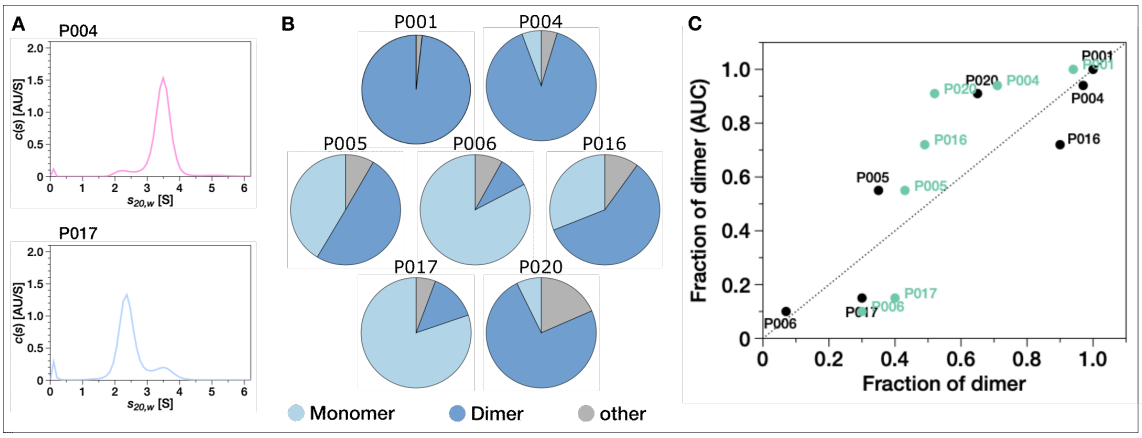

Figure 5.1: (A) The distribution of sedimentattion coefficients (c(s)) determined by sedimentation velocity AUC experiments at 60.000 rpm of two light chains (P004 and P017) as an example. (B) The monomer (light blue), dimer (dark blue) and other (grey) content measured by AUC. (C) The fraction of dimer measured in relation to the overall amount of native light chains (monomer and dimer) by the AUC against the fraction detected by MS-measurements (black) and by SDS-PAGE (green) [17].

The fractions of monomer and dimer displayed in Figure 5.1 A are extracted from sedimentation velocity c(s) profiles derived from the AUC SV measurements (Figure 5.14). Both species could be fitted as two distinct distributions in the displayed samples. As "other", we denote the additional contents of the samples, for example HSA (in P020) or aggregates, but also particles which are not sedimenting. The measured average s-value for the monomer is 2.32 S±0.07 and for the dimer 3.53 S±0.18. The c(s) profiles of P007 and P013 displayed only one species situated between the s-value of a monomer and a dimer. Applying the c(s, *ff0*)-model to the SV experiments, where the form-factor is fitted for each individual species, it becomes discoverable, that the structure of the dimer differ greatly within the sample set. The dimers can be very globular e.g. P020 with a f/f_0 of 1.01 or elongated such as P006 f/f_0 of 2.17 and P007, P013 and P017 f/f_0 between 1.62 and 1.79. Therefore the intriguing characteristic of dimers appears to be the their structure and interface. This should be analysed in greater detail in the future, for example with crystallisation experiments or NMR.

5.4.2 Thermal and chemical stability and thermally induced aggregation

We had previously characterised the thermal stabilities of these and other IgLCs by differential scanning calorimetry (DSC, [17]), and we had observed that very different percentages of the light chains re-folded upon cooling after complete thermal unfolding. Here we performed similar experiments at high resolution by monitoring the intrinsic Trp fluorescence of the IgLC samples as a function of temperature at different protein concentration, while simultaneously performing dynamic light scattering (DLS) experiments. Examples of such experiments (for P007 and P017) are shown in Figure 5.2 a and d. At the beginning of the experiment, the monomeric protein dominates the DLS signal in all cases. We found a dependence of both the unfolding temperature, as well as the temperature of onset of aggregation, on the protein concentration. Furthermore, the onset and degree of aggregation vary considerably between the samples. Aggregation can start significantly before (e.g. P001) or after (e.g. P006) the midpoint of unfolding. Furthermore, the aggregate sizes vary between sizes below 10 nm (e.g. P016) and sizes of several μM (e.g. P007). We also followed the degree of re-folding by cooling the samples down and found that most samples (except P006 and P017) show no re-folding.

Next, we extended these measurements by analysing samples at different denaturant concentrations, and performing a temperature ramp; examples are shown in Figure 5.2 b and e, where the fluorescence ratio (350 nm/330 nm) and the DLS size distributions are shown. As expected, the proteins become increasingly destabilised at higher temperatures. Interestingly, we find that significant aggregation is only observed in the absence of urea, as well as for the 1-2 lowest urea concentrations. This information allowed us to perform a global fit to a model of the temperature-dependent IgLC thermodynamic stability where we excluded the samples where aggregation was observed. Details of the modelling, which was performed directly on the fluorescence intensity rather than the ratio, can be found in the methods section. All the global fits can be found in supplementary figure 5.18. While this analysis allows to define the stability at any temperature in the measured interval, see Figure 5.2 c and f, we report only the folding free energy, ΔG, at 37 °C as a measure for the protein stability in table 5.2.

5.4.3 Effect of reducing conditions on the light chain proteins

Based on the rapid emergence of the aggregates formed upon thermal unfolding, it seems likely that these are disordered, amorphous aggregates. However, in our previous study we had observed the formation of amyloid fibrils by these IgLCs under some conditions, despite the fact that

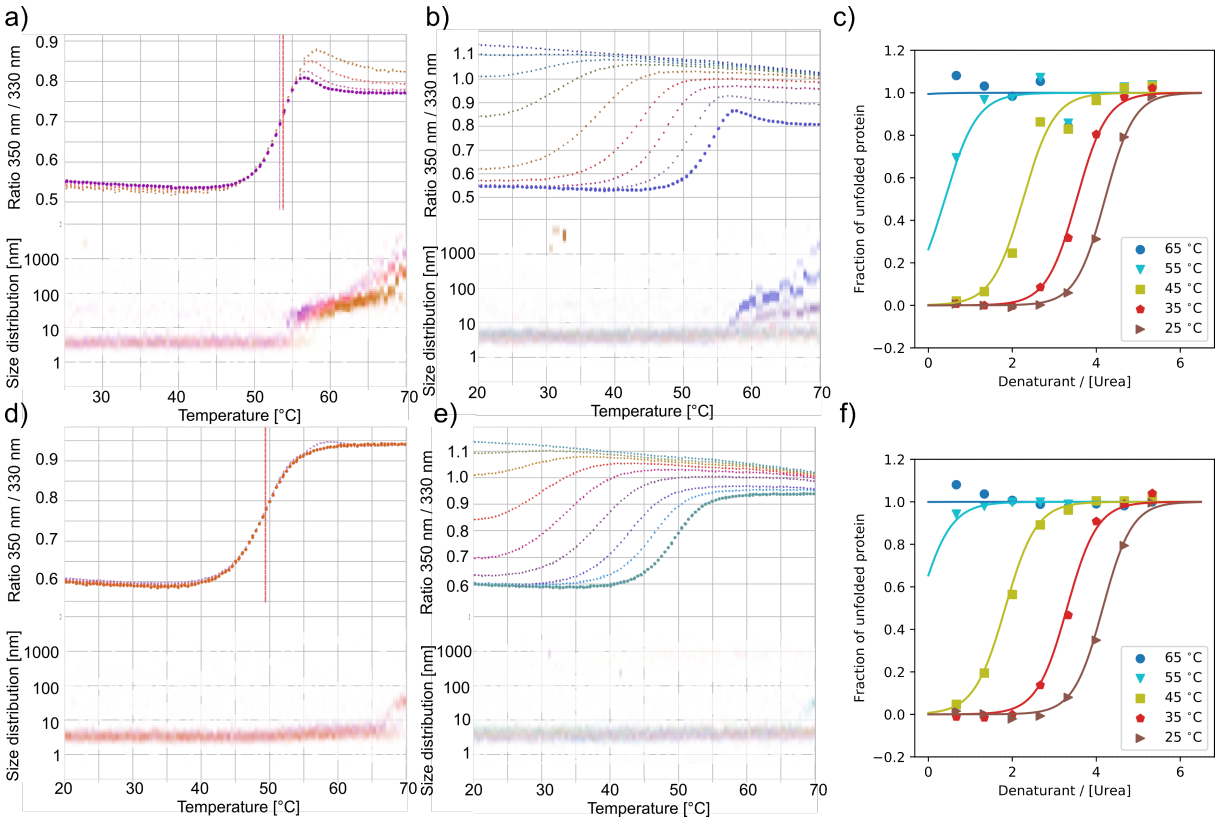

Figure 5.2: Differential scanning fluorimetry and dynamic light scattering of IgLCs. The principle of the experiment is illustrated with two samples, P007 (Panels a,b,c) and P017 (d,e,f). Experimental details can be found in the methods section. a),d) Thermal unfolding and aggregation at different protein concentrations. b),e) Thermal unfolding at different concentrations of urea. c),f) fractions of unfolded protein as a function of urea concentration (0 to 5.36 M in 8 steps) at different temperatures. The fits to the raw data can be found in supplementary figure 5.18

these samples stem from patients that did not have confirmed LC amyloidosis in most cases. We therefore set out to investigate this phenomenon systematically and in more depth. The light chain monomer solutions are highly stable at neutral pH at room temperature and at 4 °C, which was confirmed by SDS-PAGE and sedimentation velocity experiments after incubation over a number of days (data not shown). Hence we investigated the aggregation behaviour of the LCs under native-like conditions by incubating the samples in 30 mM Tris-HCl, pH 7.4 at 37 °C under permanent shaking in the presence of the fluorescent, amyloid specific dye Thioflavin-T (ThT). We could not observe any positive ThT-signal (supplementary figure 5.20), which is in agreement with published studies [244, 267].

Since previous studies showed a possible aggregation inducing effect on light chain proteins [267, 498], we examined the influence of reducing conditions (7 mM TCEP) on the aggregation behaviour by incubating different monomer concentrations (5 µM, 35 µM and 100 µM) at 37 °C under shaking conditions. The extracted increase of fluorescence intensities compared to the lowest signal and aggregation halftimes are shown in Figure 5.3. The halftimes correspond to the time point when the ThT intensity has reached half of the value between the initial baseline and the final plateau value and can be used as a macroscopic parameter to describe the aggregation kinetics. The halftimes are only displayed if an increase in ThT fluorescence intensity indicates amyloid fibril formation. All investigated LCs except of P001, P013 and

P020 showed ThT-positive aggregation. The aggregation time courses are qualitatively similar, and P005 displays the most rapid aggregation with halftimes of 4.01 h±0.04 h (5 µM monomer concentration), 1.96 h±0.13 h (35 µM monomer concentration) and 1.12 h±0.09 h (100 µM monomer concentration) and P016 the slowest with halftimes of 49.9 h±0.52 h (5 µM monomer concentration), 25.34 h±1.61 h (35 µM monomer concentration) and 13.21 h±0.91 h (100 µM monomer concentration). We therefore see a clear concentration-dependence of the aggregation kinetics, as expected for a nucleated polymerisation process, such as amyloid fibril formation. The observed fluorescence signal at the end of the experiment of the samples with 5 µM initial monomer concentration is quite weak, suggesting that only modest quantities of fibrils are formed at this low concentration. The time courses of the aggregation did not present the typical sigmoidal shape of unseeded amyloid fibril formation. No significant lag time was observed, and the ThT-signal decreases briefly in the beginning prior to the subsequent substantial increase. The initial decrease in signal can be explained to some extent by the influence of the increase in temperature on the fluorescence, when the multiwell plate is brought from room temperature to the temperature of the experiment. However in some cases the initial decrease lasts several hours and cannot fully be explained by temperature effects. The relative increase in ThT signal was derived by comparing the fluorescence intensities between the lowest and highest values of the time course. The three replicate samples per condition were combined after the aggregation experiment and the soluble protein concentration was determined. P006, P016 and P017 were found to not having fully converted into aggregates, even though a plateau value in fluorescence was reached. AFM imaging confirmed a mixture of amorphous and fibril-like structures in the ThT-positive samples. In the LCs which showed no ThT-positive aggregation (P001, P013 and P020), the protein was nevertheless found to have aggregated almost completely and to have formed large, amorphous aggregates, which are even visible by eye.

The aggregation kinetics of ThT-negative aggregates can be monitored by dynamic light scattering (DLS, Figure 5.3) and AUC sedimentation velocity experiments. While DLS allows the emergence of aggregates to be determined at high sensitivity, AUC allows to follow the change in relative populations between dimer and monomer through the time dependence of the c(s) distribution. The dimeric P001 appears to be stable over the the 15 h incubation, but monomerization can be followed using the weight average $s_{20,w}$ (Figure 5.3 D). The sedimentation velocity experiments moreover provided evidence for an additional fragmentation of the proteins, which is, however, distinctly slower than at acidic pH values as described below (supplementary figure 5.22). The secondary structure of the native LCs is dominated by β-sheet secondary structures. The amount of β-sheet structure is reduced over time when the LCs are incubated under reducing conditions. The formation of amorphous aggregates can not be distinguished from the ThT-positive aggregation with the aids of CD-spectroscopy and their analysis with BeStSel [**?**] (supplementary figure 5.21). The CD-spectra were measured with samples which were incubated in phosphate buffer, because Tris-HCl is not transparent below 230 nm, hence we checked the comparability of aggregation behaviour under both buffer conditions for P006 as an example (supplementary figure 5.20 B).

5.4.4 LC aggregation at acidic pH values

In our previous study we found that some of the investigated light chains formed amyloid fibrils at mildly acidic pH values (pH 4). These aggregation experiments were conducted in non-binding surface plates under mild mechanical agitation [17]. As we detected a strong influence of the nature of the surface on the aggregation kinetics, particularly at acidic pH values, we examined the aggregation behaviour of the selected light chains at pH 2, pH 3 and pH 4 in high-binding

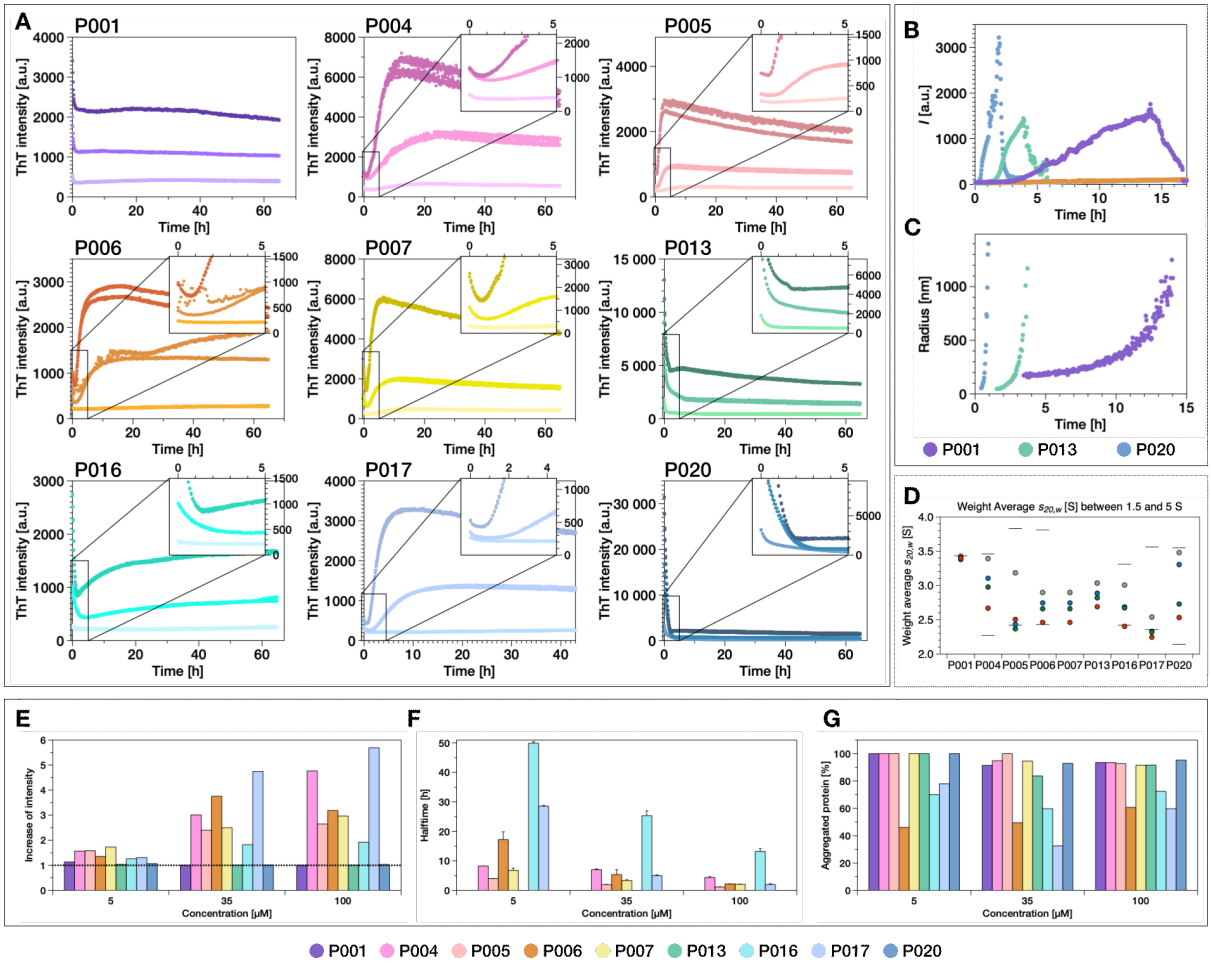

Figure 5.3: (A) ThT fluorescence aggregation assay of the LC samples in the presence of 7 mM TCEP at pH 7.4 measured in high-binding surface plate under agitation conditions. The different colour shades indicate the different monomer concentrations: light: 5 µM ; intermediate: 35 µM ; darK: 100 µM . (B)(C) Aggregation assays of P001, P013 and P020 (35 µM) in the presence of 7 mM TCEP under quiescent conditions monitored by light scattering. (B) Time evolution of the averaged total scattered intensity I and (C) of the mean hydrodynamic radius R. (D) Weight average $s_{20,\,w}$ of the c(s) distribution between 1.5 S and 5 S. The higher line (approximately 3.5 S) represents the s-value of the dimer determined in the absence of TCEP, the lower line (approximately 2.4 S) represents the s-value of the monomer. The average s-value was determined between 1.5 S and 5 S for the samples without TCEP (grey), after 75 min (blue), 5 h (green) and 15 h (red) incubation with 7 mM TCEP. Overview of the effect of TCEP on LC aggregation assayed by (E) increase of ThT fluorescence intensity compared to the lowest signal, (F) the halftime of the aggregation and (G) relative fraction of aggregated protein determined by measuring the remaining soluble content after centrifuging the endproduct of the aggregation reactions. The three replicated per condition were combined before centrifugation. The halftimes are only displayed, if any fibril formation is detected by an increase in ThT fluoresence intensity.

plates (Figure 5.4). All samples displayed an increase in ThT fluorescence intensity, except of P001 and P017 at pH 4, but the relative increase in the fluorescence intensity differs significantly between the samples. The fastest aggregation kinetics can be detected at pH 3. When the aggregation experiment was conducted in a non-binding surface plate (in the presence of glass beads and under agitation conditions) only some of the IgLCs featured ThT-positive aggregation (data not shown). P013 formed fibrils in a non-binding surface plate at all pH conditions (pH 2-pH 4), P005 at pH 4 and pH 3, P001 only at pH 3 and P020 at pH 2. In figure 5.4G, AFM height

images of products from the aggregation experiment at pH 2 are shown. The detected amyloid fibrils appeared very differently in the different samples: as mature short fibrils (P004), as mature long fibrils, which are associated with amorphous aggregates (P006), as a mixture of mature and single-stranded fibrils (P005) or as mainly single-stranded and protofibrils (P013, P020). We found no correlation between the time scale of the aggregation and the appearance of the fibrils.

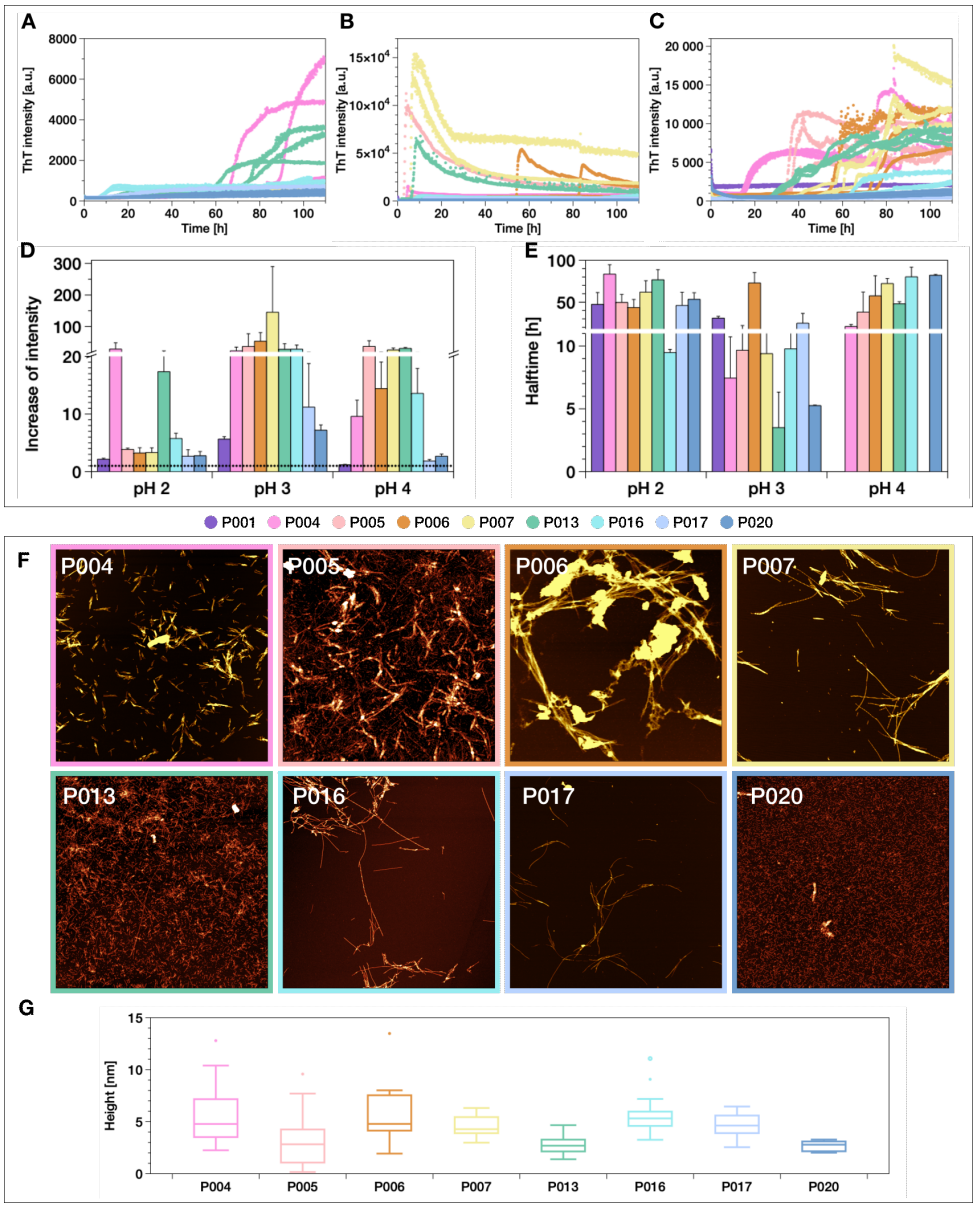

Figure 5.4: ThT fluorescence aggregation assay of the LC samples at (A) pH 2, (B) pH 3 and (C) pH 4 monitored in high-binding plates in the presence of glass beads under conditions of mechanical agitation (top). The aggregation kinetics are analysed by the (D) increase of intensity and (E) aggregation halftime. (F) AFM-height-images of LC samples after aggregation at pH 2. The image scale is 5 x 5 m. The colour range represents the height from -2 to 15 nm, (G) distribution of the fibril height in nm.

Since the aggregation at pH 3 is the most rapid we examined the aggregation behaviour of the LCs at different monomer concentrations (5 µM, 35 µM and 100 µM) under this pH condition. The plate was shaken in the absence of glass beads. Apart from P001, whose aggregation had no lag time, the aggregation kinetics followed the typical amyloid formation reaction at first glance. But solely P004, P006 (35 µM and 100 µM), P007 and P017 displayed a lag phase, a rapid growth

phase and a steady-state phase. The lag phase can last for several hours, but as soon as the growth phase started, the aggregation reaction was very fast. After reaching the steady-state phase, the ThT-signal was found to decrease in the case of the samples at 100 µM concentrations. This decrease can be explained by the formation of insoluble, big aggregates, which sediment and disappear out of the focus of detection. The relative increase in fluorescence intensity was found to be very substantial in some cases; for example for P004 and P007 the intensity increased by a factor of over 1000. P004 aggregated as one of the fastest at the concentrations of 35 µM and 100 µM, however showed a twice longer halftime at 5 µM. The aggregation process of the remaining samples (P005, P013, P016 and P020) was found to be more complex, because it features a bi- or triphasic behaviour.

Interestingly, compared to the aggregation behaviour under reducing conditions, the supernatant still contained a significant amount of soluble protein after the aggregation assays. We tested the influence of glass beads and preformed fibrils (seeds) on the aggregation kinetics of P016 in more detail as an example (supplementary figure 5.23). We pre-incubated the protein (35 µM monomer concentration) at pH 3 and pH 4 in a high-binding surface plate and added glass beads after 24 h or preformed fibrils after 6 h. The glass beads which were added after the pre-incubation had no accelerating effect on the amyloid formation compared to glass beads added at the start of the aggregation assay (pH 4) or merely shaking (pH 3). We found that the amyloid fibril formation could be seeded by adding pre-formed fibrils (seeds). However the amyloid kinetics were not typical for strongly seeding experiments, especially at pH 4. At this condition, even though the seeds accelerated the fibril formation significantly, a lag time was still observed. If the proteins were pre-incubated at this mildly acidic pH, on the other hand, rapid aggregation was observed from the moment of addition of the seeds at pH 3.

We used as seeds both fibrils which had been prepared in a high-binding surface plate in the presence of glass beads, as well as fibrils which had been prepared in the same volume in an 2 ml Eppendorf tube with glass beads. The presence of fibrils were confirmed using atomic force microscopy. A selection of AFM images from fibrils prepared in a plate and an Eppendorf tube can be found in supplementary figure 5.24. Although the presence could be validated, the total ThT-fluorescence intensity was lower if seeds prepared in an Eppendorf tube were used.

The influence of the pre-incubation of the monomer at acidic pH suggests a possible modification that the monomeric proteins might undergo under these conditions. We therefore set out to probe whether the proteins can undergo fragmentation. For this purpose the samples were incubated in an Eppendorf tube at 37 °C under quiescent conditions, in order to slow down as much as possible the formation of amyloid fibrils. The samples were analysed at different time points using SDS-PAGE and the microfluidic diffusional sizing [408] device FluidityOne (Figure 5.6). The time course of the relative proportions of native LCs (monomer and dimer combined) was determined by SDS-PAGE. Incubation at pH 3 was found to have a strong effect on the size of the monomeric protein; already after one hour incubation, almost no full length protein was found to remain. Only P001, which occurs only in a dimeric form, partly resisted acid induced degradation over several hours. At pH 4 the samples were found to be more resistant, but after an incubation of 24 h the LCs were found to be fragmented to between 50 and 100 percent. The fragmentation at pH 2 was found to be faster than at pH 4, but slower than at pH 3. P013 and particular P001 were found to be comparatively more resistant against the pH 2 fragmentation. The fragmentation of the LCs at pH 3 and pH 4 could also be observed with the FluidityOne instrument, which allows to measure the average radius of the samples and the protein concentration. The rapid fragmentation of the light chains at pH 3 was also

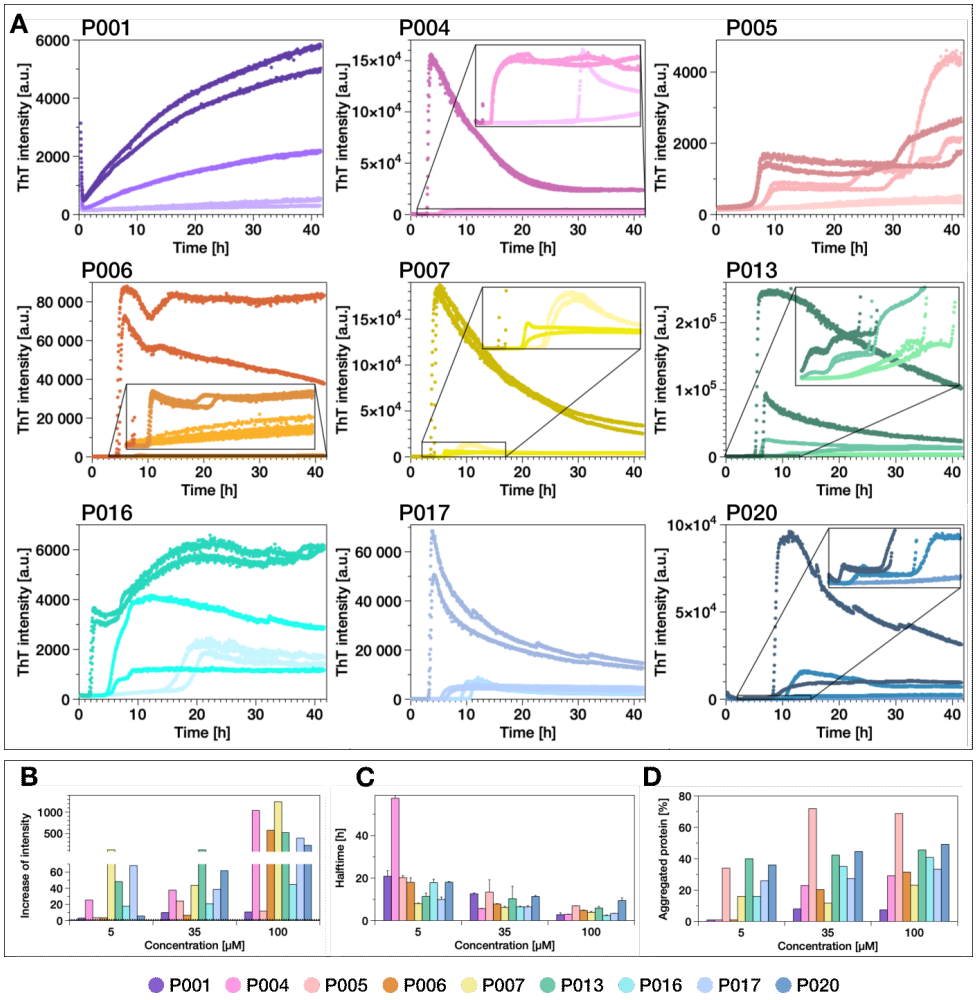

Figure 5.5: (A) ThT fluorescence aggregation assay of the LC samples at pH 3 in the presence of glass beads measured in high-binding surface plate under agitation conditions. The different colour shades indicate the different monomer concentrations: light: 5 µM intermediate: 35 µM; darK: 100 µM. Overview of the effect of pH 3 on LC aggregation assayed by (B) increase of ThT fluorescence intensity, (C) the halftime of the aggregation and (D) relative fraction of aggregated protein determined by measuring the remaining soluble content after centrifuging the end product of the aggregation reactions. The three replicates per condition were combined before centrifugation.

visible in the FluidityOne, the radius decreased in the first hour by about 1 nm and the LC samples have an average radius of around 1 nm after 160 h, which comply approximately to the average radius at pH 4 after the incubation duration. P013 appeared stable at pH 4, but the measured concentration displayed a strong decrease, which can possibly be explained through the formation of aggregates. Both amorphous aggregates and amyloid fibrils are not detected in the same quantitative manner by the FluidityOne instrument, because large aggregates may not be able to enter the microfluidic channels. Furthermore, aggregates may not be as efficiently stained by the fluorescent modification used for protein quantification in the FluidityOne (Figure 5.6 B).

Such an efficient fragmentation of the IgLCs at mildly acidic pH and room temperature cannot easily be explained by hydrolysis of the polypeptide backbone. We therefore investigated the results of our mass spectrometric analysis REF of the patient-derived samples for the possible presence of proteases. The mass spectrometric data indeed revealed the presence of different cathepsins in the LC samples purified from patients urine. The list of cathepsins detected in

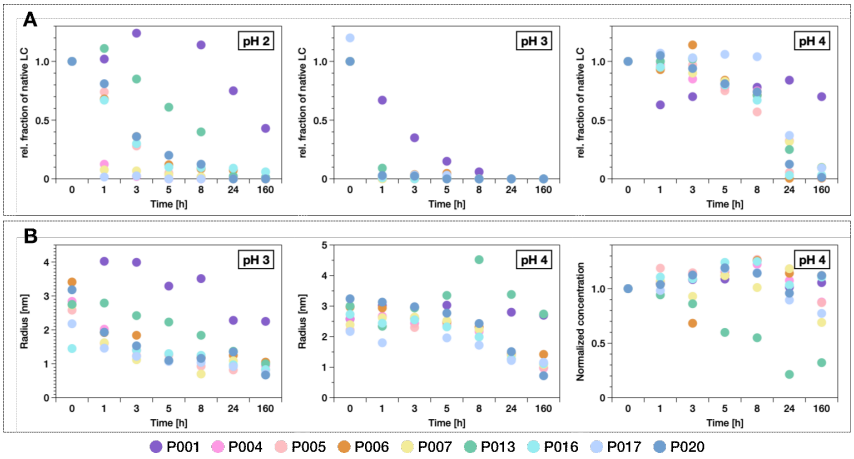

Figure 5.6: The influence of acidic pH (left: pH 2, middle: pH 3, right: pH 4) on the LC samples. (A) The fraction of native protein (monomer and dimer combined) at different incubation times determined by SDS-PAGE and (B) the radius in nm and the normalized concentration measured by FluidityOne.

the samples can be found in table 5.1. Cathepsins are predominantly endopeptidases, which are located intracellularly in endolysosomal vesicles, but can furthermore be found in the extracellular space. They are important regulators and signalling molecules of various biological processes and are involved in the production of inflammatory cytokines and enhancement of tumour development [525, 526]. The activity of cysteine cathepsins are increased at slightly acidic pH values and are mostly unstable at neutral pH [526, 527].

Table 5.1: List of different cathepsins which were found in the samples by means of their MS/MS count. The MS/MS count represents the number of MS/MS spectra leading to an identified protein. The black numbers indicate an confident identification of the protein. Proteins, which are only found with one peptide, are not valid (number coloured in grey).

Protease	P001	P004	P005	P006	P016	P017	P020
Cathepsin Z	7	6	10	12	9	9	7
Cathepsin D	3	2	11	6	2	13	8
Cathepsin B	1	1	7	3	5	7	8
Cathepsin L2	0	0	8	1	7	0	4
Pro-Cathepsin H	0	0	1	1	0	0	1
Pro-Cathepsin L	0	0	1	1	0	0	1
Catepsin S	0	0	0	0	0	0	0

In order to probe whether the fragmentation of the IgLCs at acidic pH values was caused by the present cathepsins, we incubated the samples with protease inhibitors. As inhibitors we choose E-64 and pepstatin A. E-64 (trans-Epoxysuccinyl-L-leucylamido(4-guanidino)butane) is an active-site directed, irreversible inhibitor of cysteine proteases and is known to inhibit cathepsin B, cathepsin L, cathepsin H and cathepsin Z [528, 529, 530, 531, 532]. Pepstatin A (isocaleryl-L-valyl-L-valyl-4-amino-3-hydroxy-6-methylheptanoyl-L-alanyl-4-amino-3-hydroxy-6-methylheptanoic acid) is a very selective and potent inhibitor of cathepsin D, which is one of the major aspartyl endopeptidases in mammalian cells and has an pH-optimum at a pH of 3.5-5 [533]. Cathepsin D was the second most frequently cathepsin present in the samples (in P017 it had the highest fraction) [534].

The LCs (35 µM monomer concentration) were incubated at pH 3 in the presence of 10 µM pepstatin A and E-64 in a high-binding plate and the potential aggregation was followed by the increase of ThT-fluorescence intensity (Figure 5.7). With the exception of P005 and P006, all samples showed an increase in ThT-signal. However, the ThT intensity was found to only increase by a factor of approximately two, which is almost negligible compared to the increase observed in the absence of protease inhibitor. As control, pepstatin A and E-64 alone and in combination did not display an increase in ThT signal.

AFM-imaging of the samples displayed small, globular oligomeric structures, very different from the mature aggregates observed to form in the absence of the protease inhibitors. P006 and P016, which did not or slowly aggregate, showed slightly elongated aggregates, which may be pre-fibrillar structures. While the incubation of the samples at pH 3 led to a complete fragmentation of the native LCs, the presence of the inhibitors was found to maintain the IgLCs in their original size, even after incubation for 50 h (Figure 5.7 C).

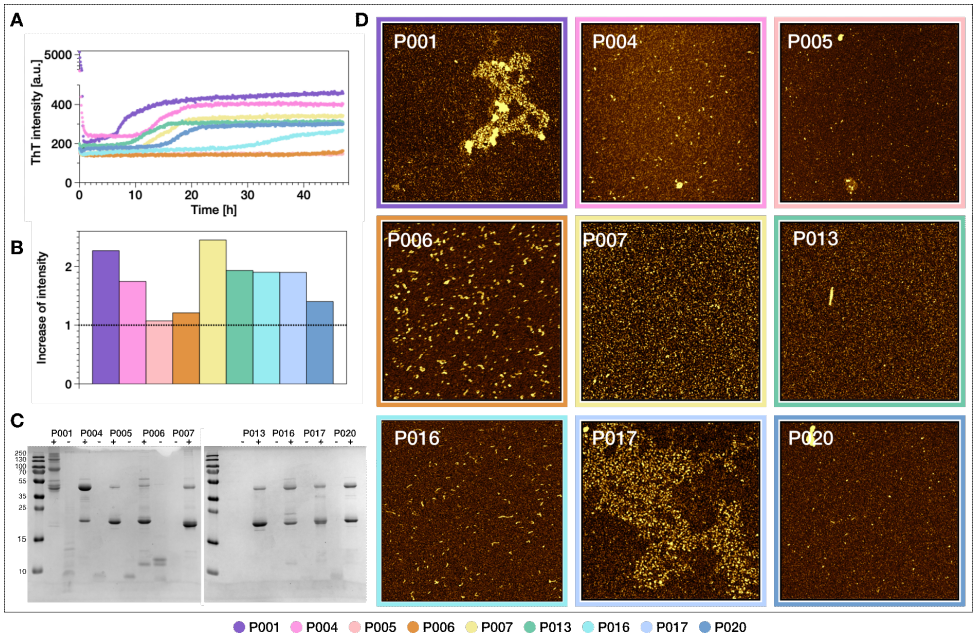

Figure 5.7: (A) ThT-fluorescence aggregation assay of the LC samples at pH 3 in the presence of 10 µM pepstatin A and 10 µM E-64 measured in a high-binding surface plate at 37 °C and (B) the extracted factor of the intensity increase. (C) The light chains were analysed by non-reducing SDS-PAGE after incubation for 50 h in presence of the inhibitors (+) and without (-). (D) AFM-height-images of the products of the aggregation assay after 50 h. The image scale is 2 x 2 μM. The colour range represents the height from -1 to 5 nm.

The influence of the two different protease inhibitors was further examined at pH 3 and pH 4 for the aggregation of P005 and P016 under agitation conditions. The light chains were incubated with 10 µM or 1 µM both inhibitors or with 1 µM of only one inhibitor. E-64 alone showed no effect on the aggregation kinetics of P005, but prolonged the aggregation of P016 at pH 3. Even though there was only a weak increase in ThT signal, we could confirm the presence of fibrillar structures in P016 at pH 3 in the presence of the inhibitors. In addition to the fibrils, also some small elongated oligomers could be seen in the AFM images of P016 incubated with inhibitor. The fibrils were twisted, even though the fibrils of P016 at pH 3 usually displayed no twist. The period of the twist were not equivalent to that of the fibrils formed at pH 2 and pH 4 in the absence of protease inhibitor.

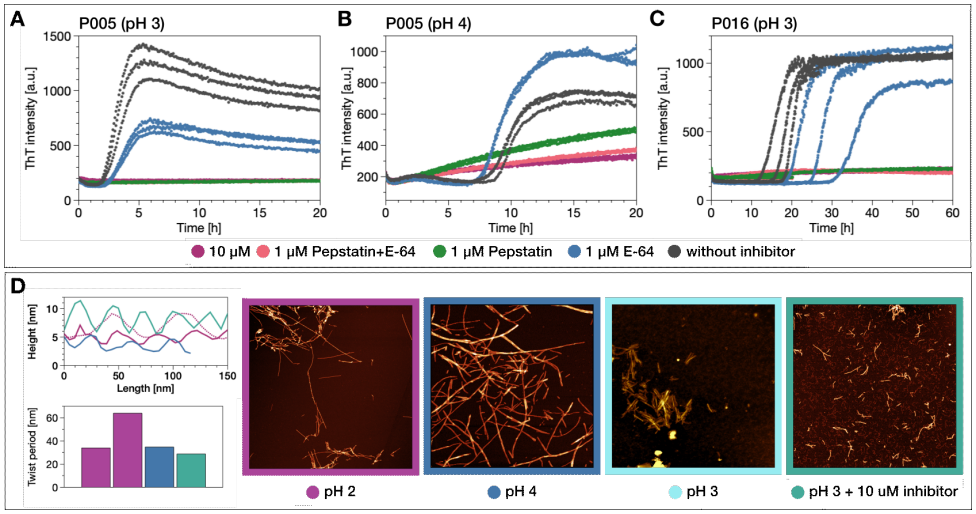

Figure 5.8: Influence of two different protease inhibitors pepstatin A and E-64 on the aggregation kinetics of the samples P005 at (A) pH 3 and (B) pH 4 and (C) P016 at pH 3 monitored in a high-binding plate under agitation conditions. (D) AFM-height-images of aggregated P016 at pH 2 (purple), pH 4 (blue), pH 3 (cyan) and pH 3 in presence of 10 µM pepstatin A and E-64 after 70 h and the extracted height profiles of different fibrils (top left) and the width of the twist (bottom left). Fibrils at pH 3 do not display any twist. The image scale is 5 x 5 μM. The colour range represents the height from -2 to 15 nm.

Finally, we tested whether the fibrils which form from the fragmented light chains can induce the aggregation of the intact light chain. Therefore we incubated the proteins at 55 °C, where the IgLCs are partly to fully unfolded (see supplementary figure 5.16) and added seeds which were produced at pH 3 or pH 4 (supplementary figure 5.26). Except for P006 and P017, no increase in ThT fluorescence intensity was observed.

5.5. Discussion

The problem of rationalising the aggregation behaviour of immunoglobulin light chain is a formidable one, given the fact that every single patient will present a light chain with a different amino acid sequence. In particular the question as to which factors determine whether a given light chain forms amyloid fibrils or amorphous aggregates has been extensively studied in recent years []. Various biochemical and biophysical properties, such as thermodynamic stability [257, 258, 264], propensity to form dimers [272, 498], ability to refold [264] or proteolytic digestibility as a proxy for protein dynamics [] have been proposed to correlate with one or the other type of aggregate formation. In this study, we have performed an in depth characterisation of these and additional factors for 9 patient-derived light chains. A complete overview over the data can be found in table 5.2. None of these 9 samples stems from an amyloidosis patient, and yet the aforementioned biophysical and biochemical properties span the full range of dimerisation, thermal and chemical stability, refolding, digestability etc. In addition to these parameters, we also characterise the overall aggregation behaviour, induced by heat, reducing conditions and low pH. Overall, our ThAgg-Fip approach yields a unique thermodynamic and aggregation fingerprint of each of the light chains. While different patient-derived light chain may appear similar if characterised only in a single dimension, such as thermal stability, a multiparametric investigation, such as the one we present here, highlights the uniqueness of each light chain. However, despite this uniqueness in overall behaviour, we made the remarkable discovery that

Table 5.2: Overview over the thermodynamic and aggregation fingerprints of the IgLCs of this study. *m-value fixed for all samples **different m-value allowed in fit ***Only one population with intermediate S-value detected

	P001	P004	P005	P006	P007	P013	P016	P017	P020
T_m-DSF (lowest conc.)	62.8	54.3	51	50.3	53.9	52.9	54.3	49.3	50.3
T_m - DSF (highest conc.)	62.5	53.7	49.9	51.1	53.4	51.9	54.3	49.5	50.5
T_m - DSC (Chapter 3)	64.6	58.5	51.2	50.4	55.4	52.2	56.8	51.7	53.5
T_{agg} (lowest conc.)	55	53.3	53.8	55	55.9	51.3	n/a	~65	52.2
T_{agg} (highest conc.)	50.5	50.8	49.6	53.7	53	47.6	58.9	~51	48
Agg size range (nm)	>1000	>1000	>1000	<30	~1000	<30	<10	<50	>1000
Refold DSF	small	small	small	large	small	small	medium	large	small
Refold % DSC	0	0.18	0.36	0.68	0.33	0.38	0.41	0.70	0.22
ΔG [kJ/mol] at 37°C	26.3±1.5	25.3±0.4	20.8±2.1	20.8±0.8	23.7±0.6	21.2±0.7	10.0±0.7	21.8±1.1	20.2±0.5
m-value	7.1*	7.1*	7.1*	7.1*	7.1*	7.1*	2.3±0.5**	7.1*	7.1*
digestability by trypsin (Chaper 3)	0.1	1	0.7	0.24	1	1	0.17	0.98	18
dimerisation SDS-PAGE	0.96	0.71	0.43	0.3	0.32	0.36	0.49	0.4	0.52
dimerisation MS	1	0.97	0.35	0.07	n/a	n/a	0.9	0.3	0.65
dimerisation AUC	1	0.94	0.55	0.1	***	***	0.72	0.15	0.91
TCEP induced aggreg.	x	✓	✓	✓	✓	x	✓	✓	x
acid induced aggreg.	✓	✓	✓	✓	✓	✓	✓	✓	✓

every one of the IgLCs of our study can form amyloid fibrils under physiologically relevant conditions. While the physiological relevance of strongly reducing conditions is debatable, mildly acidic pH values are physiologically relevant and can be encountered by IgLCs in the kidney due to lysosomal proteolysis [380] and a decreased pH with a progressive chronic kidney disease (CKD) [535]. Low pH values have also previously been reported to facilitate IgLC aggregation [264, 536]. We were able to confirm the formation of amyloid fibrils within all investigated LCs, using ThT-fluorescence assays and AFM. Furthermore, we were able to identify the presence of proteases, most notably cathepsins, as decisive for amyloid fibril formation, because of their ability to fragment the full-length protein under physiological relevant mildly acidic conditions.

It has been reported before that fragments of LCs, particularly of the variable domains are able to form amyloid fibrils [241], and it has even been proposed that the cleavage of the C-terminal is important to initiate the aggregation process [537]. It has, however, also been proposed that proteolytic cleavage may occur after fibril formation [238]. Similarly, reducing conditions can also in most, but not all, cases facilitate the formation of amyloid fibrils. The finding that all our investigated samples are able to form amyloid fibrils is ever more remarkable, as none of our IgLCs appear to form amyloid fibrils in the patient. In order to understand this discrepancy, we determined the amino acid sequences of all 9 samples investigated in this work, and in addition the sequence of the single IgLC from an amyloidosis patient (P011) in our larger data set [17]. The amino acid sequences of the light chain proteins was determined by a combination of top-down and bottom-up proteomics with specific data analysis for patient-derived light chains. The development and details of this workflow are the subject of a separate publication (Chapter 4), where we also discuss some of the specific features of the individual IgLCs. An alignments of the full length amino acid sequences of the two λ light chains P001 and P011 and of the eight κ light chains P004, P005, P006, P007, P013, P016, P017 and P020 are presented in the supplementary materials (supplementary figures 5.11 and 5.12). The constant regions of the κ light chains are identical, apart from P013, which has a valine mutated to a leucine. An alignment of only the variable regions can be found in Figure 5.9.

The sequences contain five cysteine residues which stabilise the monomers by two disulfide bridges between C23 and C87-89 and between C133-C135 and C193-195. The fifth cysteine is cysteinylated in the monomer and is responsible for the disulfide bridge in the dimer. However P001 contains two additional adjacent cysteins at position 99 and 100. Besides the displayed sequence we detected an additional LC proteoform in two samples (P004 and P017), and we were able to determine the sequence of the second isoform in P004, which contains two homodimers and one heterodimer, while P017 contains only one homodimer and one heterodimer. By means of the intact mass analysis by mass spectrometry we detected in the sample P011, which stems from the only confirmed amyloidosis patient in our cohort, two other proteins with a similar mass of 20,9 and 21.1 kDa at high abundance in addition to the light chain. This contamination prevented a detailed and accurate biophysical analysis of this sample. Therefore we excluded P011 from the further experiments and analysed solely its amino acid sequence. We used the international immunogenetics information system (IMGT) to search for the germline sequences of the investigated light chains. Both lambda LCs have a different origin; P001 from IGLV2-11 and P011 from IGLV1-40, which explains the large differences between the sequences (Figure 5.9 A). P001 is very similar to the germline sequence; it contains only three mutations: from a serine and an asparagine to a threonine and an additional threonine to alanine mutation.

The kappa LCs origin from four different germline sequences. P005 from IGKV1-39, P004 from IGKV3-20, P007 P013 and P020 from IGKV1-5 and P006, P016 and P017 from IGKV1-33 (Figure 5.9 B). The secondary structure of light chains is dominated by β-strands. In order to be able to judge a possible influence of the mutations on the native structures, we searched the pdb for three-dimensional structures of the variable regions of the appropriate germline sequence and highlighted the positions of the mutated amino acids (Figure 5.9 C). The sequence changes of P004 and P005 could have a significant impact on the structure, because they affect different βstrand regions. The sequence changes identified for P013, P020, P016 and P017, on the other hand, are mainly in the loop regions. In future work we will attempt to crystallize the patient-derived light chains in order to elucidate the impact of the mutations on protein structure. A previous study applied computational predictions using ZipperDB [483] to identify so called steric zippers that drive the assembly of amyloid fibrils in IgLCs [472]. Our determination of the

amino acid sequences enabled us to apply various bioinformatic prediction tools with the aim to rationalise the universal ability of our samples to form amyloid fibrils.

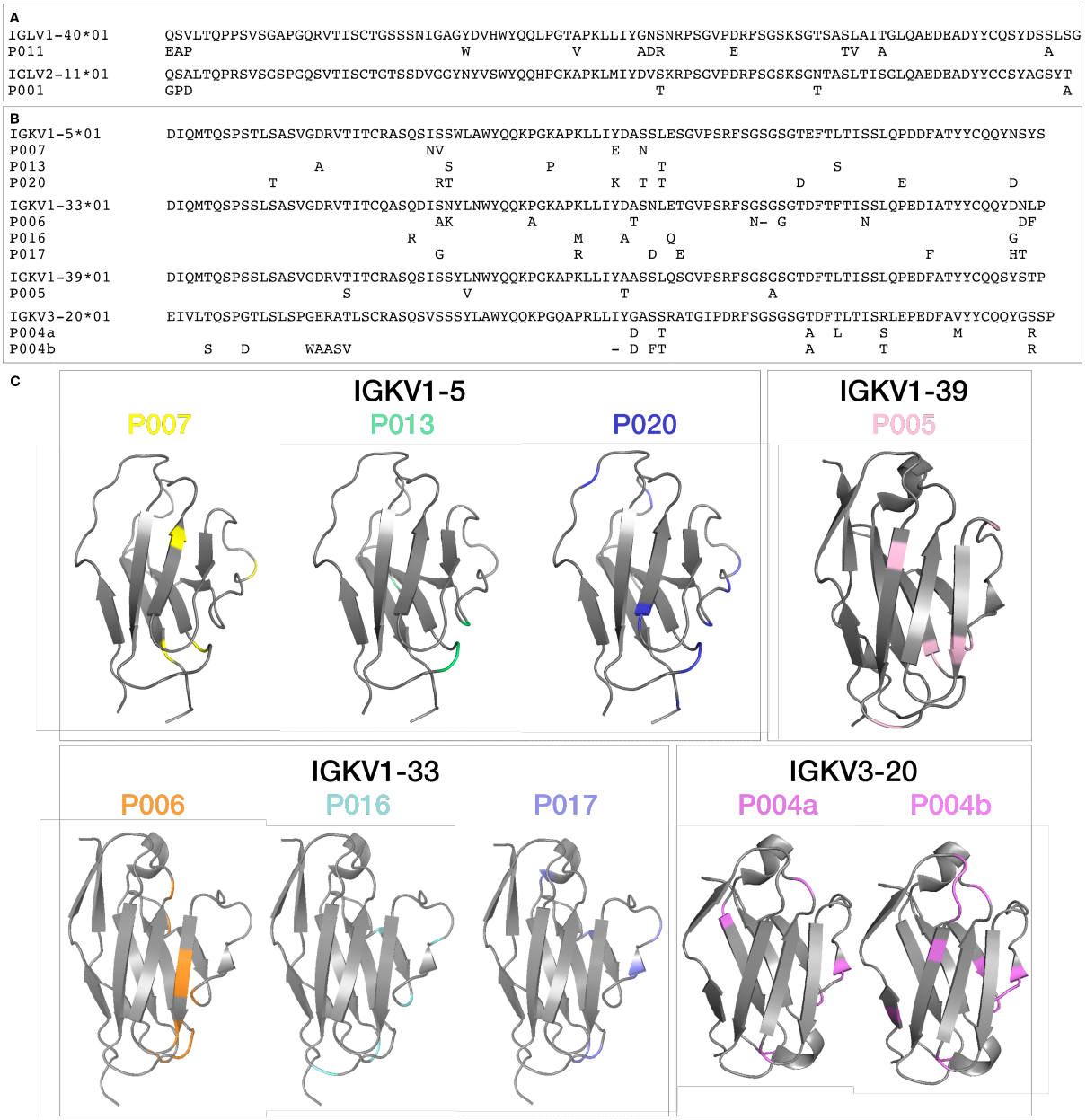

Figure 5.9: Sequences of the (A) λ and (B) κ variable domain of the germline sequences. The mutations in the sequences of the LC samples compared to the corresponding germline sequence are labelled. Mutations between isoleucine and leucine are not indicated due to the uncertainty of sequencing.(C) Three-dimensional structure of the variable regions of the κ germline sequences from the RSCB protein data bank (5I1C, 3CDF, 3UPA) and UniProtKB (P01602) visualized with PyMOL 2.4. (Schrödinger). The mutated amino acids in the investigated LCs are highlighted in colour.

We tested the amyloid propensity of the sequences with several freely available computational algorithms such as ZipperDB [483], Waltz [486], Tango [469] and Pasta [489] (supplementary figures 5.27 , 5.28, 5.29 and 5.30). Tango revealed the largest differences within the sequences, whereas pasta displayed no amyloid potential in the variable domain. We also determined the aggregation propensities of a range of κ and λ sequences from different germlines selected from AL-Base [490] as a representative collection. The sequences were categorized depending on

whether the patient was suffering from AL-Amyloidosis or MM. The algorithm does not identify any clear distinctions between amyloidogenic and non-amyloid forming light chains.

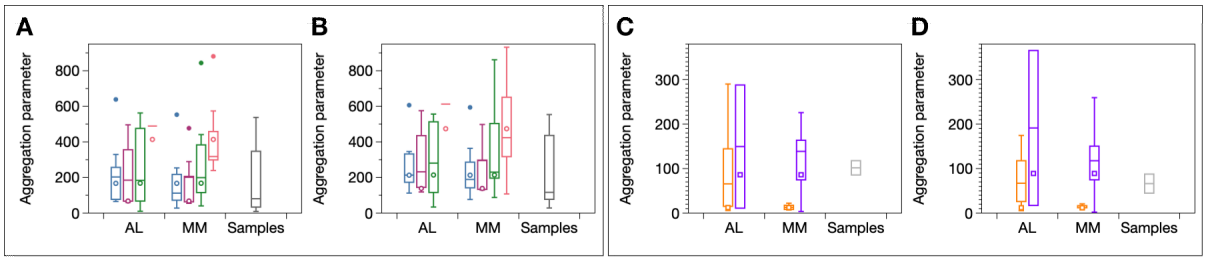

Figure 5.10: Variable kappa region sequences were analyzed with Tango at (A) pH 7 and pH 3 (B). The sequences, which originate from different germline sequences were selected from AL-Base and were categorized whether the patient was suffering from AL-Amyloidosis or MM. IGKV1-5 (blue) AL n=10, MM n=9; IGKV1-33 (violet) AL n=8, MM n=10; IGKV1-39 (green) AL n=10, MM n=10; IGKV3-20 (orange) AL n=7, MM n=10. Variable lambda region sequences were analyzed with Tango at (C) pH 7 and pH 3 (D). The sequences, which originate from different germline sequences were selected from AL-Base and were categorized whether the patient was suffering from AL-Amyloidosis or MM. IGLV1-40 (orange) AL n=10, MM n=5; IGLV2-11 (violet) AL n=2, MM n=11. The not-filled circle indicates the germline sequence.

These results derived from state of the art amyloid prediction algorithms validate our findings that the origin of the differential amyloidogenicity of IgLCs in patinets is not primarily determined by their amino acid sequence. Our main discovery can therefore be summarised as all immunoglobulin light chains having a comparable intrinsic amyloidgenic potential, and the reason that only some are able to realise this potential is to be found in the complex interplay between intrinsic physical properties of the peptide and environmental conditions *in vivo*. In particular the presence and action of proteases such as cathepsins in a patient enables the deposition in the form of amyloid fibrils. This conclusion corresponds to a major paradigm shift in the field of IgLC aggregation, where the origin of *in vivo* deposition behaviour has almost exclusively been searched for in the sequence alone. Our findings might also hint towards a possible mechanism for the preferential deposition of light chains in specific organs that is often observed. The biochemical micro-environment conducive to IgLC cleavage is likely to differ both between patients, as well as in different organs within a given patient. It is also important to stress tht it may not be necessary to cleave the light chain quantitatively in order to allow the conversion into amyloid fibrils. We have provided evidence in our study that full length IgLCs can be seeded in some cases with fibrils formed under conditions that favour cleavage (see supplementary figure 5.26). While this seeding could be very inefficient, it may still be relevant over clinical time scales. In a previous study we tried to correlate the severity of kidney damage of the patients which is possibly caused by various degrees of protein deposition, with the biophysical and biochemical characteristics of the LCs [17]. In the present, significantly extended study, we employed ThAgg-fingerprinting and found that apart from the universal amyloidogenicity, every IgLC has a unique fingerprint. Our results, which show a large spread of the values of the individual parameters, render it very unlikely that a single biophysical or biochemical parameter can be found to correlate with the complex *in vivo* aggregation behaviour of IgLCs, or indeed proteins in general. The multidimensional nature of this problem requires a multiparametric approach, such as the ThAgg-Fip method we present here. We are confident that if this type of approach is applied at large scale to patient-derived samples and combined with a maximal amount of patient-derived information (disease severity, proteomics data) then modern machine

learning and AI approaches will allow us to unravel the origin and mechanisms of such protein aggregation and deposition diseases.

5.5.1 Supplementary information

```
P001      GPDLTQPRSVSGSPGQSVTLSCTGTSSDVGGYNYVSWYQQHPGKAPKLMLYDVTKRPSGVPDRFSGSKSGTTASLTLSGLQAEDEADYYCC
P011      EAPLTQPPSVSGAPGQRVTLSCTGSSSNLGAGWDVHWYQQLPGTVPKLLLYADRNRPSGVPERFSGSKSGTSATVALAGLQAEDEADYYCQ
             **** ****:*** *******:**::*.   * **** **..***:**   :******:*********:*:::*:************

P001      SYAG-LDLFVLFGGGTKLTVLGQPKAAPSVTLFPPSSEELQANKATLVCLLSDFYPQVTVAWKADSSPVKAGVETTTPSKQSNNKYAASSY
P011      SYDSALSGFYVFGTGTKVLVLGQPKANPTVTLFPPSSEELQANKATLVCLLSDFYPQVTVAWKADGSPVKAGVETTKPSKQSNNKYAASSY
          ** . *. * :** ***: ******* *:************************************.**********.**************

P001      LSLTPEQWKSHRSYSCQVTHEGSTVEKTVAPTECS
P011      LSLTPEQWKSHRSYSCQVTHEGSTVEKTVAPTECS
          **********************************
```

Figure 5.11: Full length sequence alignment of the λ light chains of our study.

```
P004a     EIVLTQSPGTLSLSPGERATLSCRASQSVSSSYLAWYQQKPGQAPRLLIYDASTRATGIPDRFSGSGSGADFLLTISSLEPEDFAMYYCQQ
P004b     EIVLSQSPDTLSLSPWAASVLSCRASQSVSSSYLAWYQQKPGQAPRL-LYDAFTRATGLPDRFSGSGSGADFTLTLSTLEPEDFAVYYCQQ
P006      DLQMTQSPSSLSASVGDRVTLTCQASQDL-AKYLNWYQQKPGKPPKLLLYDTSNLETGVPSRFSN-GGGTDFTFTLNSLQPEDLATYYCQQ
P016      DLQMTQSPSSLSASVGDRVTLTCQASRDL-SNYLNWYQQKPGKAPMLLLYAASNLQTGVPSRFSGSGSGTDFTFTLSSLQPEDLATYYCQQ
P017      DLQMTQSPSSLSASVGDRVTLTCQASQDL-GNYLNWYQQKPGKAPRLLLYDASDLEEGVPSRFSGSGSGTDFTFTLSSLQPEDFATYYCQQ
P005      DLQMTQSPSSLSASVGDRVSLTCRASESL-SSYVNWYQQKPGKAPKLLLYTASSLQSGVPPRFSGSASGTDFTLTLSSLQPEDFATYYCQQ
P013      DLQMTQSPSTLSASVGDAVTLTCRASQSL-NVWLAWYQQKPGKPPKLLLYEASNLESGVPSRFSGSGSGTEFTLTLSSLQPDDFATYYCQQ
P007      DLQMTQSPSTLSASVGDRVTLTCRASQSL-SSSLAWYQQKPGKAPKLLLYDASSLETGVPSRFSGSGSGTEFTLSLSSLQPDDFATYYCQH
P020      DLQMTQSPSTLSTSVGDRVTLTCRASQSL-RTWLAWYQQKPGKAPKLLLYKASTLETGVPSRFSGSGSGTDFTLTLSSLQPEDFATYYCQQ
          :: ::***.:** *      *:*:**..:    : *******: * * :* :     *:* ***. ..*::* :::.:*:*:*:* ****:
P004a     YGRS-PYTFGPGTKVDIKRTVAAPSVFIF-PPSDEQLKSGTASVVCLLNNFYPREAKVQWKVDNALQSGNSQESVTEQDSKDSTYSLSSTL
P004b     YGRS-PYTFGPGTKVDLKRTVAAPSVFLFFPPSDEQLKSGTASVVCLLNNFYPREAKVQWKVDNALQSGNSQESVTEQDSKDSTYSLSSTL
P006      YDDF-PLTFGPGTKVDLKRTVAAPSVFLF-PPSDEQLKSGTASVVCLLNNFYPREAKVQWKVDNALQSGNSQESVTEQDSKDSTYSLSSTL
P016      YGNL-PLTFGGGTKVELKGTVAAPSVFLF-PPSDEQLKSGTASVVCLLNNFYPREAKVQWKVDNALQSGNSQESVTEQDSKDSTYSLSSTL
P017      YHTLPPLTFGGGTKVDVKRSLAAPSVFLF-PPSDEQLKSGTASVVCLLNNFYPREAKVQWKVDNALQSGNSQESVTEQDSKDSTYSLSSTL
P005      SYST-PLTFGQGTRLELKRTVAAPSVFLF-PPSDEQLKSGTASVVCLLNNFYPREAKVQWKVDNALQSGNSQESVTEQDSKDSTYSLSSTL
P013      YNSY-PYTFGQGAKLELKRTVAAPSVFLF-PPSDEQLKSGTASVVCLLNNFYPREAKVQWKVDNALQSGNSQESVTEQDSKDSTYSLSSTL
P007      YNSY-SLTFGQGTKVELKRTVAAPSVFLF-PPSDEQLKSGTASVVCLLNNFYPREAKVQWKVDNALQSGNSQESVTEQDSKDSTYSLSSTL
P020      YNDY-SGTFGQGTKLELKRTLAAPSVFLF-PPSDEQLKSGTASVVCLLNNFYPREAKVQWKVDNALQSGNSQESVTEQDSKDSTYSLSSTL
          :      *** *:::::* ::******:* ************************************************************

P004a     TLSKADYEKHKVYACEVTHQGLSSPVTKSFNRGEC
P004b     TLSKADYEKHKVYACEVTHQGLSSPVTKSFNRGEC
P006      TLSKADYEKHKVYACEVTHQGLSSPVTKSFNRGEC
P016      TLSKADYEKHKVYACEVTHQGLSSPVTKSFNRGEC
P017      TLSKADYEKHKVYACEVTHQGLSSPVTKSFNRGEC
P005      TLSKADYEKHKVYACEVTHQGLSSPVTKSFNRGEC
P013      TLSKADYEKHKLYACEVTHQGLSSPVTKSFNRGEC
P007      TLSKADYEKHKVYACEVTHQGLSSPVTKSFNRGEC
P020      TLSKADYEKHKVYACEVTHQGLSSPVTKSFNRGEC
          ***********:**********************
```

Figure 5.12: Full length sequence alignment of the κ light chains of our study.

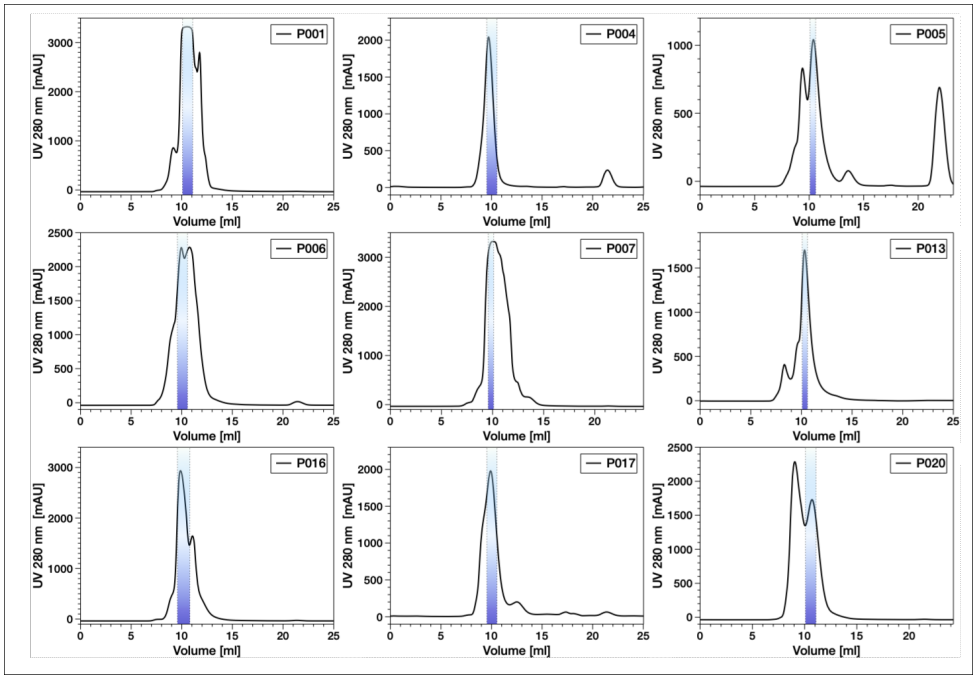

Figure 5.13: Size exclusion chromatograms of the different IgLC samples of this study. The fractions used for the remaining experiments in this study are marked in blue.

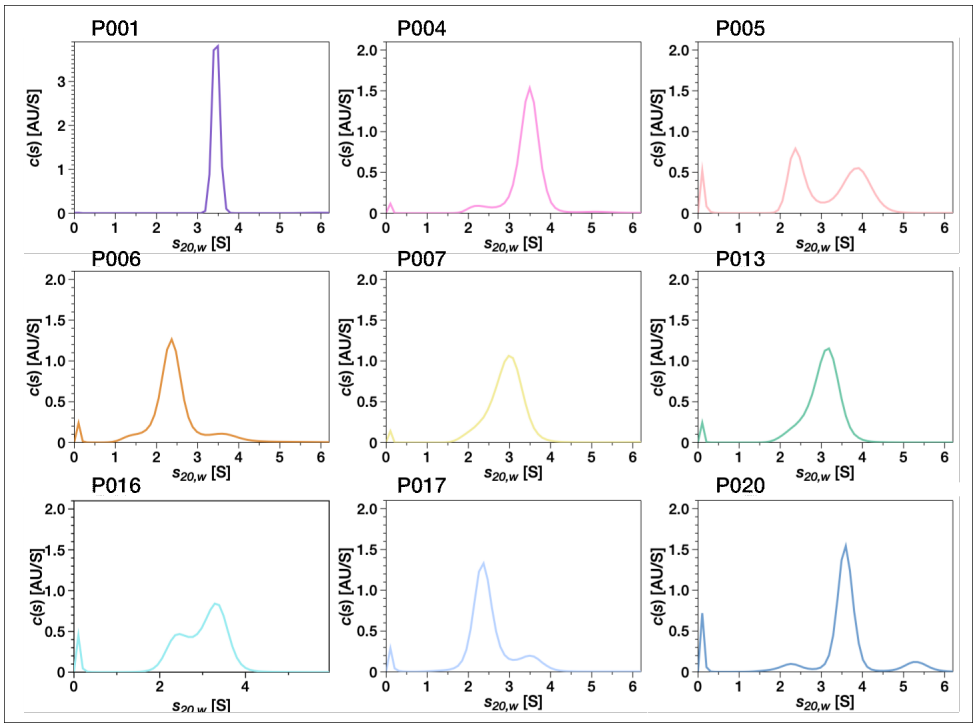

Figure 5.14: Distribution of sedimentation coefficients (c(s)) of the IgLC samples of this study determined by sedimentation velocity experiments at 60,000 rpm.

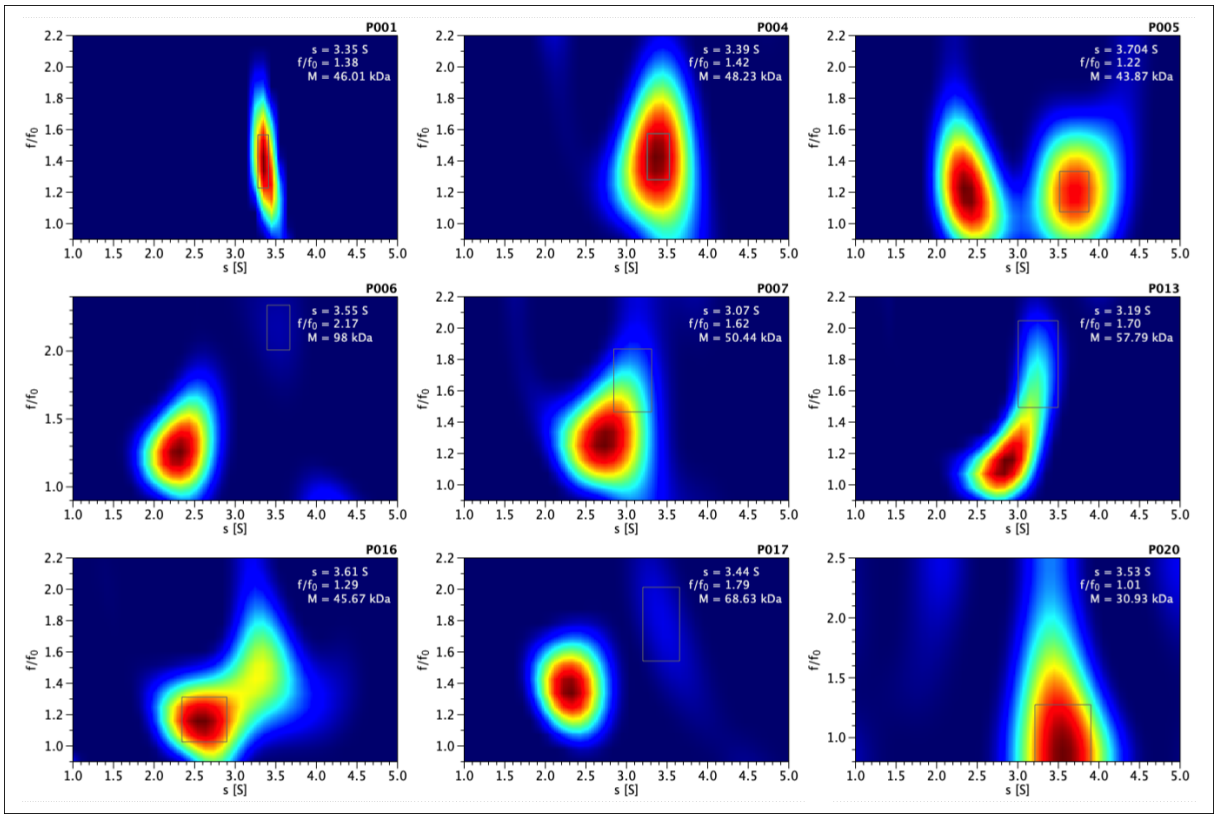

Figure 5.15: Application of the c(s, *ff0*)-model to the SV experiments of the IgLC samples at 60,000 rpm.

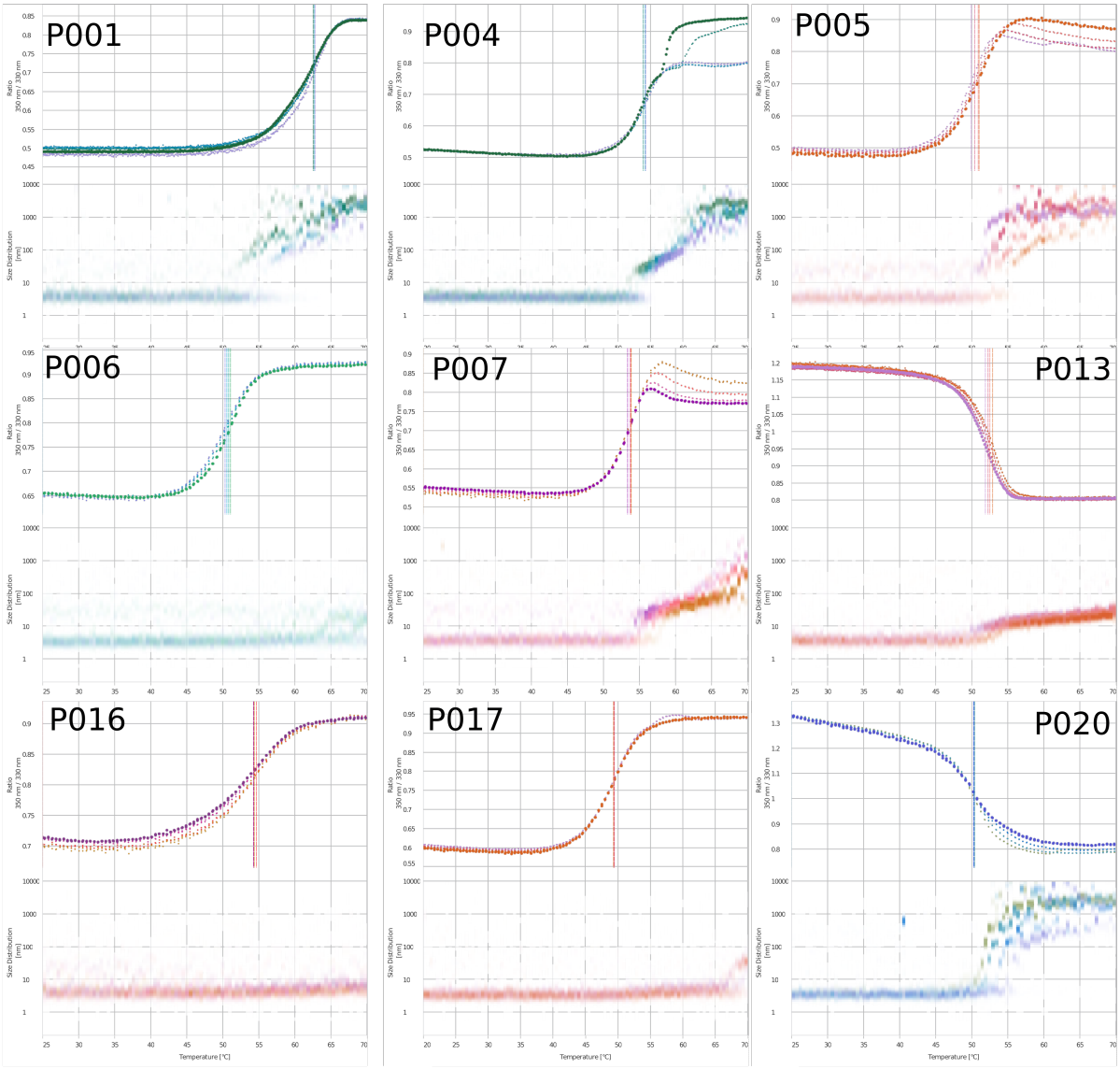

Figure 5.16: Concentration dependent thermal unfolding experiments of the IgLC samples of our study. The samples were scanned from 25 −70 °C at 1 °C per minute. In each case, the evolution of the ratio of the intrinsic fluorescence intensities at 350 and 330 nm is shown on top, and the evolution of the size distribution, measured by dynamic light scattering (DLS) is shown on a logarithmic scale on the bottom. Each sample was measured at 4 concentrations, as the undiluted stock solution as well as 3 dilutions by a factor of 2 each. The concentrations of the stock solutions are 97 µM (P001), 150 µM (P004), 91 µM (P005), 139 µM (P006), 103 µM (P007), 97 µM (P013), 99 µM(P016), 158 µM (P017) and 81 µM (P020)

.

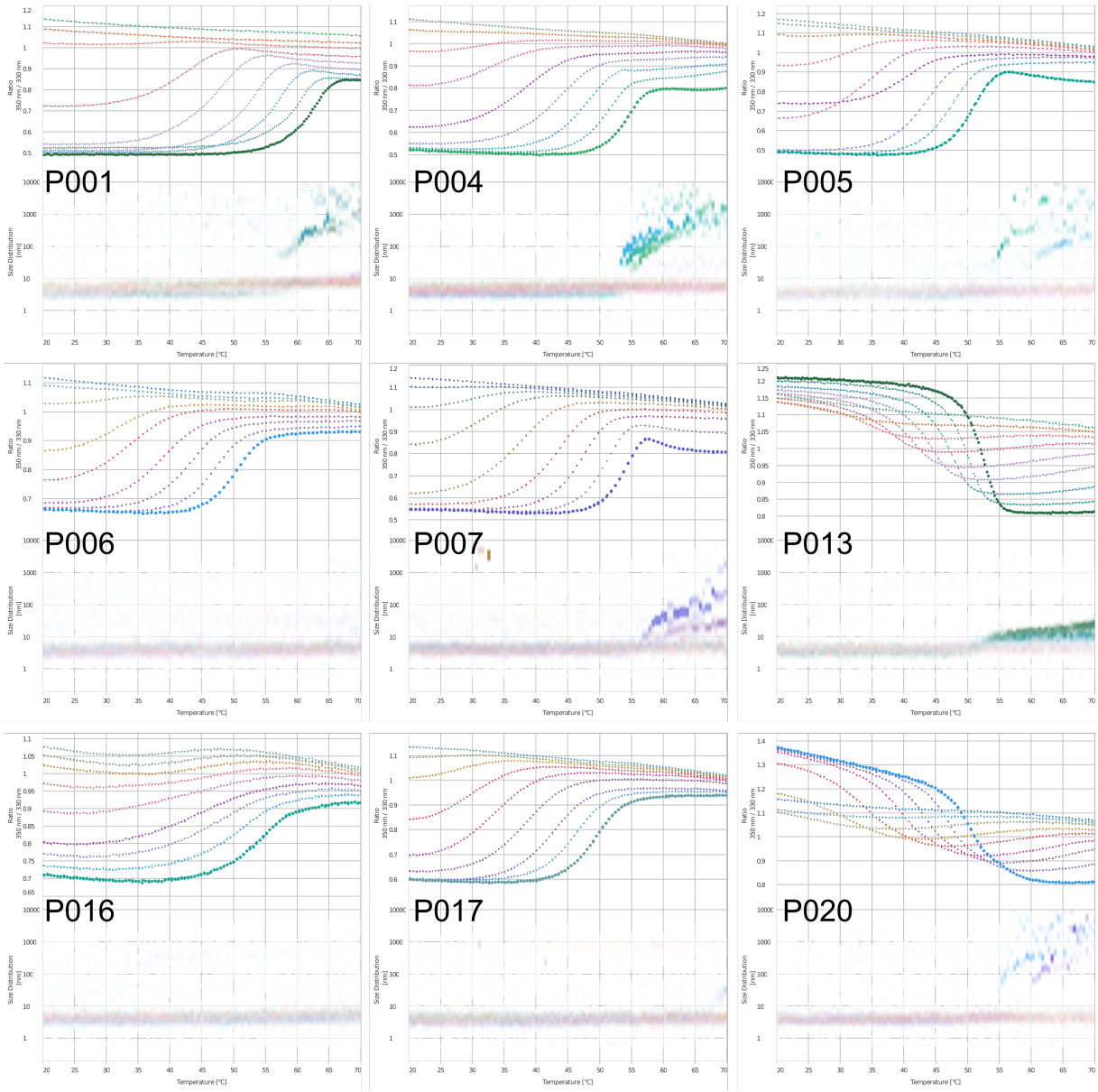

Figure 5.17: Temperature-dependent chemical denaturation of the IgLC samples of this study by urea. In each case, the evolution of the ratio of the intrinsic fluorescence intensities at 350 and 330 ,nm is shown on top, and the evolution of the size distribution, measured by DLS is shown on a logarithmic scale on the bottom. The protein concentration corresponds to a 5-fold dilution of the stock solution used for the thermal denaturation in Figure 5.16. The urea concentrations are in each case 0, 0.67,1.34, 2.01, 2.68, 3.35, 4.02, 4.69, 5.36 M. The samples were scanned from 20 −70 °C at 1 °C per minute.

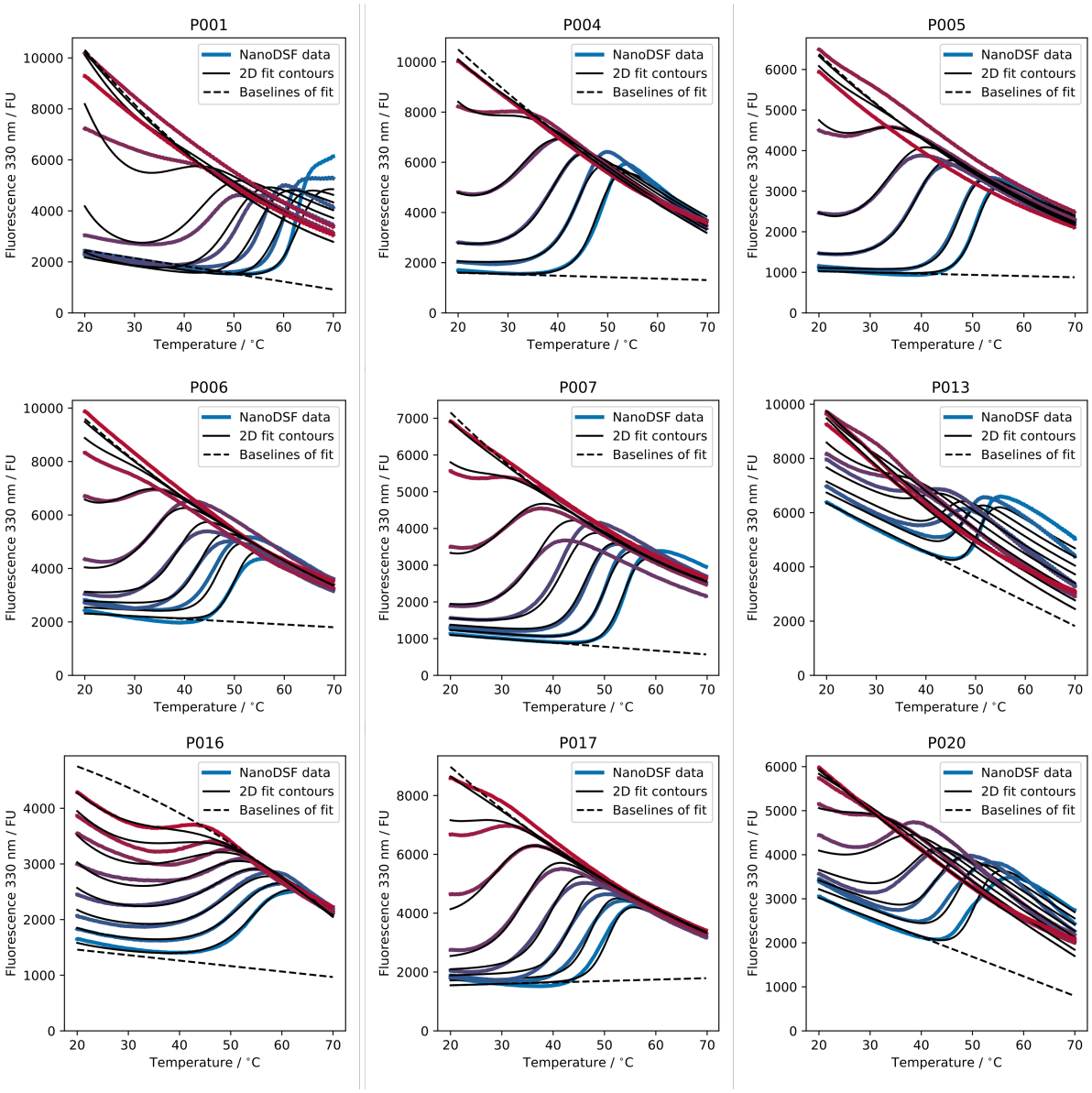

Figure 5.18: Global fits of the temperature-dependent chemical denaturation of the IgLC samples of this study by urea. The data is the same as in the previous figure, but instead of using the fluorescence intensity ratio, the fits are performed simultaneously on the fluorescence intensities at both 330 nm (shown here) and 350 nm .

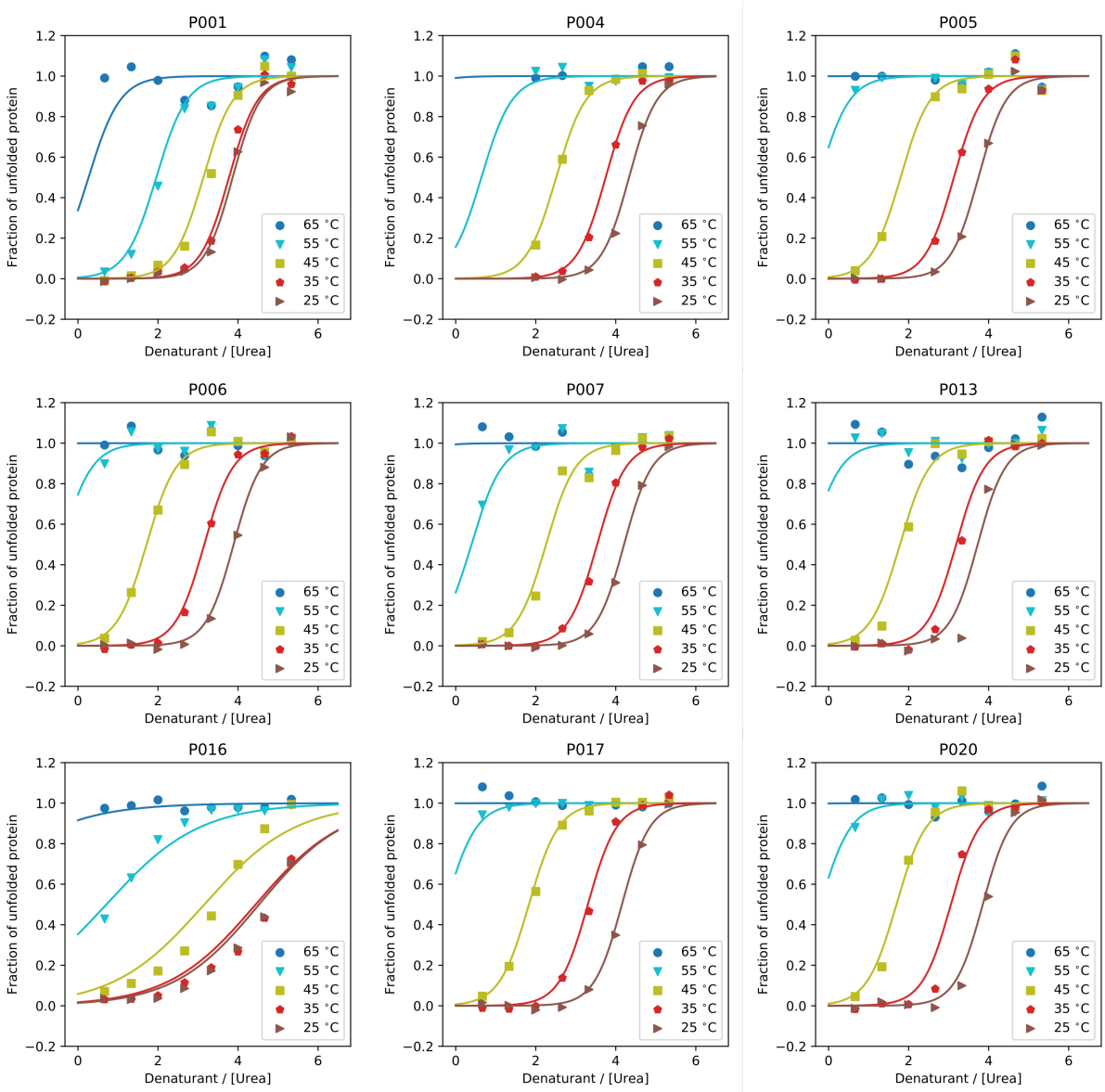

Figure 5.19: Results from the global fits of the temperature-dependent chemical denaturation of the IgLC samples of this study by urea. Shown is the fraction of unfolded protein as a function of urea concentration at different temperatures.

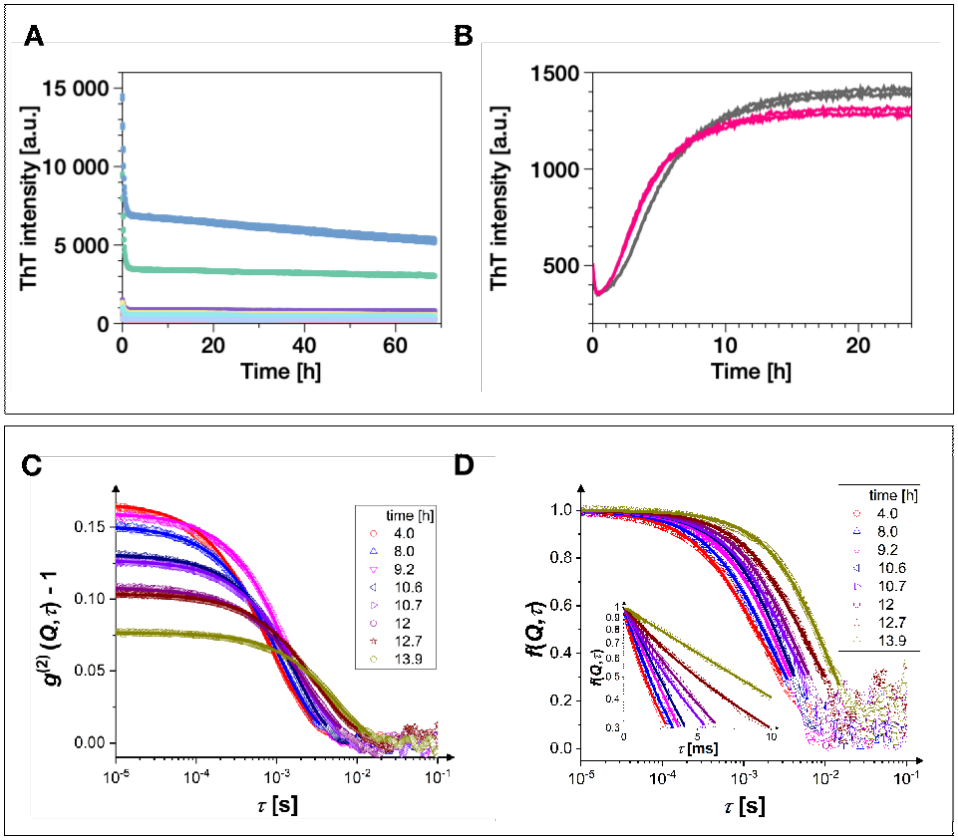

Figure 5.20: (A) Aggregation kinetic assay of the IgLC samples of this study (35 µM monomer concentration) in Tris-HCl, pH 7.4, in a high-binding surface plate under conditions of mechanical agitation. (B) Comparison of the kinetics of amyloid fibril formation of the sample P006 under reducing conditions in Tris-HCl, pH 7.4, and phosphate buffer, pH 7.4. The kinetic traces are similar, with the aggregation in phosphate buffer being slightly faster, with an average halftime of 2.52 h (3.89 h in Tris-HCl).(C)(D) Exemplary dynamic light scattering data corresponding to the time evolution of the mean hydrodynamic radius shown in Figure 5.3 C. (C) Intensity cross-correlation functions, $g^{(2)}(Q,\tau)$-1, as a function of lag time τ taken at selected times, as indicated, during the amorphous aggregation of P001 induced by TCEP and at a scattering vector Q=18.7 µm^{-1}; measurements (symbols) and cumulant fits (solid lines). (D) Data shown in (C) replotted as dynamic structure factor, $f(Q,\tau)$, as a function of lag time τ. (Inslet) Data shown in (D) on a log-lin scale. With increasing time, the decay of the correlation function shifts to larger lag times, indicating smaller diffusion coefficient and thus an increasing mean hydrodynamic size.

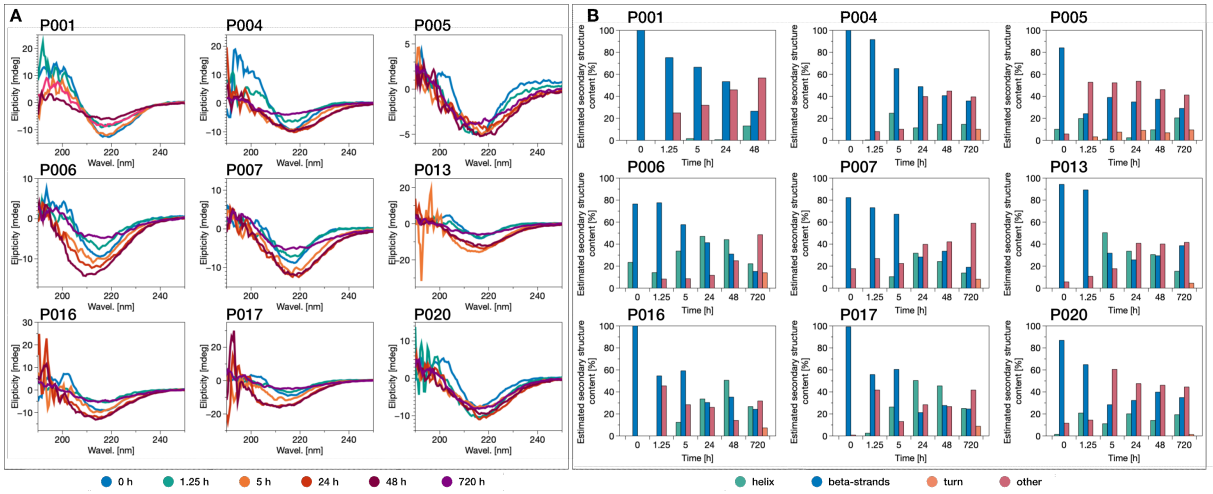

Figure 5.21: (A) Circular dichroism (CD) spectra of the IgLC samples of this study in the presence of 7 mM TCEP at different time points. (B) Analysis of the secondary structure content using BeStSel.

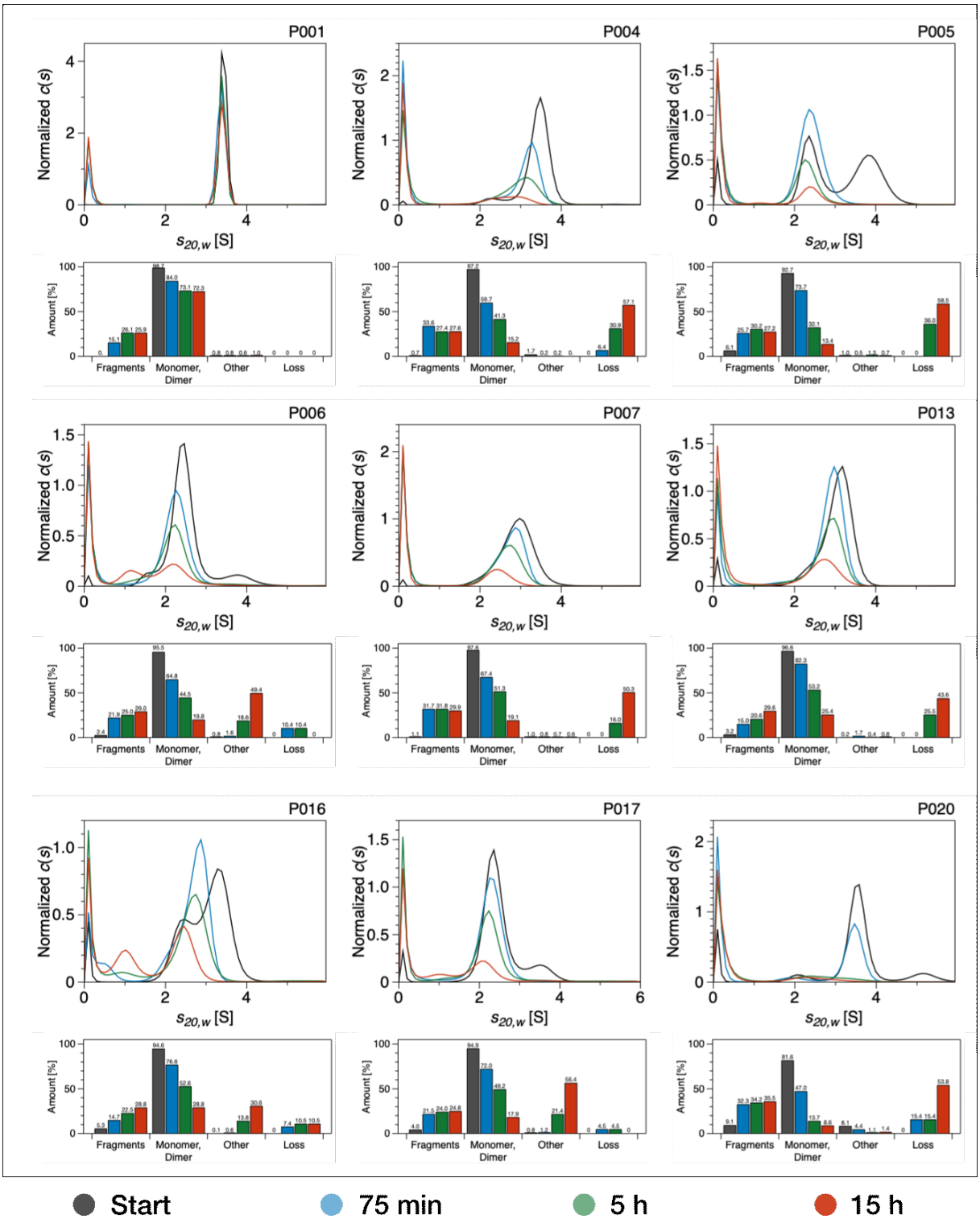

Figure 5.22: The c(s) distribution in the range between 0 and 6 S and the corresponding ratio of the species of the LC samples incubated with 7 mM TCEP. The fragments resemble the species between 0 and 1.5 S, monomer and dimer between 1.5 and 5 S and other from 5 S till the maximal value. The data was fitted for a range between 0 and 50 S or 150 S. The loss represents bigger aggregates, which sediment during the acceleration to 60.000 rpm. The c(s) distributions were normalized to the total monomer concentration. The monomer and dimer could not always be separated, therefore the average s-value was analyzed.

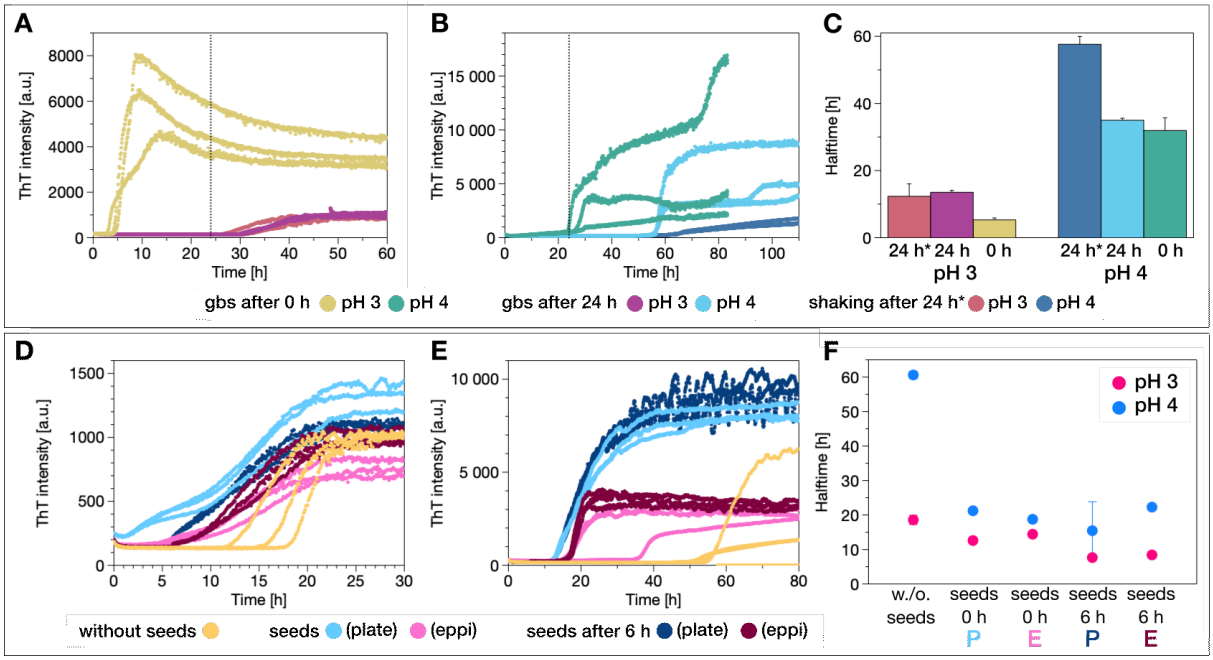

Figure 5.23: Aggregation assays of P016 at (A) pH 3 and (B) pH 4 monitored in a high-binding surface plate in the presence of glass beads and conditions of mechanical agitation and with addition of glass beads after 24 h pre-incubation without shaking and the (C) aggregation halftimes (top). Aggregation assays of P016 at (D) pH 3 and (E) pH 4 in a high-binding plate under quiescent conditions. Seeds prepared in a high-binding plate and prepared in an Eppendorf tube are added at the beginning and after 6 h pre-incubation and (F) the halftimes are analysed. The pre-incubation times (24 or 6 h) are subtracted from the halftimes.

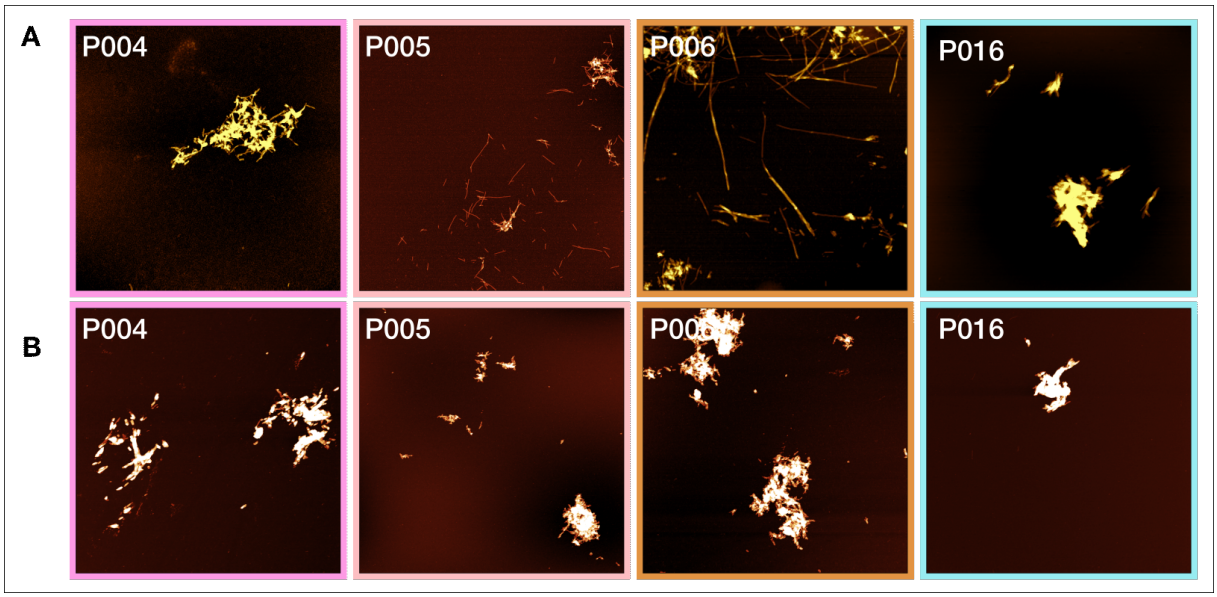

Figure 5.24: AFM-height-images of aggregates prepared in a (A) high-binding surface plate and in (B) Eppendorf tubes. The image scale is 5 x 5 µm. The colour range represents the height from -2 to 15 nm.

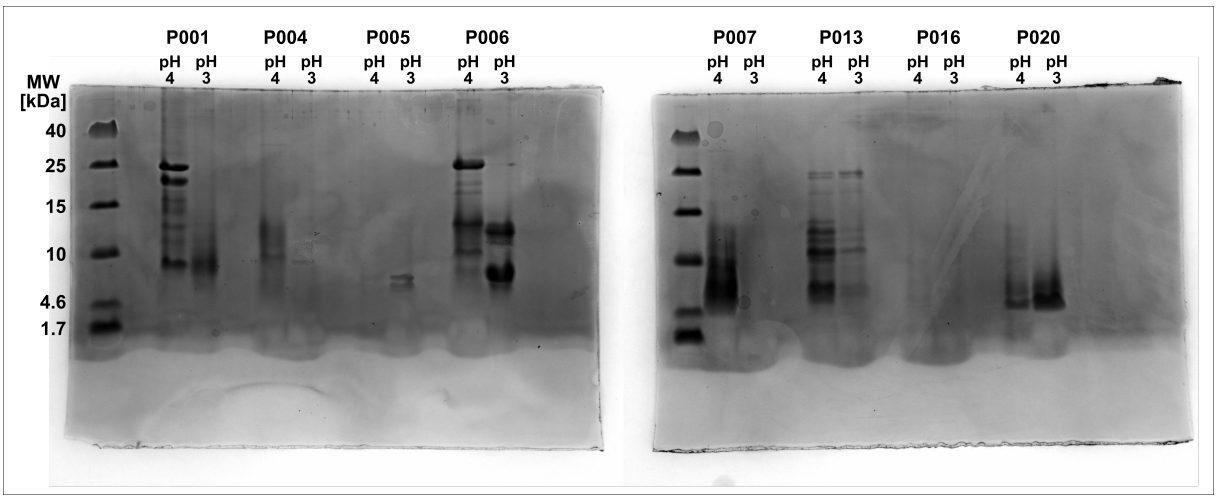

Figure 5.25: Tris Tricine SDS-PAGE of the depolymerised LC aggregates formed at acidic pH values. The aggregation products formed in Eppendorf tubes under agitation conditions were centrifuged using an Optima MAX-XP ultracentrifuge (Beckman Coulter) in a TLA-55 rotor at 40.000 rpm at 20 °C for 45 min. The pellet was resuspended in 150 mM citric acid (pH 3 or pH 4) and centrifuged again for 45 min. This washing procedure to remove the soluble fragments was conducted three times. The washed aggregates were dissolved in 6 M urea and subsequently ran on a Tris Tricine SDS-PAGE. The gels were stained with colloidal coomassie G-250 [18].

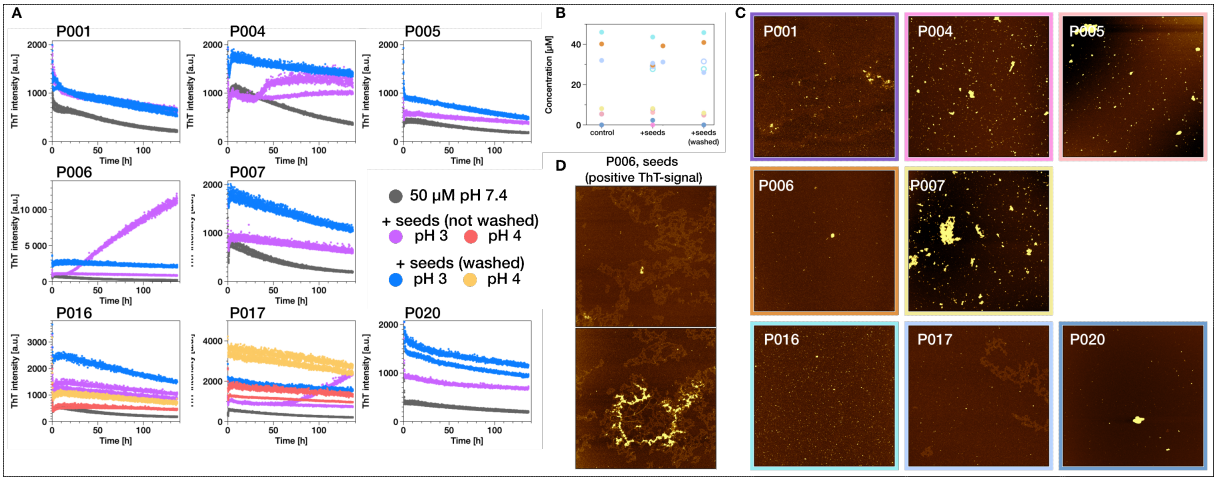

Figure 5.26: (A) Aggregation experiment at 55 °C monitored in a non-binding surface plate under agitation conditions in the presence of glass beads. 5% Seeds which were produced at pH 3 or pH 4 in an Eppendorf tube were added to 50 μM light chain. (B) The soluble content was determined after the experiment by UV-absorbance. AFM-height-images of the light chains at the end of the experiments (C) and of aggregated P006 with the positive ThT-signal (D). Fibrils at pH 3 do not display any twist. The image scale is 5 x 5 µm. The colour range represents the height from -2 to 5 nm.

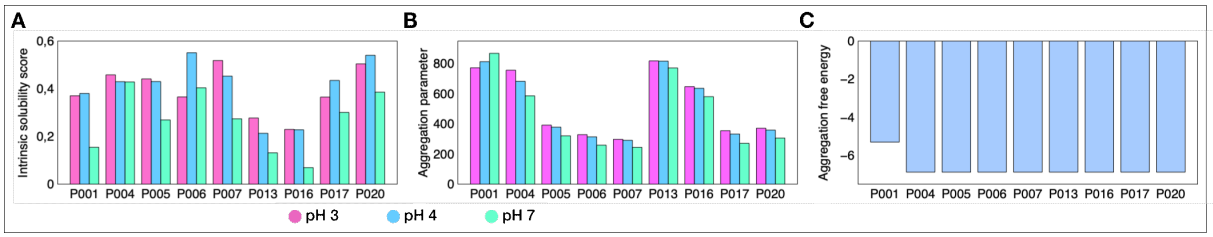

Figure 5.27: (A) Intrinsic solubility score measured by CamSol and (B) aggregation parameter determined by the Tango algorithm at pH 3, pH 4 and pH7, (C) aggregation free energy computed with the Pasta algorithm.

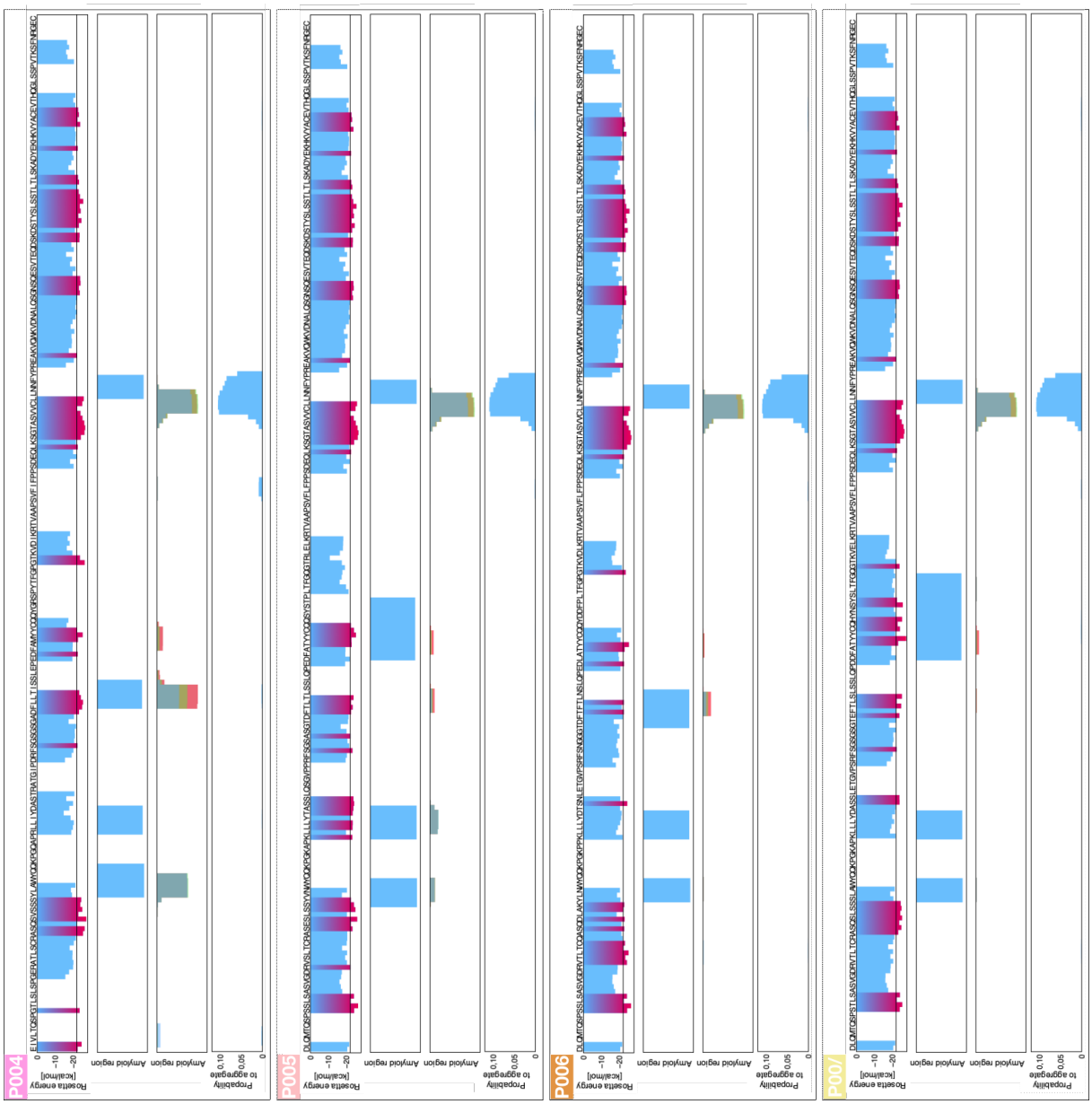

Figure 5.28: The κ IgLC sequences P004, P005, P006 and P007 were analysed with different amyloid prediction tools and the results visualised on the sequence. Rosetta energy was determined by ZipperDB, amyloidogenic sequence regions with the algorithms Waltz, Tango and Pasta. The analyses with Tango were performed at pH 3 (red), pH 4 (green) and pH 7 (blue).

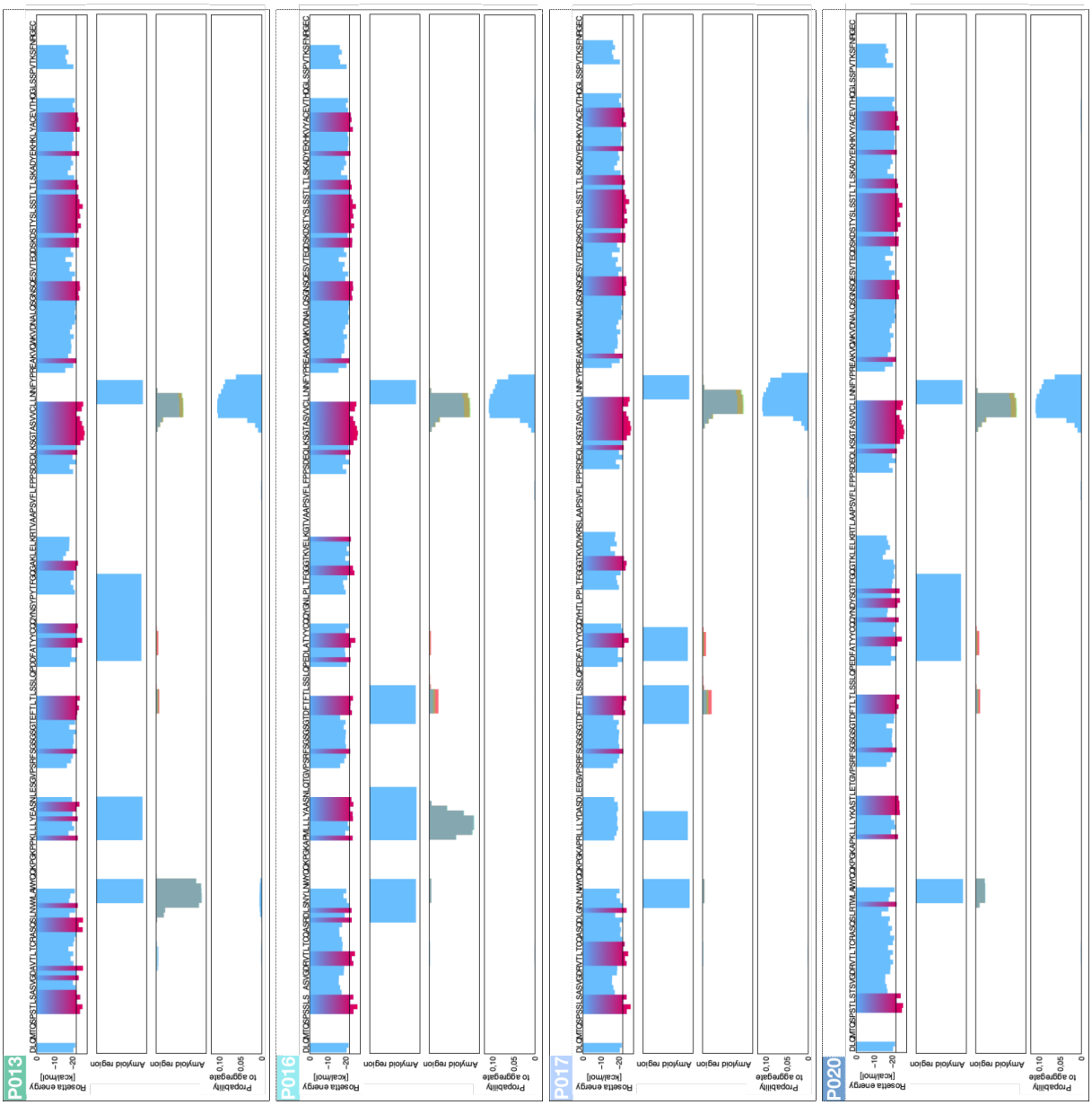

Figure 5.29: The κ IgLC sequences P013, P016, P017 and P020 were analysed with different amyloid prediction tools and visualised on the sequence. Rosetta energy was determined by ZipperDB, amyloidogenic sequence regions with the algorithms Waltz, Tango and Pasta. The analyses with Tango were performed at pH 3 (red), pH 4 (green) and pH 7 (blue).

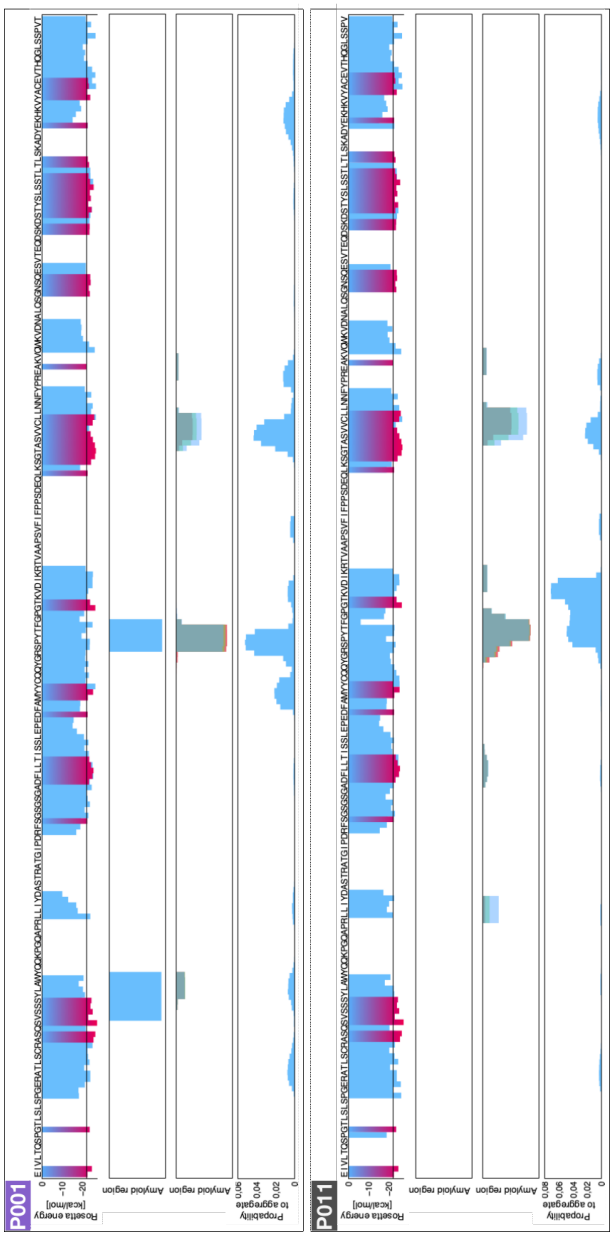

Figure 5.30: The λ IgLC sequences P001 and P011 were analysed with different amyloid prediction tools and visualised on the sequence. Rosetta energy was determined by ZipperDB, amyloidogenic sequence regions with the algorithms Waltz, Tango and Pasta. The analyses with Tango were performed at pH 3 (red), pH 4 (green) and pH 7 (blue).

6

THE AGGREGATION CONDITIONS DEFINE WHETHER EGCG IS AN INHIBITOR OR ENHANCER OF α-SYNUCLEIN AMYLOID FIBRIL FORMATION

Rebecca Sternke-Hoffmann [1], Amelie Boquoi [2], David Lopez [2], Florian Platten [3], Roland Fenk [2], Rainer Haas [2] and Alexander K. Buell [1,4]*

[1] Institute of Physical Biology, Heinrich-Heine-University, Düsseldorf, Germany
[2] Department of Hematology, Oncology and Clinical Oncology, Heinrich-Heine-University, Düsseldorf, Germany
[3] Condensed Matter Physics Laboratory, Heinrich-Heine-University, Düsseldorf, Germany
[4] Department of Biotechnology and Biomedicine, Technical University of Denmark, Lyngby, Denmark

Correspondence: alebu@dtu.dk (A.K.B.)

Keywords:

6.1. Abstract

The amyloid fibril formation by α-synuclein is a hallmark of various neurodegenerative disorders, most notably Parkinson's disease. Epigallocatechin gallate (EGCG) has been reported to be an efficient aggregation inhibitor of numerous proteins, among them α-synuclein. Here we show that this applies only to a small region of relevant parameter space and that under some conditions, EGCG can even accelerate α-synuclein amyloid fibril formation through facilitating its heterogeneous primary nucleation. Furthermore, we show through quantitative seeding experiments that, contrary to previous reports, EGCG is not able to re-model α-synuclein amyloid fibrils into seeding-incompetent structures. Taken together, our results paint a complex picture of EGCG as a compound that can under some conditions inhibit the amyloid fibril formation of α-synuclein, but the inhibitory action is not robust against various physiologically relevant changes in experimental conditions. Our results are important for the development of strategies to identify and characterise promising amyloid inhibitors.

6.2. Introduction

The misfolding and uncontrolled aggregation of proteins is linked to the onset and progression of a range of neurological disorders, such as Parkinson's disease (PD) and Alzheimer's disease [492, 520, 521]. PD is a progressive disorder of the nervous system that affects movement, but it also has non-motor symptoms. A pathological characteristic of PD are Lewy bodies [538]. The major filamentous component of Lewy bodies is the presynaptic protein α-synuclein [129, 539, 540].

α-synuclein is a 140-residue neuronal protein, which can aggregate into highly ordered, cross-β-sheet structured amyloid fibrils [375]. The aggregation mechanism of α-synuclein is a complex nucleation-dependent polymerization process, which manifests itself in test tube experiments of aggregation kinetics through a lag phase, followed by a growth and a steady state phases [376]. At a molecular level, this involves different microscopic steps, in particular (heterogeneous) primary nucleation and growth, and, depending on the solution conditions, fragmentation and secondary nucleation [379, 492].

At neutral pH α-synuclein carries a net negative charge, due to its isoelectric point of 4.0-4.7 [541]. The protein adopts a primarily disordered conformation without well defined secondary or tertiary structure (intrinsically disordered conformation) [373, 374]. At low pH, α-synuclein displays a more compact conformation due to a collapse of the normally highly acidic and extended C-terminal tail [378]. The C-terminal tail becomes fully protonated, thus uncharged, and it forms a compact conformational ensemble with increased hydrophobicity, resulting in an accelerated α-synuclein fibril formation at low pH [379]; a similar effect can be achieved by truncating the C-terminus [542]. Compared to aggregation at neutral pH, the aggregation process is strongly enhanced at mildly acidic pH values (pH < 6), through an efficient production of new growing fibrils catalysed by the binding to the surfaces of pre-existing fibrils (secondary nucleation) [81, 379]. The investigation of the behaviour of α-synuclein at mildly acidic pH values is physiologically relevant, because α-synculein can experience such solution conditions during its life cycle in endosomes and lysosomes, which maintain an acidic pH value between 4 and 5 [380, 381, 382]. This lower pH has to be considered when designing a possible therapeutic strategy for the treatment of neurodegenerative disorders.

Once formed, amyloid aggregates are often highly stable and it is difficult to reverse the aggregation process and to prevent it from spreading through secondary processes. Therefore the development of inhibitors that are able to prevent the initial formation of amyloid aggregates is crucial. In particular, a target of these substances are small oligomeric species, which are suspected to be the most cytotoxic [543], has been proposed to be an efficient strategy to combat neurodegenerative diseases. Viable therapeutic strategies for prevention and treatment of amyloid-related diseases are 1) the maintenance of the amyloidogenic protein in its soluble state, 2) the redirection of the amyloidogenic proteins into unstructured, nontoxic and off-pathway aggregates and 3) remodeling and/or dissociation of the mature amyloid fibrils. One class of inhibitors of α-synuclein amyloid fibril formation is formed by molecules that can interact with amyloidogenic monomers in order to prevent their inter-molecular associations, such as antibodies or affibodies [544, 545]. Small molecules have also been proposed as inhibitors of α-synuclein amyloid fibril formation [546, 547, 548, 549]. These include polyols, polyphenols or other aromatic molecules containing hydrogen-bonding functionalities. Polyphenols are naturally occurring secondary metabolites of plants characterized by the presence of two or more phenol rings [550]. A well-studied polyphenol is Epigallocatechin-3-gallate (EGCG), the main polyphenol found in green tea. Biochemical studies indicate the neuroprotective action of EGCG, which has been suggested to effectively inhibit the aggregation of a number of amyloidogenic peptides and proteins, including α-synuclein [355, 356, 357, 358, 359], amyloid-β (related to AD) [355, 360], islet amyloid polypeptide (related to type-II diabetes) [361, 362], huntingtin exon 1 (related to Huntington's disease) [363], tau (related to AD and tauopathies) [364], superoxide dismutase (related to amyotrophic lateral sclerosis) [365], prion proteins (related to prion diseases) [366, 367] and others. EGCG has the ability to prevent the formation of toxic prefibrillar oligomers as well as to inhibit amyloid fibril formation and has been proposed to remodel existing amyloid fibrils. Most of the studies are performed at physiological pH, where EGCG is unstable and auto-oxidises fast into various products [371]. Decreasing the pH to slight acidic pH values ($\leq$ pH 6), results in a considerable increase in EGCG stability, which we have recently shown to lead to a strongly impaired ability of EGCG to inhibit α-synuclein aggregation [19]. Considering that both α-synuclein and EGCG are likely to encounter such pH environments *in vivo*, the aim of the present study is to characterise in more detail the dependence of EGCG inhibition of α-synuclein aggregation on the solution conditions. The *in vitro* amyloid fibril formation of α-synuclein is an intrinsically slow process, due to the fact that the primary nucleation process is heterogeneous and requires a combination of appropriate surfaces (e.g. air-water interface [551], polymer-water interface [552] or lipid-water interface [553]) and constant agitation of the sample. The nucleation step can be bypassed by the addition of exogenous fibrils (seeds). Seeding, in particular at high seed concentrations (where all molecular processes other than fibril growth can be neglected [20]) can improve the reproducibility of the aggregation kinetics of α-synuclein. In this study we payed special attention on how the effect of EGCG on the fibril formation is altered, when the aggregation of α-synuclein is studied under different conditions, such as different surfaces and the presence and absence of glass beads. By systematically examining a wide range of pH values, we probe the influence of EGCG oxidation and the interplay between the solution conditions and the action of EGCG. Overall we find that EGCG is an efficient inhibitor of α-synuclein aggregation only in a small range of parameter space. Under some conditions, especially those that lead to enhanced stability of EGCG, it can either have no effect on the amyloid fibril formation of α-synuclein or even promote the latter.

6.3. Material and Methods

Materials and Solutions

α-synuclein in the pT7-7 vector was expressed in *E. coli* BL21 (DE3) and purified as previously described [85]. As a last step α-synuclein was purified by size-exclusion chromatography on an ÄKTA pure chromatography system (GE Healthcare) using a Superdex 200 Increase 10/300 GL (GE Healthcare) and 20 mM citric acid, pH 7, as an elution buffer. α-synuclein concentration was determined by measuring UV-absorption at 275 nm (extinction coefficient of 5600 M^{-1} cm^{-1}). For the α-synuclein inhibition experiments, 5 mM solutions of EGCG (Tocris #4524) were prepared by dissolving EGCG in dH_2O. The EGCG solutions were frozen and stored at −20 °C, after monitoring no difference between freshly dissolved and thawed EGCG. $EGCG_{ox}$ was prepared by dissolving 10 mM of EGCG in 20 mM citric acid, pH 7, and incubating for at least 6 hours at 60 °C in a thermomixer compact (Eppendorf) at 1000 rpm. Subsequently, it was diluted to a final concentration of 5 mM, frozen and stored at −20 °C.

Measurements of Aggregation Kinetics

In order to study the effect of EGCG of the amyloid fibril formation by α-synuclein, solutions of 25 µM of α-synuclein were prepared with EGCG or $EGCG_{ox}$ solutions in a 1:1 and 1:5 (protein:compound) ratio, 20 µM ThT and 150 mM citric acid at the desired pH value (pH 3, pH 4, pH 5, pH 6 or pH 7). 3 replicates of each solution were then pipetted into a high-binding surface plate (Corning #3601) or a non-binding surface plate (Corning #3881). The aggregation kinetics were monitored in the presence and absence of small glass beads (SiLibeads Typ M, 3.0 mm). The plates were sealed using SealPlate film (Sigma-Aldrich #Z369667). The kinetics of amyloid fibril formation were monitored at 37 °C under continuous shaking (300 rpm) or quiescent conditions by measuring ThT fluorescence intensity through the bottom of the plate using a FLUOstar (BMG LABTECH, Germany) microplate reader (readings were taken every 5 min).

In order to investigate the interactions of EGCG and the surface of the non-binding surface plate, 130 µl of solutions of EGCG or $EGCG_{ox}$ (25 µM and 125 µM) were pipetted into a well and incubated at room temperature for 2 h. After incubation, the solutions were removed, the concentration of EGCG and $EGCG_{ox}$ were measured by UV-absorption and a solution of 25 µM α-synuclein, 20 µM ThT and 150 mM citric acid pH 4 was added to the pre-treated wells. 3 replicates per condition were measured. The $EGCG_{ox}$ concentration was compared to a solution which was incubated in an Eppendorf tube. The highest ThT fluorescence emission value within each time course was taken to be I_{max}. The half-times (t_{50}) of the aggregation reaction were obtained as described by Meisl *et al.* [554].

Seeded Aggregation Experiments

In order to probe the effects of EGCG and $EGCG_{ox}$ particularly on the elongation process and on preformed fibrils, the aggregation kinetics of α-synuclein were monitored in the presence of 5 % and 0.5 % seeds in relation to the used monomer concentration. For the preparation of the seeds, solutions of 50 µM α-synuclein were incubated at 37 °C in a high-binding surface plate, in the presence of glass beads and under continuous shaking at the desired pH-values (pH 3, pH 4, pH 5, pH 6 or pH 7). The end product after 24 h of incubation, when the reaction was found to be completed under all conditions, was used to seed fresh solutions of 50 µM α-synuclein, which were incubated at 37 °C for 24 h in an Eppendorf Thermomixer with continuous shaking

(1200 rpm). The product of this seeded aggregation experiment was used to seed the kinetic experiments in the presence and absence of EGCG and $EGCG_{ox}$. For the calculation of the seed concentration, it was assumed that the monomer had quantitatively converted to amyloid fibrils. Before performing the experiment, the seed-solutions were homogenized using an ultrasonication bath Sonorex RK 100 H (Bandelin, Germany) for 180 s. The seeded aggregation experiments were performed in non-binding surface plates with 25 µM α-synuclein monomer and the preformed fibrils were added as seeds to a final concentration of 0.5 % or 5 % of the monomer solution at the desired pH value. For the experiment with seeds that were to be pre-incubated with EGCG, we added 50 µM EGCG or $EGCG_{ox}$ to a solution of 50 µM α-synuclein fibrils, at pH 5, pH 6 and pH 7. After 2 h the fibrils were added to 25 µM monomer at the corresponding pH value to a final concentration of 5 % and the aggregation kinetics were recorded every 150 s. In order to investigate if EGCG can remodel pre-formed fibrils, we incubated 10 µM fibril solutions, which were sonicated beforehand, with 10 µM EGCG or $EGCG_{ox}$ in a non-binding surface plate at 37 °C under shaking conditions at pH 6 or pH 7 for over 100 h. The fluorescence intensity was recorded using a FLUOstar (BMG LABTECH) microplate reader (readouts were taken every 5 min). After the incubation 50 µM fresh monomer was added to the solutions and the measurement was continued, with readings taken every 150 s, allowing a potential change in the seeding efficiency to be detected.

Atomic Force Microscopy (AFM)

AFM images were acquired directly after the aggregation kinetic measurements. 10 µl of each sample was deposited onto freshly cleaved mica. After drying, the samples were washed 5 times with 100 µl of dH_2O and dried under gentle flow of nitrogen. AFM images were obtained using a NanoScope V (Bruker) atomic force microscope equipped with a silicon cantilever ScanAsyst-Air with a tip radius of 2-12 nm.

Microfluidic diffusional sizing and concentration measurements

Fluidity One is a microfluidic diffusional sizing (MDS, [408]) device, which measures the rate of diffusion of protein species under steady state laminar flow and determines the average particle size from the overall diffusion coefficient. The protein concentration is determined by fluorescence intensity, as the protein is mixed with ortho-phthalaldehyde (OPA) after the diffusion, a compound which reacts with primary amines, producing a fluorescent compound [409]. To measure the concentration of the soluble α-synuclein, the samples were centrifuged for 60 min at 16100 g at 25 °C using centrifuge 5415 R (Eppendorf) directly after the kinetic measurements. The top half of the supernatant was removed and 6 µl of this solution was pipetted onto a disposable microfluidic chip and measured with the Fluidity One (F1, Fluidic Analytics, Cambridge, UK). For the measurement of the amount of protein in the pellet, the pellet was re-suspended in the remaining liquid and 6 µl of this solution was pipetted onto a microfluidic chip and analysed with the F1 instrument.

6.4. Results

Non-seeded experiments in high-binding plates

We performed α-synuclein amyloid fibril formation experiments in high-binding surface plates in the presence and absence of glass beads under shaking conditions (Figure 6.1). α-synuclein monomer solutions are kinetically highly stable, because the homogeneous primary nucleation

rate is slow, in particular around neutral pH. Under most conditions, the primary nucleation of α-synuclein is triggered by surfaces that have an affinity for the protein. When α-synuclein binds to a suitable surface or interface, the N-terminal domain can adopt a helical structure [555], which seems to facilitate the formation of fibril nuclei and oligomers. The air-water-interface [551], the surface of the plate [552] and, under mildly acidic pH conditions, the surface of already formed fibrils [81, 379] function as a nucleation assistance. The growing fibrils can then be fragmented by the shaking, in particular in the presence of glass beads [379], which leads to accelerated aggregation kinetics. We therefore performed aggregation experiments either in the presence or absence of glass beads.

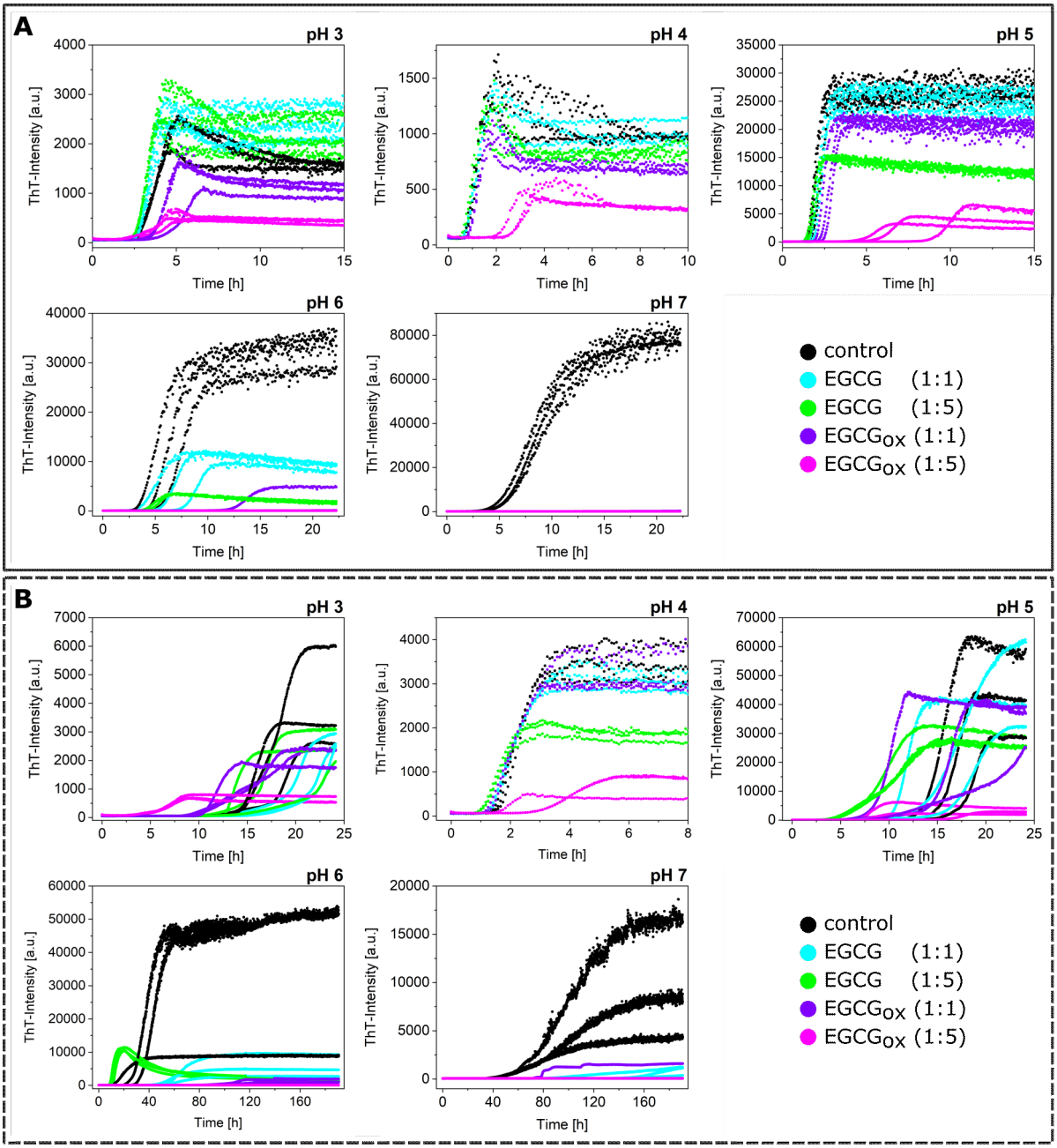

Figure 6.1: The effects of different ratios (1:1 and 5:1 with respect to protein) of EGCG and EGCG$_{ox}$ on the aggregation kinetics of α-synuclein at different pH values (pH 3 to pH 7), monitored in high-binding surface plates in the presence (A) and absence (B) of glass beads. A small subset of this data (pH 6 and pH 7, 1:1 EGCG and 1:1 EGCG$_{ox}$) is from [19].

α-synuclein monomers were combined with the compound EGCG or $EGCG_{ox}$ in a protein:compound ratio of 1:1 (25 µM:25 µM) or 1:5 (25 µM:125 µM) and the aggregation was monitored through the change in Thioflavin-T (ThT) fluorescence intensity. An increase in the intensity indicates the formation of ThT-positive aggregates specifically amyloid fibrils. The results of these initial experiments in polystyrene plates are shown in Figure 6.1, and the extracted maximal fluorescence intensities and aggregation half times are shown in Figure 6.2. The half time (t_{50}) is the time point when the ThT intensity has reached half the value between the initial baseline and the final plateau value and can be used as a macroscopic parameter to describe the aggregation kinetics. α-synuclein displayed the fastest aggregation kinetics at pH 4 with a t_{50} of 1.1 h when glass beads were added. Without glass beads the fibril formation was slowed down by a factor of 2. The *de novo* aggregation at pH 3 and pH 5 is similar, and the kinetics under these two conditions are slower by a factor of 2-3 (with added glass beads) and 8 (without additional glass beads), compared to pH 4. The aggregation at pH 5 is slightly faster than at pH 3 and the influence of the glass beads on the kinetics is bigger. The glass beads have the strongest aggregation enhancing influence at pH 7. α-synuclein can not form amyloid fibrils very efficiently at pH 7, possibly due to the high negative charge under these conditions, which is not strongly screened at the moderate ionic strength values of our experiments. Since the secondary nucleation is suppressed at neutral pH, the dominating aggregation events are only primary nucleation and elongation of the newly formed fibrils. In the presence of glass beads the enhanced fragmentation leads to a t_{50} of 9 h, whereby the absence of glass beads leads to an almost complete absence of secondary processes and a t_{50} of 96 h.

Due to the spectroscopic features of the ThT to increase its fluorescence intensity upon binding to amyloid fibrils, it is possible to consider the enhanced ThT fluorescence intensity as an increase in the concentration of aggregates that are formed. When the maximal ThT fluorescence intensities are compared to I_{max} of the control, i.e. the absence of either EGCG or $EGCG_{ox}$, almost all conditions show a decrease, in particular at neutral and slightly acidic pH (pH 7 - pH 6) (Figure 6.2). Only the aggregation at pH 3 shows an increased fluorescence intensity in the presence of EGCG. In the presence of $EGCG_{ox}$ the intensities are decreased under all conditions indicating either an inhibitory effect on the aggregation or an interference with the ThT-signal. When the experiments were performed without glass beads, I_{max} showed a similar outcome. However, at pH 3 the intensities are decreased in the presence of EGCG and $EGCG_{ox}$ when the glass beads were removed.

If rather than Ithe half-time of the aggregation reaction, t_{50}, is used as a read out, the observed inhibitory effects of EGCG at neutral and slightly acidic pH (pH 7 and pH 6) are different. At pH 7 and in the presence of EGCG there is no increase in ThT-signal observable in the presence of glass beads, whereas there is a slight increase in fluorescence intensity over time in the absence of glass beads. In one of the three repeats in the presence of $EGCG_{ox}$, a minor fluorescence intensity increase has been also observed in the case of the equimolar ratio EGCG to protein. The t_{50} of the aggregation in the presence of EGCG is clearly increased at pH 7. The picture at pH 6, however, is different. Where in the presence of EGCG (1:1) the intensity was significantly ($p \leq 0.01$) decreased, the t_{50} is not distinguishable from the control. In the presence of a high concentration of EGCG, the kinetics are faster both with and without additional glass beads. However the ThT-intensity curves without glass beads did not show the typical sigmoidal shape. The decrease of the signal at longer times could be explained by higher order assembly or surface adsorption of the amyloid fibrils [556], or else a time dependent interference of EGCG with ThT fluorescence. In the presence of $EGCG_{ox}$ the kinetics are prolonged and even completely inhibited, both with and without glass beads. However, quantification of the soluble protein

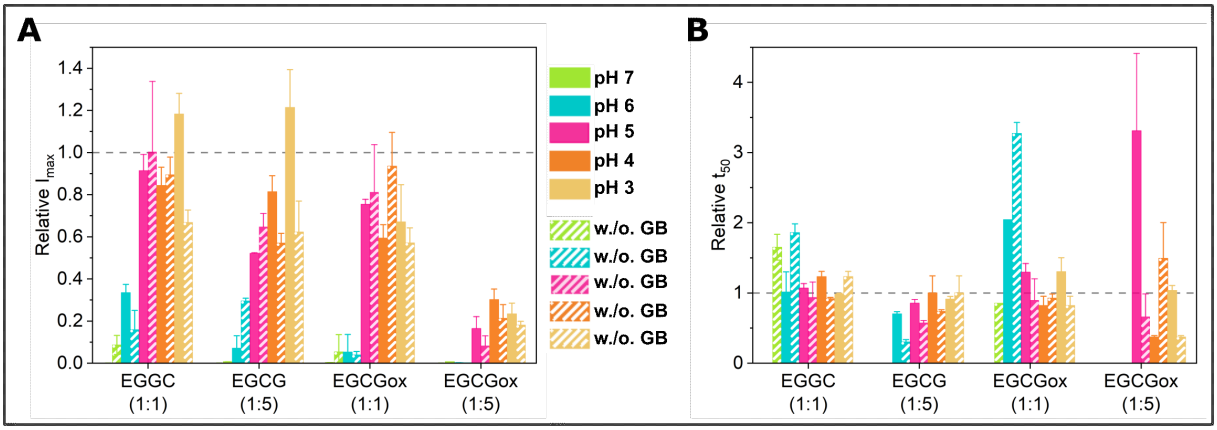

Figure 6.2: Overview of the effects of EGCG and $EGCG_{ox}$ on α-synuclein aggregation monitored in a high-binding surface plates assayed by (A) maximum ThT fluorescence intensity and (B) t_{50} of the aggregation time course. Filled bars represent aggregation in the presence of glass beads, striped bars in the absence of glass beads. Error bars are standard deviations. The data is normalized to the control of the corresponding condition, i.e. the aggregation in the absence of EGCG or $EGCG_{ox}$, the kinetic parameters of which are indicated with the horizontal dashed line at a factor of 1. Relative t_{50} values are only displayed, if any fibril formation is detected by an increase in ThT fluorescence intensity.

in the supernatant at the end of the experiment with additional glass beads showed a loss of in the presence of $EGCG_{ox}$ (1:1) and (1:5). The formed aggregates are accordingly either not ThT-positive or else the EGCG interferes too strongly with their ThT fluorescence.

At more acidic pH values, only the oxidised form of the EGCG showed any clear effect on the aggregation kinetics. At pH 5 and pH 4 the $EGCG_{ox}$ (1:5) showed a significant increase of t_{50}, but in the absence of glass beads the EGCG showed an accelerating effect at pH 5 and pH 3. At pH 4 the aggregation kinetics are slowed down slightly, but not as much as in the presence of glass beads and it is not statistically significant. The variability in the kinetics of the three replicates per condition, especially at pH 3 and pH 5, is high, rendering a thorough statistical analysis difficult with such a small number of replicates.

Non-seeded experiments in non-binding plates

The amyloid formation of α-synuclein is favoured in high-binding surface plates, due to the ability of the polystyrene-water interface to provide nucleation sites. In an attempt to try and disentangle the effects of EGCG and $EGCG_{ox}$ on the polystyrene surface-induced nucleation from that on other relevant processes, we also performed aggregation experiments in non-binding surface plates, i.e. plates where the surface is coated with a protein-repellent PEG layer (Figure 6.3). These non-binding surface plates are often used in kinetic experiments of amyloid fibril formation in order to minimize the contribution of heterogeneous nucleation processes and therefore simplify the kinetic analysis [82, 379, 553]. As expected, therefore, the kinetics of *de novo* aggregation in the non-binding surface plates are slowed down with respect to the high-binding plates, but the high fragmentation rate in the presence of glass beads allows fibril formation to be observed within an experimentally accessible time scale. The enhanced fragmentation amplifies the fibrils that form at the air-water interface [551]. This difference in lag times between high and low binding plates is particularly pronounced at the pH values which lead to very fast aggregation kinetics in the high-binding surface plates: at pH 4 the t_{50} is increased by a factor of 3.4, whereas it is only increased by a factor of 1.3 at pH 7.

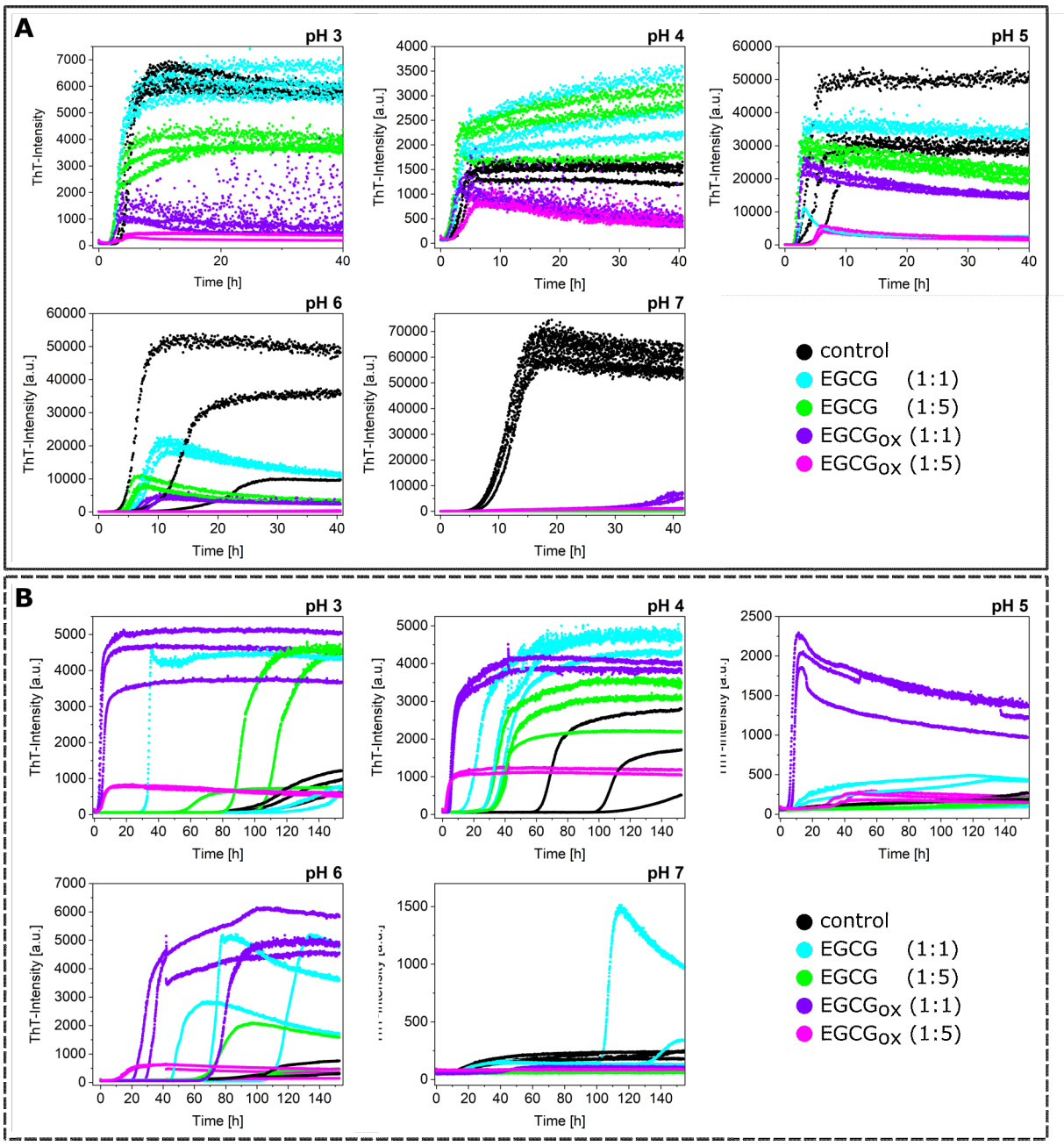

Figure 6.3: The effects of EGCG and EGCG$_{ox}$ on the aggregation kinetics of α-synuclein at different pH values (pH 3 to pH 7) monitored in a non-binding surface plate in the presence (A) and absence (B) of glass beads.

While the maximal ThT-intensities in the presence of glass beads and EGCG or EGCG$_{ox}$ in non-binding plates are comparable to the aggregation experiments conducted in a high-binding surface plate, the t_{50}s indicated an aggregation-enhancing effect of both oxidized and fresh EGCG (Figure 6.4).

The enhanced fragmentation of the fibrils by the use of glass beads leads in general to more reproducible data, both in binding and non-binding plates. However, the aggregation kinetics under some conditions (e.g. pH 6) is still rather variable, as both I_{max} and t_{50} differ between the three replicates of the control sample. In order to obtain an independent (of ThT fluorescence intensity) measurement of aggregate mass in this case, we centrifuged the samples at the end

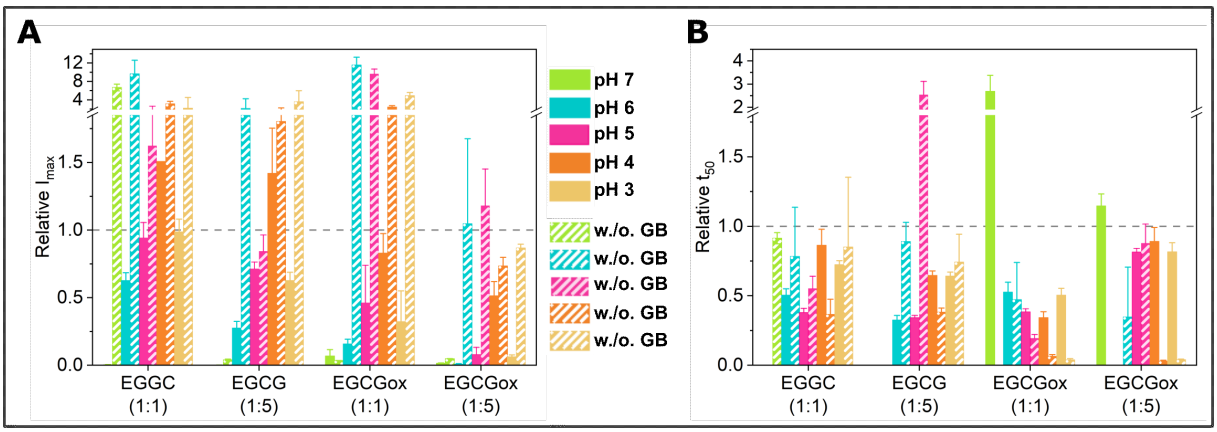

Figure 6.4: Overview of the effects of EGCG and $EGCG_{ox}$ on α-synuclein aggregation monitored in a non-binding surface plate assayed by (A) maximum ThT fluorescence intensity and (B) t_{50} of the aggregation. Filled bars represent aggregation in presence of glass beads, striped bars without glass beads. Error bars are standard deviations. The data is normalized to the control of the corresponding condition, the comparison is outlined with the dashed line (at 1).

point of the experiments and measured the size and concentration of the soluble α-synuclein in the supernatant (Figure 6.5 A, left panel) by microfluidic diffusional sizing (MDS) [408]. We found that while the ThT-signal displayed a clear difference, the amount of soluble protein in the supernatant is similar. In all three samples α-synuclein converts near-quantitatively into aggregates, and the average size of the supernatant fraction is that of monomeric protein. Overall, the picture that emerges from these ThT experiments in non-binding plates with added glass beads is that EGCG and $EGCG_{ox}$ only have an inhibitory effect at pH 7 and in addition at pH 6 in the presence of a 5-fold excess of $EGCG_{ox}$. This conclusion is confirmed by MDS experiments under all conditions (Figure 6.5 A, central panel), which show that despite the variable final ThT intensity, the protein is quantitatively converted into fibrils, illustrating that EGCG and $EGCG_{ox}$ can have a strong influence on ThT intensity [19].

In the absence of glass beads, the aggregation curves are generally more variable also in the non-binding surface plate. The absolute fluorescence intensities at the plateau were increased by a factor of up to almost 10 in the presence of EGCG (for example at pH 6 with EGCG and $EGCG_{ox}$ (1:1) and pH 5 with $EGCG_{ox}$ (1:1)), and only in the presence of the 5-fold excess of oxidised EGCG we could detect similar or slightly decreased maximal intensities compared to the control. Importantly, the aggregation kinetics in the absence of glass beads are accelerated with respect to the control in the presence of both oxidised and fresh EGCG, in particular by the former. This accelerating effect is particularly pronounced at acidic pH (pH 3 and 4), but also observed at pH 5 and 6. Again, only at pH 7, an inhibitory effect is observed. The control aggregation (no EGCG) at pH 7 in the absence of glass beads displayed a peculiar characteristic: the ThT fluorescence increase starts already after ca. 10 h, but the rate of increase in fluorescence intensity was slow. The analysis of the supernatant after more than 100 h demonstrated that over 80 % of the protein was still soluble and had an average radius of 3.12 nm (Figure 6.5 B), corresponding to the expected size of the monomer [557]. The lag time of the sample with an equimolar concentration of EGCG was slightly longer, but the reaction reached a much higher final fluorescence level. All the other samples at pH 7 without glass beads did not show any fluorescence intensity increase. We also probed for the presence of fibrils and the degree of aggregation under those conditions with the help of AFM-imaging and MDS. In these MDS experiments, we measured both the

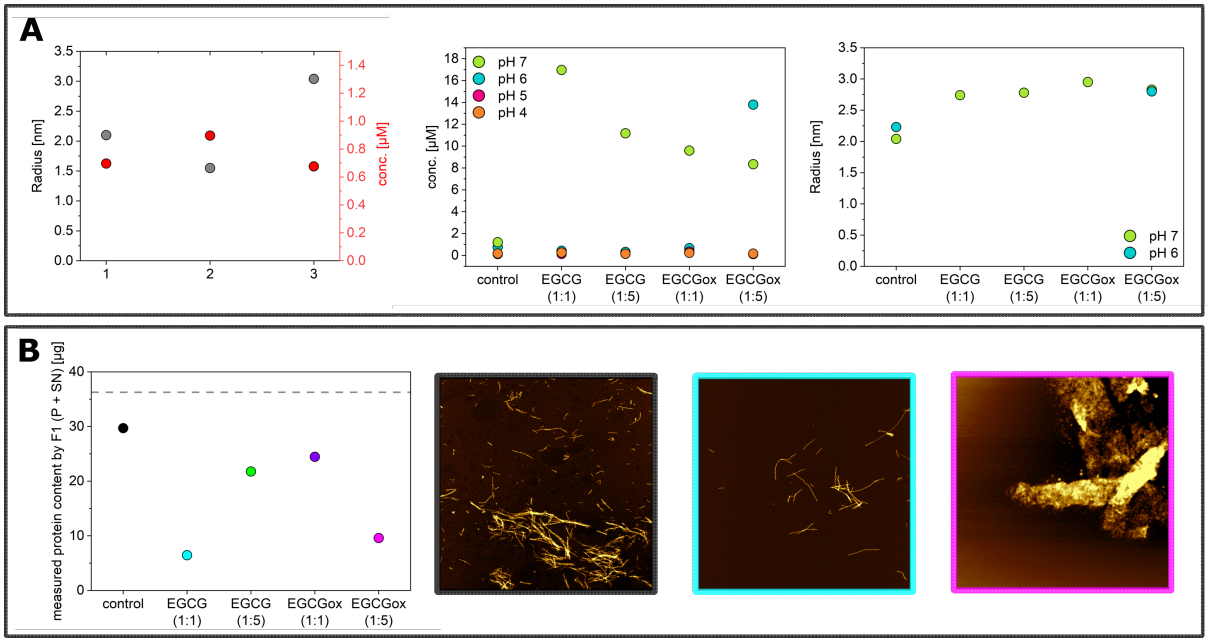

Figure 6.5: (A) Soluble α-synuclein concentration measured in the supernatant after centrifuging the end product of the aggregation reactions in a non-binding surface plate in the presence of glass beads. Radius in nm and concentration in µM of the three replicates of α-synuclein at pH 6 (control) (left), concentration in µM (middle) and radius in nm (right) of the end product of the aggregation reactions at pH 4, pH 5, pH 6 and pH 7. The three replicates per condition were combined before centrifugation (except for the control at pH 6, where each replicate sample was analysed separately, see A). (B) Amount of protein measurable with the Fluidity One (F1) MDS instrument (supernatant + pellet) in μg in the end-product of α-synuclein at pH 7 in a non-binding surface plate without additional glass beads (left). The dotted line indicates the used amount of protein. AFM-height-images of the control (black frame), α-synuclein with EGCG (1:1) (cyan frame) and of α-synuclein with EGCG$_{ox}$ (1:5) (magenta frame). The image scale is 5 x 5 μm. The colour range represents the height from -2 to 10 nm (left and middle) and -10 to 25 nm (right).

pellet and the supernatant and calculated the total concentration that the MDS data could account for. Based on the observation that the combined concentrations in both pellet and supernatant did not add up to the initially used concentration, we concluded that the samples with 1:5 EGCG and those 1:1 and 1:5 EGCG $_{ox}$ also aggregated, but the aggregates were not ThT-positive (either due to their non-fibrillar nature or due to quenching by EGCG) and were probably too big to be quantifiable by MDS. This is compatible with the observation that in all samples, except for the one with 1:1 EGCG, the α-synuclein was still primarily monomeric with radii between 2.4 and 3 nm.

At pH 4, in non-binding plates and in the absence of glass beads, all EGCG and EGCG$_{ox}$ containing samples showed faster and more reproducible aggregation than the control samples. In order to probe whether the type of aggregates formed under all these conditions is the same, we performed time-resolved AFM imaging experiments. Aliquots were taken at different time points directly out of the plate during the measurement (Figure 6.3B) and imaged by AFM (Figure 6.6). The sample of α-synuclein with a 5-fold excess of EGCG$_{ox}$ (1:5) (magenta frame) displayed many short fibrils and some amorphous structures after 17 h, when the ThT-signal had already reached the plateau-phase for several hours. For the other samples, we only found fibrils under all conditions in the last time point. At 17 h and 42 h, for example, we could not

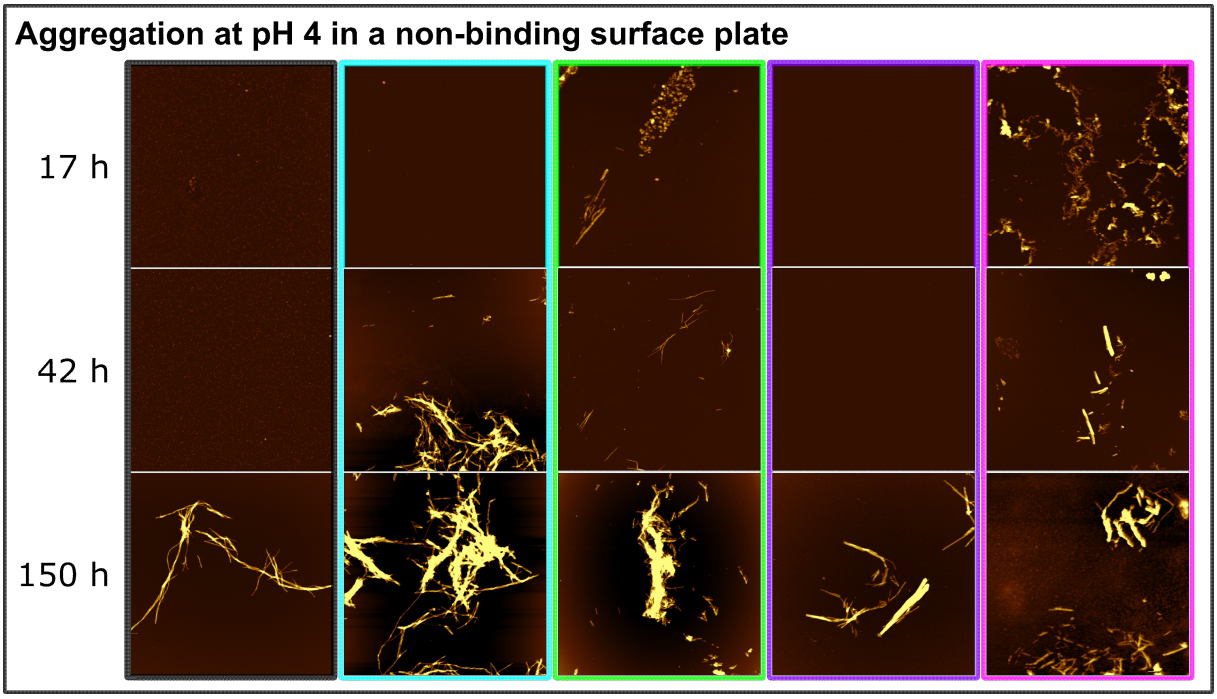

Figure 6.6: Time-resolved AFM-height-images of α-synuclein aggregation at pH 4 in a non-binding surface plate without glass beads. The colors of the frame correspond to the condition (Figure 6.3): control (black frame), EGCG (1:1) (cyan frame), EGCG (1:5) (green frame), $EGCG_{ox}$ (1:1) (purple frame) and $EGCG_{ox}$ (1:5) (magenta frame). The image scale is 5 x 5 μm. The colour range represents the height from -5 to 20 nm.

find any aggregates in the control and 1:1 $EGCG_{ox}$ samples, even if the ThT-signal displayed fibril formation, highlighting the fact that imaging-based analysis alone can be unreliable in some cases. Overall, we found no clear difference in appearance of the fibrils made under any of the different EGCG regimes at pH 4, confirming that neither EGCG nor $EGCG_{ox}$ displays an inhibiting effect under these conditions, and that the observed accelerated emergence of ThT fluorecence can indeed be ascribed to an enhancing effect of the EGCG.

As described above, α-synuclein normally requires an appropriate surface or interface, to induce the nucleation of its amyloid fibrils. Therefore the question arises as to how EGCG is able to accelerate the formation of amyloid fibrils in non-binding surface plates. It could be that EGCG directly interacts with the monomeric α-synuclein and facilitates nucleation or else, the EGCG interacts with the non-binding plate surface and renders it conducive to induce α-synuclein amyloid fibril nucleation. We hypothesised that if EGCG has a high affinity for the non-binding plate surface, pre-treatment of the plate with EGCG should have a comparable effect as if the ECGG was present during the entire aggregation experiment. Therefore, we incubated wells for two hours at room temperature with solutions of 25 µM (corresponding to 1:1 EGCG) or 125 µM EGCG or $EGCG_{ox}$ (corresponding to 1:5 EGCG). After incubation the solution was removed and the concentration of EGCG in the removed solution was determined. We found that the concentration of the 1:1 $EGCG_{ox}$ solution was decreased by 20 % and of the 1:5 $EGCG_{ox}$ solution by 28 % compared to solutions, which were incubated in an Eppendorf tube for the same time duration. The loss of ca. 6 µM from the 1:1 EGCG solution, is compatible with the formation of a monolayer of EGCG on the surface of the well, assuming that one molecule can occupy a surface area of approximately 1 nm x 1 nm. It is interesting that at the higher concentration, the EGCG solution is decreases by an approximately proportional amount, which could suggest the

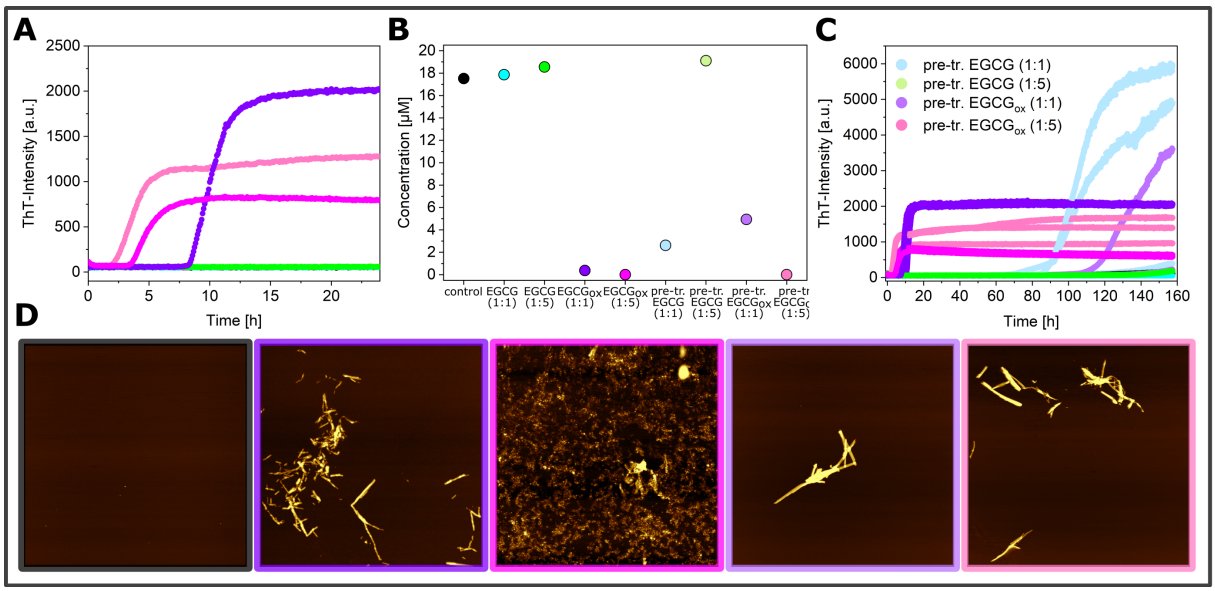

Figure 6.7: Aggregation kinetics of α-synuclein at pH 4 in a non-binding surface plate under quiescent conditions in absense of glass beads. The fibril formation was monitored in the presence and absence of EGCG or $EGCG_{ox}$, and in wells which were pre-treated with EGCG-solutions (A) and the corresponding concentration measurement by Fluidity One after 160 h (B) with AFM-height-images (D) of the aggregation products of α-synuclein (black frame) in presence of $EGCG_{ox}$ (1:1) (purple frame), (1:5) (magenta frame) and in the pre-treated wells with $EGCG_{ox}$ (1:1) (light purple frame) and (1:5) (light magenta frame) and the overview of the three replicates per condition (C). The image scale is 5 x 5 μm. The colour range represents the height from -3 to 12 nm.

formation of supramolecular EGCG structures either in solution or at the surface. Alternatively it could also be explained by a weak binding affinity that leads to saturation of all surface binding sites only at concentrations much higher than the ones used here. Aggregation in the wells treated in this way was indeed found to be accelerated in many cases with respect to the control (Figure 6.7). In particular, the pre-treatment with $EGCG_{ox}$ was found to be an efficient way to enable the plate to induce α-synuclein aggregation. Most notably, the surface pre-treated with 125 µM $EGCG_{ox}$ is even more efficient (t_{50} of 4.2 h $\pm$ 0.33h) than if the same concentration of 125 µM $EGCG_{ox}$ is present during the aggregation reaction (t_{50} of 4.6 h$\pm$ 0.74 h). In the case of 25 µM $EGCG_{ox}$, pre-treatment was found to be less efficient (t_{50} of more than 120 h) than the presence of the compound (t_{50} of 10.5 h $\pm$ 1.14), suggesting that 25 µM $EGCG_{ox}$ may not be enough to saturate the surface during pre-treatment. This conclusion is in agreement with the one drawn from the EGCG depletion experiments described above. These experiments were performed under quiescent conditions, explaining why some reactions displayed a slower kinetics compared to the equivalent solution conditions in Figure 6.3 B (control and EGCG 1:1 and 1:5). After the aggregation experiment, we centrifuged the samples and quantified the average size and concentration of the soluble protein by MDS. The samples which did not display an increase in the ThT-fluorescence had indeed remained mostly soluble, whereas the samples with $EGCG_{ox}$ aggregated nearly completely. The intensity I_{max} of the samples in pre-treated wells is higher than the corresponding ones with the same concentrations of EGCG in solution, even though the samples in the wells pre-treated with 25 µM EGCG and $EGCG_{ox}$ contained still a small amount of soluble protein. We could confirm the presence of fibrils of α-synuclein in the pre-treated wells by AFM. The sample with $EGCG_{ox}$ (1:5) present, which corresponds to the time resolved AFM sample in Figure 6.6 showed mostly amorphous material this time, even

though we had seen fibril formation (Figures 6.3 and 6.6) with almost identical kinetic traces. This variability in imaging but not in kinetic traces illustrates the fact that AFM imaging is not always representative of the distribution of species in the solution. In addition, the chemical nature of any structure is difficult to ascertain by AFM. The amorphous material in Figure 6.6 could be protein but also could correspond to the EGCG content of the solution.

Seeded experiments in the presence of EGCG and EGCG$_{ox}$

In all the experiments described above, nucleation and growth of α-synuclein amyloid fibrils proceeds simultaneously, in some cases (pH $<$ 6) in combination with secondary nucleation. A common strategy in the mechanistic analysis of protein aggregation is to perform seeded experiments which can strongly accelerate the overall aggregation time course and which, at high enough seed concentration, allows to study the process of fibril elongation in isolation [20, 379]. Experiments at weaker seeding can be useful if the contribution of secondary processes, such as fibril fragmentation or surface-catalysed secondary nucleation is to be studied [379]. In the case of α-synuclein, seeded experiments are often performed under quiescent conditions in a non-binding surface plate, in order to minimize the *de novo* formation of fibrils. In order to investigate the effects of EGCG and EGCG$_{ox}$ on the elongation process, we added 5 % seeds to monomeric α-synuclein with and without a 5-fold excess of EGCG and EGCG$_{ox}$ with respect to the concentration of monomeric α-synuclein at different pH values (Figure 6.8). We have recently proposed a definition of a measure for the seeding efficiency of a given batch of seed fibrils, based on the analysis of strongly seeded kinetic data [20]. A seeding efficiency of 1 seeding unit (s.u.) corresponds to an effective exponential constant of 1 h^{-1} under conditions where the normalised kinetic traces of the seeded experiments can be well-fitted by the function 1-e^{-kt}, with the time t in hours. We have quantified the following seeded experiments within this framework, allowing for a convenient comparison of the effects of EGCG and EGCG$_{ox}$. It has to be kept in mind, however, that in this framework, the effects of the inhibitor are entirely attributed to their action on the seed fibrils, and interactions with the soluble protein are not included. Therefore this framework is most appropriate for the experiments with pre-incubated seeds.

Fresh EGCG does not show an inhibitory influence on the seeding efficiency, but the fluorescence intensities are decreased in a pH-dependent manner compared to the absence of EGCG. At both pH 3 and 6, the seeding efficiency in the presence of EGCG appears even to be somewhat increased with respect to the control. The strongly seeded aggregation kinetics of α-synuclein at pH 7 in the presence EGCG appear unusual. After a fast increase, the ThT fluorescence intensity decreased strongly. However, by AFM we were able to verify the presence of fibrillar structures. The fibrils were present as big aggregates on the mica substrate (Figure 6.8 A), which is somewhat unexpected at neutral pH, given that higher order assembly of α-synuclein fibrils is most pronounced at pH values close to the isoelectric point [379]. The observed decrease in ThT signal could be due to this higher order assembly of the fibrils, or alternatively to the fact that the initial seeded aggregation is faster than the EGCG oxidation, but the latter will ultimately be responsible for a decrease in fluorescence intensity through quenching by the EGCG$_{ox}$. Due to this unusual shape, we did not quantify the seeding efficiency in the presence of EGCG at pH 7. Furthermore, the seeded aggregation at pH 4, both in the presence and absence of EGCG, shows biphasic behaviour, indicative of a contribution of secondary processes, also preventing the application of the simplified framework for the determination of seeding efficiencies. Such behaviour is unexpected at high seed concentrations, but could be explained by higher order assembly which is particularly pronounced close to the isoelectric point [379],

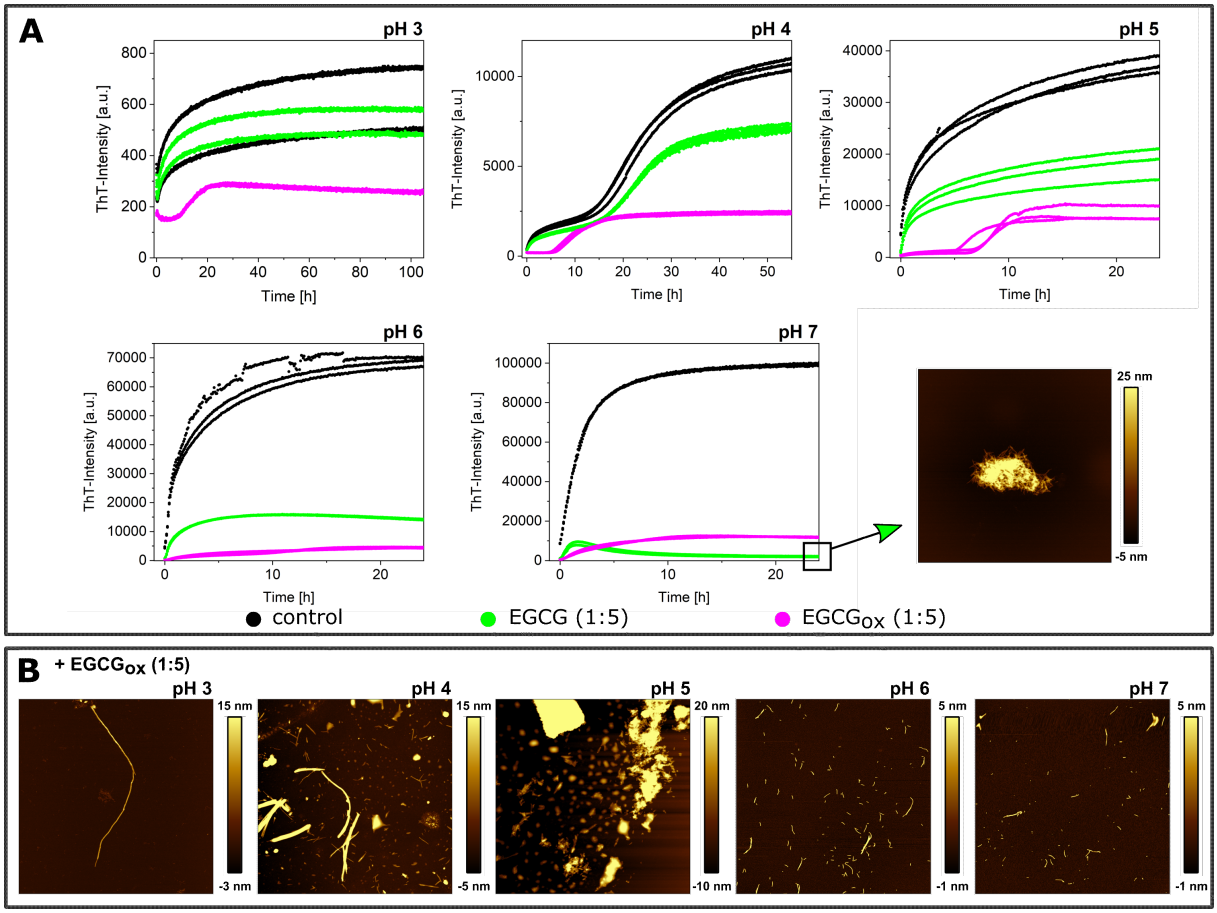

Figure 6.8: (A) The effects of EGCG and EGCG$_{ox}$ on the aggregation kinetics of α-synuclein, in particular the growth of fibrils, at different pH values (pH 3 to pH 7) in the presence of 5 % seeds monitored in a non-binding surface plate under quiescent conditions and a AFM-height-image of the sample at pH 7 in presence of EGCG (1:5) (B) AFM-height-images of α-synuclein in the presence of EGCG$_{ox}$ (1:5) at different pH values after the aggregation experiment. The image scale is 5 x 5 μm.

and which decreases the seeding efficiency. However the similarity of the kinetic traces indicates that also at pH 4, EGCG has no inhibitory effect on the seeding efficiency. The situation is quite different for 1:5 EGCG$_{ox}$, which dramatically reduces the seeding efficiency and leads to sigmoidal aggregation curves at pH 3-5 even at this high seed concentration of 5 %. The observed lag times are even longer than in experiments without added seeds in non-binding plates (Figure 6.9 C). However, these experiments cannot be compared in a straightforward manner, because the non-seeded experiments were performed under shaking conditions and the seeded experiments quiescently. Nevertheless, this result suggests that at the most acidic pH values (3-5), EGCG$_{ox}$ inactivates the pre-formed seeds and the observed ThT intensity increase is due to *de novo* formation of fibrils. AFM-measurement confirmed the presence of fibrils in the samples with EGCG$_{ox}$ under all pH conditions. The fitting of the kinetics which showed the expected shape for strongly seeded experiments (i.e. single exponential function, pH 6-7) reveals a somewhat decreased seeding efficiency with repsect to the control (Figure 6.9 A).

When less seeds are added to the experiments (0.5 % seeds in monomer equivalents), the aggregation kinetics are considerably slower than at the 10-fold higher seed concentration of the previous experiments (Figure 6.9B), potentially allowing the impact of EGCG and EGCG$_{ox}$ on secondary processes to be studied. An inhibitory effect of both EGCG and EGCG$_{ox}$ is clearly

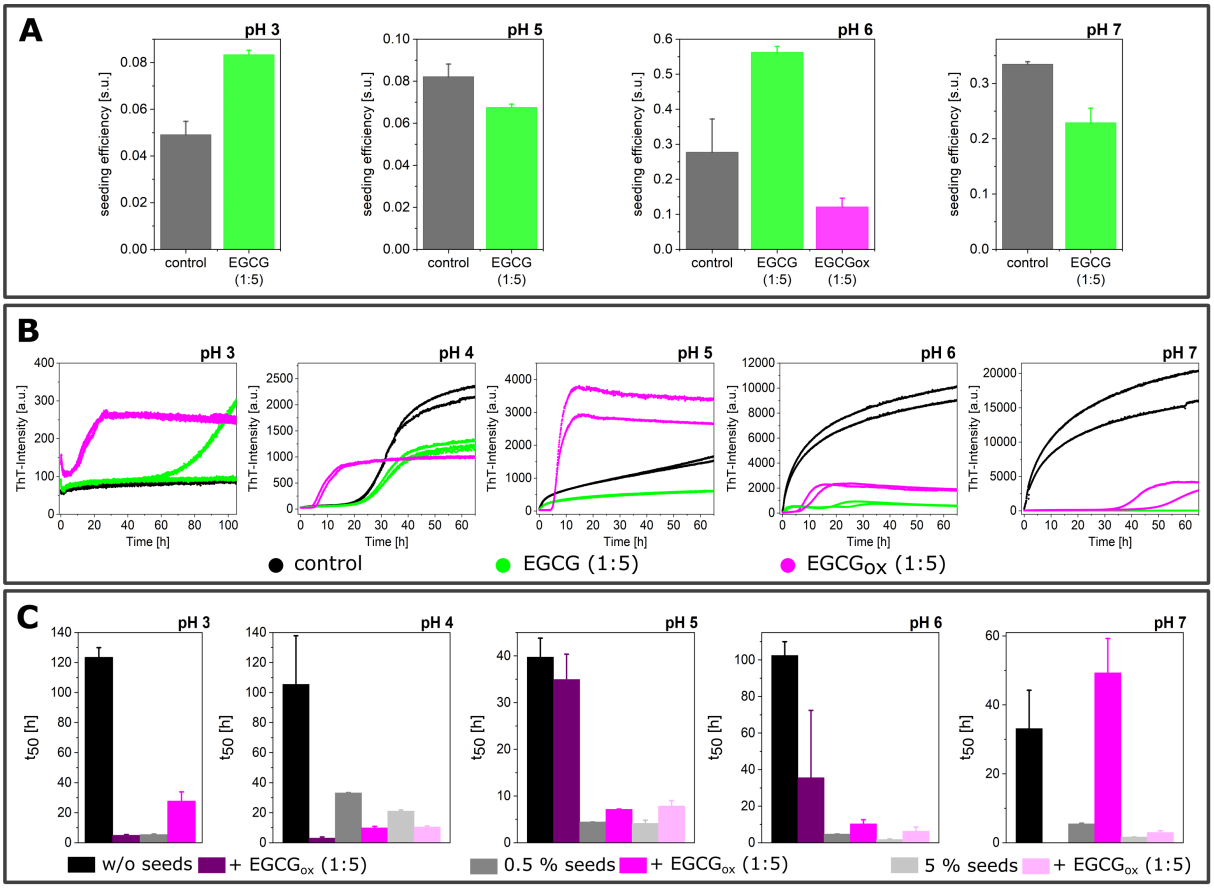

Figure 6.9: (A) The seeding efficiency, expressed in seeding units (s.u., [20]), determined by fitting the kinetics of the 5 % seeding experiments with y=1-e^{-kt} after normalisation between 0 and 1. Only the kinetics which showed the shape expected for a strongly seeded aggregation curve [20] were analysed. (B) The effects of EGCG and EGCG$_{ox}$ on the aggregation kinetics of α-synuclein at different pH values (pH 4 to pH 7) in the presence of 0.5 % seeds monitored in a non-binding surface plate under quiescent conditions. (C) The t_{50} of α-synuclein at different pH values (pH 3 to pH 7) in a non-binding surface plate without additional seeds with shaking (filled bar), with 0.5 % seeds (striped bar) and 5 % seeds (chequered bar) under quiescent conditions and in presence of 1:5 EGCG$_{ox}$ (violet).

visible at pH 7. The aggregation starts immediately, without a lag phase, in the control sample, with EGCG$_{ox}$ after over 30 h and in the presence of EGCG, no increase in ThT signal was observed after over 60 h. Compared to the aggregation with 5 % seeds, EGCG was therefore found to have a stronger impact on the aggregation kinetics at the decreased seed concentration. EGCG$_{ox}$ also delays the aggregation reaction at pH 5 and pH 6, whereas it has an accelerating effect at pH 4. At the latter pH, the weakly seeded data in the absence of EGCG or EGCG$_{ox}$ has the expected sigmoidal shape indicative of secondary nucleation. The aggregation kinetics in the presence of EGCG$_{ox}$ resembles that in the absence of seeds (Figure 6.3 and 6.7), where the EGCG$_{ox}$ induces *de novo* formation of fibrils by changing the properties of the non-binding plate surfaces. Overall, it appears that in these seeded experiments in non-binding plates, several competing effects are at work, all of which are pH-dependent. Fresh EGCG mostly exert its inhibitory effect at pH 7, consistent with the non-seeded experiments. EGCG$_{ox}$, on the other hand, is able to effectively interfere with seeded aggregation at acidic pH values, while at the same time being able to render the non-binding plate conducive to nucleate α-synuclein amyloid fibrils.

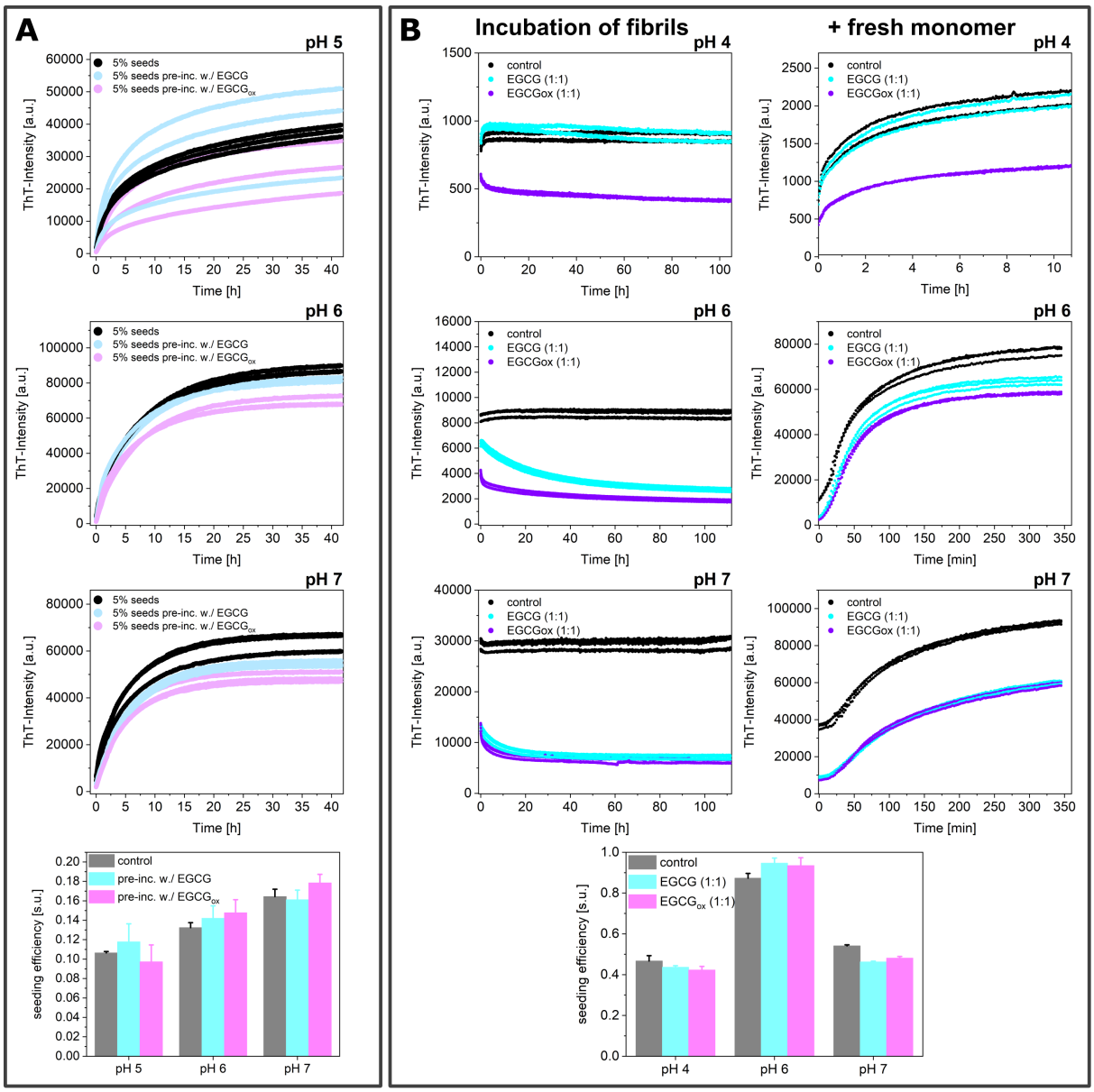

Figure 6.10: (A) The effects of EGCG and EGCG$_{ox}$ on the seeded aggregation, when the seeds were pre-incubated with stoichiometric amounts of the compound for 2 h at RT before adding them to a 25 µM monomer-solution at pH 5, pH 6 and pH 7 to a final concentration of 5 % (in monomer equivalents). The samples, where the fibrils were pre-incubated with the compound, contained still 1.25 µM EGCG or EGCG$_{ox}$. (B) 10 µM fibrils at pH 4, pH 6 and pH 7 were incubated in presence of 10 µM EGCG or EGCG$_{ox}$ in a non-binding surface plate at 37 °C for over 100 h (left) and then 50 µM fresh monomer were added (right).

Experiments in the presence of seeds pre-incubated with EGCG and EGCG$_{ox}$

In order to separate the effects of EGCG on the seeds and on the soluble α-synuclein, we also performed experiments where we incubated seed fibrils for 2 h at room temperature with stoichiometric amounts of EGCG and EGCG$_{ox}$ and added them to a final concentration of 5 % (in monomer equivalents) to 25 µM monomeric α-synuclein. This corresponds at the same time to a strong dilution of the EGCG, such that the ratio of soluble α-synuclein to EGCG/EGCG$_{ox}$ is 20:1 during the seeded experiments. If the EGCG either binds with high affinity to the

fibrils and/or is able to remodel the fibrils into non-fibrillar structures [355] then a reduction in seeding efficiency can be expected. However, the observed aggregation kinetics are very similar, particularly when they are normalized to the same final level of fluorescence intensity (Figure 6.10A). A quantitative analysis shows that the seeding efficiency showed no significant difference between the samples, suggesting that during the time scale of this experiment, the fibrils have not undergone a significant structural change. In order to investigate whether fibril remodeling into seeding-incompetent species can occur over longer time scales, we incubated 10 µM pre-formed seeds in a non-binding surface plate at 37 °C for over 100 h at pH 4, 6 and pH 7 with equimolar concentrations of EGCG or $EGCG_{ox}$ (Figure 6.10 B). The ThT-intensity of the control did not change over time, but the ThT intensity of the fibrillar sample with added EGCG decreased by a factor of 2.4 at pH 6 and 1.8 at pH 7, whereby the decrease at pH 6 was slower. The fluorescence intensity in the presence of oxidised EGCG was reduced by a factor of 2.2 at pH 6 and 2.1 at pH 7. The intensities of the samples with both EGCG and $EGCG_{ox}$ were very similar, the $EGCG_{ox}$ did not lead to a stronger quenching of the fluorescence. Compared to the control, the intensities after over 100 h are lowered by a factor of 3.2 at pH 6 and 4.2 at pH 7 in presence of EGCG and 4.7 in presence of $EGCG_{ox}$. Despite the fact that the significant decrease in ThT fluorescence intensity suggested a change of the seed fibril structure or concentration, and correspondingly a different seeding efficiency, the observed kinetics after addition of 50 µM monomer were virtually identical between all samples. We quantified the seeding efficiencies and found no statistically significant differences induced by the long incubation with EGCG or $EGCG_{ox}$. Therefore an equimolar concentration of EGCG is not able to induce changes in the seeding efficiency of preformed fibrils even after prlonged incubation.

6.5. Discussion

The effects of the potential anti-amyloid component EGCG and its auto-oxidised form on the process of amyloid fibril formation of the protein α-synuclein was analysed under distinct environmental conditions. We probed the effect of pH in the range from pH 3 to pH 7, the effect of presence of a glass bead, the influence of the type of plate surface, as well as the presence and absence of seeds, which were either freshly prepared or pre-incubated with EGCG or $EGCG_{ox}$. By examining the change of the maximum ThT-intensity and/or the kinetics of the aggregation (quantified by the t_{50} of the reaction) in presence of the compound, the effects on the *de novo* (i.e. un-seeded) amyloid formation were assessed and a summary is presented in table 6.1.

The overall picture that emerges from table 6.1 is that only at pH 7, both I_{max} and t_{50} suggest an inhibitory effect of EGCG under all tested conditions. This is confirmed by microfluidic diffusional sizing experiments, which show that α-synuclein is maintained in its soluble, probably monomeric state by both EGCG and $EGCG_{ox}$. Already at pH 6, the picture becomes more complex and the two parameters I_{max} and t_{50} do not yield a consistent picture: while I_{max} still largely suggests inhibition, t_{50} shows mostly no effect of EGCG but still inhibition for $EGCG_{ox}$. At neutral pH (i.e. pH 7), corresponding to the solution condition most often investigated in previous studies, EGCG is highly unstable. EGCG oxidises rapidly under the investigated buffer conditions within several hours [19] in a similar time scale as the aggregation process itself in presence of glass beads. A decrease of the pH value to pH 6 leads to a significant increase in the stability of EGCG and accordingly to a less strong inhibitory effect on α-synuclein aggregation. In particular at even lower pH values, where EGCG is highly stable, no significant effects on the *de novo* amyloid fibril formation of α-synuclein are observed. Therefore, mostly the auto-oxidised EGCG is able to inhibit amyloid formation. The fact that I_{max} and t_{50} do not always

Table 6.1: Evaluation of the effects of EGCG and $EGCG_{ox}$ on the *de novo* α-synuclein aggregation process established by comparing experimental values of I_{max} or t_{50} of the control samples (α-synuclein) with the ones determined in the presence of the component using one-way ANOVA (*:$p < 0.05$; **:$p < 0.01$; ***:$p < 0.001$). If the effect is defined as inhibitory without indication of the p-value, the sample showed no aggregation during the term. The abbreviations HBS stands for high-binding surface, NBS for non-binding surface and GB for glass bead.

Assessed by change in I_{max}

physiologically relevant conditions	Conditions	EGCG (1:1)	EGCG (1:5)	$EGCG_{OX}$ (1:1)	$EGCG_{OX}$ (1:5)
pH 7	HBS + GB	Inhibitory***	Inhibitory***	Inhibitory***	Inhibitory***
	HBS - GB	Inhibitory*	Inhibitory*	Inhibitory*	Inhibitory*
	NBS + GB	Inhibitory***	Inhibitory***	Inhibitory***	Inhibitory***
	NBS - GB	No effect	Inhibitory***	Inhibitory***	Inhibitory***
pH 6	HBS + GB	Inhibitory***	Inhibitory***	Inhibitory***	Inhibitory***
	HBS - GB	Inhibitory*	No effect	Inhibitory*	Inhibitory*
	NBS + GB	No effect	No effect	Inhibitory*	Inhibitory*
	NBS - GB	Enhancing**	No effect	Enhancing**	No effect
pH 5	HBS + GB	No effect	Inhibitory***	Inhibitory***	Inhibitory***
	HBS - GB	No effect	No effect	No effect	Inhibitory**
	NBS + GB	No effect	No effect	No effect	Inhibitory***
	NBS - GB	No effect	No effect	Enhancing***	No effect
pH 4	HBS + GB	No effect	No effect	Inhibitory*	Inhibitory***
	HBS - GB	No effect	Inhibitory**	No effect	Inhibitory***
	NBS + GB	No effect	No effect	No effect	No effect
	NBS - GB	Enhancing**	No effect	Enhancing*	No effect
pH 3	HBS + GB	No effect	No effect	No effect	Inhibitory***
	HBS - GB	No effect	No effect	No effect	Inhibitory**
	NBS + GB	No effect	Inhibitory*	Inhibitory***	Inhibitory***
	NBS - GB	No effect	No effect	No effect	No effect

Assessed by change in t_{50}

physiologically relevant conditions	Conditions	EGCG (1:1)	EGCG (1:5)	$EGCG_{OX}$ (1:1)	$EGCG_{OX}$ (1:5)
pH 7	HBS + GB	Inhibitory	Inhibitory	Inhibitory	Inhibitory
	HBS - GB	Inhibitory**	Inhibitory	Inhibitory	Inhibitory
	NBS + GB	Inhibitory	Inhibitory	Inhibitory**	No effect
	NBS - GB	No effect	Inhibitory	No effect	Inhibitory
pH 6	HBS + GB	No effect	No effect	Inhibitory*	Inhibitory
	HBS - GB	Inhibitory**	Enhancing	Inhibitory***	Inhibitory
	NBS + GB	No effect	No effect	No efffect	Inhibitory
	NBS - GB	No effect	No effect	No effect	No effect
pH 5	HBS + GB	No effect	No effect	No effect	Inhibitory**
	HBS - GB	No effect	No effect	No effect	No effect
	NBS + GB	Enhancing**	Enhancing**	Enhancing**	No effect
	NBS - GB	No effect	Inhibitory***	Enhancing***	No effect
pH 4	HBS + GB	No effect	No effect	No effect	Inhibitory***
	HBS - GB	No effect	No effect	No effect	No effect
	NBS + GB	No effect	Enhancing**	Enhancing***	No effect
	NBS - GB	Enhancing**	Enhancing**	Enhancing***	Enhancing***
pH 3	HBS + GB	No effect	No effect	Inhibitory*	No effect
	HBS - GB	No effect	No effect	No effect	Enhancing**
	NBS + GB	Enhancing**	Enhancing***	Enhancing***	Enhancing*
	NBS - GB	No effect	No effect	Enhancing**	Enhancing**

yield a consistent result strongly suggests that both EGCG and $EGCG_{ox}$ can interfere with ThT fluorescence. It is therefore important to not only rely on ThT intensity alone when assessing the

inhibitory effects of EGCG, or indeed any other compound. The inclusion of imaging techniques, such as AFM can help to avoid false positives, but we also show in this work that it can be challenging to obtain representative images of the content of an aggregated protein solution. We therefore employ an additional method in this work, MDS, that allows us to quantify both the concentration and average size of the protein remaining in the supernatant of the completed aggregation reaction after centrifugation. This study reveals the strong influence of the *de novo* aggregation conditions on the mode of action of a given compound. In a non-binding surface plate the presence of EGCG was observed to result in a faster kinetics of aggregation. Unlike the protein, the compound can bind to the non-binding surface and thereby enables α-synuclein monomer to bind to the so-modified surface. This paves the way to the nucleation of amyloid fibrils and starts the amyloid cascade. Consistent with this model, pre-incubation of the wells of a non-binding plate can also lead to efficient induction of aggregation, and a clear concentration dependence of this effect is visible.

To rely solely on the change in ThT intensity as a readout for the extent of inhibition can lead to erroneous interpretation of a given compound as an inhibitor (e.g. EGCG seemed to inhibit the aggregation at pH 6 in a high-binding plate with glass beads, but the t_{50} and the soluble protein at the end of the measurement showed no effect on the amyloid formation). In particular the oxidised EGCG strongly quenches ThT fluorescence, rather than inhibiting amyloid fibril growth. The compound either interferes with ThT-fluorescence [558] or binds to amyloid fibrils, preventing the binding of ThT [19, 559].

A *de novo* experiment involves different microscopic steps. At neutral pH conditions the process is dominated by primary nucleation, growth and fragmentation. Secondary nucleation on the surface of preformed α-synuclein fibrils becomes more important, when the pH is decreased towards the isoelectric point. By performing seeded experiments the investigation of the process of fibril elongation in isolation is feasible. In strongly seeded (5 % seeds in monomer equivalents), mostly $EGCG_{ox}$ exerts an effect on the seeding efficiency, and this inhibitory effect appears most pronounced at acidic pH values. At the lowest pH values, *de novo* aggregation, aided by the coating of the wells by EGCG, become efficient enough to lead to rapid aggregation despite the lack of seeding. More weakly seeded experiments (0.5 % seeds in monomer equivalents) are more susceptible to inhibition, probably because the relative concentration ratio of inhibitor to seed is higher. These seeded experiments provide clear evidence for an interaction between α-synuclein fibrils and both EGCG and $EGCG_{ox}$ under most pH conditions. This is consistent with a previous study that has reported an affinity of EGCG for α-synuclein fibrils in the low µM range at neutral pH [**?**]. Indeed, in this previous work, it was noted that the affinity of EGCG to α-synuclein fibrils appeared to become more tight over the course of minutes to hours. This corresponds to the time scale of EGCG oxidation under these conditions and is consistent with our finding here that $EGCG_{ox}$ has a stronger inhibitory effect at equivalent concentrations. We also performed an experiment to probe whether $EGCG_{ox}$ interacts with fibrils at more acidic pH than what had been shown in the previous study. When 25 µM α-synuclein fibrils are incubated with a stoichiometric quantity of $EGCG_{ox}$, approximately two thirds of the compound can be centrifuged down with the fibrils. This result confirms that α-synuclein fibrils interact with $EGCG_{ox}$ also at acidic pH with a stoichiometry not very different from 1:1.

Since we detected an inhibitory effect of $EGCG_{ox}$ in seeded experiments, particularly in the experiments at low seed concentrations, we tested whether incubating the seeds with EGCG or $EGCG_{ox}$ before the experiment was able to influence their seeding efficiency. In experiments where the seeds were incubated for 1 h and then added at a final concentration of 5 % in monomer

equivalents at pH 5-7, the aggregation kinetics and the efficiency of the seeds did not reveal any differences between pre-incubated seeds and those that had not been in contact with EGCG or $EGCG_{ox}$. We then tested whether the seeds were altered by a substantially longer incubation ($> 100\ h$) at 37 °C, followed by addition of fresh monomer. Also here we found no influence on the seeding efficiency, but the ThT fluorescence intensity was strongly decreased by the compounds. In these pre-incubation experiments, the concentrations of EGCG/$EGCG_{ox}$ is sub-stoichiometric during the actual elongation reaction. Taken together, our seeded experiments show therefore that EGCG and/or its oxidation products can only act on the seeding efficiency if present at high enough concentrations and that the interactions between the seeds and the compound are not able to permanently alter the seeding efficiency.

This finding agrees with a previous observation for κ-casein fibrils, which interact with high affinity with EGCG, but showed no indication of modification the structure or of redirection of the aggregation pathway [560]. However, various studies have reported the EGCG-induced remodelling of diverse amyloid fibrils and a formation of soluble amorphous aggregates at neutral pH [355, 356, 559, 561, 562, 563, 564, 565, 566]. Our seeding data did not suggest a seeding efficiency change or dissociation of the pre-formed α-synuclein fibrils; EGCG interacts with the fibril surface and therefore changes the interaction with ThT, as well as being able to interfere with the seeding if present at sufficiently high concentrations. However, an equimolar concentration is not sufficient to change the structure of preformed fibrils in such a way to render them less efficient as seeds.

All together, our results paint a much more complex picture of the inhibitory effects of EGCG on the amyloid fibril formation by α-synuclein than what the available literature suggests. We summarize our findings in Figure 6.11. First of all, EGCG itself seems to be very ineffective as inhibitor, whereas its oxidation products are much more efficient [19]. This finding explains why in general EGCG is a rather inefficient inhibitor in *de novo* experiments under pH conditions where EGCG is stable, i.e. mildly acidic pH. Furthermore, EGCG can interact with non-binding surfaces of plates and transform them into efficient surfaces for the heterogeneous primary nucleation of α-synuclein amyloid fibrils. Finally, $EGCG_{ox}$ is able to effectively interfere with seeded aggregation if present at a high enough ratio with respect to the seeds. However, upon dilution and subsequent unbinding, the fibrils recover their seeding efficiency. Our seeded experiments were carried out under quiescent conditons, where fibril fragmentation is negligible and no new ends are therefore generated, explaining the efficient inhibition. Under conditions of vigorous mechanical shaking, such as the ones we have employed in our *de novo* experiments, the constant generation of new ends through primary nucleation and fragmentation [379] renders the inhibitory effect of $EGCG_{ox}$ much weaker. Our study represents the most detailed investigation of the inhibitory effects of EGCG on α-synuclein amyloid fibril formation. From our study emerges a complete picture of the EGCG effect on α-synuclein aggregation. This data suggest that an extensive characterisation of potential amyloid fibril inhibitors is required in order to be able to conclude whether a given molecule is a useful inhibitor.

Conclusions

In conclusion, we have shown that EGCG only inhibits the amyloid fibril formation by α-synuclein under very specific conditions, and that this compound can even act as an enhancer of amyloid fibril formation through facilitating heterogeneous primary nucleation. The oxidation products of EGCG are significantly more efficient inhibitory agents than the unmodified EGCG, but at the same time it is also more efficient in inducing primary nucleation. This leads to a

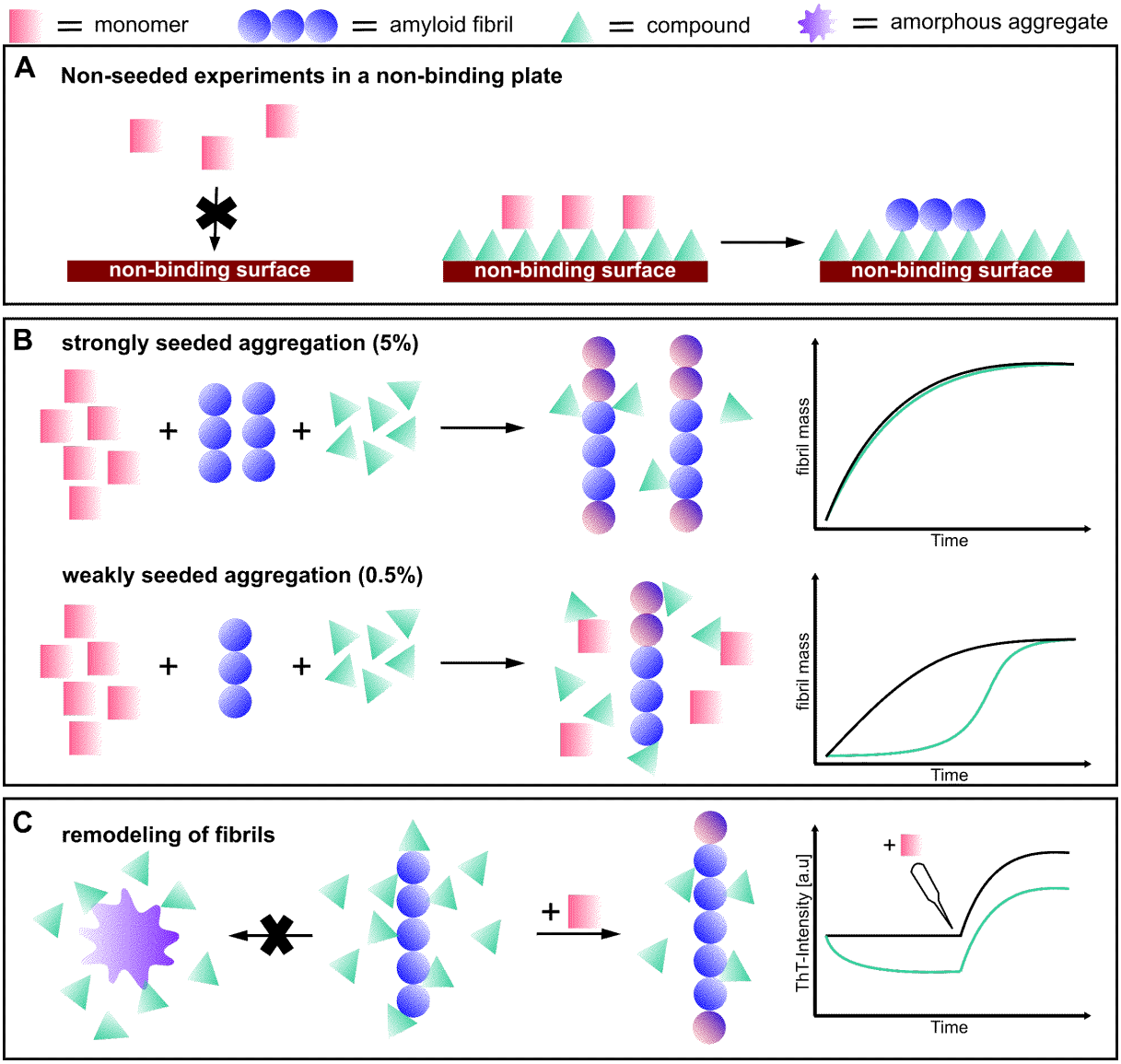

Figure 6.11: Schematic depiction of monitored effects of the anti-amyloid compound EGCG on the α-synuclein fibril formation. (A) shows that α-synuclein can not bind to the non-binding surface of the plate, while the compound EGCG can bind to the surface and facilitate the formation of amyloid fibrils. (B) EGCG displayed almost no effect on a strongly seeded aggregation (5 % seeds), whereas a weakly seeded aggregation (0.5 % seeds) could be retarded through interactions with the monomer. (C) The compound seems to interact with amyloid fibrils, but was not able to remodel the fibril into amorphous aggregates. When fresh monomer was added, the fibrils could elongate like the control.

complex interplay of the inhibitory and enhancing effects of EGCG and $EGCG_{ox}$, the net effects of which depend on the pH of the solution, the presence or absence of seeds, as well as the type of reaction vessel and the general conditions of the aggregation reaction. Importantly, we also establish that EGCG is not able to remodel α-synuclein into seed-incompetent structures. Taken together our results highlight the complexity of even such a supposedly well-established amyloid inhibitor as EGCG and establish a detailed experimental strategy to evaluate the true potential of a compound to interfere with amyloid fibril formation.

7

Discussion

A lot of scientific work has been carried out on light chain characteristics and their aggregation behaviour. But only in the last two decades studies with the full-length LC were conducted. In the past solely the variable domains were intensively investigated, because they were mainly found in amyloid deposits. The main focus was examining the variable domains REC, REI, SMA and LEN, Rhe [184, 197, 214, 257, 298, 413, 499, 567, 568, 569, 570, 571, 572, 573, 574]. All of these peptides derived from a patient and the amino acid sequence was determined, since the *de novo* sequencing of light chains is even nowadays challenging, former studies concentrated on the known sequences. REC and SMA were extracted from an AL patient, while LEN, REI and Rhe were excreted free a patient without indication of having amyloid deposits.

Only recently the full-length LC gained importance in the research field [232], but the question of amyloidogenesis of full-length LC remains unsolved. The aim of my project was to shed light on the aggregation behaviour of patient-derived full-length LCs. I have purified 20 LC proteins mainly from MM patients, characterized their biophysical properties in correlation to the patient's pathology (Chapter 3,, and performed a detailed Thermodynamic Aggregation Fingerprinting (ThAgg-Fip) of a subset of nine LC proteins. With the help of my collaboration partners from the Institut Pasteur we were able to to determine the amino acid sequence of a subset of nine LC proteins (Chapter 4).The inclusion criterion of a given sample was the availability of a sufficient amount of LC at high purity. A more detailed biophysical investigation of the selected samples was performed, which we denoted Thermodynamic and Aggregation Fingerprinting (ThAgg-Fip), because it revealed a unique set of biophysical and biochemical properties of every patient-derived light chain (Chapter 5).

All together I could establish a simple, but efficient protocol to purify light chains from urine samples of patients. The samples displayed a high purity, which enables a detailed biophysical characterization, though I had to exclude three samples from the study. The kidneys of these patients were massively damaged, hence they excreted mainly human serum albumin (HSA). The intrinsic physical properties which were claimed to correlate with the amyloidogenicity of a LC, such as thermodynamic stability, dimer content, ability of refolding and proteolytic resistance, could not be used as a discriminator of kidney damage severity.

However, LCs derived from a patient with a significantkidney impairment were resistant to proteolytic cleavage by trypsin. Even though a fast fragmentation could lead to the formation of fibrillar structures *in vitro*. Mass spectrometry could not only determine the unique amino acid of the structure, but also revealed the presence of different cathepsins in the LC samples purified from urine. Cathepsins are predominantly endopeptidases, which are intracellular

located in endolysosomal vesicles. Lysosomal lumen has an acidic pH close to 4.5 and contains approximately 60 different soluble hydrolytic enzymes, which are directly involved in the degradation of metabolites [380, 381, 382, 575]. This is the reason why cysteine cathepsins are active at slightly acidic pH values and mostly unstable at neutral pH [527, 528].

In vivo extracellular material reaches lysosomes mainly through endocytosis and phagocytosis, and intracellular materials are delivered through autophagy [575]. Studies demonstrated that the interaction with mesangial cells plays a key role in the pathogenesis of AL and LCDD. The glomerulus persists to approximately one third of mesangial cells. In contrast to light chains from an LCDD patient, amyloidogenic LCs are endocytosed by mesangial cells and delivered to lysosomes, where the LCs are exposed to secretases [576, 577, 578]. An *in vitro* study performed by Tagouri indicated, that amyloid formation in the kidney requires the intracellular processing of mesangial cells [579]. Kjeldsberg found intracellular amyloid fibrils within plasma cells, histiocytes, renal tubule cells and hepatocytes, suggesting that amyloid fibrils may form in the Golgi apparatus and within lysosomes [580]. It was postulated that the excessively produced LCs were transported to the Golgi apparatus, where they were transformed into crystalline inclusions, and thereafter, digested by lysosomal enzymes to form amyloid fibrils [247]. This is consistent with the presented findings of generic amyloidogenicity where the LCs are fragmented by cathepsins at low pH. Reiter and colleagues could detect the presence of cathepsin B in urinary cast in AL and MM patients [581].

Protein maturation occurs in the endoplasmic reticulum (ER) implying chaperone-assisted folding, post-translational modifications and disulfide bond formation [289, 290]. Native folded proteins which pass the quality control are delivered to the Golgi apparatus before they are secreted to the extracellular space [291, 292]. Excess light chains are usually secreted without assembly to the corresponding heavy chains. But the expression of SMA and LEN in COS cells, revealed that the secretion of a LC presenting an unstable conformation can fail due to the quality control of the ER [297, 298].

During the expression of SMA and LEN in COS cells, non-amyloidogenic LEN is rapidly oxidized in the ER, transferred to the Golgi apparatus and subsequently secreted, whereas newly synthesized amyloidogenic SMA remains in the reduced state, and gets dislocated out of the ER into the cytosol, where the protein gets ubiquitinylated and degraded by proteasomes. If the degradation fails, SMA can be found in perinuclear aggresomes surrounded by vimentin-containing intermediate filaments [297, 298]. LC amyloid deposits are extracellular. Only rarely patients having additional intracellular aggregates localized for instance in the rough endoplasmic reticulum are found [582, 583]. Usually altered conformations do not transit from the ER to the Golgi. Rather they are retained in the ER, dislocated in the cytosol and targeted for degradation by proteasomes [584, 585]. In patients the quality control in the ER is not always successful, otherwise e.g. SMA could not have been found in amyloid deposits in a patient. Nevertheless, activating the unfolding protein response significantly decreases the amount of secreted LCs.

Critical protein concentration for the aggregation of SMA was reported as 4 µM, which is approximately the concentration of LC in the ER of the plasma cell [586]. The lowest concentration used in my aggregation experiments was 5 µM. The ThT-signal was dramatically reduced compared to the fluorescence intensity for the aggregation experiment with 100 µM, but was still detectable at acidic pH. Under reducing conditions the signal was hardly analysable, but the aggregation under reducing conditions was very heterogeneous. Some of the LCs formed only ThT-negative aggregates (P001, P013 and P020) and the other LCs formed a mixture of amorphous and fibrillar aggregates. In addition to the reduction of the disulfide bond, the LCs

also got fragmented. But compared to the fragmentation at lower pH values, this fragmentation was very slow. The proportion of fragments did rarely change over an incubation time of 15 h, whereas the aggregation continued. Therefore the driving force is probably not the fragmentation of the LCs, but rather the reduced dimer. Unlike the other samples, which already comprised very large aggregates after 75 min or 5 h, P006, P016 and P017 formed oligomeric species, which grew more slowly. The size of the other aggregates was so enlarged, that they sediment during the acceleration to 60,000 rpm or even scattered the light immense at 3000 rpm. But except for sample P016, which aggregates fairly slow, these differences in the behaviour cannot be revealed in the ThT-kinetics. The fact, that reducing conditions can induce the formation of oligomeric species, was already reported by Andrich *et al.* [267].

Nevertheless, the data at pH 3 suggest, that the critical concentration for fragments is considerably smaller.

The aggregation of SMA could be accelerated with pre-formed fibrils and these seeds could also be used to seed LEN [587]. A possible cross-seeding of a non-amyloidogenic LC with fibrils of an amyloidogenic LC, raises a more complex picture. This implies, that only a small proportion of an aggregation prone LC is needed to induce the aggregation of a LC, which would not self-assemble.

In vitro fibril formation of LCs, which did not aggregate *in vivo* could be induced by low concentrations of denaturant, indicating that there are no structural or sequence-specific features other than the greater stability [257].

The injection of LCs derived from patients with different clinical appearances in six-week-old mice manifest in a comparable deposition similar to the patients deposits, however the biophysical characteristics of the used light chain proteins showed no correlation [588, 589].

The systemic analysis of the LC sequences using different computational approaches, emphasizes the universal amyloidogenicity of patient-derived light chains, in particular together with sequences derived from different germlines selected from AL-Base. The pathology of the patients was known, therefore they could be categorized in amyloidogenic and non-amyloidogenic LCs. TANGO determined similar aggregation propensities. This reveals that there is no significant difference within the sample set. The TANGO calculations have not been compared to other proteins, because they displayed very diverse aggregation propensities irrelevant of their *in vivo* behaviour. Thus the algorithms are merely useful to compare similar sequences.

PASTA could not display the amyloidogenicity, whereas waltz determined no amyloid propensity for the LC derived from an AL-patient. According to this, the different approaches have to be considered critically.

Surfaces can catalyze the formation of amyloid fibrils. Surface-induced aggregation of SMA was orders of magnitude faster on negatively charged mica surface than aggregation in bulk solution. On positively or nonpolar modified mica no fibril formation was monitored. Large mature fibrils were absent on the surface [590]. High rate of blood velocity, destabilizing lower pH, higher salt and urea concentration in the kidney lead to *in vivo* deposits.

The comprehensive picture which arises, is that LC aggregation seems to be influenced by several factors, of which some are dependent on the intrinsic protein properties whereas others depend on the environment. In addition to the already mentioned proteases, the composition of the extracellular matrix, such as glycosaminoglycans (GAGs) [495, 591], lipid compositions [592], the ionic strength [593], pH [594] and the redox status [501, 595, 596] is highly relevant. *In*

vitro aggregation could be induced by biologically relevant lipid-derived aldehydes by altering the secondary structure to an increased β-sheet conformation. This was primarily dependent upon the lipid aldehyde and not the primary structure of the examined LCs [592].

Since the aggregation of light chains seems to be dependent on different external factors, the study of the impact of the polyphenol epigallocatechin-3-gallate (EGCG) is unfeasible to be carried out with LCs in particular without a deeper understanding of the potential course of action of EGCG. Therefore I conducted aggregation experiments with the well-studied Parkinson protein α-synuclein. The mode of action was very dependent on the aggregation conditions and range from enhancement to inhibition (Chapter 6). EGCG only inhibits amyloid formation at pH 7, where EGCG auto-oxidises fast into various products. $EGCG_{ox}$ is a significantly more efficient inhibitor agent than unmodified EGCG. Both compounds can interfere with ThT-fluorescence, which can result in false positives (Figure 7.1).

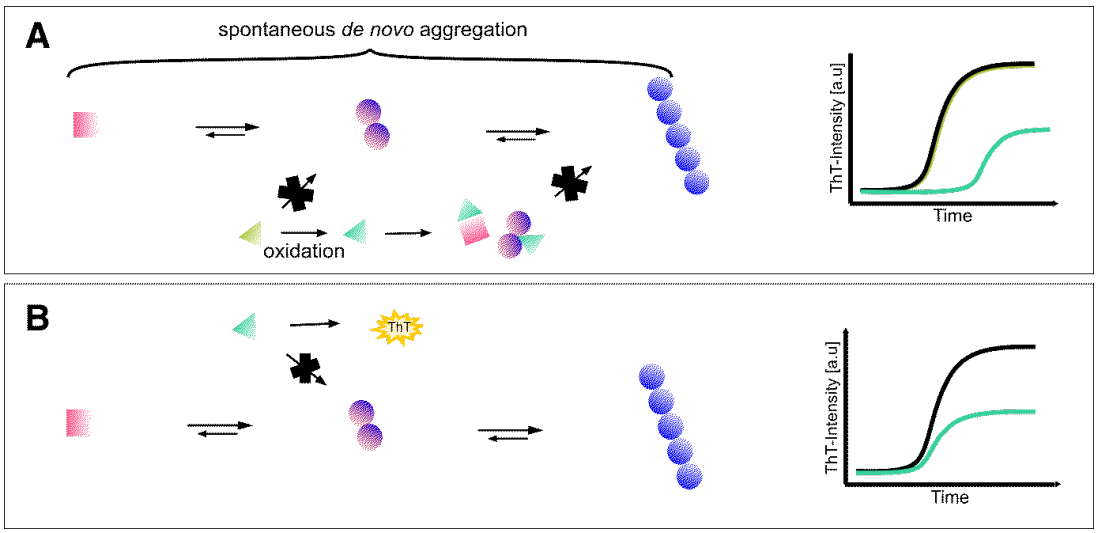

Figure 7.1: Impact of the compound EGCG on spontaneous *de novo* aggregation. (A) EGCG auto-oxidises rapidly at neutral pH and this oxidised compound can inhibit the fibril formation, which results in an prolonged lag-time. (B) EGCG and $EGCG_{ox}$ can interfere with ThT-fluorescence, which may lead to false positives.

To assess the impact of the compound, the used conditions played a key factor. For instance, *de novo* aggregation of α-synuclein was dramatically accelerated in non-binding plates. A-synuclein requires a hydrophobic surface to promote primary nucleation. This surface can either be provided by lipids, the air-water interface or the surface of the reaction vessel. A-synuclein cannot bind to the non-binding surface plates, but EGCG covers the modified surface, whereby enabling the binding of the protein.

EGCG displayed almost no effect on a strongly seeded aggregation reaction, whereas a weakly seeded aggregation reaction is more strongly inhibited. Even though EGCG interacted with the fibrils, the compound was not found to be able to remodel the fibrils into amorphous, seeding-incompetent aggregates. They presented the same seeding efficiency as the control fibrils.

Summarising, the anti-amyloidogenic compound EGCG is strongly dependend on the environmental conditions, such as the pH value of the solution, the type of the reaction vessel, the presence or absence of seeds. This complexity, in particular of a supposedly well-established amyloid inhibitor, raised awareness to a comprehensive study design.

7.1. Outlook

The idea of an intrinsic universal amyloidogenicity challenge the current paradigm of the link between amino acid sequence and amyloid fibril formation of pathogenic LCs. The primary sequence may play a role in their behaviour in a patient, but under appropriate, physiological conditions all light chains formed amyloid structures. The external factors *in vivo* appear to be essential requirements. This aggravates the experimental study design and in particular the forecast of the behaviour in a patient.

To understand the effect of the intrinsic protein properties the amount of samples has to be increased and our developed fingerprinting approach has to be performed. With a high amount of ThAgg-Fip data sets, deep learning can be accomplished. This may reveal certain characteristics, which tend to be overlooked in standard approaches. In addition, this raises the question, if more precise knowledge of the patient's environment is required.

In the future, *in vitro* studies better mimicking *in vivo* conditions, have to be performed. In particular the affinity to different proteins have to be examined.

The non-fibrillar glycoprotein serum amyloid P component (SAP) was found to bind and deposit universally to amyloid fibrils and was present in amyloid deposits of Ig light chains [597]. SAP is a plasma protein, which belongs to the pentraxin family [598]. The interaction with fibrils may involve glycosaminoglycans, but SAP also binds to *in vitro* formed fibrils. Patients with Waldenström's macroglobulinaemia, who possess high levels of IgM monoclonal protein [599], have elevated SAP levels ($83\pm34\,\mu g/ml$) compared to patients with MM ($39\pm17\,\mu g/ml$) and to a healthy control group ($35\pm11\,\mu g/ml$) [600]. SAP bound to amyloid fibrils, protects the fibrils from degradation by proteolytic enzymes, e.g. cathepsin G in the presence of calcium [601], whereby amyloid can be fostered. SAP could not be detected in non-amyloid deposits of LCDD-patients [602, 603]. *In vitro* aggregation kinetics in the presence of SAP are troublesome, because it has a high tendency to precipitate. Therefore it is questionable, whether SAP promotes aggregation by facilitating nucleation or solely by protecting formed fibrils. Nevertheless, SAP can be used to detect amyloid deposits, diagnose amyloidosis and potentially treat amyloidosis for example by using radioiodinated SAP [604] or the anti-SAP antibody Dezamizumab [336, 348].

Moreover, light chains can non-covalently bind to the glycosylated protein uromodulin, also known as Tamm-Horsfall protein, which is the most abundant protein in normal human urine [605]. The formation of heterotypic aggregation of these proteins form myeloma casts in the distal nephron of the kidney and results in renal failure [606]. These aggregates displayed a low digestability by proteases [607]. Uromodulin could be detected in all the investigated samples using MS.

The investigation of patient-derived LCs has the advantage that the samples still comprise patient-specific additional components such as cathepsins. However, this hampers the analysis of the intrinsic protein characteristics. To overcome this burden, the LCs can be produced recombinantly. A protocol to express LCs in *E. coli* and purify them from the periplasmic space and from insoluble inclusion bodies was established using an amyloidogenic LC sequence from literature tagged with an His-Tag. This protocol can be used to express the LCs, which primary sequence has been determined. Furthermore, an established LC, such as LEN, can be expressed and examined using the outlined approaches in the presence and absence of additional lysosomal proteases.

8

LITERATUR

[1] Elizabeth R Morris and Mark S Searle. Overview of protein folding mechanisms: experimental and theoretical approaches to probing energy landscapes. *Current protocols in protein science*, 68(1):28–2, 2012.

[2] Ania C Muntau, João Leandro, Michael Staudigl, Felix Mayer, and Søren W Gersting. Innovative strategies to treat protein misfolding in inborn errors of metabolism: pharmacological chaperones and proteostasis regulators. *Journal of inherited metabolic disease*, 37(4):505–523, 2014.

[3] Jozef Adamcik and Raffaele Mezzenga. Amyloid polymorphism in the protein folding and aggregation energy landscape. *Angewandte Chemie International Edition*, 57(28):8370–8382, 2018.

[4] Jason Greenwald and Roland Riek. Biology of amyloid: structure, function, and regulation. *Structure*, 18(10):1244–1260, 2010.

[5] Paolo Swuec, Francesca Lavatelli, Masayoshi Tasaki, Cristina Paissoni, Paola Rognoni, Martina Maritan, Francesca Brambilla, Paolo Milani, Pierluigi Mauri, Carlo Camilloni, et al. Cryo-em structure of cardiac amyloid fibrils from an immunoglobulin light chain al amyloidosis patient. *Nature communications*, 10(1):1–9, 2019.

[6] Alexander J Dear, Thomas CT Michaels, Georg Meisl, David Klenerman, Si Wu, Sarah Perrett, Sara Linse, Christopher M Dobson, and Tuomas PJ Knowles. Kinetic diversity of amyloid oligomers. *Proceedings of the National Academy of Sciences*, 117(22):12087–12094, 2020.

[7] Alexander J Dear, Georg Meisl, Anđela Šarić, Thomas CT Michaels, Magnus Kjaergaard, Sara Linse, and Tuomas PJ Knowles. Identification of on-and off-pathway oligomers in amyloid fibril formation. *Chemical Science*, 2020.

[8] Ivan Konstantinov. Antibody immunoglobulin g (igg). https://visual-science.com/projects/antibody-immunoglobulin-G/illustration, december 2020.

[9] Kathryn R Ely, James N Herron, Melani Harker, and Allen B Edmundson. Three-dimensional structure of a light chain dimer crystallized in water: conformational flexibility of a molecule in two crystal forms. *Journal of molecular biology*, 210(3):601–615, 1989.

[10] Alain Roussel, Silvia Spinelli, Sophie Déret, Jorge Navaza, Pierre Aucouturier, and Christian Cambillau. The structure of an entire noncovalent immunoglobulin kappa light-chain dimer (bence-jones protein) reveals a weak and unusual constant domains association. *European journal of biochemistry*, 260(1):192–199, 1999.

[11] Helen M Berman, Talapady N Bhat, Philip E Bourne, Zukang Feng, Gary Gilliland, Helge Weissig, and John Westbrook. The protein data bank and the challenge of structural genomics. *Nature structural biology*, 7(11):957–959, 2000.

[12] Sunghwan Kim, Paul A Thiessen, Evan E Bolton, Jie Chen, Gang Fu, Asta Gindulyte, Lianyi Han, Jane He, Siqian He, Benjamin A Shoemaker, et al. Pubchem substance and compound databases. *Nucleic acids research*, 44(D1):D1202–D1213, 2016.

[13] Sameer Velankar, Younes Alhroub, Anaëlle Alili, Christoph Best, Harry C Boutselakis, Ségolène Caboche, Matthew J Conroy, Jose M Dana, Glen van Ginkel, Adel Golovin, et al. Pdbe: protein data bank in europe. *Nucleic acids research*, 39(suppl_1):D402–D410, 2010.

[14] Eva Kowalinski, Chloe Zubieta, Andrea Wolkerstorfer, Oliver HJ Szolar, Rob WH Ruigrok, and Stephen Cusack. Structural analysis of specific metal chelating inhibitor binding to the endonuclease domain of influenza ph1n1 (2009) polymerase. *PLoS Pathog*, 8(8):e1002831, 2012.

[15] Greg Ralston. *Introduction to analytical ultracentrifugation*, volume 1. Beckman California:, 1993.

[16] James L Cole, Jeffrey W Lary, Thomas P Moody, and Thomas M Laue. Analytical ultracentrifugation: sedimentation velocity and sedimentation equilibrium. *Methods in cell biology*, 84:143–179, 2008.

[17] Rebecca Sternke-Hoffmann, Amelie Boquoi, David Lopez Y Niedenhoff, Florian Platten, Roland Fenk, Rainer Haas, and Alexander K Buell. Biochemical and biophysical characterisation of immunoglobulin free light chains derived from an initially unbiased population of patients with light chain disease. *PeerJ*, 8:e8771, 2020.

[18] Nadine Dyballa and Sabine Metzger. Fast and sensitive colloidal coomassie g-250 staining for proteins in polyacrylamide gels. *JoVE (Journal of Visualized Experiments)*, (30):e1431, 2009.

[19] Tomas Sneideris, Andrius Sakalauskas, Rebecca Sternke-Hoffmann, Alessia Peduzzo, Mantas Ziaunys, Alexander K Buell, and Vytautas Smirnovas. The environment is a key factor in determining the anti-amyloid efficacy of egcg. *Biomolecules*, 9(12):855, 2019.

[20] Alexander K Buell. The growth of amyloid fibrils: rates and mechanisms. *Biochemical Journal*, 476(19):2677–2703, 2019.

[21] Yujin E Kim, Mark S Hipp, Andreas Bracher, Manajit Hayer-Hartl, and F Ulrich Hartl. Molecular chaperone functions in protein folding and proteostasis. *Annual review of biochemistry*, 82:323–355, 2013.

[22] Christian B Anfinsen. Principles that govern the folding of protein chains. *Science*, 181(4096):223–230, 1973.

[23] Guo-Wei Wei. Protein structure prediction beyond alphafold. *Nature Machine Intelligence*, 1(8):336–337, 2019.

[24] Andrew W Senior, Richard Evans, John Jumper, James Kirkpatrick, Laurent Sifre, Tim Green, Chongli Qin, Augustin Žídek, Alexander WR Nelson, Alex Bridgland, et al. Improved protein structure prediction using potentials from deep learning. *Nature*, 577(7792):706–710, 2020.

[25] Linlin Qiu, Suzette A Pabit, Adrian E Roitberg, and Stephen J Hagen. Smaller and faster: The 20-residue trp-cage protein folds in 4 μs. *Journal of the American Chemical Society*, 124(44):12952–12953, 2002.

[26] Dmitry N Ivankov and Alexei V Finkelstein. Prediction of protein folding rates from the amino acid sequence-predicted secondary structure. *Proceedings of the National Academy of Sciences*, 101(24):8942–8944, 2004.

[27] Athi N Naganathan and Victor Muñoz. Scaling of folding times with protein size. *Journal of the American Chemical Society*, 127(2):480–481, 2005.

[28] Cyrus Levinthal. Mossbauer spectroscopy in biological systems. In *Proceedings of a meeting held at Allerton House. P. Debrunner, JCM Tsibris, and E. Munck, editors. University of Illinois Press, Urbana, IL*, 1969.

[29] Robert Zwanzig, Attila Szabo, and Biman Bagchi. Levinthal's paradox. *Proceedings of the National Academy of Sciences*, 89(1):20–22, 1992.

[30] Martin Karplus. The levinthal paradox: yesterday and today. *Folding and design*, 2:S69–S75, 1997.

[31] Donald B Wetlaufer. Nucleation, rapid folding, and globular intrachain regions in proteins. *Proceedings of the National Academy of Sciences*, 70(3):697–701, 1973.

[32] Alan R Fersht. Optimization of rates of protein folding: the nucleation-condensation mechanism and its implications. *Proceedings of the National Academy of Sciences*, 92(24):10869–10873, 1995.

[33] Haripada Maity, Mita Maity, Mallela MG Krishna, Leland Mayne, and S Walter Englander. Protein folding: the stepwise assembly of foldon units. *Proceedings of the National Academy of Sciences*, 102(13):4741–4746, 2005.

[34] Tanya M Raschke, Joan Kho, and Susan Marqusee. Confirmation of the hierarchical folding of rnase h: a protein engineering study. *Nature structural biology*, 6(9):825–831, 1999.

[35] Peter S Kim and Robert L Baldwin. Specific intermediates in the folding reactions of small proteins and the mechanism of protein folding. *Annual review of biochemistry*, 51(1):459–489, 1982.

[36] Martin Karplus and David L Weaver. Protein folding dynamics: The diffusion-collision model and experimental data. *Protein science*, 3(4):650–668, 1994.

[37] Robert L Baldwin. How does protein folding get started? *Trends in biochemical sciences*, 14(7):291–294, 1989.

[38] Peter E Leopold, Mauricio Montal, and José N Onuchic. Protein folding funnels: a kinetic approach to the sequence-structure relationship. *Proceedings of the National Academy of Sciences*, 89(18):8721–8725, 1992.

[39] Ken A Dill and Hue Sun Chan. From levinthal to pathways to funnels. *Nature structural biology*, 4(1):10–19, 1997.

[40] José Nelson Onuchic, Nicholas D Socci, Zaida Luthey-Schulten, and Peter G Wolynes. Protein folding funnels: the nature of the transition state ensemble. *Folding and Design*, 1(6):441–450, 1996.

[41] F Ulrich Hartl and Manajit Hayer-Hartl. Converging concepts of protein folding in vitro and in vivo. *Nature structural & molecular biology*, 16(6):574, 2009.

[42] Christopher M Dobson. Protein misfolding, evolution and disease. *Trends in biochemical sciences*, 24(9):329–332, 1999.

[43] Christopher M Dobson. Protein folding and misfolding. *Nature*, 426(6968):884–890, 2003.

[44] Yoshikazu Aso, Kentaro Shiraki, and Masahiro Takagi. Systematic analysis of aggregates from 38 kinds of non disease-related proteins: identifying the intrinsic propensity of polypeptides to form amyloid fibrils. *Bioscience, biotechnology, and biochemistry*, 71(5):1313–1321, 2007.

[45] Sarah Perrett, Chi LL Pham, Ann H Kwan, and Margaret Sunde. Functional amyloid: widespread in nature, diverse in purpose. *Essays in biochemistry*, 56:207–219, 2014.

[46] Nani Van Gerven, Roger D Klein, Scott J Hultgren, and Han Remaut. Bacterial amyloid formation: structural insights into curli biogensis. *Trends in microbiology*, 23(11):693–706, 2015.

[47] Vassiliki A Iconomidou, Georgios D Chryssikos, Vassilis Gionis, Athanassios S Galanis, Paul Cordopatis, Andreas Hoenger, and Stavros J Hamodrakas. Amyloid fibril formation propensity is inherent into the hexapeptide tandemly repeating sequence of the central domain of silkmoth chorion proteins of the a-family. *Journal of structural biology*, 156(3):480–488, 2006.

[48] Fabrizio Chiti and Christopher M Dobson. Protein misfolding, amyloid formation, and human disease: a summary of progress over the last decade. *Annual review of biochemistry*, 86:27–68, 2017.

[49] Robert A Kyle. Amyloidosis: a convoluted story. *British journal of haematology*, 114(3):529–538, 2001.

[50] HOLDE PUCHTLER and FAYE SWEAT. A review of early concepts of amyloid in context with contemporary chemical literature from 1839 to 1859. *Journal of Histochemistry & Cytochemistry*, 14(2):123–134, 1966.

[51] Jean D Sipe and Alan S Cohen. History of the amyloid fibril. *Journal of structural biology*, 130(2-3):88–98, 2000.

[52] C Schmidt. Ueber das sogenannte ?thierische amyloïd? ? (substanz der corpuscula amylacea). *Justus Liebigs Annalen der Chemie*, 110(2):250–254, 1859.

[53] N Friedreich and A Kekule. Zur amyloidfrage. *Archiv für pathologische Anatomie und Physiologie und für klinische Medicin*, 16(1-2):50–65, 1859.

[54] H Bennhold. Specific staining of amyloid by congo red. *Muenchen. Med. Wochenschr*, 30(1537-1538):31, 1922.

[55] Peter Ladewig. Double-refringence of the amyloid-congo-red-complex in histological sections. *Nature*, 156(3951):81–82, 1945.

[56] HD Attwood, CG Price, and RJ Riddell. Primary diffuse tracheobronchial amyloidosis. *Thorax*, 27(5):620–624, 1972.

[57] Alan S Cohen and Evan Calkins. Electron microscopic observations on a fibrous component in amyloid of diverse origins. *Nature*, 183(4669):1202–1203, 1959.

[58] ED Eanes and GG Glenner. X-ray diffraction studies on amyloid filaments. *Journal of Histochemistry & Cytochemistry*, 16(11):673–677, 1968.

[59] Laurence Bonar, Alan S Cohen, and Martha M Skinner. Characterization of the amyloid fibril as a cross-β protein. *Proceedings of the Society for Experimental Biology and Medicine*, 131(4):1373–1375, 1969.

[60] Louise C Serpell, Paul E Fraser, and Margaret Sunde. [34] x-ray fiber diffraction of amyloid fibrils. In *Methods in enzymology*, volume 309, pages 526–536. Elsevier, 1999.

[61] Robert Tycko. Solid-state nmr studies of amyloid fibril structure. *Annual review of physical chemistry*, 62:279–299, 2011.

[62] Yaowang Li, Chunyu Zhao, Feng Luo, Zhenying Liu, Xinrui Gui, Zhipu Luo, Xiang Zhang, Dan Li, Cong Liu, and Xueming Li. Amyloid fibril structure of α-synuclein determined by cryo-electron microscopy. *Cell research*, 28(9):897–903, 2018.

[63] Yunpeng Sun, Shouqiao Hou, Kun Zhao, Houfang Long, Zhenying Liu, Jing Gao, Yaoyang Zhang, Xiao-Dong Su, Dan Li, and Cong Liu. Cryo-em structure of full-length α-synuclein amyloid fibril with parkinson?s disease familial a53t mutation. *Cell Research*, 30(4):360–362, 2020.

[64] Matthias Schmidt, Sebastian Wiese, Volkan Adak, Jonas Engler, Shubhangi Agarwal, Günter Fritz, Per Westermark, Martin Zacharias, and Marcus Fändrich. Cryo-em structure of a transthyretin-derived amyloid fibril from a patient with hereditary attr amyloidosis. *Nature communications*, 10(1):1–9, 2019.

[65] Lothar Gremer, Daniel Schölzel, Carla Schenk, Elke Reinartz, Jörg Labahn, Raimond BG Ravelli, Markus Tusche, Carmen Lopez-Iglesias, Wolfgang Hoyer, Henrike Heise, et al. Fibril structure of amyloid-β (1–42) by cryo–electron microscopy. *Science*, 358(6359):116–119, 2017.

[66] Lynn Radamaker, Yin-Hsi Lin, Karthikeyan Annamalai, Stefanie Huhn, Ute Hegenbart, Stefan O Schönland, Günter Fritz, Matthias Schmidt, and Marcus Fändrich. Cryo-em structure of a light chain-derived amyloid fibril from a patient with systemic al amyloidosis. *Nature communications*, 10(1):1–8, 2019.

[67] Christine Röder, Nicola Vettore, Lena N Mangels, Lothar Gremer, Raimond BG Ravelli, Dieter Willbold, Wolfgang Hoyer, Alexander K Buell, and Gunnar F Schröder. Atomic structure of pi3-kinase sh3 amyloid fibrils by cryo-electron microscopy. *Nature communications*, 10(1):1–9, 2019.

[68] Marcus Fändrich, Vincent Forge, Katrin Buder, Marlis Kittler, Christopher M Dobson, and Stephan Diekmann. Myoglobin forms amyloid fibrils by association of unfolded polypeptide segments. *Proceedings of the National Academy of Sciences*, 100(26):15463–15468, 2003.

[69] Giorgia Zandomeneghi, Mark RH Krebs, Margaret G McCammon, and Marcus Fändrich. Ftir reveals structural differences between native β-sheet proteins and amyloid fibrils. *Protein Science*, 13(12):3314–3321, 2004.

[70] Paolo Arosio, Tuomas PJ Knowles, and Sara Linse. On the lag phase in amyloid fibril formation. *Physical Chemistry Chemical Physics*, 17(12):7606–7618, 2015.

[71] Aneta T Petkova, Richard D Leapman, Zhihong Guo, Wai-Ming Yau, Mark P Mattson, and Robert Tycko. Self-propagating, molecular-level polymorphism in alzheimer's ß-amyloid fibrils. *Science*, 307(5707):262–265, 2005.

[72] Arshdeep Sidhu, Ine Segers-Nolten, and Vinod Subramaniam. Solution conditions define morphological homogeneity of α-synuclein fibrils. *Biochimica et Biophysica Acta (BBA)-Proteins and Proteomics*, 1844(12):2127–2134, 2014.

[73] Jiangtao Zhou, Leonardo Venturelli, Ludovic Keiser, Sergey K Sekatskii, François Gallaire, Sandor Kasas, Giovanni Longo, Tuomas PJ Knowles, Francesco S Ruggeri, and Giovanni Dietler. Environmental control of amyloid polymorphism by modulation of hydrodynamic stress. *ACS nano*, 2020.

[74] Götz Heilbronner, Yvonne S Eisele, Franziska Langer, Stephan A Kaeser, Renata Novotny, Amudha Nagarathinam, Andreas Åslund, Per Hammarström, K Peter R Nilsson, and Mathias Jucker. Seeded strain-like transmission of β-amyloid morphotypes in app transgenic mice. *EMBO reports*, 14(11):1017–1022, 2013.

[75] Jan Stöhr, Carlo Condello, Joel C Watts, Lillian Bloch, Abby Oehler, Mimi Nick, Stephen J DeArmond, Kurt Giles, William F DeGrado, and Stanley B Prusiner. Distinct synthetic aβ prion strains producing different amyloid deposits in bigenic mice. *Proceedings of the National Academy of Sciences*, 111(28):10329–10334, 2014.

[76] Chao Peng, Ronald J Gathagan, and Virginia M-Y Lee. Distinct α-synuclein strains and implications for heterogeneity among α-synucleinopathies. *Neurobiology of disease*, 109:209–218, 2018.

[77] Matthew Biancalana and Shohei Koide. Molecular mechanism of thioflavin-t binding to amyloid fibrils. *Biochimica et Biophysica Acta (BBA)-Proteins and Proteomics*, 1804(7):1405–1412, 2010.

[78] Harry Levine III. Stopped-flow kinetics reveal multiple phases of thioflavin t binding to alzheimer β (1-40) amyloid fibrils. *Archives of biochemistry and biophysics*, 342(2):306–316, 1997.

[79] Frank Ferrone. [17] analysis of protein aggregation kinetics. In *Methods in enzymology*, volume 309, pages 256–274. Elsevier, 1999.

[80] Wei-Feng Xue, Steve W Homans, and Sheena E Radford. Systematic analysis of nucleation-dependent polymerization reveals new insights into the mechanism of amyloid self-assembly. *Proceedings of the National Academy of Sciences*, 105(26):8926–8931, 2008.

[81] Ricardo Gaspar, Georg Meisl, Alexander K Buell, Laurence Young, Clemens F Kaminski, Tuomas PJ Knowles, Emma Sparr, and Sara Linse. Secondary nucleation of monomers on fibril surface dominates α-synuclein aggregation and provides autocatalytic amyloid amplification. *Quart Rev Biophys*, 50, 2017.

[82] Samuel IA Cohen, Sara Linse, Leila M Luheshi, Erik Hellstrand, Duncan A White, Luke Rajah, Daniel E Otzen, Michele Vendruscolo, Christopher M Dobson, and Tuomas PJ Knowles. Proliferation of amyloid-β42 aggregates occurs through a secondary nucleation mechanism. *Proceedings of the National Academy of Sciences*, 110(24):9758–9763, 2013.

[83] Alexander J Dear, Georg Meisl, Thomas CT Michaels, Manuela R Zimmermann, Sara Linse, and Tuomas PJ Knowles. The catalytic nature of protein aggregation. *The Journal of Chemical Physics*, 152(4):045101, 2020.

[84] Dev Thacker, Kalyani Sanagavarapu, Birgitta Frohm, Georg Meisl, Tuomas PJ Knowles, and Sara Linse. The role of fibril structure and surface hydrophobicity in secondary nucleation of amyloid fibrils. *Proceedings of the National Academy of Sciences*, 117(41):25272–25283, 2020.

[85] Alessia Peduzzo, Sara Linse, and Alexander Buell. The properties of α-synuclein secondary nuclei are dominated by the solution conditions rather than the seed fibril strain. 2019.

[86] Edward P O'brien, Yuko Okamoto, John E Straub, Bernard R Brooks, and D Thirumalai. Thermodynamic perspective on the dock- lock growth mechanism of amyloid fibrils. *The Journal of Physical Chemistry B*, 113(43):14421–14430, 2009.

[87] Michelle J Cannon, Angela D Williams, Ronald Wetzel, and David G Myszka. Kinetic analysis of beta-amyloid fibril elongation. *Analytical biochemistry*, 328(1):67–75, 2004.

[88] Alexander K Buell, Jamie R Blundell, Christopher M Dobson, Mark E Welland, Eugene M Terentjev, and Tuomas PJ Knowles. Frequency factors in a landscape model of filamentous protein aggregation. *Physical review letters*, 104(22):228101, 2010.

[89] Liu Hong, Xizhou Liu, Thomas CT Michaels, and Tuomas PJ Knowles. Hamiltonian dynamics of saturated elongation in amyloid fiber formation. *arXiv preprint arXiv:2011.06222*, 2020.

[90] Travis B Thompson, Georg Meisl, Tuomas Knowles, and Alain Goriely. The role of clearance mechanisms in the kinetics of toxic protein aggregates involved in neurodegenerative diseases. *arXiv preprint arXiv:2009.14135*, 2020.

[91] Valérie Wilquet and Bart De Strooper. Amyloid-beta precursor protein processing in neurodegeneration. *Current opinion in neurobiology*, 14(5):582–588, 2004.

[92] Panchika Prangkio, Erik C Yusko, David Sept, Jerry Yang, and Michael Mayer. Multivariate analyses of amyloid-beta oligomer populations indicate a connection between pore formation and cytotoxicity. *PloS one*, 7(10):e47261, 2012.

[93] Urmi Sengupta, Marcos J Guerrero-Muñoz, Diana L Castillo-Carranza, Cristian A Lasagna-Reeves, Julia E Gerson, Adriana A Paulucci-Holthauzen, Shashirekha Krishnamurthy, Malika Farhed, George R Jackson, and Rakez Kayed. Pathological interface between oligomeric alpha-synuclein and tau in synucleinopathies. *Biological psychiatry*, 78(10):672–683, 2015.

[94] Urmi Sengupta and Rakez Kayed. Amyloid oligomer interactions and polymorphisms: disease-relevant distinct assembly of α-synuclein and tau. *Neuropsychopharmacology*, 44(1):222, 2019.

[95] Walraj S Gosal, Isobel J Morten, Eric W Hewitt, D Alastair Smith, Neil H Thomson, and Sheena E Radford. Competing pathways determine fibril morphology in the self-assembly of β2-microglobulin into amyloid. *Journal of molecular biology*, 351(4):850–864, 2005.

[96] Hilal A Lashuel, Christine Wurth, Linda Woo, and Jeffery W Kelly. The most pathogenic transthyretin variant, l55p, forms amyloid fibrils under acidic conditions and protofilaments under physiological conditions. *Biochemistry*, 38(41):13560–13573, 1999.

[97] Tatiana Miti, Mentor Mulaj, Jeremy D Schmit, and Martin Muschol. Stable, metastable, and kinetically trapped amyloid aggregate phases. *Biomacromolecules*, 16(1):326–335, 2015.

[98] Alessandra Bigi, Gilda Loffredo, Roberta Cascella, and Cristina Cecchi. Targeting pathological amyloid aggregates with conformation-sensitive antibodies. *Current Alzheimer Research*, 2020.

[99] Nora Bengoa-Vergniory, Rosalind F Roberts, Richard Wade-Martins, and Javier Alegre-Abarrategui. Alpha-synuclein oligomers: a new hope. *Acta neuropathologica*, 134(6):819–838, 2017.

[100] Janusz Frackowiak, Albina Zoltowska, and Henryk M Wisniewski. Non-fibrillar β-amyloid protein is associated with smooth muscle cells of vessel walls in alzheimer disease. *Journal of Neuropathology & Experimental Neurology*, 53(6):637–645, 1994.

[101] Yuesong Gong, Lei Chang, Kirsten L Viola, Pascale N Lacor, Mary P Lambert, Caleb E Finch, Grant A Krafft, and William L Klein. Alzheimer's disease-affected brain: presence of oligomeric aβ ligands (addls) suggests a molecular basis for reversible memory loss. *Proceedings of the National Academy of Sciences*, 100(18):10417–10422, 2003.

[102] Rakez Kayed, Elizabeth Head, Jennifer L Thompson, Theresa M McIntire, Saskia C Milton, Carl W Cotman, and Charles G Glabe. Common structure of soluble amyloid oligomers implies common mechanism of pathogenesis. *Science*, 300(5618):486–489, 2003.

[103] Akihiko Noguchi, Satoko Matsumura, Mari Dezawa, Mari Tada, Masako Yanazawa, Akane Ito, Manami Akioka, Satoru Kikuchi, Michio Sato, Shouji Ideno, et al. Isolation and characterization of patient-derived, toxic, high mass amyloid β-protein (aβ) assembly from alzheimer disease brains. *Journal of Biological Chemistry*, 284(47):32895–32905, 2009.

[104] Emiley Pham, Leslie Crews, Kiren Ubhi, Lawrence Hansen, Anthony Adame, Anna Cartier, David Salmon, Douglas Galasko, Sarah Michael, Jeffrey N Savas, et al. Progressive accumulation of amyloid-β oligomers in alzheimer's disease and in amyloid precursor protein transgenic mice is accompanied by selective alterations in synaptic scaffold proteins. *The FEBS journal*, 277(14):3051–3067, 2010.

[105] Thomas J Esparza, Hanzhi Zhao, John R Cirrito, Nigel J Cairns, Randall J Bateman, David M Holtzman, and David L Brody. Amyloid-beta oligomerization in alzheimer dementia versus high-pathology controls. *Annals of neurology*, 73(1):104–119, 2013.

[106] Sylvain E Lesne, Mathew A Sherman, Marianne Grant, Michael Kuskowski, Julie A Schneider, David A Bennett, and Karen H Ashe. Brain amyloid-β oligomers in ageing and alzheimer's disease. *Brain*, 136(5):1383–1398, 2013.

[107] Takami Tomiyama, Shogo Matsuyama, Hiroyuki Iso, Tomohiro Umeda, Hiroshi Takuma, Kiyouhisa Ohnishi, Kenichi Ishibashi, Rie Teraoka, Naomi Sakama, Takenari Yamashita, et al. A mouse model of amyloid β oligomers: their contribution to synaptic alteration, abnormal tau phosphorylation, glial activation, and neuronal loss in vivo. *Journal of Neuroscience*, 30(14):4845–4856, 2010.

[108] Asad Jan, Dean M Hartley, and Hilal A Lashuel. Preparation and characterization of toxic aβ aggregates for structural and functional studies in alzheimer's disease research. *Nature protocols*, 5(6):1186–1209, 2010.

[109] Erika N Cline, Maíra Assunção Bicca, Kirsten L Viola, and William L Klein. The amyloid-β oligomer hypothesis: Beginning of the third decade. *Journal of Alzheimer's Disease*, 64(s1):S567–S610, 2018.

[110] Dimitra G Georganopoulou, Lei Chang, Jwa-Min Nam, C Shad Thaxton, Elliott J Mufson, William L Klein, and Chad A Mirkin. Nanoparticle-based detection in cerebral spinal fluid of a soluble pathogenic biomarker for alzheimer's disease. *Proceedings of the National Academy of Sciences*, 102(7):2273–2276, 2005.

[111] Ting Yang, Tiernan T O'Malley, Daniel Kanmert, Jasna Jerecic, Lynn R Zieske, Henrik Zetterberg, Bradley T Hyman, Dominic M Walsh, and Dennis J Selkoe. A highly sensitive novel immunoassay specifically detects low levels of soluble aβ oligomers in human cerebrospinal fluid. *Alzheimer's research & therapy*, 7(1):14, 2015.

[112] Wesley Jongbloed, Kim A Bruggink, Maartje I Kester, Pieter-Jelle Visser, Philip Scheltens, Marinus A Blankenstein, Marcel M Verbeek, Charlotte E Teunissen, and Robert Veerhuis. Amyloid-β oligomers relate to cognitive decline in alzheimer's disease. *Journal of Alzheimer's Disease*, 45(1):35–43, 2015.

[113] Filip Hasecke, Chamani Niyangoda, Gustavo Borjas, Jianjun Pan, Garrett Matthews, Martin Muschol, and Wolfgang Hoyer. Protofibril–fibril interactions inhibit amyloid fibril assembly by obstructing secondary nucleation. *Angewandte Chemie International Edition*, 2020.

[114] Brett A Chromy, Richard J Nowak, Mary P Lambert, Kirsten L Viola, Lei Chang, Pauline T Velasco, Bryan W Jones, Sara J Fernandez, Pascale N Lacor, Peleg Horowitz, et al. Self-assembly of aβ1-42 into globular neurotoxins. *Biochemistry*, 42(44):12749–12760, 2003.

[115] Clara SR Grüning, Stefan Klinker, Martin Wolff, Mario Schneider, Küpra Toksöz, Antonia N Klein, Luitgard Nagel-Steger, Dieter Willbold, and Wolfgang Hoyer. The off-rate of monomers dissociating from amyloid-β protofibrils. *Journal of Biological Chemistry*, 288(52):37104–37111, 2013.

[116] Marie P Schützmann, Filip Hasecke, Sarah Bachmann, Mara Zielinski, Sebastian Hänsch, Gunnar F Schröder, Hans Zempel, and Wolfgang Hoyer. Endo-lysosomal aβ concentration and ph enable formation of aβ oligomers that potently induce tau missorting. *bioRxiv*, 2020.

[117] Jie Yang, Alexander J Dear, Qiong-Qiong Yao, Zhenyan Liu, Christopher M Dobson, Tuomas PJ Knowles, Si Wu, and Sarah Perrett. Amelioration of aggregate cytotoxicity by catalytic conversion of protein oligomers into amyloid fibrils. *Nanoscale*, 12(36):18663–18672, 2020.

[118] Thomas CT Michaels, Andela Šarić, Samo Curk, Katja Bernfur, Paolo Arosio, Georg Meisl, Alexander J Dear, Samuel IA Cohen, Christopher M Dobson, Michele Vendruscolo, et al. Dynamics of oligomer populations formed during the aggregation of alzheimer's aβ42 peptide. *Nature Chemistry*, 12(5):445–451, 2020.

[119] Kenjiro Ono and Mayumi Tsuji. Protofibrils of amyloid-β are important targets of a disease-modifying approach for alzheimer's disease. *International Journal of Molecular Sciences*, 21(3):952, 2020.

[120] Ravindra Kodali and Ronald Wetzel. Polymorphism in the intermediates and products of amyloid assembly. *Current opinion in structural biology*, 17(1):48–57, 2007.

[121] Stanley B Prusiner. Prion diseases and the bse crisis. *Science*, 278(5336):245–251, 1997.

[122] Stanley B Prusiner. Prions. *Proceedings of the National Academy of Sciences*, 95(23):13363–13383, 1998.

[123] John W Wilesmith, GA Wells, Mick P Cranwell, and JB Ryan. Bovine spongiform encephalopathy: epidemiological studies. *The Veterinary Record*, 123(25):638, 1988.

[124] JD Foster, J Hope, and H Fraser. Transmission of bovine spongiform encephalopathy to sheep and goats. *The Veterinary Record*, 133(14):339–341, 1993.

[125] Brandon B Holmes and Marc I Diamond. Cellular mechanisms of protein aggregate propagation. *Current opinion in neurology*, 25(6):721, 2012.

[126] Valerie R Osterberg, Kateri J Spinelli, Leah J Weston, Kelvin C Luk, Randall L Woltjer, and Vivek K Unni. Progressive aggregation of alpha-synuclein and selective degeneration of lewy inclusion-bearing neurons in a mouse model of parkinsonism. *Cell reports*, 10(8):1252–1260, 2015.

[127] Rodrigo Morales, Javiera Bravo-Alegria, Claudia Duran-Aniotz, and Claudio Soto. Titration of biologically active amyloid–β seeds in a transgenic mouse model of alzheimer's disease. *Scientific reports*, 5(1):1–8, 2015.

[128] M Lewandowsky. Handbuch der neurologie, 1912.

[129] Minami Baba, Shigeo Nakajo, Pang-Hsien Tu, Taisuke Tomita, Kazuyasu Nakaya, VM Lee, John Q Trojanowski, and Takeshi Iwatsubo. Aggregation of alpha-synuclein in lewy bodies of sporadic parkinson's disease and dementia with lewy bodies. *The American journal of pathology*, 152(4):879, 1998.

[130] Takashi Ishizawa, Petri Mattila, Peter Davies, Dengshun Wang, and Dennis W Dickson. Colocalization of tau and alpha-synuclein epitopes in lewy bodies. *Journal of Neuropathology & Experimental Neurology*, 62(4):389–397, 2003.

[131] M. G. Spillantini, M. L. Schmidt, V. M. Lee, J. Q. Trojanowski, R. Jakes, and M. Goedert. Alpha-synuclein in lewy bodies. *Nature*, 388(6645):839–840, Aug 1997.

[132] J Parkinson. Essay on the shaking palsy. london. reprint in: Macdonald critchley (ed)(1955). james parkinson, 1817.

[133] Werner Poewe, Klaus Seppi, Caroline M Tanner, Glenda M Halliday, Patrik Brundin, Jens Volkmann, Anette-Eleonore Schrag, and Anthony E Lang. Parkinson disease. *Nature reviews Disease primers*, 3(1):1–21, 2017.

[134] Maarten C De Rijk, Walter A Rocca, DW Anderson, MO Melcon, MMB Breteler, and DM Maraganore. A population perspective on diagnostic criteria for parkinson's disease. *Neurology*, 48(5):1277–1281, 1997.

[135] AB Singleton, M Farrer, J Johnson, A Singleton, S Hague, J Kachergus, M Hulihan, T Peuralinna, A Nussbaum Dutra, S Lincoln, et al. [alpha]-synuclein locus triplication causes parkinson's disease. *Science*, 302(5646):841–842, 2003.

[136] Michel Goedert. Alpha-synuclein and neurodegenerative diseases. *Nature Reviews Neuroscience*, 2(7):492–501, 2001.

[137] Kay Seidel, Ludger Schöls, Silke Nuber, Elisabeth Petrasch-Parwez, Kristin Gierga, Zbigniew Wszolek, Dennis Dickson, Wei P Gai, Antje Bornemann, Olaf Riess, et al. First appraisal of brain pathology owing to a30p mutant alpha-synuclein. *Annals of neurology*, 67(5):684–689, 2010.

[138] Józef Opara, Andrzej Małecki, Elżbieta Małecka, and Teresa Socha. Motor assessment in parkinsons disease. *Ann Agric Environ Med*, 24(3):411–415, 2017.

[139] Julian M Fearnley and Andrew J Lees. Ageing and parkinson's disease: substantia nigra regional selectivity. *Brain*, 114(5):2283–2301, 1991.

[140] A Kastner, EC Hirsch, O Lejeune, F Javoy-Agid, O Rascol, and Y Agid. Is the vulnerability of neurons in the substantia nigra of patients with parkinson's disease related to their neuromelanin content? *Journal of neurochemistry*, 59(3):1080–1089, 1992.

[141] WR Gibb and AJ1033142 Lees. The relevance of the lewy body to the pathogenesis of idiopathic parkinson's disease. *Journal of Neurology, Neurosurgery & Psychiatry*, 51(6):745–752, 1988.

[142] Leonid Breydo, Jessica W Wu, and Vladimir N Uversky. α-synuclein misfolding and parkinson's disease. *Biochimica et Biophysica Acta (BBA)-Molecular Basis of Disease*, 1822(2):261–285, 2012.

[143] CB Lücking and A Brice. Alpha-synuclein and parkinson's disease. *Cellular and Molecular Life Sciences CMLS*, 57(13-14):1894–1908, 2000.

[144] Vladimir N Uversky and David Eliezer. Biophysics of parkinson's disease: structure and aggregation of α-synuclein. *Current Protein and Peptide Science*, 10(5):483–499, 2009.

[145] KA Ansari and A Johnson. Olfactory function in patients with parkinson's disease. *Journal of chronic diseases*, 28(9):493–497, 1975.

[146] Richard L Doty. Olfaction in parkinson's disease and related disorders. *Neurobiology of disease*, 46(3):527–552, 2012.

[147] Stephanie Lohmann, Maria E Bernis, Babila J Tachu, Alexandra Ziemski, Jessica Grigoletto, and Gültekin Tamgüney. Oral and intravenous transmission of α-synuclein fibrils to mice. *Acta neuropathologica*, 138(4):515–533, 2019.

[148] Joel C Watts. Calling α-synuclein a prion is scientifically justifiable. *Acta neuropathologica*, 138(4):505–508, 2019.

[149] Heiko Braak, Estifanos Ghebremedhin, Udo Rüb, Hansjürgen Bratzke, and Kelly Del Tredici. Stages in the development of parkinson's disease-related pathology. *Cell and tissue research*, 318(1):121–134, 2004.

[150] Álvaro Sánchez-Ferro, Alberto Rábano, María José Catalán, Fernando Canga Rodríguez-Valcárcel, Servando Fernández Díez, Jaime Herreros-Rodríguez, Elvira García-Cobos, Marina Mata Álvarez-Santullano, Lydia López-Manzanares, Antonio J Mosqueira, et al. In vivo gastric detection of α-synuclein inclusions in parkinson's disease. *Movement Disorders*, 30(4):517–524, 2015.

[151] Kathleen M Shannon, Ali Keshavarzian, Ece Mutlu, Hemraj B Dodiya, Delia Daian, Jean A Jaglin, and Jeffrey H Kordower. Alpha-synuclein in colonic submucosa in early untreated parkinson's disease. *Movement Disorders*, 27(6):709–715, 2012.

[152] Sangjune Kim, Seung-Hwan Kwon, Tae-In Kam, Nikhil Panicker, Senthilkumar S Karuppagounder, Saebom Lee, Jun Hee Lee, Wonjoong Richard Kim, Minjee Kook, Catherine A

Foss, et al. Transneuronal propagation of pathologic α-synuclein from the gut to the brain models parkinson's disease. *Neuron*, 103(4):627–641, 2019.

[153] Staffan Holmqvist, Oldriska Chutna, Luc Bousset, Patrick Aldrin-Kirk, Wen Li, Tomas Björklund, Zhan-You Wang, Laurent Roybon, Ronald Melki, and Jia-Yi Li. Direct evidence of parkinson pathology spread from the gastrointestinal tract to the brain in rats. *Acta neuropathologica*, 128(6):805–820, 2014.

[154] Collin Challis, Acacia Hori, Timothy R Sampson, Bryan B Yoo, Rosemary C Challis, Adam M Hamilton, Sarkis K Mazmanian, Laura A Volpicelli-Daley, and Viviana Gradinaru. Gut-seeded α-synuclein fibrils promote gut dysfunction and brain pathology specifically in aged mice. *Nature Neuroscience*, 23(3):327–336, 2020.

[155] Ethan Stolzenberg, Deborah Berry, DE Yang, Ernest Y Lee, Alexander Kroemer, Stuart Kaufman, Gerard CL Wong, Joost J Oppenheim, Supti Sen, Thomas Fishbein, et al. A role for neuronal alpha-synuclein in gastrointestinal immunity. *Journal of innate immunity*, 9(5):456–463, 2017.

[156] Emily Fitzgerald, Sarah Murphy, and Holly A Martinson. Alpha-synuclein pathology and the role of the microbiota in parkinson's disease. *Frontiers in neuroscience*, 13:369, 2019.

[157] Serena Bellani, Vitor L Sousa, Giuseppe Ronzitti, Flavia Valtorta, Jacopo Meldolesi, and Evelina Chieregatti. The regulation of synaptic function by α-synuclein. *Communicative & Integrative Biology*, 3(2):106–109, 2010.

[158] Laura Calo, Michal Wegrzynowicz, Jessica Santivañez-Perez, and Maria Grazia Spillantini. Synaptic failure and α-synuclein. *Movement Disorders*, 31(2):169–177, 2016.

[159] Pablo Garcia-Reitboeck, Oleg Anichtchik, Jeffrey W Dalley, Natalia Ninkina, George K Tofaris, Vladimir L Buchman, and Maria Grazia Spillantini. Endogenous alpha-synuclein influences the number of dopaminergic neurons in mouse substantia nigra. *Experimental neurology*, 248:541–545, 2013.

[160] Barbara S Connolly and Anthony E Lang. Pharmacological treatment of parkinson disease: a review. *Jama*, 311(16):1670–1683, 2014.

[161] Gunilla T Westermark and Per Westermark. Prion-like aggregates: infectious agents in human disease. *Trends in molecular medicine*, 16(11):501–507, 2010.

[162] Tomoaki Murakami, Yasuo Inoshima, and Naotaka Ishiguro. Systemic aa amyloidosis as a prion-like disorder. *Virus research*, 207:76–81, 2015.

[163] Miriam Hernández-Zamora, Fernando Martínez-Jerónimo, Eliseo Cristiani-Urbina, and Rosa Olivia Cañizares-Villanueva. Congo red dye affects survival and reproduction in the cladoceran ceriodaphnia dubia. effects of direct and dietary exposure. *Ecotoxicology*, 25(10):1832–1840, 2016.

[164] MARGUERITE STEAMMERMAN and OSCAR AUERBACH. The value and limitations of the congo red test for amyloidosis. *The American Journal of the Medical Sciences*, 208(3):305–309, 1944.

[165] Paul N Unger, Morris Zuckerbrod, Gustav J Beck, J Murray Steele, Yetta Porosowska, et al. Study of the disappearance of congo red from the blood of non-amyloid subjects and patients with amyloidosis. *The Journal of clinical investigation*, 27(1):111–118, 1948.

[166] O Lubarsch. Zur kenntnis ungewöhnlicher amyloidablagerungen. *Virchows Archiv für pathologische Anatomie und Physiologie und für klinische Medizin*, 271(3):867–889, 1929.

[167] W St C Symmers. Primary amyloidosis: a review. *Journal of clinical pathology*, 9(3):187, 1956.

[168] Robert A Kyle, Dirk R Larson, Paul J Kurtin, Shaji Kumar, James R Cerhan, Terry M Therneau, S Vincent Rajkumar, Celine M Vachon, and Angela Dispenzieri. Incidence of al amyloidosis in olmsted county, minnesota, 1990 through 2015. In *Mayo Clinic Proceedings*, volume 94, pages 465–471. Elsevier, 2019.

[169] Vaishali Sanchorawala. Light-chain (al) amyloidosis: diagnosis and treatment. *Clinical Journal of the American Society of Nephrology*, 1(6):1331–1341, 2006.

[170] Estelle Desport, Frank Bridoux, Christophe Sirac, Sébastien Delbes, Sébastien Bender, Béatrice Fernandez, Nathalie Quellard, Corinne Lacombe, Jean-Michel Goujon, David Lavergne, et al. Al amyloidosis. *Orphanet journal of rare diseases*, 7(1):54, 2012.

[171] Robert A Kyle and Morie A Gertz. Primary systemic amyloidosis: clinical and laboratory features in 474 cases. In *Seminars in hematology*, volume 32, pages 45–59. [Sheboygan, Wis.]: Grune & Stratton,[c1964-, 1995.

[172] Carlo Aprile, Gabriella Marinone, Raffaella Saponaro, Chiara Bonino, and Giampaolo Merlini. Cardiac and pleuropulmonary al amyloid imaging with technetium-99m labelled aprotinin. *European journal of nuclear medicine*, 22(12):1393–1401, 1995.

[173] Raymond L Comenzo, Yana Zhang, Carmen Martinez, Keren Osman, and Guillermo A Herrera. The tropism of organ involvement in primary systemic amyloidosis: contributions of ig vl germ line gene use and clonal plasma cell burden. *Blood, The Journal of the American Society of Hematology*, 98(3):714–720, 2001.

[174] Rodney H Falk. Diagnosis and management of the cardiac amyloidoses. *Circulation*, 112(13):2047–2060, 2005.

[175] Daniel A Brenner, Mohit Jain, David R Pimentel, Bo Wang, Lawreen H Connors, Martha Skinner, Carl S Apstein, and Ronglih Liao. Human amyloidogenic light chains directly impair cardiomyocyte function through an increase in cellular oxidant stress. *Circulation research*, 94(8):1008–1010, 2004.

[176] Tatiana Prokaeva, Brian Spencer, Maurya Kaut, Al Ozonoff, Gheorghe Doros, Lawreen H Connors, Martha Skinner, and David C Seldin. Soft tissue, joint, and bone manifestations of al amyloidosis: clinical presentation, molecular features, and survival. *Arthritis & Rheumatism: Official Journal of the American College of Rheumatology*, 56(11):3858–3868, 2007.

[177] SW Dubrey, K Cha, J Anderson, B Chamarthi, J Reisinger, M Skinner, and RH Falk. The clinical features of immunoglobulin light-chain (al) amyloidosis with heart involvement. *QJM: monthly journal of the Association of Physicians*, 91(2):141–157, 1998.

[178] Caryn A Libbey, Martha Skinner, and Alan S Cohen. Use of abdominal fat tissue aspirate in the diagnosis of systemic amyloidosis. *Archives of internal medicine*, 143(8):1549–1552, 1983.

[179] GM Delman and JA Gally. The nature of bence-jones proteins: chemical similarities to polypeptide chains of myeloma globulins and normal γ-globulins. *The Journal of experimental medicine*, 116(2):207–227, 1962.

[180] Florence Magrangeas, Marie-Laure Cormier, Géraldine Descamps, Nadège Gouy, Laurence Lodé, Marie-Paule Mellerin, Jean-Luc Harousseau, Régis Bataille, Stéphane Minvielle, Hervé Avet-Loiseau, et al. Light-chain only multiple myeloma is due to the absence of functional (productive) rearrangement of the igh gene at the dna level. *Blood*, 103(10):3869–3875, 2004.

[181] Guillermo A Herrera. Renal lesions associated with plasma cell dyscrasias: practical approach to diagnosis, new concepts, and challenges. *Archives of pathology & laboratory medicine*, 133(2):249–267, 2009.

[182] Takanari Nakano, Masanori Matsui, Ikuo Inoue, Takuya Awata, Shigehiro Katayama, and Takayuki Murakoshi. Free immunoglobulin light chain: its biology and implications in diseases. *Clinica chimica acta*, 412(11-12):843–849, 2011.

[183] Mohammad R Nowrousian, Dieter Brandhorst, Christiane Sammet, Michaela Kellert, Rainer Daniels, Philipp Schuett, Miriam Poser, Siemke Mueller, Peter Ebeling, Anja Welt, et al. Serum free light chain analysis and urine immunofixation electrophoresis in patients with multiple myeloma. *Clinical Cancer Research*, 11(24):8706–8714, 2005.

[184] Alan Solomon, Carla L McLaughlin, Chin Hsuan Wei, and J Ralph Einstein. Bence-jones proteins and light chains of immunoglobulins v. x-ray crystallographic investigation of the amino-terminal half of a κ bence-jones protein. *Journal of Biological Chemistry*, 245(20):5289–5291, 1970.

[185] RA Kyle, BGM Durie, SV Rajkumar, O Landgren, Joan Bladé, Giampaolo Merlini, Nicolaus Kröger, Hermann Einsele, DH Vesole, Meletios Dimopoulos, et al. Monoclonal gammopathy of undetermined significance (mgus) and smoldering (asymptomatic) multiple myeloma: Imwg consensus perspectives risk factors for progression and guidelines for monitoring and management. *Leukemia*, 24(6):1121–1127, 2010.

[186] Giampaolo Talamo, Umar Farooq, Maurizio Zangari, Jason Liao, Nathan G Dolloff, Thomas P Loughran Jr, and Elliot Epner. Beyond the crab symptoms: a study of presenting clinical manifestations of multiple myeloma. *Clinical Lymphoma Myeloma and Leukemia*, 10(6):464–468, 2010.

[187] Giovanni Tonon. Molecular pathogenesis of multiple myeloma. *Hematology/oncology clinics of North America*, 21(6):985–1006, 2007.

[188] Taxiarchis V Kourelis, Shaji K Kumar, Morie A Gertz, Martha Q Lacy, Francis K Buadi, Suzanne R Hayman, Steven Zeldenrust, Nelson Leung, Robert A Kyle, Stephen Russell, et al. Coexistent multiple myeloma or increased bone marrow plasma cells define equally high-risk populations in patients with immunoglobulin light chain amyloidosis. *Journal of clinical oncology*, 31(34):4319, 2013.

[189] Yusuke Furukawa and Jiro Kikuchi. Molecular pathogenesis of multiple myeloma. *International journal of clinical oncology*, 20(3):413–422, 2015.

[190] George G Glenner, Daniel Ein, and William D Terry. The immunoglobulin origin of amyloid. *The American journal of medicine*, 52(2):141–147, 1972.

[191] Paul W Sanders and Beverly B Booker. Pathobiology of cast nephropathy from human bence jones proteins. *The Journal of clinical investigation*, 89(2):630–639, 1992.

[192] Joel Buxbaum and Gloria Gallo. Nonamyloidotic monoclonal immunoglobulin deposition disease: light-chain, heavy-chain, and light-and heavy-chain deposition diseases. *Hematology/oncology clinics of North America*, 13(6):1235–1248, 1999.

[193] Michael Barry Stokes, Jaishree Jagirdar, Omar Burchstin, Susan Kornacki, Asok Kumar, and Gloria Gallo. Nodular pulmonary immunoglobulin light chain deposits with coexistent amyloid and nonamyloid features in an hiv-infected patient. *Modern pathology: an official journal of the United States and Canadian Academy of Pathology, Inc*, 10(10):1059–1065, 1997.

[194] C Jacquot, JP Saint-Andre, G Touchard, D Nochy, C de Lamartinie D'Auzac, R Oriol, P Druet, and J Bariety. Association of systemic light-chain deposition disease and amyloidosis: a report of three patients with renal involvement. *Clinical nephrology*, 24(2):93–98, 1985.

[195] Gavino Faa, Peter Van Eyken, Rita De Vos, Johan Fevery, Boudewijn Van Damme, Jan De Groote, and Valeer J Desmet. Light chain deposition disease of the liver associated with al-type amyloidosis and severe cholestasis: a case report and literature review. *Journal of hepatology*, 12(1):75–82, 1991.

[196] NM Smith and AJ Malcolm. Simultaneous al-type amyloid and light chain deposit disease in a liver biopsy: a case report. *Histopathology*, 10(10):1057–1064, 1986.

[197] David P Davis, Gloria Gallo, Shawn M Vogen, Jeanne L Dul, Kimberly L Sciarretta, Asok Kumar, Rosemarie Raffen, Fred J Stevens, and Yair Argon. Both the environment and somatic mutations govern the aggregation pathway of pathogenic immunoglobulin light chain. *Journal of molecular biology*, 313(5):1021–1034, 2001.

[198] Dandan Liang, Jing Liu, Shaoshan Liang, Feng Xu, Zhen Cheng, Xianghua Huang, Caihong Zeng, and Zhihong Liu. Types of m protein and clinicopathological profiles in patients with monoclonal gammopathy of renal significance. *Journal of Nephrology*, pages 1–10, 2020.

[199] Ryuta Abe, Nagaaki Katoh, Yusuke Takahashi, Ken Takasone, Tsuneaki Yoshinaga, Masahide Yazaki, Fuyuki Kametani, and Yoshiki Sekijima. Distribution of amyloidosis subtypes based on tissue biopsy site- consecutive analysis of 729 patients at a single amyloidosis center in japan. *Pathology international*, 2020.

[200] Shun Manabe, Michiyasu Hatano, Masahide Yazaki, Kosaku Nitta, and Michio Nagata. Renal ah amyloidosis associated with a truncated immunoglobulin heavy chain undetectable by immunostaining. *American Journal of Kidney Diseases*, 66(6):1095–1100, 2015.

[201] Sanjeev Sethi, Jason D Theis, Nelson Leung, Angela Dispenzieri, Samih H Nasr, Mary E Fidler, Lynn D Cornell, Jeffrey D Gamez, Julie A Vrana, and Ahmet Dogan. Mass spectrometry–based proteomic diagnosis of renal immunoglobulin heavy chain amyloidosis. *Clinical Journal of the American Society of Nephrology*, 5(12):2180–2187, 2010.

[202] Manfred Eulitz, Deborah T Weiss, and Alan Solomon. Immunoglobulin heavy-chain-associated amyloidosis. *Proceedings of the National Academy of Sciences*, 87(17):6542–6546, 1990.

[203] Frank Bridoux, Vincent Javaugue, Sébastien Bender, Fannie Leroy, Pierre Aucouturier, Céline Debiais-Delpech, Jean-Michel Goujon, Nathalie Quellard, Amélie Bonaud, Marie Clavel, et al. Unravelling the immunopathological mechanisms of heavy chain deposition disease with implications for clinical management. *Kidney International*, 91(2):423–434, 2017.

[204] Samih H Nasr, Samar M Said, Anthony M Valeri, Sanjeev Sethi, Mary E Fidler, Lynn D Cornell, Morie A Gertz, Angela Dispenzieri, Francis K Buadi, Julie A Vrana, et al. The diagnosis and characteristics of renal heavy-chain and heavy/light-chain amyloidosis and their comparison with renal light-chain amyloidosis. *Kidney international*, 83(3):463–470, 2013.

[205] Elena S Klimtchuk, Tatiana B Prokaeva, Brian H Spencer, Olga Gursky, and Lawreen H Connors. In vitro co-expression of human amyloidogenic immunoglobulin light and heavy chain proteins: a relevant cell-based model of al amyloidosis. *Amyloid*, 24(2):115–122, 2017.

[206] PM Ronco and P Aucouturier. The molecular bases of plasma cell dyscrasia-related renal diseases. *Nephrology, dialysis, transplantation: official publication of the European Dialysis and Transplant Association-European Renal Association*, 14(suppl_1):4–8, 1999.

[207] Colin A Hutchison, Vecihi Batuman, Judith Behrens, Frank Bridoux, Christophe Sirac, Angela Dispenzieri, Guillermo A Herrera, Helen Lachmann, and Paul W Sanders. The pathogenesis and diagnosis of acute kidney injury in multiple myeloma. *Nature Reviews Nephrology*, 8(1):43–51, 2012.

[208] Mingyu Cheng, Xin Gu, Elba A Turbat-Herrera, and Guillermo A Herrera. Tubular injury and dendritic cell activation are integral components of light chain–associated acute tubulointerstitial nephritis. *Archives of pathology & laboratory medicine*, 143(10):1212–1224, 2019.

[209] Vittorio Bellotti, Mario Nuvolone, Sofia Giorgetti, Laura Obici, Giovanni Palladini, Paola Russo, Francesca Lavatelli, Vittorio Perfetti, and Giampaolo Merlini. The workings of the amyloid diseases. *Annals of medicine*, 39(3):200–207, 2007.

[210] Marie-Paule Lefranc and Gérard Lefranc. *The immunoglobulin factsbook*. Academic press, 2001.

[211] Max D Cooper and Matthew N Alder. The evolution of adaptive immune systems. *Cell*, 124(4):815–822, 2006.

[212] L Mario Amzel and Roberto J Poljak. Three-dimensional structure of immunoglobulins. *Annual review of biochemistry*, 48(1):961–997, 1979.

[213] M Schiffer, C-H Chang, and FJ Stevens. Formation of an infinite β-sheet arrangement dominates the crystallization behavior of λ-type antibody light chains. *Journal of molecular biology*, 186(2):475–478, 1985.

[214] Christian Frisch, Harald Kolmar, Arno Schmidt, Gerd Kleemann, Astrid Reinhardt, Ehmke Pohl, Isabel Usón, Thomas R Schneider, and Hans-Joachim Fritz. Contribution of the intramolecular disulfide bridge to the folding stability of reiv, the variable domain of a human immunoglobulin κ light chain. *Folding and Design*, 1(6):431–440, 1996.

[215] ALAN Solomon, BLAS Frangione, EDWARD C Franklin, et al. Bence jones proteins and light chains of immunoglobulins. preferential association of the v lambda vi subgroup of human light chains with amyloidosis al (lambda). *The Journal of clinical investigation*, 70(2):453–460, 1982.

[216] Roshini S Abraham, Susan M Geyer, Tammy L Price-Troska, Cristine Allmer, Robert A Kyle, Morie A Gertz, and Rafael Fonseca. Immunoglobulin light chain variable (v) region genes influence clinical presentation and outcome in light chain–associated amyloidosis (al). *Blood*, 101(10):3801–3807, 2003.

[217] Dennis R Livesay and Shankar Subramaniam. Conserved sequence and structure association motifs in antibody–protein and antibody–hapten complexes. *Protein Engineering Design and Selection*, 17(5):463–472, 2004.

[218] Hitoshi Sakano, Konrad Hüppi, Günther Heinrich, and Susumu Tonegawa. Sequences at the somatic recombination sites of immunoglobulin light-chain genes. *Nature*, 280(5720):288–294, 1979.

[219] Grace Teng and F Nina Papavasiliou. Immunoglobulin somatic hypermutation. *Annu. Rev. Genet.*, 41:107–120, 2007.

[220] Patricia J Gearhart, Nelson D Johnson, Richard Douglas, and Leroy Hood. Igg antibodies to phosphorylcholine exhibit more diversity than their igm counterparts. *Nature*, 291(5810):29–34, 1981.

[221] O WESLEY McBRIDE, PA Heiter, GREGORY F Hollis, DAVID Swan, MILES C Otey, and PHILIP Leder. Chromosomal location of human kappa and lambda immunoglobulin light chain constant region genes. *The Journal of experimental medicine*, 155(5):1480–1490, 1982.

[222] Susan Malcolm, P Barton, C Murphy, MA Ferguson-Smith, DL Bentley, and TH Rabbitts. Localization of human immunoglobulin kappa light chain variable region genes to the short arm of chromosome 2 by in situ hybridization. *Proceedings of the National Academy of Sciences*, 79(16):4957–4961, 1982.

[223] Takashi Isobe and Elliott F Osserman. Patterns of amyloidosis and their association with plasma-cell dyscrasia, monoclonal immunoglobulins and bence-jones proteins. *New England Journal of Medicine*, 290(9):473–477, 1974.

[224] Vittorio Bellotti, Palma Mangione, and Giampaolo Merlini. immunoglobulin light chain amyloidosis?the archetype of structural and pathogenic variability. *Journal of structural biology*, 130(2-3):280–289, 2000.

[225] Miryam I Villalba, Juan C Canul-Tec, Oscar D Luna-Martínez, Rosalba Sánchez-Alcalá, Timoteo Olamendi-Portugal, Enrique Rudiño-Piñera, Sonia Rojas, Rosana Sánchez-López, Daniel A Fernández-Velasco, and Baltazar Becerril. Site-directed mutagenesis reveals regions implicated in the stability and fiber formation of human λ3r light chains. *Journal of Biological Chemistry*, 290(5):2577–2592, 2015.

[226] Dominique Scaviner, Valérie Barbié, Manuel Ruiz, and Marie-Paule Lefranc. Protein displays of the human immunoglobulin heavy, kappa and lambda variable and joining regions. *Experimental and clinical immunogenetics*, 16(4):234–240, 1999.

[227] George G Glenner. Amyloid deposits and amyloidosis. the beta-fibrilloses (first of two parts). *The New England journal of medicine*, 302(23):1283–1292, 1980.

[228] Hanne M Ramstad, Knut Sletten, and Gunnar Husby. The amino acid sequence and carbohydrate composition of an immunoglobulin kappa light chain amyloid fibril protein (al) of variable subgroup i. *Amyloid*, 2(4):223–228, 1995.

[229] Stina Enqvist, Knut Sletten, Fred J Stevens, Ulf Hellman, and Per Westermark. Germ line origin and somatic mutations determine the target tissues in systemic al-amyloidosis. *PLoS One*, 2(10), 2007.

[230] Cardine N Nokwe, Manuel Hora, Martin Zacharias, Hisashi Yagi, Christine John, Bernd Reif, Yuji Goto, and Johannes Buchner. The antibody light-chain linker is important for domain stability and amyloid formation. *Journal of molecular biology*, 427(22):3572–3586, 2015.

[231] Giovanni Palladini, Francesca Lavatelli, Paola Russo, Stefano Perlini, Vittorio Perfetti, Tiziana Bosoni, Laura Obici, Arthur R Bradwell, GianVico Melzi D'Eril, Roberto Fogari, et al. Circulating amyloidogenic free light chains and serum n-terminal natriuretic peptide type b decrease simultaneously in association with improvement of survival in al. *Blood*, 107(10):3854–3858, 2006.

[232] Pamina Kazman, Marie-Theres Vielberg, María Daniela Pulido Cendales, Lioba Hunziger, Benedikt Weber, Ute Hegenbart, Martin Zacharias, Rolf Köhler, Stefan Schönland, Michael Groll, et al. Fatal amyloid formation in a patient?s antibody light chain is caused by a single point mutation. *Elife*, 9:e52300, 2020.

[233] Mark R Hurle, Larry R Helms, LIN Li, Winnie Chan, and Ronald Wetzel. A role for destabilizing amino acid replacements in light-chain amyloidosis. *Proceedings of the National Academy of Sciences*, 91(12):5446–5450, 1994.

[234] Alan Solomon, Deborah T Weiss, Charles L Murphy, Rudi Hrncic, Jonathan S Wall, and Maria Schell. Light chain-associated amyloid deposits comprised of a novel κ constant domain. *Proceedings of the National Academy of Sciences*, 95(16):9547–9551, 1998.

[235] Karen Ege Olsen, Knut Sletten, and Per Westermark. Fragments of the constant region of immunoglobulin light chains are constituents of al-amyloid proteins. *Biochemical and biophysical research communications*, 251(2):642–647, 1998.

[236] Francesca Lavatelli, David H Perlman, Brian Spencer, Tatiana Prokaeva, Mark E McComb, Roger Théberge, Lawreen H Connors, Vittorio Bellotti, David C Seldin, Giampaolo Merlini, et al. Amyloidogenic and associated proteins in systemic amyloidosis proteome of adipose tissue. *Molecular & Cellular Proteomics*, 7(8):1570–1583, 2008.

[237] Julie A Vrana, Jeffrey D Gamez, Benjamin J Madden, Jason D Theis, H Robert Bergen III, and Ahmet Dogan. Classification of amyloidosis by laser microdissection and mass spectrometry–based proteomic analysis in clinical biopsy specimens. *Blood, The Journal of the American Society of Hematology*, 114(24):4957–4959, 2009.

[238] Stina Enqvist, Knut Sletten, and Per Westermark. Fibril protein fragmentation pattern in systemic al-amyloidosis. *The Journal of Pathology: A Journal of the Pathological Society of Great Britain and Ireland*, 219(4):473–480, 2009.

[239] MM Picken, B Frangione, B Barlogie, M Luna, and G Gallo. Light chain deposition disease derived from the kappa i light chain subgroup. biochemical characterization. *The American journal of pathology*, 134(4):749, 1989.

[240] Lawreen H Connors, Yan Jiang, Marianna Budnik, Roger Théberge, Tatiana Prokaeva, Kip L Bodi, David C Seldin, Catherine E Costello, and Martha Skinner. Heterogeneity in primary structure, post-translational modifications, and germline gene usage of nine full-length amyloidogenic κ1 immunoglobulin light chains. *Biochemistry*, 46(49):14259–14271, 2007.

[241] Francesca Lavatelli, Giulia Mazzini, Stefano Ricagno, Federica Iavarone, Paola Rognoni, Paolo Milani, Mario Nuvolone, Paolo Swuec, Serena Caminito, Masayoshi Tasaki, et al. Mass spectrometry characterization of light chain fragmentation sites in cardiac al amyloidosis: insights into the timing of proteolysis. *Journal of Biological Chemistry*, 295(49):16572–16584, 2020.

[242] Margaret Tan and Wallace Epstein. Polymer formation during the degradation of human light chain and bence-jones proteins by an extract of the lysosomal fraction of normal human kidney. *Immunochemistry*, 9(1):9–16, 1972.

[243] Wallace V Epstein, Margaret Tan, and Irmgard S Wood. Formation of ?amyloid? fibrils in vitro by action of human kidney lysosomal enzymes on bence jones proteins. *The Journal of Laboratory and Clinical Medicine*, 84(1):107–110, 1974.

[244] Gareth J Morgan and Jeffery W Kelly. The kinetic stability of a full-length antibody light chain dimer determines whether endoproteolysis can release amyloidogenic variable domains. *Journal of molecular biology*, 428(21):4280–4297, 2016.

[245] Robin Axel Ruiz-Zamora, Simon Guillaumé, Youssra K Al-Hilaly, Zahraa Al-Garawi, Francisco Javier Rodríguez-Alvarez, Guadalupe Zavala-Padilla, Julio I Pérez-Carreón, Sandra L Rodríguez-Ambriz, Guillermo A Herrera, Baltazar Becerril-Luján, et al. The cdr1 and other regions of immunoglobulin light chains are hot spots for amyloid aggregation. *Scientific reports*, 9(1):1–18, 2019.

[246] Gareth J Morgan, Grace A Usher, and Jeffery W Kelly. Incomplete refolding of antibody light chains to non-native, protease-sensitive conformations leads to aggregation: A mechanism of amyloidogenesis in patients? *Biochemistry*, 56(50):6597–6614, 2017.

[247] Shigeo Nomura, Tadashi Kanoh, and Haruto Uchino. Intracellular formation of amyloid fibrils in myeloma. cytochemical, immunochemical, and electron microscopic observations. *Cancer*, 54(2):303–307, 1984.

[248] GG Glenner, D Ein, ED Eanes, HA Bladen, W Terry, and DL Page. Creation of" amyloid" fibrils from bence jones proteins in vitro. *Science*, 174(4010):712–714, 1971.

[249] RP Linke, D Zucker-Franklin, and EC Franklin. Morphologic, chemical, and immunologic studies of amyloid-like fibrils formed from bence jones proteins by proteolysis. *The Journal of Immunology*, 111(1):10–23, 1973.

[250] Michael A Chapman, Michael S Lawrence, Jonathan J Keats, Kristian Cibulskis, Carrie Sougnez, Anna C Schinzel, Christina L Harview, Jean-Philippe Brunet, Gregory J Ahmann, Mazhar Adli, et al. Initial genome sequencing and analysis of multiple myeloma. *Nature*, 471(7339):467–472, 2011.

[251] Amit A Upadhyay, Robert C Kauffman, Amber N Wolabaugh, Alice Cho, Nirav B Patel, Samantha M Reiss, Colin Havenar-Daughton, Reem A Dawoud, Gregory K Tharp, Iñaki Sanz, et al. Baldr: a computational pipeline for paired heavy and light chain immunoglobulin reconstruction in single-cell rna-seq data. *Genome medicine*, 10(1):1–18, 2018.

[252] Sanjay Kumar, David Murray, Surendra Dasari, Paolo Milani, David Barnidge, Benjamin Madden, Taxiarchis Kourelis, Bonnie Arendt, Giampaolo Merlini, Marina Ramirez-Alvarado, et al. Assay to rapidly screen for immunoglobulin light chain glycosylation: a potential path to earlier al diagnosis for a subset of patients. *Leukemia*, 33(1):254–257, 2019.

[253] Lone A Omtvedt, David Bailey, David V Renouf, Michael J Davies, Nikolay A Paramonov, Svein Haavik, Gunnar Husby, Knut Sletten, and Elizabeth F Hounsell. Glycosylation of immunoglobulin light chains associated with amyloidosis. *Amyloid*, 7(4):227–244, 2000.

[254] Amareth Lim, Jeremy Wally, Mary T Walsh, Martha Skinner, and Catherine E Costello. Identification and location of a cysteinyl posttranslational modification in an amyloidogenic κ1 light chain protein by electrospray ionization and matrix-assisted laser desorption/ionization mass spectrometry. *Analytical biochemistry*, 295(1):45–56, 2001.

[255] Noriko Iwamoto and Takashi Shimada. Recent advances in mass spectrometry-based approaches for proteomics and biologics: Great contribution for developing therapeutic antibodies. *Pharmacology & Therapeutics*, 185:147–154, 2018.

[256] Paula M Ladwig, David R Barnidge, and Maria AV Willrich. Mass spectrometry approaches for identification and quantitation of therapeutic monoclonal antibodies in the clinical laboratory. *Clinical and Vaccine Immunology*, 24(5), 2017.

[257] Rosemarie Raffen, Lynda J Dieckman, Meredith Szpunar, Christine Wunschl, Phani R Pokkuluri, Poras Dave, Priscilla Wilkins Stevens, Xiaoyin Cai, Marianne Schiffer, and Fred J Stevens. Physicochemical consequences of amino acid variations that contribute to fibril formation by immunoglobulin light chains. *Protein Science*, 8(3):509–517, 1999.

[258] Yong-sung Kim, Jonathan S Wall, Jeffrey Meyer, Charles Murphy, Theodore W Randolph, Mark C Manning, Alan Solomon, and John F Carpenter. Thermodynamic modulation of light chain amyloid fibril formation. *Journal of Biological Chemistry*, 275(3):1570–1574, 2000.

[259] Jonathan S Wall, Vibha Gupta, Matthew Wilkerson, Maria Schell, Remy Loris, Paul Adams, Alan Solomon, Fred Stevens, and Chris Dealwis. Structural basis of light chain amyloidogenicity: comparison of the thermodynamic properties, fibrillogenic potential and tertiary structural features of four vλ6 proteins. *Journal of Molecular Recognition*, 17(4):323–331, 2004.

[260] Martín González-Andrade, Baltazar Becerril-Luján, Rosana Sánchez-López, Héctor Ceceña-Álvarez, Julio I Pérez-Carreón, Ernesto Ortiz, D Alejandro Fernández-Velasco, and Luis del Pozo-Yauner. Mutational and genetic determinants of λ6 light chain amyloidogenesis. *The FEBS journal*, 280(23):6173–6183, 2013.

[261] Tanya L Poshusta, Laura A Sikkink, Nelson Leung, Raynell J Clark, Angela Dispenzieri, and Marina Ramirez-Alvarado. Mutations in specific structural regions of immunoglobulin light chains

are associated with free light chain levels in patients with al amyloidosis. *PloS one*, 4(4):e5169, 2009.

[262] Elena S Klimtchuk, Olga Gursky, Rupesh S Patel, Kathryn L Laporte, Lawreen H Connors, Martha Skinner, and David C Seldin. The critical role of the constant region in thermal stability and aggregation of amyloidogenic immunoglobulin light chain. *Biochemistry*, 49(45):9848–9857, 2010.

[263] Luis del Pozo-Yauner, Jonathan S Wall, Martín González Andrade, Rosana Sánchez-López, Sandra L Rodríguez-Ambriz, Julio I Pérez Carreón, Adrián Ochoa-Leyva, and D Alejandro Fernández-Velasco. The n-terminal strand modulates immunoglobulin light chain fibrillogenesis. *Biochemical and biophysical research communications*, 443(2):495–499, 2014.

[264] Luis M Blancas-Mejía, Timothy J Horn, Marta Marin-Argany, Matthew Auton, Alexander Tischer, and Marina Ramirez-Alvarado. Thermodynamic and fibril formation studies of full length immunoglobulin light chain al-09 and its germline protein using scan rate dependent thermal unfolding. *Biophysical chemistry*, 207:13–20, 2015.

[265] Laura A Sikkink and Marina Ramirez-Alvarado. Biochemical and aggregation analysis of bence jones proteins from different light chain diseases. *Amyloid*, 15(1):29–39, 2008.

[266] Luis del Pozo Yauner, Ernesto Ortiz, Rosalba Sánchez, Rosana Sánchez-López, Leopoldo Güereca, Charles L Murphy, Amy Allen, Jonathan S Wall, D Alejandro Fernández-Velasco, Alan Solomon, et al. Influence of the germline sequence on the thermodynamic stability and fibrillogenicity of human lambda 6 light chains. *Proteins: Structure, Function, and Bioinformatics*, 72(2):684–692, 2008.

[267] Kathrin Andrich, Ute Hegenbart, Christoph Kimmich, Niraja Kedia, H. Robert Bergen, Stefan Schönland, Erich Wanker, and Jan Bieschke. Aggregation of full-length immunoglobulin light chains from systemic light chain amyloidosis (AL) patients is remodeled by epigallocatechin-3-gallate. *Journal of Biological Chemistry*, 292(6):2328–2344, 2017.

[268] Zhijie Qin, Dongmei Hu, Min Zhu, and Anthony L Fink. Structural characterization of the partially folded intermediates of an immunoglobulin light chain leading to amyloid fibrillation and amorphous aggregation. *Biochemistry*, 46(11):3521–3531, 2007.

[269] Manikanthan Bhavaraju and Ulrich HE Hansmann. Effect of single point mutations in a form of systemic amyloidosis. *Protein Science*, 24(9):1451–1462, 2015.

[270] Elizabeth M Baden, Edward G Randles, Awo K Aboagye, James R Thompson, and Marina Ramirez-Alvarado. Structural insights into the role of mutations in amyloidogenesis. *Journal of Biological Chemistry*, 283(45):30950–30956, 2008.

[271] Mathieu Laporte Wolwertz, Phuong Trang Nguyen, Noé Quittot, and Steve Bourgault. Probing the role of $\lambda 6$ immunoglobulin light chain dimerization in amyloid formation. *Biochimica et Biophysica Acta (BBA)-Proteins and Proteomics*, 1864(4):409–418, 2016.

[272] Moshe E Gatt, Batia Kaplan, Dean Yogev, Elana Slyusarevsky, Galina Pogrebijski, Sizilia Golderman, Olga Kukuy, and Avi Livneh. The use of serum free light chain dimerization patterns assist in the diagnosis of al amyloidosis. *British Journal of Haematology*, 182(1):86–92, 2018.

[273] Olga Kukuy, Batia Kaplan, Sizilia Golderman, Alexander Volkov, Adrian Duek, Merav Leiba, Ilan Ben-Zvi, and Avi Livneh. Kidney disease and plasma cell dyscrasias: ambiguous cases solved by serum free light chain dimerization analysis. *Clinical and Experimental Nephrology*, 23(6):763–772, 2019.

[274] Batia Kaplan, Sizilia Golderman, Boris Aizenbud, Konstantin Esev, Olga Kukuy, Merav Leiba, Avi Livneh, and Ilan Ben-Zvi. Immunoglobulin-free light chain monomer-dimer patterns help to distinguish malignant from premalignant monoclonal gammopathies: a pilot study. *American Journal of Hematology*, 89(9):882–888, 2014.

[275] Sarmad Said, Chad J Cooper, Azikiwe C Nwosu, Jorge E Bilbao, and German T Hernandez. Hypertension, renal failure, and edema in a 38-year-old man: light chain deposition disease; a case report and review of the literature. *Journal of nephropathology*, 3(2):63, 2014.

[276] K Sölling. Polymeric forms of free light chains in serum from normal individuals and from patients with renal diseases. *Scandinavian Journal of Clinical and Laboratory Investigation*, 36(5):447–452, 1976.

[277] K Sølling. Light chain polymerism in normal individuals, in patients with severe proteinuria and in normals with inhibited tubular protein reabsorption by lysine. *Scandinavian journal of clinical and laboratory investigation*, 40(2):129–134, 1980.

[278] Roshini S Abraham, M Cristine Charlesworth, Barbara AL Owen, Linda M Benson, Jerry A Katzmann, Craig B Reeder, and Robert A Kyle. Trimolecular complexes of λ light chain dimers in serum of a patient with multiple myeloma. *Clinical chemistry*, 48(10):1805–1811, 2002.

[279] Jun Zhao, Baohong Zhang, Jianwei Zhu, Ruth Nussinov, and Buyong Ma. Structure and energetic basis of overrepresented λ light chain in systemic light chain amyloidosis patients. *Biochimica et Biophysica Acta (BBA)-Molecular Basis of Disease*, 1864(6):2294–2303, 2018.

[280] Pierre O Souillac, Vladimir N Uversky, Ian S Millett, Ritu Khurana, Sebastian Doniach, and Anthony L Fink. Elucidation of the molecular mechanism during the early events in immunoglobulin light chain amyloid fibrillation evidence for an off-pathway oligomer at acidic ph. *Journal of Biological Chemistry*, 277(15):12666–12679, 2002.

[281] Batia Kaplan, Marina Ramirez-Alvarado, Laura Sikkink, Sicilia Golderman, Angela Dispenzieri, Avi Livneh, and Gloria Gallo. Free light chains in plasma of patients with light chain amyloidosis and non-amyloid light chain deposition disease. high proportion and heterogeneity of disulfide-linked monoclonal free light chains as pathogenic features of amyloid disease. *British journal of haematology*, 144(5):705–715, 2009.

[282] Changqiang Chen, Peizhan Chen, and Xuqian Fang. The flc dimer with lambda type may false-migrate to the position of "albumin" band by urine protein electrophoresis on sebia agarose gel-based detection system. *Journal of clinical laboratory analysis*, 33(2):e22658, 2019.

[283] Colin A Hutchison, Stephen Harding, Graham Mead, Hermann Goehl, Markus Storr, Arthur Bradwell, and Paul Cockwell. Serum free-light chain removal by high cutoff hemodialysis: Optimizing removal and supportive care. *Artificial organs*, 32(12):910–917, 2008.

[284] Luca Oberti, Paola Rognoni, Alberto Barbiroli, Francesca Lavatelli, Rosaria Russo, Martina Maritan, Giovanni Palladini, Martino Bolognesi, Giampaolo Merlini, and Stefano Ricagno. Concurrent structural and biophysical traits link with immunoglobulin light chains amyloid propensity. *Scientific reports*, 7(1):1–11, 2017.

[285] Sujoy Mukherjee, Simon P Pondaven, Kieran Hand, Jillian Madine, and Christopher P Jaroniec. Effect of amino acid mutations on the conformational dynamics of amyloidogenic immunoglobulin light-chains: A combined nmr and in silico study. *Scientific reports*, 7(1):1–13, 2017.

[286] Dipankar Nandi, Pankaj Tahiliani, Anujith Kumar, and Dilip Chandu. The ubiquitin-proteasome system. *Journal of biosciences*, 31(1):137–155, 2006.

[287] Eeva-Liisa Eskelinen and Paul Saftig. Autophagy: a lysosomal degradation pathway with a central role in health and disease. *Biochimica et Biophysica Acta (BBA)-Molecular Cell Research*, 1793(4):664–673, 2009.

[288] Tianhong Pan, Seiji Kondo, Weidong Le, and Joseph Jankovic. The role of autophagy-lysosome pathway in neurodegeneration associated with parkinson's disease. *Brain*, 131(8):1969–1978, 2008.

[289] E Sergio Trombetta and Ari Helenius. Conformational requirements for glycoprotein reglucosylation in the endoplasmic reticulum. *The Journal of cell biology*, 148(6):1123–1130, 2000.

[290] Jyoti D Malhotra and Randal J Kaufman. The endoplasmic reticulum and the unfolded protein response. In *Seminars in cell & developmental biology*, volume 18, pages 716–731. Elsevier, 2007.

[291] Patrick G Needham and Jeffrey L Brodsky. How early studies on secreted and membrane protein quality control gave rise to the er associated degradation (erad) pathway: the early history of erad. *Biochimica et Biophysica Acta (BBA)-Molecular Cell Research*, 1833(11):2447–2457, 2013.

[292] Tiziana Anelli and Roberto Sitia. Protein quality control in the early secretory pathway. *The EMBO journal*, 27(2):315–327, 2008.

[293] Stewart Siyan Cao and Randal J Kaufman. Unfolded protein response. *Current biology*, 22(16):R622–R626, 2012.

[294] Christina B Cooley, Lisa M Ryno, Lars Plate, Gareth J Morgan, John D Hulleman, Jeffery W Kelly, and R Luke Wiseman. Unfolded protein response activation reduces secretion and extracellular aggregation of amyloidogenic immunoglobulin light chain. *Proceedings of the National Academy of Sciences*, 111(36):13046–13051, 2014.

[295] Lars Plate, Bibiana Rius, Bianca Nguyen, Joseph C Genereux, Jeffery W Kelly, and R Luke Wiseman. Quantitative interactome proteomics reveals a molecular basis for atf6-dependent regulation of a destabilized amyloidogenic protein. *Cell Chemical Biology*, 26(7):913–925, 2019.

[296] Bibiana Rius, Jaleh S Mesgarzadeh, Isabelle C Romine, Ryan J Paxman, Jeffery W Kelly, and Luke Wiseman. Small molecule er proteostasis regulators reduce amyloidogenic immunoglobulin light chain secretion through an on-target, atf6-independent mechanism. *BioRxiv*, 2020.

[297] AM Gardner, S Aviel, and Y Argon. Rapid degradation of an unassembled immunoglobulin light chain is mediated by a serine protease and occurs in a pre-golgi compartment. *Journal of Biological Chemistry*, 268(34):25940–25947, 1993.

[298] Jeanne L Dul, David P Davis, Edward K Williamson, Fred J Stevens, and Yair Argon. Hsp70 and antifibrillogenic peptides promote degradation and inhibit intracellular aggregation of amyloidogenic light chains. *The Journal of Cell Biology*, 152(4):705–716, 2001.

[299] Cheng E Chee, Martha Q Lacy, Ahmet Dogan, Steven R Zeldenrust, and Morie A Gertz. Pitfalls in the diagnosis of primary amyloidosis. *Clinical Lymphoma Myeloma and Leukemia*, 10(3):177–180, 2010.

[300] Ashutosh D Wechalekar, Stefan O Schonland, Efstathios Kastritis, Julian D Gillmore, Meletios A Dimopoulos, Thirusha Lane, Andrea Foli, Darren Foard, Paolo Milani, Lisa Rannigan, et al. A european collaborative study of treatment outcomes in 346 patients with cardiac stage iii al amyloidosis. *Blood*, 121(17):3420–3427, 2013.

[301] Giovanni Palladini, Ute Hegenbart, Paolo Milani, Christoph Kimmich, Andrea Foli, Anthony D Ho, Marta Vidus Rosin, Riccardo Albertini, Remigio Moratti, Giampaolo Merlini, et al. A staging system for renal outcome and early markers of renal response to chemotherapy in al amyloidosis. *Blood, The Journal of the American Society of Hematology*, 124(15):2325–2332, 2014.

[302] Maria Teresa Cibeira, Vaishali Sanchorawala, David C Seldin, Karen Quillen, John L Berk, Laura M Dember, Adam Segal, Frederick Ruberg, Hans Meier-Ewert, Nancy T Andrea, et al. Outcome of al amyloidosis after high-dose melphalan and autologous stem cell transplantation: long-term results in a series of 421 patients. *Blood, The Journal of the American Society of Hematology*, 118(16):4346–4352, 2011.

[303] Saulius Girnius, David C Seldin, Martha Skinner, Kathleen T Finn, Karen Quillen, Gheorghe Doros, and Vaishali Sanchorawala. Short and long-term outcome of treatment with high-dose melphalan and stem cell transplantation for multiple myeloma-associated al amyloidosis. *Annals of hematology*, 89(6):579–584, 2010.

[304] Sabrina Browning, Karen Quillen, J Mark Sloan, Gheorghe Doros, Shayna Sarosiek, and Vaishali Sanchorawala. Hematologic relapse in al amyloidosis after high-dose melphalan and stem cell transplantation. *Blood, The Journal of the American Society of Hematology*, 130(11):1383–1386, 2017.

[305] Michel Attal, Jean-Luc Harousseau, Thierry Facon, François Guilhot, Chantal Doyen, Jean-Gabriel Fuzibet, Mathieu Monconduit, Cyrille Hulin, Denis Caillot, Reda Bouabdallah, et al. Single versus double autologous stem-cell transplantation for multiple myeloma. *New England Journal of Medicine*, 349(26):2495–2502, 2003.

[306] Martha Skinner, Vaishali Sanchorawala, David C Seldin, Laura M Dember, Rodney H Falk, John L Berk, Jennifer J Anderson, Carl O'Hara, Kathleen T Finn, Caryn A Libbey, et al. High-dose melphalan and autologous stem-cell transplantation in patients with al amyloidosis: an 8-year study. *Annals of internal medicine*, 140(2):85–93, 2004.

[307] Efstathios Kastritis, Magdalini Migkou, Maria Gavriatopoulou, Panos Zirogiannis, Valsamakis Hadjikonstantinou, and Meletios A Dimopoulos. Treatment of light chain deposition disease with bortezomib and dexamethasone. *Haematologica*, 94(2):300, 2009.

[308] Julian Adams, Vito J Palombella, Edward A Sausville, Jill Johnson, Antonia Destree, Douglas D Lazarus, Jochen Maas, Christine S Pien, Samuel Prakash, and Peter J Elliott. Proteasome inhibitors: a novel class of potent and effective antitumor agents. *Cancer research*, 59(11):2615–2622, 1999.

[309] WG An, SG Hwang, JB Trepel, and MV Blagosklonny. Protease inhibitor-induced apoptosis: accumulation of wt p53, p21 waf1/cip1, and induction of apoptosis are independent markers of proteasome inhibition. *Leukemia*, 14(7):1276–1283, 2000.

[310] Randall W King, Raymond J Deshaies, Jan-Michael Peters, and Marc W Kirschner. How proteolysis drives the cell cycle. *Science*, 274(5293):1652–1659, 1996.

[311] Julian Adams and Michael Kauffman. Development of the proteasome inhibitor velcade™(bortezomib). *Cancer investigation*, 22(2):304–311, 2004.

[312] Monique P Curran and Kate McKeage. Bortezomib. *Drugs*, 69(7):859–888, 2009.

[313] Jesús F San Miguel, Rudolf Schlag, Nuriet K Khuageva, Meletios A Dimopoulos, Ofer Shpilberg, Martin Kropff, Ivan Spicka, Maria T Petrucci, Antonio Palumbo, Olga S Samoilova, et al. Bortezomib plus melphalan and prednisone for initial treatment of multiple myeloma. *New England Journal of Medicine*, 359(9):906–917, 2008.

[314] Paul G Richardson, Pieter Sonneveld, Michael W Schuster, David Irwin, Edward A Stadtmauer, Thierry Facon, Jean-Luc Harousseau, Dina Ben-Yehuda, Sagar Lonial, Hartmut Goldschmidt, et al. Bortezomib or high-dose dexamethasone for relapsed multiple myeloma. *New England journal of medicine*, 352(24):2487–2498, 2005.

[315] Asher A Chanan-Khan, Jonathan L Kaufman, Jayesh Mehta, Paul G Richardson, Kena C Miller, Sagar Lonial, Nikhil C Munshi, Robert Schlossman, Joseph Tariman, and Seema Singhal. Activity and safety of bortezomib in multiple myeloma patients with advanced renal failure: a multicenter retrospective study. *Blood*, 109(6):2604–2606, 2007.

[316] Efstathios Kastritis, Athanasios Anagnostopoulos, Maria Roussou, Savvas Toumanidis, Constantinos Pamboukas, Magdalini Migkou, Anna Tassidou, Irini Xilouri, Sossana Delibasi, Erasmia Psimenou, et al. Treatment of light chain (al) amyloidosis with the combination of bortezomib and dexamethasone. *Haematologica*, 92(10):1351–1358, 2007.

[317] Giovanni Palladini and Giampaolo Merlini. When should treatment of al amyloidosis start at relapse? early, to prevent organ progression. *Blood advances*, 3(2):212–215, 2019.

[318] Talha Badar, Anita D'Souza, and Parameswaran Hari. Recent advances in understanding and treating immunoglobulin light chain amyloidosis. *F1000Research*, 7, 2018.

[319] Bruce D Cheson and Mathias J Rummel. Bendamustine: rebirth of an old drug. *Journal of Clinical Oncology*, 27(9):1492–1501, 2009.

[320] Massimo Gentile, Ernesto Vigna, Anna Grazia Recchia, Lucio Morabito, Francesco Mendicino, Giovanna Giagnuolo, and Fortunato Morabito. Bendamustine in multiple myeloma. *European Journal of Haematology*, 95(5):377–388, 2015.

[321] Heinz Ludwig, Hedwig Kasparu, Clemens Leitgeb, Elisabeth Rauch, Werner Linkesch, Niklas Zojer, Richard Greil, Adelheid Seebacher, Ludek Pour, Adalbert Weißmann, et al. Bendamustine-bortezomib-dexamethasone is an active and well-tolerated regimen in patients with relapsed or refractory multiple myeloma. *Blood, The Journal of the American Society of Hematology*, 123(7):985–991, 2014.

[322] Massimo Alessio, Stefano Roggero, Ada Funaro, LB De Monte, Licia Peruzzi, Massimo Geuna, and Fabio Malavasi. Cd38 molecule: structural and biochemical analysis on human t lymphocytes, thymocytes, and plasma cells. *The Journal of Immunology*, 145(3):878–884, 1990.

[323] D Kim, CY Park, BC Medeiros, and IL Weissman. Cd19- cd45 low/- cd38 high/cd138+ plasma cells enrich for human tumorigenic myeloma cells. *Leukemia*, 26(12):2530–2537, 2012.

[324] Antonio Palumbo, Asher Chanan-Khan, Katja Weisel, Ajay K Nooka, Tamas Masszi, Meral Beksac, Ivan Spicka, Vania Hungria, Markus Munder, Maria V Mateos, et al. Daratumumab, bortezomib, and dexamethasone for multiple myeloma. *New England Journal of Medicine*, 375(8):754–766, 2016.

[325] Philippe Moreau, Maria-Victoria Mateos, Joan Bladé, Lotfi Benboubker, Javier de la Rubia, Thierry Facon, Raymond L Comenzo, Joseph W Fay, Xiang Qin, Tara Masterson, et al. An open-label, multicenter, phase 1b study of daratumumab in combination with backbone regimens in patients with multiple myeloma, 2014.

[326] Christoph R Kimmich, Tobias Terzer, Axel Benner, Tobias Dittrich, Kaya Veelken, Alexander Carpinteiro, Timon Hansen, Hartmut Goldschmidt, Anja Seckinger, Dirk Hose, et al. Daratumumab for systemic al amyloidosis: prognostic factors and adverse outcome with nephrotic-range albuminuria. *Blood, The Journal of the American Society of Hematology*, 135(18):1517–1530, 2020.

[327] Vaishali Sanchorawala, Shayna Sarosiek, Amanda Schulman, Meredith Mistark, Mary Ellen Migre, Ramon Cruz, J Mark Sloan, Dina Brauneis, and Anthony C Shelton. Safety, tolerability, and response rates of daratumumab in relapsed al amyloidosis: results of a phase 2 study. *Blood, The Journal of the American Society of Hematology*, 135(18):1541–1547, 2020.

[328] Giovanni Montagna, Benedetta Cazzulani, Laura Obici, Carla Uggetti, Sofia Giorgetti, Riccardo Porcari, Rubina Ruggiero, P Patrizia Mangione, Moreno Brambilla, Jacopo Lucchetti, et al. Benefit of doxycycline treatment on articular disability caused by dialysis related amyloidosis. *Amyloid*, 20(3):173–178, 2013.

[329] Erin Karlstedt, Victor Jimenez-Zepeda, Jonathan G Howlett, James A White, and Nowell M Fine. Clinical experience with the use of doxycycline and ursodeoxycholic acid for the treatment of transthyretin cardiac amyloidosis. *Journal of cardiac failure*, 25(3):147–153, 2019.

[330] Flávia Viana Santa-Cecília, Caio Abner Leite, Elaine Del-Bel, and Rita Raisman-Vozari. The neuroprotective effect of doxycycline on neurodegenerative diseases. *Neurotoxicity research*, 35(4):981–986, 2019.

[331] Claudia Balducci and Gianluigi Forloni. Doxycycline for alzheimer's disease: fighting β-amyloid oligomers and neuroinflammation. *Frontiers in Pharmacology*, 10:738, 2019.

[332] Maurizio Pocchiari and Anna Ladogana. Rethinking of doxycycline therapy in creutzfeldt-jakob disease, 2015.

[333] María Valero-Muñoz, Richard M Wilson, Rosa Bretón-Romero, Dominique Croteau, David C Seldin, and Flora Sam. Doxycycline decreases amyloidogenic light chain-induced autophagy in isolated primary cardiac myocytes. *International journal of cardiology*, 321:133–136, 2020.

[334] Jennifer Ellis Ward, Ruiyi Ren, Gianluca Toraldo, Pam SooHoo, Jian Guan, Carl O'Hara, Ravi Jasuja, Vickery Trinkaus-Randall, Ronglih Liao, Lawreen H Connors, et al. Doxycycline reduces fibril formation in a transgenic mouse model of al amyloidosis. *Blood, The Journal of the American Society of Hematology*, 118(25):6610–6617, 2011.

[335] Anita D'Souza, Kathryn Flynn, Saurabh Chhabra, Binod Dhakal, Mehdi Hamadani, Kirsten Jacobsen, Marcelo Pasquini, Dorothee Weihrauch, and Parameswaran Hari. Rationale and design of dual study: Doxycycline to upgrade response in light chain (al) amyloidosis (dual): A phase 2 pilot study of a two-pronged approach of prolonged doxycycline with plasma cell-directed therapy in the treatment of al amyloidosis. *Contemporary clinical trials communications*, 8:33–38, 2017.

[336] Cindy Varga, Suzanne Lentzsch, and Raymond L Comenzo. Beyond neod001 for systemic light-chain amyloidosis. *Blood, The Journal of the American Society of Hematology*, 132(18):1992–1993, 2018.

[337] Ashutosh Wechalekar, Carol Whelan, Helen Lachmann, Marianna Fontana, Shameem Mahmood, Julian D Gillmore, and Philip N Hawkins. Oral doxycycline improves outcomes of stage iii al amyloidosis-a matched case control study, 2015.

[338] AD Wechalekar and C Whelan. Encouraging impact of doxycycline on early mortality in cardiac light chain (al) amyloidosis. *Blood cancer journal*, 7(3):e546–e546, 2017.

[339] Jian Guan, Shikha Mishra, Jianru Shi, Eva Plovie, Yiling Qiu, Xin Cao, Davide Gianni, Bingbing Jiang, Federica Del Monte, Lawreen H Connors, et al. Stanniocalcin1 is a key mediator of amyloidogenic light chain induced cardiotoxicity. *Basic research in cardiology*, 108(5):378, 2013.

[340] Shikha Mishra, Jian Guan, Eva Plovie, David C Seldin, Lawreen H Connors, Giampaolo Merlini, Rodney H Falk, Calum A MacRae, and Ronglih Liao. Human amyloidogenic light chain proteins result in cardiac dysfunction, cell death, and early mortality in zebrafish. *American Journal of Physiology-Heart and Circulatory Physiology*, 305(1):H95–H103, 2013.

[341] Helen P McWilliams-Koeppen, James S Foster, Nicole Hackenbrack, Marina Ramirez-Alvarado, Dallas Donohoe, Angela Williams, Sallie Macy, Craig Wooliver, Dale Wortham, Jennifer

Morrell-Falvey, et al. Light chain amyloid fibrils cause metabolic dysfunction in human cardiomyocytes. *PloS one*, 10(9):e0137716, 2015.

[342] Morie A Gertz, Heather Landau, Raymond L Comenzo, David Seldin, Brendan Weiss, Jeffrey Zonder, Giampaolo Merlini, Stefan Schönland, Jackie Walling, Gene G Kinney, et al. First-in-human phase i/ii study of neod001 in patients with light chain amyloidosis and persistent organ dysfunction. *Journal of Clinical Oncology*, 34(10):1097, 2016.

[343] Jonathan S Wall, Stephen J Kennel, Angela Williams, Tina Richey, Alan Stuckey, Ying Huang, Sallie Macy, Robert Donnell, Robin Barbour, Peter Seubert, et al. Al amyloid imaging and therapy with a monoclonal antibody to a cryptic epitope on amyloid fibrils. *PloS one*, 7(12):e52686, 2012.

[344] Mark Renz, Ronald Torres, Philip J Dolan, Stephen J Tam, Jose R Tapia, Lauri Li, Joshua R Salmans, Robin M Barbour, Paul J Shughrue, Tarlochan Nijjar, et al. 2a4 binds soluble and insoluble light chain aggregates from al amyloidosis patients and promotes clearance of amyloid deposits by phagocytosis. *Amyloid*, 23(3):168–177, 2016.

[345] Camille V Edwards, Julia Gould, Arielle L Langer, Markus Mapara, Jai Radhakrishnan, Mathew S Maurer, Shahzad Raza, John G Mears, Jonathan Wall, Alan Solomon, et al. Interim analysis of the phase 1a/b study of chimeric fibril-reactive monoclonal antibody 11-1f4 in patients with al amyloidosis. *Amyloid*, 24(sup1):58–59, 2017.

[346] Jing Fu, Alan Solomon, Patrick Carberry, John Castrillon, Jongho Kim, Suzanne Lentzsch, and Akiva Mintz. Personalizing amyloidosis therapy with real time pet imaging of fibril-reactive monoclonal antibody cael-101. *Blood*, 132(Supplement 1):1003–1003, 2018.

[347] Nikunj Bhatt, Jongho Kim, Jing Fu, John Castrillon, Patrick Carberry, Andrei Molotkov, Mikhail Doubrovin, Nadiya Pavlishyn, Vaishali Sanchorawala, Lawreen Connors, et al. Immunopet imaging with radiolabeled cael-101 for personalizing amyloidosis immunotherapy. *Journal of Nuclear Medicine*, 60(supplement 1):1010–1010, 2019.

[348] Duncan B Richards, Louise M Cookson, Alienor C Berges, Sharon V Barton, Thirusha Lane, James M Ritter, Marianna Fontana, James C Moon, Massimo Pinzani, Julian D Gillmore, et al. Therapeutic clearance of amyloid by antibodies to serum amyloid p component. *New England Journal of Medicine*, 373(12):1106–1114, 2015.

[349] PT Sattianayagam, SDJ Gibbs, JH Pinney, AD Wechalekar, HJ Lachmann, CJ Whelan, JA Gilbertson, PN Hawkins, and JD Gillmore. Solid organ transplantation in al amyloidosis. *American Journal of Transplantation*, 10(9):2124–2131, 2010.

[350] Ashutosh D Wechalekar, Philip N Hawkins, and Julian D Gillmore. Perspectives in treatment of al amyloidosis. *British journal of haematology*, 140(4):365–377, 2008.

[351] Julian D Gillmore, Hugh J Goodman, Helen J Lachmann, Mark Offer, Ashutosh D Wechalekar, Jayshree Joshi, Mark B Pepys, and Philip N Hawkins. Sequential heart and autologous stem cell transplantation for systemic al amyloidosis. *Blood*, 107(3):1227–1229, 2006.

[352] Werner Hunstein. Epigallocathechin-3-gallate in al amyloidosis: a new therapeutic option? *Blood, The Journal of the American Society of Hematology*, 110(6):2216–2216, 2007.

[353] Derliz Mereles, Erich E Wanker, and Hugo A Katus. Therapy effects of green tea in a patient with systemic light-chain amyloidosis. *Clinical Research in Cardiology*, 97(5):341–344, 2008.

[354] Jennifer R Carlson, Brent A Bauer, Ann Vincent, Paul J Limburg, and Ted Wilson. Reading the tea leaves: anticarcinogenic properties of (-)-epigallocatechin-3-gallate. In *Mayo Clinic Proceedings*, volume 82, pages 725–732. Elsevier, 2007.

[355] Jan Bieschke, Jenny Russ, Ralf P. Friedrich, Dagmar E. Ehrnhoefer, Heike Wobst, Katja Neugebauer, and Erich E. Wanker. EGCG remodels mature α-synuclein and amyloid-β fibrils and reduces cellular toxicity. *Proceedings of the National Academy of Sciences*, 107(17):7710–7715, 2010.

[356] Juan Zhao, Qingnan Liang, Qing Sun, Congheng Chen, Lihui Xu, Yu Ding, and Ping Zhou. (-)-Epigallocatechin-3-gallate (EGCG) inhibits fibrillation, disaggregates amyloid fibrils of α-synuclein, and protects PC12 cells against α-synuclein-induced toxicity. *RSC Advances*, 7(52):32508–32517, 2017.

[357] Hong Qing, Patrick L. McGeer, Yanyan Zhang, Qinghu Yang, Rongji Dai, Rongkai Zhang, Jianping Guo, Winnie Wong, Yan Xu, and Zhenzhen Quan. Epigallocatechin gallate (EGCG) inhibits alpha-synuclein aggregation: A potential agent for Parkinson's disease. *Neurochemical Research*, 41(10):2788–2796, 2016.

[358] Sneha Roy and Rajiv Bhat. Suppression, disaggregation, and modulation of γ-Synuclein fibrillation pathway by green tea polyphenol EGCG. *Protein Science*, 28(2):382–402, 2019.

[359] Yilong Teng, Juan Zhao, Lulu Ding, Yu Ding, and Ping Zhou. Complex of egcg with cu (ii) suppresses amyloid aggregation and cu (ii)-induced cytotoxicity of α-synuclein. *Molecules*, 24(16):2940, 2019.

[360] Yun Liu, Yang Liu, Shihui Wang, Shengzhao Dong, Ping Chang, and Zhaofeng Jiang. Structural characteristics of (-)-epigallocatechin-3-gallate inhibiting amyloid Aβ42 aggregation and remodeling amyloid fibers. *RSC Advances*, 5(77):62402–62413, 2015.

[361] Young-Ho Lee, Yuxi Lin, Sarah J. Cox, Misaki Kinoshita, Bikash R. Sahoo, Magdalena Ivanova, and Ayyalusamy Ramamoorthy. Zinc boosts EGCG's hIAPP amyloid Inhibition both in solution and membrane. *Biochimica et Biophysica Acta (BBA) - Proteins and Proteomics*, 1867(5):529 – 536, 2019.

[362] Zhi Xue Xu, Gong Li Ma, Qiang Zhang, Cong Heng Chen, Yan Ming He, Li Hui Xu, Guang Rong Zhou, Zhen Hua Li, Hong Jie Yang, and Ping Zhou. Inhibitory mechanism of epigallocatechin gallate on fibrillation and aggregation of amidated human islet amyloid polypeptide. *ChemPhysChem*, 18(12):1611–1619, 2017.

[363] Dagmar E. Ehrnhoefer, Martin Duennwald, Phoebe Markovic, Jennifer L. Wacker, Sabine Engemann, Margaret Roark, Justin Legleiter, J. Lawrence Marsh, Leslie M. Thompson, Susan Lindquist, Paul J. Muchowski, and Erich E. Wanker. Green tea (-)-epigallocatechin-gallate modulates early events in huntingtin misfolding and reduces toxicity in Huntington's disease models. *Human Molecular Genetics*, 15(18):2743–2751, 2006.

[364] Heike J. Wobst, Apurwa Sharma, Marc I. Diamond, Erich E. Wanker, and Jan Bieschke. The green tea polyphenol (-)-epigallocatechin gallate prevents the aggregation of tau protein into toxic oligomers at substoichiometric ratios. *FEBS Letters*, 589(1):77–83, 2015.

[365] E. Srinivasan and R. Rajasekaran. Probing the inhibitory activity of epigallocatechin-gallate on toxic aggregates of mutant (L84F) SOD1 protein through geometry based sampling and steered molecular dynamics. *Journal of Molecular Graphics and Modelling*, 74:288–295, jun 2017.

[366] Angelika S Rambold, Margit Miesbauer, Diana Olschewski, Ralf Seidel, Constanze Riemer, Lindsay Smale, Lisa Brumm, Michal Levy, Ehud Gazit, Dieter Oesterhelt, et al. Green tea extracts interfere with the stress-protective activity of prpc and the formation of prpsc. *Journal of neurochemistry*, 107(1):218–229, 2008.

[367] Blake E. Roberts, Martin L. Duennwald, Huan Wang, Chan Chung, Nicholas P. Lopreiato, Elizabeth A. Sweeny, M. Noelle Knight, and James Shorter. A synergistic small-molecule combination directly eradicates diverse prion strain structures. *Nature Chemical Biology*, 5(12):936–946, 2009.

[368] Angel E Pelaez-Aguilar, Lina Rivillas-Acevedo, Leidys French-Pacheco, Gilberto Valdes-Garcia, Roberto Maya-Martinez, Nina Pastor, and Carlos Amero. Inhibition of light chain 6ajl2-r24g amyloid fiber formation associated with light chain amyloidosis. *Biochemistry*, 54(32):4978–4986, 2015.

[369] Yoshito Abe, Naoki Odawara, Nantanat Aeimhirunkailas, Hinako Shibata, Naoki Fujisaki, Hirofumi Tachibana, and Tadashi Ueda. Inhibition of amyloid fibril formation in the variable domain of $\lambda 6$ light chain mutant wil caused by the interaction between its unfolded state and epigallocatechin-3-o-gallate. *Biochimica et Biophysica Acta (BBA)-General Subjects*, 1862(12):2570–2578, 2018.

[370] Sohsuke Meshitsuka, Sumito Shingaki, Masatoshi Hotta, Miku Goto, Makoto Kobayashi, Yuuichi Ukawa, Yuko M Sagesaka, Yasuyo Wada, Masanori Nojima, and Kenshi Suzuki. Phase 2 trial of daily, oral epigallocatechin gallate in patients with light-chain amyloidosis. *International journal of hematology*, 105(3):295–308, 2017.

[371] Yaqing Wei, Pingping Chen, Tiejun Ling, Yijun Wang, Ruixia Dong, Chen Zhang, Longjie Zhang, Manman Han, Dongxu Wang, Xiaochun Wan, and Jinsong Zhang. Certain (-)-epigallocatechin-3-gallate (EGCG) auto-oxidation products (EAOPs) retain the cytotoxic activities of EGCG. *Food Chemistry*, 204:218–226, 2016.

[372] Pietro Sormanni, Francesco A Aprile, and Michele Vendruscolo. The camsol method of rational design of protein mutants with enhanced solubility. *Journal of molecular biology*, 427(2):478–490, 2015.

[373] Carlos W Bertoncini, Young-Sang Jung, Claudio O Fernandez, Wolfgang Hoyer, Christian Griesinger, Thomas M Jovin, and Markus Zweckstetter. Release of long-range tertiary interactions potentiates aggregation of natively unstructured alpha-synuclein. *Proceedings of the National Academy of Sciences of the United States of America*, 102:1430–1435, February 2005.

[374] Francois-Xavier Theillet, Andres Binolfi, Beata Bekei, Andrea Martorana, Honor May Rose, Marchel Stuiver, Silvia Verzini, Dorothea Lorenz, Marleen van Rossum, Daniella Goldfarb, and Philipp Selenko. Structural disorder of monomeric α-synuclein persists in mammalian cells. *Nature*, 530:45–50, February 2016.

[375] Ricardo Guerrero-Ferreira, Nicholas MI Taylor, Daniel Mona, Philippe Ringler, Matthias E Lauer, Roland Riek, Markus Britschgi, and Henning Stahlberg. Cryo-em structure of alpha-synuclein fibrils. *eLife*, 7:e36402, 2018.

[376] Stephen J Wood, Jette Wypych, Shirley Steavenson, Jean-Claude Louis, Martin Citron, and Anja Leona Biere. α-synuclein fibrillogenesis is nucleation-dependent implications for the pathogenesis of parkinson's disease. *Journal of Biological Chemistry*, 274(28):19509–19512, 1999.

[377] Francesco Simone Ruggeri, Patrick Flagmeier, Janet R Kumita, Georg Meisl, Dimitri Y Chirgadze, Marie N Bongiovanni, Tuomas PJ Knowles, and Christopher M Dobson. The influence of pathogenic mutations in α-synuclein on biophysical and structural characteristics of amyloid fibrils. *ACS nano*, 14(5):5213–5222, 2020.

[378] Sebastian McClendon, Carla C Rospigliosi, and David Eliezer. Charge neutralization and collapse of the c-terminal tail of alpha-synuclein at low ph. *Protein Science*, 18(7):1531–1540, 2009.

[379] Alexander K Buell, Céline Galvagnion, Ricardo Gaspar, Emma Sparr, Michele Vendruscolo, Tuomas P J Knowles, Sara Linse, and Christopher M Dobson. Solution conditions determine the relative importance of nucleation and growth processes in α-synuclein aggregation. *Proc Natl Acad Sci U S A*, 111(21):7671–7676, May 2014.

[380] Ché S Pillay, Edith Elliott, and Clive Dennison. Endolysosomal proteolysis and its regulation. *Biochemical Journal*, 363(3):417–429, 2002.

[381] Sally K. Mak, Alison L. McCormack, Amy B. Manning-Bog, Ana Maria Cuervo, and Donato A. Di Monte. Lysosomal degradation of alpha-synuclein in vivo. *Journal of Biological Chemistry*, 285:13621–13629, 2010.

[382] Mathieu Bourdenx, Erwan Bezard, and Benjamin Dehay. Lysosomes and α-synuclein form a dangerous duet leading to neuronal cell death. *Frontiers in Neuroanatomy*, 8:83, 2014.

[383] Keith Wilson and John Walker. *Principles and techniques of biochemistry and molecular biology*. Cambridge university press, 2010.

[384] Bas JH Kuipers and Harry Gruppen. Prediction of molar extinction coefficients of proteins and peptides using uv absorption of the constituent amino acids at 214 nm to enable quantitative reverse phase high-performance liquid chromatography- mass spectrometry analysis. *Journal of agricultural and food chemistry*, 55(14):5445–5451, 2007.

[385] Michael H Simonian and John A Smith. Spectrophotometric and colorimetric determination of protein concentration. *Current protocols in molecular biology*, 76(1):10–1, 2006.

[386] Donald F Swinehart. The beer-lambert law. *Journal of chemical education*, 39(7):333, 1962.

[387] Maurice R Eftink. Intrinsic fluorescence of proteins. In *Topics in fluorescence spectroscopy*, pages 1–15. Springer, 2002.

[388] Valentina Villari and Norberto Micali. Light scattering as spectroscopic tool for the study of disperse systems useful in pharmaceutical sciences. *Journal of pharmaceutical sciences*, 97(5):1703–1730, 2008.

[389] Thomas Wriedt. Mie theory: a review. In *The Mie Theory*, pages 53–71. Springer, 2012.

[390] Jörg Stetefeld, Sean A McKenna, and Trushar R Patel. Dynamic light scattering: a practical guide and applications in biomedical sciences. *Biophysical reviews*, 8(4):409–427, 2016.

[391] Carole Fraschini, Grégory Chauve, Jean-François Le Berre, Steven Ellis, Myriam Méthot, Brian O'Connor, and Jean Bouchard. Critical discussion of light scattering and microscopy techniques for cnc particle sizing. *Nordic Pulp & Paper Research Journal*, 29(1):31–40, 2014.

[392] Bruce J Berne and Robert Pecora. *Dynamic light scattering: with applications to chemistry, biology, and physics*. Courier Corporation, 2000.

[393] Hermann Schägger. Tricine–sds-page. *Nature protocols*, 1(1):16, 2006.

[394] Wayne S Rasband et al. Imagej, 1997.

[395] Howard K Schachman. *Ultracentrifugation in biochemistry*. Elsevier, 2013.

[396] Ole Lamm. *Die differentialgleichung der ultrazentrifugierung*. Almqvist & Wiksell, 1929.

[397] Peter Schuck. Size-distribution analysis of macromolecules by sedimentation velocity ultracentrifugation and lamm equation modeling. *Biophysical journal*, 78(3):1606–1619, 2000.

[398] Nertila Siuti and Neil L Kelleher. Decoding protein modifications using top-down mass spectrometry. *Nature methods*, 4(10):817–821, 2007.

[399] Timothy K Toby, Luca Fornelli, and Neil L Kelleher. Progress in top-down proteomics and the analysis of proteoforms. *Annual review of analytical chemistry*, 9:499–519, 2016.

[400] Faye Vazvaei and Jeffrey X Duggan. Validation of lc–ms/ms bioanalytical methods for protein therapeutics. *Bioanalysis*, 6(13):1739–1742, 2014.

[401] Lijuan Kang, Naidong Weng, and Wenying Jian. Lc–ms bioanalysis of intact proteins and peptides. *Biomedical Chromatography*, 34(1):e4633, 2020.

[402] Wenying Jian, Lijuan Kang, Lyle Burton, and Naidong Weng. A workflow for absolute quantitation of large therapeutic proteins in biological samples at intact level using lc-hrms. *Bioanalysis*, 8(16):1679–1691, 2016.

[403] Lijuan Kang, Raul C Camacho, Wenyu Li, Katharine D'Aquino, Seohee You, Vanessa Chuo, Naidong Weng, and Wenying Jian. Simultaneous catabolite identification and quantitation of large therapeutic protein at the intact level by immunoaffinity capture liquid chromatography–high-resolution mass spectrometry. *Analytical chemistry*, 89(11):6065–6075, 2017.

[404] Xi Qiu, Lijuan Kang, Martin Case, Naidong Weng, and Wenying Jian. Quantitation of intact monoclonal antibody in biological samples: comparison of different data processing strategies. *Bioanalysis*, 10(13):1055–1067, 2018.

[405] Christian Lanshoeft, Sarah Cianférani, and Olivier Heudi. Generic hybrid ligand binding assay liquid chromatography high-resolution mass spectrometry-based workflow for multiplexed human immunoglobulin g1 quantification at the intact protein level: application to preclinical pharmacokinetic studies. *Analytical chemistry*, 89(4):2628–2635, 2017.

[406] Leah V Schaffer, Robert J Millikin, Rachel M Miller, Lissa C Anderson, Ryan T Fellers, Ying Ge, Neil L Kelleher, Richard D LeDuc, Xiaowen Liu, Samuel H Payne, et al. Identification and quantification of proteoforms by mass spectrometry. *Proteomics*, 19(10):1800361, 2019.

[407] John F Carpenter, Theodore W Randolph, Wim Jiskoot, Daan JA Crommelin, C Russell Middaugh, and Gerhard Winter. Potential inaccurate quantitation and sizing of protein aggregates by size exclusion chromatography: essential need to use orthogonal methods to assure the quality of therapeutic protein products. *Journal of pharmaceutical sciences*, 99(5):2200–2208, 2010.

[408] Paolo Arosio, Thomas Muüller, Luke Rajah, Emma V Yates, Francesco A Aprile, Yingbo Zhang, Samuel IA Cohen, Duncan A White, Therese W Herling, Erwin J De Genst, et al. Microfluidic diffusion analysis of the sizes and interactions of proteins under native solution conditions. *ACS nano*, 10(1):333–341, 2015.

[409] Emma V Yates, Thomas Müller, Luke Rajah, Erwin J De Genst, Paolo Arosio, Sara Linse, Michele Vendruscolo, Christopher M Dobson, and Tuomas P J Knowles. Latent analysis of unmodified biomolecules and their complexes in solution with attomole detection sensitivity. *Nature chemistry*, 7:802–809, Oct 2015.

[410] Yuval Erez, Nadav Amdursky, Rinat Gepshtein, and Dan Huppert. Temperature and viscosity dependence of the nonradiative decay rates of auramine-o and thioflavin-t in glass-forming solvents. *The Journal of Physical Chemistry A*, 116(49):12056–12064, 2012.

[411] Mark RH Krebs, Eric HC Bromley, and Athene M Donald. The binding of thioflavin-t to amyloid fibrils: localisation and implications. *Journal of structural biology*, 149(1):30–37, 2005.

[412] Chun Wu, Matthew Biancalana, Shohei Koide, and Joan-Emma Shea. Binding modes of thioflavin-t to the single-layer β-sheet of the peptide self-assembly mimics. *Journal of molecular biology*, 394(4):627–633, 2009.

[413] Ritu Khurana, Joel R Gillespie, Anupam Talapatra, Lauren J Minert, Cristian Ionescu-Zanetti, Ian Millett, and Anthony L Fink. Partially folded intermediates as critical precursors of light chain amyloid fibrils and amorphous aggregates. *Biochemistry*, 40(12):3525–3535, 2001.

[414] Anna I Sulatskaya, Andrey V Lavysh, Alexander A Maskevich, Irina M Kuznetsova, and Konstantin K Turoverov. Thioflavin t fluoresces as excimer in highly concentrated aqueous solutions and as monomer being incorporated in amyloid fibrils. *Scientific reports*, 7(1):1–11, 2017.

[415] AA Maskevich, AV Lavysh, IM Kuznetsova, AI Sulatskaya, and KK Turoverov. Spectral manifestations of thioflavin t aggregation. *Journal of applied spectroscopy*, 82(1):33–39, 2015.

[416] AI Sulatskaya, KK Turoverov, and IM Kuznetsova. Spectral properties and factors determining high quantum yield of thioflavin t incorporated in amyloid fibrils. *Spectroscopy*, 24(1-2):169–172, 2010.

[417] Giancarlo V De Ferrari, William D Mallender, Nibaldo C Inestrosa, and Terrone L Rosenberry. Thioflavin t is a fluorescent probe of the acetylcholinesterase peripheral site that reveals conformational interactions between the peripheral and acylation sites. *Journal of Biological Chemistry*, 276(26):23282–23287, 2001.

[418] Michal Harel, Leilani K Sonoda, Israel Silman, Joel L Sussman, and Terrone L Rosenberry. Crystal structure of thioflavin t bound to the peripheral site of torpedo californica acetylcholinesterase reveals how thioflavin t acts as a sensitive fluorescent reporter of ligand binding to the acylation site. *Journal of the American Chemical Society*, 130(25):7856–7861, 2008.

[419] Viktoria Babenko and Wojciech Dzwolak. Thioflavin t forms a non-fluorescent complex with α-helical poly-l-glutamic acid. *Chemical Communications*, 47(38):10686–10688, 2011.

[420] Priyankar Sen, Sadaf Fatima, Basir Ahmad, and Rizwan Hasan Khan. Interactions of thioflavin t with serum albumins: spectroscopic analyses. *Spectrochimica Acta Part A: Molecular and Biomolecular Spectroscopy*, 74(1):94–99, 2009.

[421] Nataliya R Rovnyagina, Nikolai N Sluchanko, Tatiana N Tikhonova, Victor V Fadeev, Artur Yu Litskevich, Alexander A Maskevich, and Evgeny A Shirshin. Binding of thioflavin t by albumins: An underestimated role of protein oligomeric heterogeneity. *International journal of biological macromolecules*, 108:284–290, 2018.

[422] Hengzhi Zhao, Qiang Liu, Mei Liu, Yan Jin, and Baoxin Li. Label-free fluorescent assay of t4 polynucleotide kinase phosphatase activity based on g-quadruplexe- thioflavin t complex. *Talanta*, 165:653–658, 2017.

[423] Kefeng Wu, Changbei Ma, Zhiyi Deng, Ning Fang, Zhenwei Tang, Xingxing Zhu, and Kemin Wang. Label-free and nicking enzyme-assisted fluorescence signal amplification for rnase h determination based on a g-quadruplexe/thioflavin t complex. *Talanta*, 182:142–147, 2018.

[424] Eric D Routh, Steven D Creacy, Peter E Beerbower, Steven A Akman, James P Vaughn, and Philip J Smaldino. A g-quadruplex dna-affinity approach for purification of enzymatically active g4 resolvase1. *JoVE (Journal of Visualized Experiments)*, (121):e55496, 2017.

[425] Christine Xue, Tiffany Yuwen Lin, Dennis Chang, and Zhefeng Guo. Thioflavin t as an amyloid dye: fibril quantification, optimal concentration and effect on aggregation. *Royal Society open science*, 4(1):160696, 2017.

[426] Shuai Chen, Yong-Liang Yu, and Jian-Hua Wang. Inner filter effect-based fluorescent sensing systems: a review. *Analytica chimica acta*, 999:13–26, 2018.

[427] Yuval Erez, Yu-Hui Liu, Nadav Amdursky, and Dan Huppert. Modeling the nonradiative decay rate of electronically excited thioflavin t. *The Journal of Physical Chemistry A*, 115(30):8479–8487, 2011.

[428] Natalia P Rodina, Maksim I Sulatsky, Anna I Sulatskaya, Irina M Kuznetsova, Vladimir N Uversky, and Konstantin K Turoverov. Photophysical properties of fluorescent probe thioflavin t in crowded milieu. *Journal of Spectroscopy*, 2017, 2017.

[429] Ellen V Hackl, Joseph Darkwah, Geoff Smith, and Irina Ermolina. Effect of acidic and basic ph on thioflavin t absorbance and fluorescence. *European Biophysics Journal*, 44(4):249–261, 2015.

[430] Mantas Ziaunys, Andrius Sakalauskas, and Vytautas Smirnovas. Identifying insulin fibril conformational differences by thioflavin-t binding characteristics. *Biomacromolecules*, 2020.

[431] Anna I Sulatskaya, Natalia P Rodina, Maksim I Sulatsky, Olga I Povarova, Iuliia A Antifeeva, Irina M Kuznetsova, and Konstantin K Turoverov. Investigation of α-synuclein amyloid fibrils using the fluorescent probe thioflavin t. *International journal of molecular sciences*, 19(9):2486, 2018.

[432] Maria M Picken and Guillermo A Herrera. Thioflavin t stain: an easier and more sensitive method for amyloid detection. In *Amyloid and Related Disorders*, pages 225–227. Springer, 2015.

[433] Alexander K Buell, Christopher M Dobson, Tuomas PJ Knowles, and Mark E Welland. Interactions between amyloidophilic dyes and their relevance to studies of amyloid inhibitors. *Biophysical journal*, 99(10):3492–3497, 2010.

[434] Sean A Hudson, Heath Ecroyd, Tak W Kee, and John A Carver. The thioflavin t fluorescence assay for amyloid fibril detection can be biased by the presence of exogenous compounds. *The FEBS journal*, 276(20):5960–5972, 2009.

[435] Kirsten Gade Malmos, Luis M Blancas-Mejia, Benedikt Weber, Johannes Buchner, Marina Ramirez-Alvarado, Hironobu Naiki, and Daniel Otzen. Tht 101: a primer on the use of thioflavin t to investigate amyloid formation. *Amyloid*, 24(1):1–16, 2017.

[436] Johanna Wiesbauer, Ruth Prassl, and Bernd Nidetzky. Renewal of the air–water interface as a critical system parameter of protein stability: aggregation of the human growth hormone and its prevention by surface-active compounds. *Langmuir*, 29(49):15240–15250, 2013.

[437] Carol L Ladner-Keay, Bethany J Griffith, and David S Wishart. Shaking alone induces de novo conversion of recombinant prion proteins to β-sheet rich oligomers and fibrils. *PloS one*, 9(6):e98753, 2014.

[438] Dave E Dunstan, Paul Hamilton-Brown, Peter Asimakis, William Ducker, and Joseph Bertolini. Shear flow promotes amyloid-β fibrilization. *Protein Engineering, Design & Selection*, 22(12):741–746, 2009.

[439] Mark Duerkop, Eva Berger, Astrid Dürauer, and Alois Jungbauer. Impact of cavitation, high shear stress and air/liquid interfaces on protein aggregation. *Biotechnology journal*, 13(7):1800062, 2018.

[440] Alireza Abdolvahabi, Yunhua Shi, Sanaz Rasouli, Corbin M Croom, Aleksandra Chuprin, and Bryan F Shaw. How do gyrating beads accelerate amyloid fibrillization? *Biophysical journal*, 112(2):250–264, 2017.

[441] Maria F Mossuto, Benedetta Bolognesi, Bernat Guixer, Anne Dhulesia, Federico Agostini, Janet R Kumita, Gian G Tartaglia, Mireille Dumoulin, Christopher M Dobson, and Xavier Salvatella. Disulfide bonds reduce the toxicity of the amyloid fibrils formed by an extracellular protein. *Angewandte Chemie*, 123(31):7186–7189, 2011.

[442] Maulik V Trivedi, Jennifer S Laurence, and Teruna J Siahaan. The role of thiols and disulfides on protein stability. *Current Protein and Peptide Science*, 10(6):614–625, 2009.

[443] Nian E Zhou, Cyril M Kay, and Robert S Hodges. Disulfide bond contribution to protein stability: Positional effects of substitution in the hydrophobic core of the two-stranded. alpha.-helical coiled-coil. *Biochemistry*, 32(12):3178–3187, 1993.

[444] Mateusz Banach, Barbara Kalinowska, Leszek Konieczny, and Irena Roterman. Role of disulfide bonds in stabilizing the conformation of selected enzymes—an approach based on divergence entropy applied to the structure of hydrophobic core in proteins. *Entropy*, 18(3):67, 2016.

[445] Yuji Goto and Kozo Hamaguchi. Formation of the intrachain disulfide bond in the constant fragment of the immunoglobulin light chain. *Journal of molecular biology*, 146(3):321–340, 1981.

[446] Yang Li, Juan Yan, Xin Zhang, and Kun Huang. Disulfide bonds in amyloidogenesis diseases related proteins. *Proteins: Structure, Function, and Bioinformatics*, 81(11):1862–1873, 2013.

[447] Ryosuke Maeda, Kazuyoshi Ado, Naohiro Takeda, and Yoshihiro Taniguchi. Promotion of insulin aggregation by protein disulfide isomerase. *Biochimica et Biophysica Acta (BBA)-Proteins and Proteomics*, 1774(12):1619–1627, 2007.

[448] Zeynep A Oztug Durer, Jeffrey A Cohlberg, Phong Dinh, Shelby Padua, Krista Ehrenclou, Sean Downes, James K Tan, Yoko Nakano, Christopher J Bowman, Jessica L Hoskins, et al. Loss of metal ions, disulfide reduction and mutations related to familial als promote formation of amyloid-like aggregates from superoxide dismutase. *PloS one*, 4(3):e5004, 2009.

[449] Ryo Honda. Role of the disulfide bond in prion protein amyloid formation: a thermodynamic and kinetic analysis. *Biophysical journal*, 114(4):885–892, 2018.

[450] Mu Yang, Colina Dutta, and Ashutosh Tiwari. Disulfide-bond scrambling promotes amorphous aggregates in lysozyme and bovine serum albumin. *The Journal of Physical Chemistry B*, 119(10):3969–3981, 2015.

[451] Yumiko Ohhashi, Yoshihisa Hagihara, Gennady Kozhukh, Masaru Hoshino, Kazuhiro Hasegawa, Itaru Yamaguchi, Hironobu Naiki, and Yuji Goto. The intrachain disulfide bond of β2-microglobulin is not essential for the immunoglobulin fold at neutral ph, but is essential for amyloid fibril formation at acidic ph. *The Journal of Biochemistry*, 131(1):45–52, 2002.

[452] Bon W Koo and Andrew D Miranker. Contribution of the intrinsic disulfide to the assembly mechanism of islet amyloid. *Protein Science*, 14(1):231–239, 2005.

[453] Nandini Sarkar, Manjeet Kumar, and Vikash Kumar Dubey. Effect of sodium tetrathionate on amyloid fibril: Insight into the role of disulfide bond in amyloid progression. *Biochimie*, 93(5):962–968, 2011.

[454] Lee Whitmore and Bonnie A Wallace. Protein secondary structure analyses from circular dichroism spectroscopy: methods and reference databases. *Biopolymers: Original Research on Biomolecules*, 89(5):392–400, 2008.

[455] Jen Tsi Yang, Chuen-Shang C Wu, and Hugo M Martinez. [11] calculation of protein conformation from circular dichroism. *Methods in enzymology*, 130:208–269, 1986.

[456] András Micsonai, Frank Wien, Linda Kernya, Young-Ho Lee, Yuji Goto, Matthieu Réfrégiers, and József Kardos. Accurate secondary structure prediction and fold recognition for circular dichroism spectroscopy. *Proceedings of the National Academy of Sciences*, 112(24):E3095–E3103, 2015.

[457] Claus Urban and Peter Schurtenberger. Characterization of turbid colloidal suspensions using light scattering techniques combined with cross-correlation methods. *Journal of colloid and interface science*, 207(1):150–158, 1998.

[458] Dennis E Koppel. Analysis of macromolecular polydispersity in intensity correlation spectroscopy: the method of cumulants. *The Journal of Chemical Physics*, 57(11):4814–4820, 1972.

[459] UD Schwarz, H Haefke, P Reimann, and H-J Güntherodt. Tip artefacts in scanning force microscopy. *Journal of Microscopy*, 173(3):183–197, 1994.

[460] Q Zhong, D Inniss, K Kjoller, and VB Elings. Fractured polymer/silica fiber surface studied by tapping mode atomic force microscopy. *Surface science*, 290(1-2):L688–L692, 1993.

[461] Per M Claesson, Peter C Herder, Christina E Blom, and Barry W Ninham. Interactions between a positively charged hydrophobic surface and a negatively charged bare mica surface. *Journal of colloid and interface science*, 118(1):68–79, 1987.

[462] Xingfei Zhou, Yingying Zhang, Feng Zhang, Saju Pillai, Jianhua Liu, Rong Li, Bin Dai, Bin Li, and Yi Zhang. Hierarchical ordering of amyloid fibrils on the mica surface. *Nanoscale*, 5(11):4816–4822, 2013.

[463] HKL Blackley, GHW Sanders, MC Davies, CJ Roberts, SJB Tendler, and MJ Wilkinson. In-situ atomic force microscopy study of β-amyloid fibrillization. *Journal of molecular biology*, 298(5):833–840, 2000.

[464] Claire Goldsbury, Joerg Kistler, Ueli Aebi, Tudor Arvinte, and Garth JS Cooper. Watching amyloid fibrils grow by time-lapse atomic force microscopy. *Journal of molecular biology*, 285(1):33–39, 1999.

[465] Gjertrud Maurstad, Marcus Prass, Louise C Serpell, and Pawel Sikorski. Dehydration stability of amyloid fibrils studied by afm. *European Biophysics Journal*, 38(8):1135–1140, 2009.

[466] David Nečas and Petr Klapetek. Gwyddion: an open-source software for spm data analysis. *Open Physics*, 10(1):181–188, 2012.

[467] Satoru Fujiwara, Fumiaki Kono, Tatsuhito Matsuo, Yasunobu Sugimoto, Tomoharu Matsumoto, Akihiro Narita, and Kaoru Shibata. Dynamic properties of human α-synuclein related to propensity to amyloid fibril formation. *Journal of molecular biology*, 431(17):3229–3245, 2019.

[468] Yumiko Ohhashi, Miho Kihara, Hironobu Naiki, and Yuji Goto. Ultrasonication-induced amyloid fibril formation of β2-microglobulin. *Journal of Biological Chemistry*, 280(38):32843–32848, 2005.

[469] Ana-Maria Fernandez-Escamilla, Frederic Rousseau, Joost Schymkowitz, and Luis Serrano. Prediction of sequence-dependent and mutational effects on the aggregation of peptides and proteins. *Nature biotechnology*, 22(10):1302–1306, 2004.

[470] Antonio Trovato, Fabrizio Chiti, Amos Maritan, and Flavio Seno. Insight into the structure of amyloid fibrils from the analysis of globular proteins. *PLoS Comput Biol*, 2(12):e170, 2006.

[471] Poh K Teng and David Eisenberg. Short protein segments can drive a non-fibrillizing protein into the amyloid state. *Protein Engineering, Design & Selection*, 22(8):531–536, 2009.

[472] Boris Brumshtein, Shannon R Esswein, Michael R Sawaya, Gregory Rosenberg, Alan T Ly, Meytal Landau, and David S Eisenberg. Identification of two principal amyloid-driving segments in variable domains of ig light chains in systemic light-chain amyloidosis. *Journal of Biological Chemistry*, 293(51):19659–19671, 2018.

[473] Andreas Schmidt, Karthikeyan Annamalai, Matthias Schmidt, Nikolaus Grigorieff, and Marcus Fändrich. Cryo-em reveals the steric zipper structure of a light chain-derived amyloid fibril. *Proceedings of the National Academy of Sciences*, 113(22):6200–6205, 2016.

[474] Nikolaos Louros, Katerina Konstantoulea, Matthias De Vleeschouwer, Meine Ramakers, Joost Schymkowitz, and Frederic Rousseau. Waltz-db 2.0: an updated database containing structural information of experimentally determined amyloid-forming peptides. *Nucleic Acids Research*, 48(D1):D389–D393, 2020.

[475] Amol P Pawar, Kateri F Dubay, Jesus Zurdo, Fabrizio Chiti, Michele Vendruscolo, and Christopher M Dobson. Prediction of ?aggregation-prone? and ?aggregation-susceptible? regions in proteins associated with neurodegenerative diseases. *Journal of molecular biology*, 350(2):379–392, 2005.

[476] Fabrizio Chiti, Massimo Stefani, Niccolò Taddei, Giampietro Ramponi, and Christopher M Dobson. Rationalization of the effects of mutations on peptide andprotein aggregation rates. *Nature*, 424(6950):805–808, 2003.

[477] Gian Gaetano Tartaglia, Andrea Cavalli, Riccardo Pellarin, and Amedeo Caflisch. The role of aromaticity, exposed surface, and dipole moment in determining protein aggregation rates. *Protein Science*, 13(7):1939–1941, 2004.

[478] Antonio Trovato, Flavio Seno, and Silvio CE Tosatto. The pasta server for protein aggregation prediction. *Protein Engineering, Design & Selection*, 20(10):521–523, 2007.

[479] Oxana V Galzitskaya, Sergiy O Garbuzynskiy, and Michail Yurievich Lobanov. Prediction of amyloidogenic and disordered regions in protein chains. *PLoS Comput Biol*, 2(12):e177, 2006.

[480] Oscar Conchillo-Solé, Natalia S de Groot, Francesc X Avilés, Josep Vendrell, Xavier Daura, and Salvador Ventura. Aggrescan: a server for the prediction and evaluation of" hot spots" of aggregation in polypeptides. *BMC bioinformatics*, 8(1):65, 2007.

[481] Shahin Zibaee, O Sumner Makin, Michel Goedert, and Louise C Serpell. A simple algorithm locates β-strands in the amyloid fibril core of α-synuclein, aβ, and tau using the amino acid sequence alone. *Protein Science*, 16(5):906–918, 2007.

[482] Sebastian Maurer-Stroh, Maja Debulpaep, Nico Kuemmerer, Manuela Lopez De La Paz, Ivo Cristiano Martins, Joke Reumers, Kyle L Morris, Alastair Copland, Louise Serpell, Luis Serrano, et al. Exploring the sequence determinants of amyloid structure using position-specific scoring matrices. *Nature methods*, 7(3):237–242, 2010.

[483] Gian Gaetano Tartaglia and Michele Vendruscolo. The zyggregator method for predicting protein aggregation propensities. *Chemical Society Reviews*, 37(7):1395–1401, 2008.

[484] Mattia Belli, Matteo Ramazzotti, and Fabrizio Chiti. Prediction of amyloid aggregation in vivo. *EMBO reports*, 12(7):657–663, 2011.

[485] Lukasz Goldschmidt, Poh K Teng, Roland Riek, and David Eisenberg. Identifying the amylome, proteins capable of forming amyloid-like fibrils. *Proceedings of the National Academy of Sciences*, 107(8):3487–3492, 2010.

[486] Mikael Oliveberg. Waltz, an exciting new move in amyloid prediction. *Nature methods*, 7(3):187–188, 2010.

[487] Frederic Rousseau, Joost Schymkowitz, and Luis Serrano. Protein aggregation and amyloidosis: confusion of the kinds? *Current opinion in structural biology*, 16(1):118–126, 2006.

[488] Rune Linding, Joost Schymkowitz, Frederic Rousseau, Francesca Diella, and Luis Serrano. A comparative study of the relationship between protein structure and β-aggregation in globular and intrinsically disordered proteins. *Journal of molecular biology*, 342(1):345–353, 2004.

[489] Ian Walsh, Flavio Seno, Silvio CE Tosatto, and Antonio Trovato. Pasta 2.0: an improved server for protein aggregation prediction. *Nucleic acids research*, 42(W1):W301–W307, 2014.

[490] Kip Bodi, Tatiana Prokaeva, Brian Spencer, Maurya Eberhard, Lawreen H Connors, and David C Seldin. Al-base: a visual platform analysis tool for the study of amyloidogenic immunoglobulin light chain sequences. *Amyloid*, 16(1):1–8, 2009.

[491] Per Westermark, Merrill D Benson, Joel N Buxbaum, Alan S Cohen, Blas Frangione, Shu-Ichi Ikeda, Colin L Masters, Giampaolo Merlini, Maria J Saraiva, and Jean D Sipe. Amyloid: Toward terminology clarification report from the nomenclature committee of the international society of amyloidosis. *Amyloid*, 12(1):1–4, 2005.

[492] Tuomas P. J. Knowles, Michele Vendruscolo, and Christopher M. Dobson. The amyloid state and its association with protein misfolding diseases. *Nature reviews. Molecular cell biology*, 15(6):384–96, jun 2014.

[493] Ashutosh D Wechalekar, Julian D Gillmore, and Philip N Hawkins. Systemic amyloidosis. *The Lancet*, 387(10038):2641–2654, 2016.

[494] Paolo Arosio, Marta Owczarz, Thomas Müller-Späth, Paola Rognoni, Marten Beeg, Hua Wu, Mario Salmona, and Massimo Morbidelli. In vitro aggregation behavior of a non-amyloidogenic λ light chain dimer deriving from u266 multiple myeloma cells. *PloS one*, 7(3), 2012.

[495] Luis M Blancas-Mejía, Jared Hammernik, Marta Marin-Argany, and Marina Ramirez-Alvarado. Differential effects on light chain amyloid formation depend on mutations and type of glycosaminoglycans. *Journal of Biological Chemistry*, 290(8):4953–4965, 2015.

[496] Benedikt Weber, Manuel Hora, Pamina Kazman, Christoph Göbl, Carlo Camilloni, Bernd Reif, and Johannes Buchner. The antibody light-chain linker regulates domain orientation and amyloidogenicity. *Journal of molecular biology*, 430(24):4925–4940, 2018.

[497] Jameel Muzaffar, Abdullah Mohammad Khan, Athira Unnikrishnan, Preeti Narayan, Dara Wakefield, and Jan S Moreb. Characteristics of light chain deposition disease (lcdd) and factors affecting outcome after treatment. *Blood*, 130(Supplement 1):5513–5513, 2017.

[498] George M Bernier and Frank W Putnam. Monomer–dimer forms of bence jones proteins. *Nature*, 200(4903):223–225, 1963.

[499] Otto Epp, Eaton E Lattman, Marianne Schiffer, Robert Huber, and Walter Palm. Molecular structure of a dimer composed of the variable portions of the bence-jones protein rei refined at 2.0-å resolution. *Biochemistry*, 14(22):4943–4952, 1975.

[500] Boris Brumshtein, Shannon R Esswein, Meytal Landau, Christopher M Ryan, Julian P Whitelegge, Martin L Phillips, Duilio Cascio, Michael R Sawaya, and David S Eisenberg. Formation of amyloid fibers by monomeric light chain variable domains. *Journal of Biological Chemistry*, 289(40):27513–27525, 2014.

[501] Dongmei Hu, Zhijie Qin, Bin Xue, Anthony L Fink, and Vladimir N Uversky. Effect of methionine oxidation on the structural properties, conformational stability, and aggregation of immunoglobulin light chain len. *Biochemistry*, 47(33):8665–8677, 2008.

[502] Josef Vlasak and Roxana Ionescu. Fragmentation of monoclonal antibodies. In *MAbs*, volume 3, pages 253–263. Taylor & Francis, 2011.

[503] Joseph J Bass, Daniel J Wilkinson, Debbie Rankin, Bethan E Phillips, Nathaniel J Szewczyk, Kenneth Smith, and Philip J Atherton. An overview of technical considerations for western blotting applications to physiological research. *Scandinavian journal of medicine & science in sports*, 27(1):4–25, 2017.

[504] Nelson Leung, Morie Gertz, Robert A Kyle, Fernando C Fervenza, Maria V Irazabal, Alfonso Eirin, Shaji Kumar, Stephen S Cha, S Vincent Rajkumar, Martha Q Lacy, et al. Urinary albumin excretion patterns of patients with cast nephropathy and other monoclonal gammopathy–related kidney diseases. *Clinical Journal of the American Society of Nephrology*, 7(12):1964–1968, 2012.

[505] H Sugihara, D Chihara, K Seike, K Fukumoto, M Fujisawaa, Y Suehara, Y Nishida, M Takeuchi, and K Matsue. Percentage of urinary albumin excretion and serum-free light-chain reduction are important determinants of renal response in myeloma patients with moderate to severe renal impairment. *Blood cancer journal*, 4(8):e235–e235, 2014.

[506] MH Bakkus, Carlo Heirman, Ivan Van Riet, Ben Van Camp, and Kris Thielemans. Evidence that multiple myeloma ig heavy chain vdj genes contain somatic mutations but show no intraclonal variation. 1992.

[507] Wan Cheung Cheung, Sean A Beausoleil, Xiaowu Zhang, Shuji Sato, Sandra M Schieferl, James S Wieler, Jason G Beaudet, Ravi K Ramenani, Lana Popova, Michael J Comb, et al. A proteomics approach for the identification and cloning of monoclonal antibodies from serum. *Nature biotechnology*, 30(5):447–452, 2012.

[508] Kelly V Ruggles, Karsten Krug, Xiaojing Wang, Karl R Clauser, Jing Wang, Samuel H Payne, David Fenyö, Bing Zhang, and DR Mani. Methods, tools and current perspectives in proteogenomics. *Molecular & Cellular Proteomics*, 16(6):959–981, 2017.

[509] Rui Vitorino, Sofia Guedes, Fabio Trindade, Inês Correia, Gabriela Moura, Paulo Carvalho, Manuel AS Santos, and Francisco Amado. De novo sequencing of proteins by mass spectrometry. *Expert Review of Proteomics*, 17(7-8):595–607, 2020.

[510] Nuno Bandeira, Victoria Pham, Pavel Pevzner, David Arnott, and Jennie R Lill. Automated de novo protein sequencing of monoclonal antibodies. *Nature biotechnology*, 26(12):1336–1338, 2008.

[511] Ngoc Hieu Tran, M Ziaur Rahman, Lin He, Lei Xin, Baozhen Shan, and Ming Li. Complete de novo assembly of monoclonal antibody sequences. *Scientific reports*, 6(1):1–10, 2016.

[512] Da Ren, Gary D Pipes, David Hambly, Pavel V Bondarenko, Michael J Treuheit, and Himanshu S Gadgil. Top-down n-terminal sequencing of immunoglobulin subunits with electrospray ionization time of flight mass spectrometry. *Analytical biochemistry*, 384(1):42–48, 2009.

[513] Kristina Srzentic, Luca Fornelli, Yury O Tsybin, Joseph A Loo, Henrique Seckler, Jeffrey N Agar, Lissa C Anderson, Dina L Bai, Alain Beck, Jennifer S Brodbelt, et al. Interlaboratory study for characterizing monoclonal antibodies by top-down and middle-down mass spectrometry. *Journal of the American Society for Mass Spectrometry*, 31(9):1783–1802, 2020.

[514] David M Horn, Roman A Zubarev, and Fred W McLafferty. Automated de novo sequencing of proteins by tandem high-resolution mass spectrometry. *Proceedings of the National Academy of Sciences*, 97(19):10313–10317, 2000.

[515] Xiaowen Liu, Lennard JM Dekker, Si Wu, Martijn M Vanduijn, Theo M Luider, Nikola Tolic?, Qiang Kou, Mikhail Dvorkin, Sonya Alexandrova, Kira Vyatkina, et al. De novo protein sequencing by combining top-down and bottom-up tandem mass spectra. *Journal of proteome research*, 13(7):3241–3248, 2014.

[516] Martial Rey, Menglin Yang, Kyle M Burns, Yaping Yu, Susan P Lees-Miller, and David C Schriemer. Nepenthesin from monkey cups for hydrogen/deuterium exchange mass spectrometry. *Molecular & cellular proteomics*, 12(2):464–472, 2013.

[517] Stefka Tyanova, Tikira Temu, and Juergen Cox. The maxquant computational platform for mass spectrometry-based shotgun proteomics. *Nature protocols*, 11(12):2301, 2016.

[518] Daniel Kavan and Petr Man. Mstools?web based application for visualization and presentation of hxms data. *International journal of mass spectrometry*, 302(1-3):53–58, 2011.

[519] Himanshu S Gadgil, Pavel V Bondarenko, Gary D Pipes, Thomas M Dillon, Douglas Banks, Jeffrey Abel, Gerd R Kleemann, and Michael J Treuheit. Identification of cysteinylation of a free cysteine in the fab region of a recombinant monoclonal igg1 antibody using lys-c limited proteolysis coupled with lc/ms analysis. *Analytical biochemistry*, 355(2):165–174, 2006.

[520] Heiko Braak and Eva Braak. Neuropathological stageing of alzheimer-related changes. *Acta neuropathologica*, 82(4):239–259, 1991.

[521] Fabrizio Chiti and Christopher M. Dobson. Protein misfolding, amyloid formation, and human disease: A summary of progress over the last decade. *Annual Review of Biochemistry*, 86(1):27–68, 2017.

[522] David D Weis. *Hydrogen exchange mass spectrometry of proteins: fundamentals, methods, and applications*. John Wiley & Sons, 2016.

[523] Liza Nielsen, Ritu Khurana, Alisa Coats, Sven Frokjaer, Jens Brange, Sandip Vyas, Vladimir N Uversky, and Anthony L Fink. Effect of environmental factors on the kinetics of insulin fibril formation: elucidation of the molecular mechanism. *Biochemistry*, 40(20):6036–6046, 2001.

[524] Bruce J Berne. R. pecora dynamic light scattering. *Wdey, New York*, 1976.

[525] Mona Mostafa Mohamed and Bonnie F Sloane. Multifunctional enzymes in cancer. *Nature Reviews Cancer*, 6(10):764–775, 2006.

[526] Vito Turk, Veronika Stoka, Olga Vasiljeva, Miha Renko, Tao Sun, Boris Turk, and Dušan Turk. Cysteine cathepsins: from structure, function and regulation to new frontiers. *Biochimica et Biophysica Acta (BBA)-Proteins and Proteomics*, 1824(1):68–88, 2012.

[527] Ilaria Giusti, Sandra D?Ascenzo, Danilo Millimaggi, Giulia Taraboletti, Gaspare Carta, Nicola Franceschini, Antonio Pavan, and Vincenza Dolo. Cathepsin b mediates the ph-dependent proinvasive activity of tumor-shed microvesicles. *Neoplasia*, 10(5):481–488, 2008.

[528] Baoguang Zhao, Cheryl A Janson, Bernard Y Amegadzie, Karla D'Alessio, Charles Griffin, Charles R Hanning, Christopher Jones, Jeff Kurdyla, Michael McQueney, Xiayang Qiu, et al. Crystal structure of human osteoclast cathepsin k complex with e-64. *Nature structural biology*, 4(2):109–111, 1997.

[529] Seiichi Hashida, Takae TOWATARI, Eiki KOMINAMI, and Nobuhiko KATUNUMA. Inhibitions by e-64 derivatives of rat liver cathepsin b and cathepsin l in vitro and in vivo. *The Journal of Biochemistry*, 88(6):1805–1811, 1980.

[530] Norbert Schaschke, Irmgard Assfalg-Machleidt, Werner Machleidt, Dushan Turk, and Luis Moroder. E-64 analogues as inhibitors of cathepsin b. on the role of the absolute configuration of the epoxysuccinyl group. *Bioorganic & medicinal chemistry*, 5(9):1789–1797, 1997.

[531] Alan J Barrett, Asha A Kembhavi, Molly A Brown, Heidrun Kirschke, C Graham Knight, M Tamai, and K Hanada. L-trans-epoxysuccinyl-leucylamido (4-guanidino) butane (e-64) and its analogues as inhibitors of cysteine proteinases including cathepsins b, h and l. *Biochemical Journal*, 201(1):189–198, 1982.

[532] Iñigo Santamarı?a, Gloria Velasco, Alberto M Pendás, Antonio Fueyo, and Carlos López-Otı?n. Cathepsin z, a novel human cysteine proteinase with a short propeptide domain and a unique chromosomal location. *Journal of Biological Chemistry*, 273(27):16816–16823, 1998.

[533] JN Whitaker, PK Herman, SM Sparacio, SR Zhou, and EN Benveniste. Changes induced in astrocyte cathepsin d by cytokines and leupeptin. *Journal of neurochemistry*, 57(2):406–414, 1991.

[534] Chii-Shiarng Chen, Wan-Nan U Chen, Mingjie Zhou, Seksiri Arttamangkul, and Richard P Haugland. Probing the cathepsin d using a bodipy fl–pepstatin a: applications in fluorescence polarization and microscopy. *Journal of biochemical and biophysical methods*, 42(3):137–151, 2000.

[535] Naoko Nakanishi, Michiaki Fukui, Muhei Tanaka, Hitoshi Toda, Saeko Imai, Masahiro Yamazaki, Goji Hasegawa, Yohei Oda, and Naoto Nakamura. Low urine ph is a predictor of chronic kidney disease. *Kidney and Blood Pressure Research*, 35(2):77–81, 2012.

[536] Agueda Rostagno, Ruben Vidal, Batia Kaplan, Joseph Chuba, Ashok Kumar, James I Elliott, Blas Frangione, Gloria Gallo, and Jorge Ghiso. ph-dependent fibrillogenesis of a vκiii bence jones protein. *British journal of haematology*, 107(4):835–843, 1999.

[537] Fred J Stevens, Elizabeth A Myatt, Chong-Hwan Chang, Florence A Westholm, Manfred Eulitz, Deborah T Weiss, Charles Murphy, Alan Solomon, and Marianne Schiffer. A molecular model for self-assembly of amyloid fibrils: immunoglobulin light chains. *Biochemistry*, 34(34):10697–10702, 1995.

[538] Dag Aarsland, E Londos, and Clive Ballard. Parkinson's disease dementia and dementia with lewy bodies: different aspects of one entity. *International psychogeriatrics*, 21(2):216–219, 2009.

[539] Maria Grazia Spillantini, R Anthony Crowther, Ross Jakes, Masato Hasegawa, and Michel Goedert. α-synuclein in filamentous inclusions of lewy bodies from parkinson?s disease and dementia with lewy bodies. *Proceedings of the National Academy of Sciences*, 95(11):6469–6473, 1998.

[540] Kelvin C Luk, Victoria Kehm, Jenna Carroll, Bin Zhang, Patrick O?Brien, John Q Trojanowski, and Virginia M-Y Lee. Pathological α-synuclein transmission initiates parkinson-like neurodegeneration in nontransgenic mice. *Science*, 338(6109):949–953, 2012.

[541] Vladimir N. Uversky, Jie Li, and Anthony L. Fink. Evidence for a Partially Folded Intermediate in α-Synuclein Fibril Formation. *Journal of Biological Chemistry*, 276(14):10737–10744, 2001.

[542] Ingrid Marlou van der Wateren, Tuomas Knowles, Alexander Buell, Christopher M Dobson, and Celine Galvagnion. C-terminal truncation of α-synuclein promotes amyloid fibril amplification at physiological ph. *Chemical Science*, 2018.

[543] Monica Bucciantini, Elisa Giannoni, Fabrizio Chiti, Fabiana Baroni, Lucia Formigli, Jesús Zurdo, Niccolo Taddei, Giampietro Ramponi, Christopher M Dobson, and Massimo Stefani. Inherent toxicity of aggregates implies a common mechanism for protein misfolding diseases. *nature*, 416(6880):507, 2002.

[544] Marija Iljina, Liu Hong, Mathew H Horrocks, Marthe H Ludtmann, Minee L Choi, Craig D Hughes, Francesco S Ruggeri, Tim Guilliams, Alexander K Buell, Ji-Eun Lee, Sonia Gandhi, Steven F Lee, Clare E Bryant, Michele Vendruscolo, Tuomas P J Knowles, Christopher M Dobson, Erwin De Genst, and David Klenerman. Nanobodies raised against monomeric α-synuclein inhibit fibril formation and destabilize toxic oligomeric species. *BMC biology*, 15:57, Jul 2017.

[545] Emil D Agerschou, Patrick Flagmeier, Theodora Saridaki, Celine Galvagnion, Daniel Komnig, Akansha Nagpal, Natalie Gasterich, Laetitia Heid, Vibha Prasad, Hamed Shaykhalishahi, Dieter Willbold, Chrisopher M Dobson, Aaron Voigt, Björn Falkenburger, Wolfgang Hoyer, and Alexander K Buell. An engineered monomer binding-protein for α-synuclein efficiently inhibits the proliferation of amyloid fibrils. *eLife*, 8:e46112, 2019.

[546] Jens Wagner, Sergey Ryazanov, Andrei Leonov, Johannes Levin, Song Shi, Felix Schmidt, Catharina Prix, Francisco Pan?Montojo, Uwe Bertsch, Gerda Mitteregger?Kretzschmar, Markus Geissen, Martin Eiden, Fabienne Leidel, Thomas Hirschberger, Andreas A. Deeg, Julian J. Krauth, Wolfgang Zinth, Paul Tavan, Jens Pilger, Markus Zweckstetter, Tobias Frank, Mathias Bähr, Jochen H. Weishaupt, Manfred Uhr, Henning Urlaub, Ulrike Teichmann, Matthias Samwer, Kai Bötzel, Martin Groschup, Hans Kretzschmar, Christian Griesinger, and Armin Giese. Anle138b: a novel oligomer modulator for disease-modifying therapy of neurodegenerative diseases such as prion and parkinson?s disease. *Acta Neuropathol*, 125:795–813, 2013.

[547] Gergely Tóth, Shyra J Gardai, Wagner Zago, Carlos W Bertoncini, Nunilo Cremades, Susan L Roy, Mitali A Tambe, Jean-Christophe Rochet, Celine Galvagnion, Gaia Skibinski, Steven Finkbeiner, Michael Bova, Karin Regnstrom, San-San Chiou, Jennifer Johnston, Kari Callaway, John P Anderson, Michael F Jobling, Alexander K Buell, Ted A Yednock, Tuomas P J Knowles, Michele Vendruscolo, John Christodoulou, Christopher M Dobson, Dale Schenk, and Lisa McConlogue. Targeting the intrinsically disordered structural ensemble of α-synuclein by small molecules as a potential therapeutic strategy for parkinson's disease. *PLoS One*, 9(2):e87133, 2014.

[548] Michele Perni, Céline Galvagnion, Alexander Maltsev, Georg Meisl, Martin B. D. Müller, Pavan K. Challa, Julius B. Kirkegaard, Patrick Flagmeier, Samuel I. A. Cohen, Roberta Cascella, Serene W. Chen, Ryan Limbocker, Pietro Sormanni, Gabriella T. Heller, Francesco A. Aprile, Nunilo Cremades, Cristina Cecchi, Fabrizio Chiti, Ellen A. A. Nollen, Tuomas P. J. Knowles, Michele Vendruscolo, Adriaan Bax, Michael Zasloff, and Christopher M. Dobson. A natural product inhibits the initiation of α-synuclein aggregation and suppresses its toxicity. *Proc Nat Acad Sc*, 114(6):E1009–E1017, 2017.

[549] Samuel Pe na Díaz, Jordi Pujols, María Conde-Giménez, Anita Carija, Esther Dalfo, Jesús García, Susanna Navarro, Francisca Pinheiro, Jaime Santos, Xavier Salvatella, Javier Sancho, and Salvador Ventura. Zpd-2, a small compound that inhibits α-synuclein amyloid aggregation and its seeded polymerization. *Front Mol Neurosc*, 2019.

[550] Kanti Bhooshan Pandey and Syed Ibrahim Rizvi. Plant polyphenols as dietary antioxidants in human health and disease. *Oxidative medicine and cellular longevity*, 2(5):270–278, 2009.

[551] Silvia Campioni, Guillaume Carret, Sophia Jordens, Lucrece Nicoud, Raffaele Mezzenga, and Roland Riek. The presence of an air-water interface affects formation and elongation of alpha-synuclein fibrils. *J Am Chem Soc*, Jan 2014.

[552] Marie Grey, Sara Linse, Hanna Nilsson, Patrik Brundin, and Emma Sparr. Membrane interaction of α-synuclein in different aggregation states. *J Parkinsons Dis*, 1(4):359–371, 2011.

[553] Céline Galvagnion, Alexander K Buell, Georg Meisl, Thomas C T Michaels, Michele Vendruscolo, Tuomas P J Knowles, and Christopher M Dobson. Lipid vesicles trigger α-synuclein aggregation by stimulating primary nucleation. *Nat Chem Biol*, 11(3):229–234, Mar 2015.

[554] Georg Meisl, Julius B Kirkegaard, Paolo Arosio, Thomas C T Michaels, Michele Vendruscolo, Christopher M Dobson, Sara Linse, and Tuomas P J Knowles. Molecular mechanisms of protein aggregation from global fitting of kinetic models. *Nature Protocols*, 11(2):252–272, 2016.

[555] Giuliana Fusco, Alfonso De Simone, Tata Gopinath, Vitaly Vostrikov, Michele Vendruscolo, Christopher M Dobson, and Gianluigi Veglia. Direct observation of the three regions in α-synuclein that determine its membrane-bound behaviour. *Nat Commun*, 5:3827, 2014.

[556] Amber N. Murray, Fernando L. Palhano, Jan Bieschke, and Jeffery W. Kelly. Surface adsorption considerations when working with amyloid fibrils in multiwell plates and Eppendorf tubes. *Protein Science*, 22(11):1531–1541, 2013.

[557] Hongze Gang, Céline Galvagnion, Georg Meisl, Thomas Müller, Manuela Pfammatter, Alexander K Buell, Aviad Levin, Christopher M Dobson, Bozhong Mu, and Tuomas P J Knowles. Microfluidic diffusion platform for characterizing the sizes of lipid vesicles and the thermodynamics of protein-lipid interactions. *Analytical chemistry*, 90:3284–3290, March 2018.

[558] Alexander K Buell, Christopher M Dobson, Tuomas P J Knowles, and Mark E Welland. Interactions between amyloidophilic dyes and their relevance to studies of amyloid inhibitors. *Biophys J*, 99(10):3492–3497, Nov 2010.

[559] Fernando L. Palhano, Jiyong Lee, Neil P. Grimster, and Jeffery W. Kelly. Toward the molecular mechanism(s) by which EGCG treatment remodels mature amyloid fibrils. *Journal of the American Chemical Society*, 135(20):7503–7510, may 2013.

[560] Sean A. Hudson, Heath Ecroyd, Francis C. Dehle, Ian F. Musgrave, and John A. Carver. (?)-Epigallocatechin-3-Gallate (EGCG) Maintains κ-Casein in Its Pre-Fibrillar State without Redirecting Its Aggregation Pathway. *Journal of Molecular Biology*, 392(3):689–700, sep 2009.

[561] Hila Shoval, Lev Weiner, Ehud Gazit, Michal Levy, Ilya Pinchuk, and Dov Lichtenberg. Polyphenol-induced dissociation of various amyloid fibrils results in a methionine-independent formation of ros. *Biochimica et Biophysica Acta (BBA)-Proteins and Proteomics*, 1784(11):1570–1577, 2008.

[562] Dagmar E Ehrnhoefer, Jan Bieschke, Annett Boeddrich, Martin Herbst, Laura Masino, Rudi Lurz, Sabine Engemann, Annalisa Pastore, and Erich E Wanker. Egcg redirects amyloidogenic polypeptides into unstructured, off-pathway oligomers. *Nature structural & molecular biology*, 15(6):558, 2008.

[563] Wei Zhu, Jin-Ming Peng, Zhen-Zhen Ge, and Chun-Mei Li. A-type dimeric epigallocatechin-3-gallate (egcg) is a more potent inhibitor against the formation of insulin amyloid fibril than egcg monomer. *Biochimie*, 125:204–212, 2016.

[564] Indu R Chandrashekaran, Christopher G Adda, Christopher A MacRaild, Robin F Anders, and Raymond S Norton. Egcg disaggregates amyloid-like fibrils formed by plasmodium falciparum merozoite surface protein 2. *Archives of biochemistry and biophysics*, 513(2):153–157, 2011.

[565] Jing He, Yan-Fei Xing, Bo Huang, Yi-Zheng Zhang, and Cheng-Ming Zeng. Tea catechins induce the conversion of preformed lysozyme amyloid fibrils to amorphous aggregates. *Journal of agricultural and food chemistry*, 57(23):11391–11396, 2009.

[566] Malcolm J Daniels, J Brucker Nourse, Hanna Kim, Valerio Sainati, Marco Schiavina, Maria Grazia Murrali, Buyan Pan, John J Ferrie, Conor M Haney, Rani Moons, et al. Cyclized ndga modifies dynamic α-synuclein monomers preventing aggregation and toxicity. *Scientific reports*, 9(1):2937, 2019.

[567] Priscilla Wilkins Stevens, Rosemarie Raffen, Deborah K Hanson, Ya-Li Deng, Maria Berrios-Hammond, Florence A Westholm, Marianne Schiffer, Fred J Stevens, Charles Murphy, Alan Solomon, et al. Recombinant immunoglobulin variable domains generated from synthetic genes provide a system for in vitro characterization of light-chain amyloid proteins. *Protein Science*, 4(3):421–432, 1995.

[568] M Pras, M Schubert, D Zucker-Franklin, A Rimon, EC Franklin, et al. The characterization of soluble amyloid prepared in water. *The Journal of clinical investigation*, 47(4):924–933, 1968.

[569] Hiroshi Tonoike, Fuyuki Kametani, Akihiko Hoshi, Tomotaka Shinoda, and Takashi Isobe. Amino acid sequence of an amyloidogenic bence jones protein in myeloma-associated systemic amyloidosis. *FEBS letters*, 185(1):139–141, 1985.

[570] M Schneider and N Hilschmann. The primary structure of a monoclonic immunoglobulin-l-chain of subgroup iv of the kappa type (bence-jones protein len.). *Hoppe-Seyler's Zeitschrift fur physiologische Chemie*, 356(5):507–557, 1975.

[571] Marina Nawata, Hirotaka Tsutsumi, Yuta Kobayashi, Satoru Unzai, Shouhei Mine, Tsutomu Nakamura, Koichi Uegaki, Hironari Kamikubo, Mikio Kataoka, and Daizo Hamada. Heat-induced native dimerization prevents amyloid formation by variable domain from immunoglobulin light-chain rei. *The FEBS Journal*, 284(18):3114–3127, 2017.

[572] Bi-cheng Wang, Chung Soo Yoo, and Martin Sax. Crystal structure of bence jones protein rhe (3 å) and its unique domain-domain association. *Journal of Molecular Biology*, 129(4):657–674, 1979.

[573] Walter Palm and Norbert Hilschmann. Die primärstruktur einer kristallinen monoklonalen immunglobulin-l-kette vom κ-typ, subgruppe i (bence-jones-protein rei.), isolierung und charakterisierung der tryptischen peptide; die vollständige aminosäuresequenz des proteins. ein beitrag zur aufklärung der räumlichen struktur der antikörper, insbesondere der haftstelle. *Hoppe-Seyler´s Zeitschrift für physiologische Chemie*, 356(1):167–192, 1975.

[574] Cristian Ionescu-Zanetti, Ritu Khurana, Joel R Gillespie, Jay S Petrick, Lynne C Trabachino, Lauren J Minert, Sue A Carter, and Anthony L Fink. Monitoring the assembly of ig light-chain amyloid fibrils by atomic force microscopy. *Proceedings of the National Academy of Sciences*, 96(23):13175–13179, 1999.

[575] Andrea Ballabio. The awesome lysosome. *EMBO molecular medicine*, 8(2):73–76, 2016.

[576] John Keeling, Jiamin Teng, and Guillermo A Herrera. Al-amyloidosis and light-chain deposition disease light chains induce divergent phenotypic transformations of human mesangial cells. *Laboratory investigation*, 84(10):1322–1338, 2004.

[577] Jiamin Teng, William J Russell, Xin Gu, James Cardelli, M Lamar Jones, and Guillermo A Herrera. Different types of glomerulopathic light chains interact with mesangial cells using a common receptor but exhibit different intracellular trafficking patterns. *Laboratory investigation*, 84(4):440–451, 2004.

[578] Tsuranobu Shirahama and Alan S Cohen. Intralysosomal formation of amyloid fibrils. *The American journal of pathology*, 81(1):101, 1975.

[579] Yahia M Tagouri, Paul W Sanders, Maria M Picken, Gene P Siegal, Jeffrey D Kerby, and Guillermo A Herrera. In vitro al-amyloid formation by rat and human mesangial cells. *Laboratory investigation; a journal of technical methods and pathology*, 74(1):290–302, 1996.

[580] Carl R Kjeldsberg, Harmon J Eyre, and Henry Totzke. Evidence for intracellular amyloid formation in myeloma. 1977.

[581] Thomas Reiter, Daniela Knafl, Hermine Agis, Karl Mechtler, Ludwig Wagner, and Wolfgang Winnicki. Structural analysis of urinary light chains and proteomic analysis of hyaline tubular casts in light chain associated kidney disorders. *PeerJ*, 7:e7819, 2019.

[582] Ikuo Suzuki, Morinobu Takahashi, and Senichi Itoh. Ultrastructural study of human myeloma cells in relation to its function. *Journal of clinical pathology*, 23(4):339–350, 1970.

[583] Tokuhiro Ishihara, Mutsuo Takahashi, Mayumi Koga, Tadaaki Yokota, Yoshimi Yamashita, Fumiya Uchino, and Takako Iwata. Amyloid fibril formation in the rough endoplasmic reticulum of plasma cells from a patient with localized aλ amyloidosis. In *Amyloid and Amyloidosis 1990*, pages 535–538. Springer, 1991.

[584] Eric D Werner, Jeffrey L Brodsky, and Ardythe A McCracken. Proteasome-dependent endoplasmic reticulum-associated protein degradation: an unconventional route to a familiar fate. *Proceedings of the National Academy of Sciences*, 93(24):13797–13801, 1996.

[585] Shruthi S Vembar and Jeffrey L Brodsky. One step at a time: endoplasmic reticulum-associated degradation. *Nature reviews Molecular cell biology*, 9(12):944–957, 2008.

[586] David L Wiest, Janis K Burkhardt, Susan Hester, Michael Hortsch, David I Meyer, and Yair Argon. Membrane biogenesis during b cell differentiation: most endoplasmic reticulum proteins are expressed coordinately. *The Journal of cell biology*, 110(5):1501–1511, 1990.

[587] David P Davis, Rosemarie Raffen, Jeanne L Dul, Shawn M Vogen, Edward K Williamson, Fred J Stevens, and Yair Argon. Inhibition of amyloid fiber assembly by both bip and its target peptide. *Immunity*, 13(4):433–442, 2000.

[588] Alan Solomon, Deborah T Weiss, and Anthony A Kattine. Nephrotoxic potential of bence jones proteins. *New England Journal of Medicine*, 324(26):1845–1851, 1991.

[589] MN Koss, CL Pirani, and EF Osserman. Experimental bence jones cast nephropathy. *Laboratory investigation; a journal of technical methods and pathology*, 34(6):579–591, 1976.

[590] Min Zhu, Pierre O Souillac, Cristian Ionescu-Zanetti, Sue A Carter, and Anthony L Fink. Surface-catalyzed amyloid fibril formation. *Journal of Biological Chemistry*, 277(52):50914–50922, 2002.

[591] Douglas J Martin and Marina Ramirez-Alvarado. Glycosaminoglycans promote fibril formation by amyloidogenic immunoglobulin light chains through a transient interaction. *Biophysical chemistry*, 158(1):81–89, 2011.

[592] Jorge Nieva, Asher Shafton, Laurence J Altobell Iii, Sangeetha Tripuraneni, Joseph K Rogel, Anita D Wentworth, Richard A Lerner, and Paul Wentworth Jr. Lipid-derived aldehydes accelerate light chain amyloid and amorphous aggregation. *Biochemistry*, 47(29):7695–7705, 2008.

[593] Laura A Sikkink and Marina Ramirez-Alvarado. Salts enhance both protein stability and amyloid formation of an immunoglobulin light chain. *Biophysical chemistry*, 135(1-3):25–31, 2008.

[594] Isabel Velázquez-López, Gilberto Valdés-García, Sergio Romero Romero, Roberto Maya Martínez, Ana I Leal-Cervantes, Miguel Costas, Rosana Sánchez-López, Carlos Amero, Nina Pastor, and D Alejandro Fernández Velasco. Localized conformational changes trigger the ph-induced fibrillogenesis of an amyloidogenic λ light chain protein. *Biochimica et Biophysica Acta (BBA)-General Subjects*, 1862(7):1656–1666, 2018.

[595] Ximena Zottig, Mathieu Laporte Wolwertz, Makan Golizeh, Leanne Ohlund, Lekha Sleno, and Steve Bourgault. Effects of oxidative post-translational modifications on structural stability and self-assembly of λ6 immunoglobulin light chain. *Biophysical Chemistry*, 219:59–68, 2016.

[596] Yanyan Lu, Yan Jiang, Tatiana Prokaeva, Lawreen H Connors, and Catherine E Costello. Oxidative post-translational modifications of an amyloidogenic immunoglobulin light chain protein. *International journal of mass spectrometry*, 416:71–79, 2017.

[597] Norbert Sepp, Evelyn Pichler, Stephen M Breathnach, Peter Fritsch, and Helmut Hintner. Amyloid elastosis: analysis of the role of amyloid p component. *Journal of the American Academy of Dermatology*, 22(1):27–34, 1990.

[598] M B Pepys, DR Booth, WL Hutchinson, JR Gallimore, IM Collins, and E Hohenester. Amyloid p component. a critical review. *Amyloid*, 4(4):274–295, 1997.

[599] Morie A Gertz, Rafael Fonseca, and S Vincent Rajkumar. Waldenström's macroglobulinemia. *The Oncologist*, 5(1):63–67, 2000.

[600] AF Strachan and PM Johnson. Protein sap (serum amyloid p-component) in waldenström's macroglobulinaemia, multiple myeloma and rheumatic diseases. *Journal of clinical & laboratory immunology*, 8(3):153–156, 1982.

[601] Glenys A Tennent, LB Lovat, and MB Pepys. Serum amyloid p component prevents proteolysis of the amyloid fibrils of alzheimer disease and systemic amyloidosis. *Proceedings of the National Academy of Sciences*, 92(10):4299–4303, 1995.

[602] GMBJ Gallo, M Picken, B Frangione, and J Buxbaum. Nonamyloidotic monoclonal immunoglobulin deposits lack amyloid p component. *Modern pathology: an official journal of the United States and Canadian Academy of Pathology, Inc*, 1(6):453, 1988.

[603] Andras Khoor, Jeffrey L Myers, Henry D Tazelaar, and Paul J Kurtin. Amyloid-like pulmonary nodules, including localized light-chain deposition: clinicopathologic analysis of three cases. *American journal of clinical pathology*, 121(2):200–204, 2004.

[604] Philip N Hawkins. Serum amyloid p component scintigraphy for diagnosis and monitoring amyloidosis. *Current opinion in nephrology and hypertension*, 11(6):649–655, 2002.

[605] Olivier Devuyst, Karin Dahan, and Yves Pirson. Tamm–horsfall protein or uromodulin: new ideas about an old molecule. *Nephrology dialysis transplantation*, 20(7):1290–1294, 2005.

[606] Paul W Sanders. Pathogenesis and treatment of myeloma kidney. *The Journal of laboratory and clinical medicine*, 124(4):484–488, 1994.

[607] Zhi-Qiang Huang, Paul W Sanders, et al. Localization of a single binding site for immunoglobulin light chains on human tamm-horsfall glycoprotein. *The Journal of clinical investigation*, 99(4):732–736, 1997.